Investigating the Role of Epithelial-mesenchymal Crosstalk in the Pathology of Idiopathic Pulmonary Fibrosis

Submitted by Thomas Hames to the University of Exeter as a thesis for the degree of Doctor of Philosophy in Medical Studies, November 2017

Declarations

All experimental material presented in the results section of this thesis was performed by myself.

Signature: ……

Acknowledgements

There are numerous people to thank for enabling me to complete this project. Firstly, I would like to thank my supervisory team of Dr Chris Scotton, Prof. Paul Winyard and Dr Michael Gibbons. I would like to thank them for their support and guidance and their assistance in shaping this project. In particular, I would like to thank Dr Chris Scotton for teaching me the many lab techniques used during this project, teaching me how to conduct good research and for providing valuable feedback across all areas my research. I have also been greatly supported by the Exeter Respiratory Research Group and I would like to thank Alex Clarke, Bry McCord, Dr Phil Mitchelmore and Dr Rebecca Wollerton for their help.

Likewise, none of the experiments performed in this project would have been possible without the acquisition of human cells. For that I would like to thank Dr Michael Gibbons and the Cardiothoracic Team at the RD&E for assisting with tissue collection, Dr Gil Baker, Lidia Romanczuk and Chloe Slade, of the RD&E Clinical Research Facility, for organising tissue collection, and Dr Manish Powari, consultant histopathologist, for dissecting tissue for me. As well as this, I would like to thank Professor Ann Millar and Dr Shaney Barratt (University of Bristol) for providing additional primary fibroblast lines as well as Dr Jo Porter (University College London), for providing bronchial epithelial cells.

There are also several people to thank for their help with experiments. Investigations into the mitochondrial were made possible by the assistance of Prof. Michael Schrader and Tina Schrader, from University of Exeter Biosciences, who taught me about the mitochondrial morphology and staining techniques. I would also like to thank Dr Alicia Waters for answering my many questions regarding the mitochondria. I would like to thank Dr Giles Cory and Dr David Allard for both assisting and providing reagents for western blotting, and I would like to thank Ben Mellows (University of Reading) for his help with senescence protocols.

Finally, I have enjoyed my time in Exeter thanks to the people I have worked, socialised and lived with. I would like to thank all the people at the St. Luke's Labs for this, with a very special mention to Alex Clarke, Annie Knight, Alicia Waters, Annelie Maskell, Daniel Ferguson, Ashley Nicholls and Lorena Boquete. From the medical school, I would also like to thank Ana Miguel Cruz and Hannah Smithers, as well as a very big shout out to Ben Hall, Jeff Lambert, Myles Linton, Nick Logan and Darren Walsh. All these people have made my experience in Exeter fantastic.

One last person I would like to thank is Rose McConaghy. I'd like to thank her for all her support and for being an amazing girlfriend!

Abstract

Idiopathic pulmonary fibrosis (IPF) is a disease of unknown aetiology, characterised by the progressive and irreversible scarring of parenchymal lung tissue that leads to respiratory failure and death. The disease is understood to be driven by an impaired and aberrant wound healing response, with an inappropriate reactivation of developmental signalling. The greatest risk factor for the disease is age, which is a process intimately associated with an increase in the burden of senescent cells. Such cells acquire a unique secretory phenotype and are known to have a significant impact on their local microenvironment.

It was hypothesised that an alteration in epithelial-mesenchymal secretory communication, due to senescent-like changes in the fibroblast phenotype, may detrimentally contribute to lung homeostasis. An *in vitro* model of the lung airway was established in which primary human lung fibroblasts (HLFs) were co-cultured with human bronchial epithelial cells (HBECs). HBECs were cultured on a semi-permeable, transwell insert and co-cultured with either normal (NHLF), fibrotic (FHLF) or senescent fibroblasts. Over 72 hrs of co-culture, wound healing was assessed, via an epithelial scratch assay, and epithelial regeneration was measured, via trans-epithelial electrical resistance.

Co-culture with NHLFs improves epithelial regeneration, however, FHLFs and senescent cells in co-culture show a diminished ability to promote epithelial regeneration and wound repair. The secretory repertoire of these cells contains elevated levels of IL-6, CXCL8, CXCL1 and GCSF (when assessed at both an RNA and protein level), factors strongly associated with the senescent phenotype. Targeting this secretome via treatment with the JAK 1/2 inhibitor Ruxolitinib attenuates these impairments and may point towards a new therapeutic strategy for the treatment of IPF.

Table of Contents

List of Figures

List of Tables

Abbreviations

3D	3-dimensional
AEC1	Type I alveolar epithelial cell
AEC2	Type II alveolar epithelial cell
AER	Apical ectodermal ridge
AKAP13	A-kinase anchoring protein 13
ALI	Air-liquid interface
AQP5	Aquaporin-5
ARF	Alternative-reading-frame
ASL	Airway surface liquid
ATM	Ataxia telangiectasia mutated
ATP	Adenosine triphosphate
BAL	Broncho-alveolar lavage
BC	Basal cell
BLM	Bleomycin
BMP4	Bone morphogenic protein-4
CCL2	CC chemokine ligand-2 (Monocyte chemotactic protein-1)
CDK	Cyclin dependent kinase
CM	Conditioned medium
COL1A1	Collagen type I, alpha-1
COL2A1	Collagen type II, alpha-1
COX1	Cyclooxygenase-1
CPP	Cardiopulmonary progenitors
CXCL8	CXC chemokine ligand-8 (Interleukin-8)
D+Q	Dasatinib and Quercetin
DDR	DNA-damage response
DKC	Dyskeratosis congenita
DKK1	Dickkopf-1
DMSO	Dimethyl sulfoxide

DPLD	Diffuse parenchymal lung diseases
DSB	Double-strand breaks
ECM	Extra cellular matrix
EGFR	Epidermal growth factor receptor
ELISA	Enzyme-linked immunosorbent assay
EMT	Epithelial mesenchymal transition
ER	Endoplasmic reticulum
FBS	Foetal bovine serum
FCCP	Carbonyl cyanide-4-(trifluoromethoxy)phenylhydrazone
FGF10	Fibroblast growth factor-10
FHLF	Fibrotic human lung fibroblast
F-IPF	Familial-idiopathic pulmonary fibrosis
FOXJ1	Forkhead box protein J1
FOXO3A	Forkhead box O3a
FST	Follistatin
FVC	Forced vital capacity
GLI1	GLI family zinc finger-1
GM-CSF	Granulocyte-macrophage colony-stimulating factor
H_2O_2	Hydrogen peroxide
HA	Hyaluronan
HAS	Hyaluronan synthase
HBEC	Human bronchial epithelial cell
HGF	Hepatocyte growth factor
HLF	Human lung fibroblast
HOPX	HOP homeobox
HPLC	High-performance liquid chromatography
HRCT	High-resolution computed tomography
HSC	Hepatic stellate cells
ID2	Inhibitor of DNA binding-2
IIP	Idiopathic interstitial pneumonias

IL-1β	Interleukin 1-beta
IL-6	Interleukin-6
IPF	Idiopathic pulmonary fibrosis
ITGA6	Integrin subunit alpha-6
JAK	Janus Kinase
KGF	Keratinocyte growth factor
KRT14	Keratin-14
KRT5	Keratin-5
LN_2	Liquid nitrogen
LOXL2	Lysyl hydroxylase-2
LPS	Lipopolysaccharide
MAPK	Mitogen-activated protein kinase
MDM2	E3 ubiquitin-protein ligase
MFI	Median fluorescent intensity
MMP	Matrix metalloproteinase
mtDNA	Mitochondrial DNA
mTOR	Mammalian target of Rapamycin
MUC5AC	Mucin 5ac
NF-κB	Nuclear factor kappa-B
NGFR	Nerve growth factor receptor
NHLF	Normal human lung fibroblast
NK	Natural killer
NKX2.1	NK2 homeobox-1
NOX	NADPH oxidase
OD	Optical density
OIS	Oncogene-induced senescence
OSKM	Oct4, Sox2, Klf4, cMyc
PAI-1	Plasminogen activator inhibitor-1
PDGFRA	Platelet derived growth factor receptor-alpha
PDPN	Podoplanin

PFA	Paraformaldehyde
PGE2	Prostaglandin E2
PINK1	PTEN-induced putative kinase-1
PMK	Primary mouse keratinocytes
pSTAT-3	phosphorylated STAT-3
PTGDS	Prostaglandin D synthase
PZ	Progress zone
RB	Retinoblastoma protein
RCN	Relative cell number
RCT	Randomised control trial
RD&E	Royal Devon and Exeter Hospital
ROS	Reactive oxygen species
R_{TE}	Trans-epithelial electrical resistance
RT-qPCR	Reverse transcription - quantitative polymerase chain reaction
SADS	Senescence-associated distension of satellites
SAHF	Senescence-associated heterochromatic foci
SASP	Senescence-associated secretory phenotype
SA-βgal	Senescence-associated beta-galactosidase
SCGB1A1	Secretoglobin family 1A member 1
SDS	Sodium dodecyl sulphate
SDS	Standard deviation
SEM	Standard error of mean
SFTP	Surfactant protein
SHH	Sonic hedgehog
SIPS	Stress-induced premature senescence
SMG	Submucosal glands
SOX2	SRY-box 2
SOX9	SRY-box 9
SRY	Sex-determining region Y

STAT-3	Signal transducer and activator of transcription-3
TAZ	Transcriptional coactivator with PDZ-binding motif
TERT	Telomerase reverse transcriptase
TGF-β	Transforming growth factor beta
TMRE	Tetramethylrhodamine, ethyl ester
TNF-α	Tumour necrosis factor-alpha
TRP63	Transformation related protein-63
TUBB6	Tubulin beta-6
UIP	Usual interstitial pneumonia
VEGF	Vascular endothelial growth factor
VIM	Vimentin
WNT	Wingless-type MMTV integration site family
WISP1	WNT1-inducible signalling protein-1
YAP	Yes-associated protein-1
ZO-1	Zonula occludens-1
αMEM	alpha-minimum essential medium
αSMA	alpha-smooth muscle actin
Δp	Proton motive force
$\Delta_{\psi m}$	Mitochondrial membrane potential

1. Introduction

Idiopathic pulmonary fibrosis (IPF) is a disease of unknown aetiology, characterised by progressive and irreversible scarring of the parenchymal lung tissue, leading to respiratory failure and death. The disease is understood to be driven by an inappropriate reactivation of developmental signalling and an impaired and aberrant wound healing response, set against the backdrop of an ageing lung. Fundamental to the processes of development, repair, and maintenance of tissue function, is the relationship between the epithelium and the mesenchyme. This relationship is thought to be key to the pathology of IPF and understanding it can help better elucidate some of the driving forces of the disease. This introduction aims to outline the numerous roles of epithelialmesenchymal crosstalk in basic lung physiology, covering development, homeostasis and repair, moving then to an examination of the pathology of IPF and the key characteristics of the disease. The roles of crosstalk and the characteristics of IPF will then converge on the phenomenon of cellular senescence, highlighting its possible role in the pathology of IPF.

1.1 Epithelial-mesenchymal Crosstalk in Lung Physiology

The key to any good relationship is communication; the relationship between cell types of the lung is no exception.

A cell's function and behaviour is dictated by its local micro-environment. This environment can be determined by the cell itself, producing proteins that function in an autocrine manner, and also by communication with its neighbours. This 'crosstalk' is a paracrine mechanism of cell communication that is important to numerous physiological processes. An important example of crosstalk is the relationship between the epithelium and the mesenchyme. This relationship facilitates the development of the lung during gestation, maintains homeostasis of the adult airways and contributes heavily to the processes of repair.

By investigating crosstalk in these processes, it is possible to gain, not just an insight into intercellular communication, but also to the overall physiology of the lung, encompassing its structure, organisation and function. Likewise, what becomes apparent when looking at these aspects of physiology is that core communicatory pathways exist, with the same pathways functioning across a diverse range of roles. This section will set out to expatiate the processes of lung development, homeostasis and repair, exemplifying the role of crosstalk whilst giving a more general overview of the lungs.

1.1.1. Development of the Lung

Embryogenesis

The lung begins to develop relatively late in the human embryo, starting 4-5 weeks into gestation. The process begins with mesenchymal mesodermal cells signalling to ventral, epithelial endodermal cells on the anterior foregut, producing factors such as bone morphogenic protein-4 (BMP4) and Wingless-type MMTV integration site family (WNT) 2/2B, which specify commitment to a lung cell fate. Endodermal cells become

committed by expression of the transcription factor NK2 homeobox-1 (NKX2.1) and from this cohort of cells, over the next 35 weeks, the respiratory tree develops, going on to contain the complete repertoire of cells for the fully functioning, adult lung [1,2].

The pseudoglandular phase

Ventral mesodermal cells promote the budding of *Nkx2.1*$^{+}$ endodermal cells giving rise to the nascent trachea and bronchi **(*Figure* 1.1.1.)** [3]. Once separated from the developing oesophagus, the lung transitions from this early embryonic stage into the pseudoglandular stage. During this period the extensive respiratory tree is formed in a process of branching morphogenesis. This process is elicited by three geometrical modes of branching, which creates a highly stereotypic structure [4]. Such patterning is again largely dictated by the surrounding mesoderm. Mesenchymal cells expressing the mitogen, fibroblast growth factor-10 (FGF10), promote the proliferation of epithelial cells whilst also dictating the direction of their growth [5,6]. Regulation occurring downstream of FGF10, co-ordinates mitotic spindle orientation and promotes directed division in a distal direction, extending the respiratory network [7]. Likewise, fibronectin laid down by the mesoderm interacts with epithelial β1 integrins, promoting planar growth and preventing epithelial multilayering [8]. The strength of FGF10 signalling is greatest at the distal ends of the advancing airways and the pattern of its expression is crucial for morphogenesis. Endodermal crosstalk, involving sonic hedgehog (SHH) and BMP4, restricts mesodermal *Fgf10* expression [5,6]. This acts as an inhibitor of endodermal growth. In adjacent endoderm growth is not inhibited thereby allowing a process of branching.

Commitment to cell fate

Early in lung development cells of the endoderm are further committed to distinct lineages, occurring in a proximal-distal manner [9]. As the strength of FGF10 signalling is lost in the more proximal regions of the airways, sex-determining region Y (SRY)-box 2 (*Sox2*) expression is enabled in the epithelium. This creates and commits cells to a lineage that will give rise to the conducting portion of the developed airway. Reduced

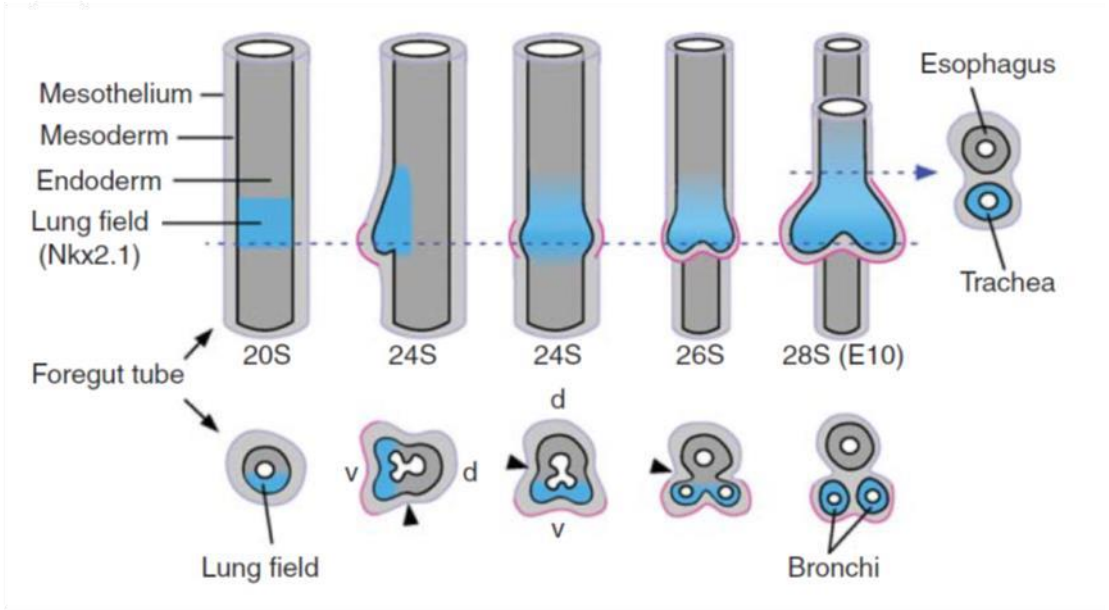

Figure 1.1.1. Lung budding from the anterior foregut. The initial lung bud is composed of epithelial endoderm surrounded by mesenchymal mesoderm. As the bud protrudes ventrally it becomes surround by a layer of mesothelium, which will go on to form the visceral pleura. The arrowheads highlight the tracheoesophageal groove, which initiates septation of the trachea and oesophagus. (Reproduced from ref. [3] with the permission of Cold Spring Harbor Laboratory Press)

WNT signalling facilitates this increase in SOX2 activity, which leads to inhibition of branching [10]. This is, in part, due to a pre-emptive induction of differentiation pathways that make the cells refractory to branching signals [11]. Conversely, at the distal, budding regions of the airway, cells establish expression of SRY-box 9 (*Sox9*) and inhibitor of DNA binding-2 (*Id2*), leading to a population of cells that act as progenitor for the gas exchange (or respiratory) portion of the lung **(*Figure* 1.1.2.)** [12]. SOX9 also further regulates distal branching and its loss leads to numerous defects in epithelial cytoskeletal arrangement and extracellular matrix (ECM) organisation, with perturbed transcriptional regulation of collagen type II, α-1 (*COL2A1*) [13].

The canalicular phase

As the process of branching morphogenesis nears completion the developing lung enters the canalicular stage. During this stage, mesodermal signalling promotes the further differentiation of $Sox9^{+}/Id2^{+}$ progenitors into the two alveolar cell types. This is discernible by the appearance of two, distinct epithelial transcriptional profiles. Type I alveolar epithelial cells (AEC1s) arise, expressing HOP homeobox (*Hopx*) and Podoplanin (*Pdpn*), developing alongside surfactant protein A-C (*SftpA-C*) expressing type II alveolar epithelial cells (AEC2s) [14]. This stage also involves a greater association of the epithelium with the underlying vasculature and a narrowing of airway tubules. The mesodermal signals that drive this process have yet to be entirely elucidated. Temporal glucocorticoid signalling has been shown to be important in mouse, as has FGF signalling, with FGF-induced branching morphogenesis antagonising alveolar differentiation via the GTPase Kras [15,16] .

The saccular phase

There is quick succession from the canalicular stage to the saccular stage, a stage in which the distal tubules bud into a series of sacs, each of which is intimately associated with the surrounding vasculature **(*Figure* 1.1.3.)**. The extensive surface area of the epithelial-endothelial interface of the lung is achieved during this stage by the formation of primary septa, which give rise to the alveoli. Mesenchymal cells migrate into the walls of the distal airway, subdividing the alveoli into numerous compartments. These

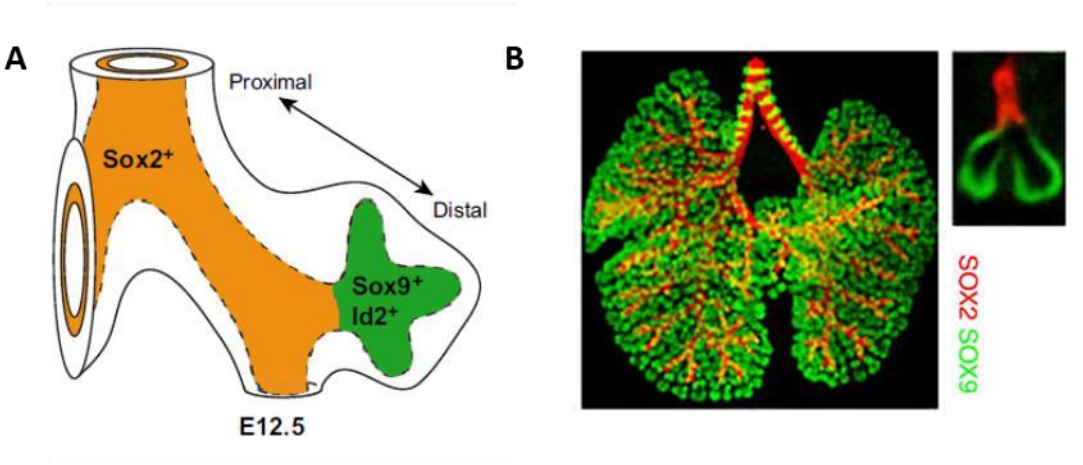

Figure 1.1.2. Commitment of lung endodermal epithelium to a conducting or acinar lineage. (A) In proximal regions of the lung, lack of certain mesodermal signals allows endodermal expression of *Sox2*, which restricts branching and enables cells to eventually form the tracheobronchial airways. In the distal airways, mesodermal signals specify *Sox9* / *Id2* expression. These cells can then act as a progenitor for AEC1 and AEC2s. (Reproduced form ref. [25] with the permission of *Development*) **(B)** Whole-mount, immuno-stained mouse lung at embryonic day 15, highlighting the proximal-distal pattern of *Sox* expression. (Reproduced from ref. [4] with the permission of Macmillan Publishers Ltd)

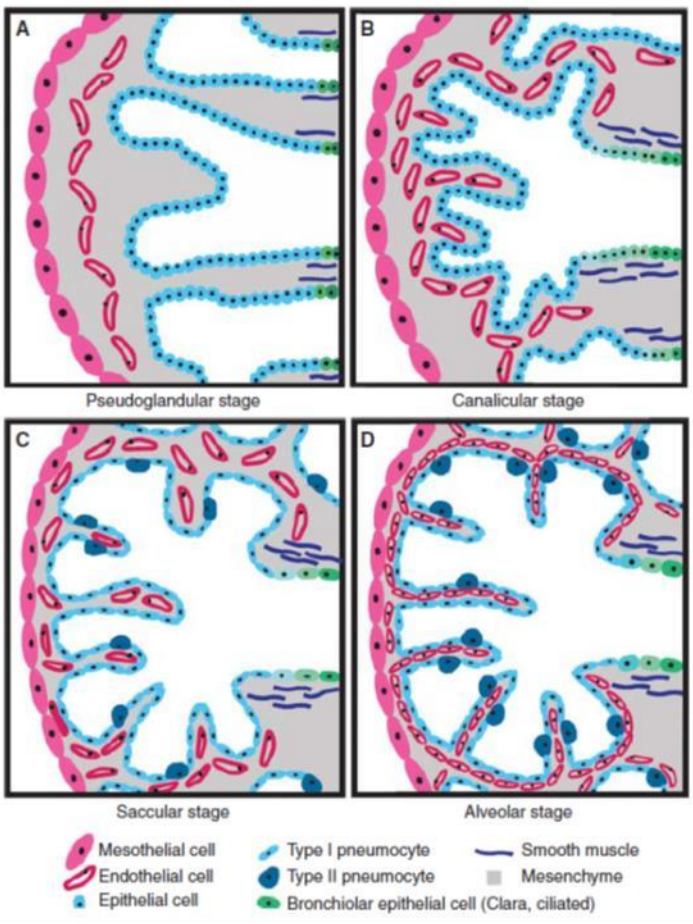

Figure 1.1.3. Stages of distal lung development. (A) The pseudoglandular stage involves epithelial advance into the mesenchyme and branching morphogenesis. **(B)** During the canalicular stage, epithelial cell fate is specified and the epithelium becomes more associated with the vasculature. **(C)** The saccular stage involves mesenchymal cell septation of distal lung buds, increasing their surface area. **(D)** The alveolar stage is the final phase of lung development, which continues into adult life. During this stage secondary septae formation further defines the alveoli and their intimate endothelial association allows efficient gas exchange. (Reproduced from ref. [3] with the permission of Cold Spring Harbor Laboratory Press)

mesenchymal cells arise from a common mesodermal progenitor termed cardiopulmonary progenitors (CPP). These ventrally located cells are identified by *Wnt2/Gli1/Isl1* expression and are regulated via SHH signalling. They give rise to both vascular and airway smooth muscle cells, pericytes and proximal endothelia [17]. Not only this, but they contribute to the generation of cardiomyocyte and endocardial cells. CPPs appear to lose their multipotency as gestation draws to a close and the continued role of this cell lineage in the adult lung remains to be elucidated. Their role in the saccular stage however is important, for both the structural and the functional development of the epithelium.

Alveologenesis

Postnatally, the process of alveolar development continues, with alveologenesis occurring several months post-term in humans. It is facilitated by further mesenchymal infiltration, by cells that migrate and differentiate into fibroblasts, myofibroblasts and lipofibroblasts. Myofibroblasts further define alveolar septation by depositing elastin at the tips of the alveolar walls **(*Figure* 1.1.4.)** [18]. The function of these myofibroblasts is under the control of SHH signalling. At the early stages of post-natal alveologenesis SHH promotes myofibroblast proliferation and differentiation, giving rise to *Gli1*$^{+}$/*Acta2*$^{+}$ cells. Inhibition of SHH signalling during this period results in enlarged alveoli, lacking secondary septa. Importantly though, with the completion of septal definition there is a decrease in SHH signalling and reduction in alveolar myofibroblast number [19].

The resultant ECM scaffolding in the alveoli integrates with an extensive, interlinking network of connective tissue fibres. These fibres provide not only structure, but allow the appropriate distribution of tensile stress, allowing even conductance of air into the alveoli [20]. Collagen is the predominating fibre in this network, which has a three-category hierarchy. Axial fibres sheath the respiratory tree from the large airways to the alveolar ducts, peripheral fibres, emanating from the visceral pleura, penetrate into the parenchyma where they are connected to axial fibres by septal fibres, which are continuous throughout the interalveolar space and form the alveolar walls [21].

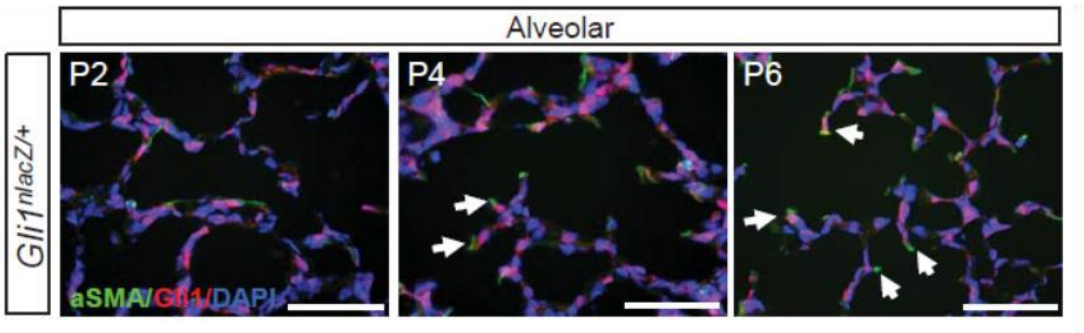

Figure 1.1.4. Myofibroblast alveolar infiltration and secondary septae formation. Immuno-stained mouse alveoli from post-natal day 2 – 6. *Gli1*$^{+}$ mesenchymal cells (red) and *Acta2*$^{+}$ mesenchymal myofibroblasts (green). Arrowheads at day 4 and 6 highlight myofibroblasts at the tips of secondary alveolar septae. These cells deposit matrix, providing structural support for the alveoli. Scale bar = 50 µm. (Reproduced from ref. [19] with the permission of The American Thoracic Society)

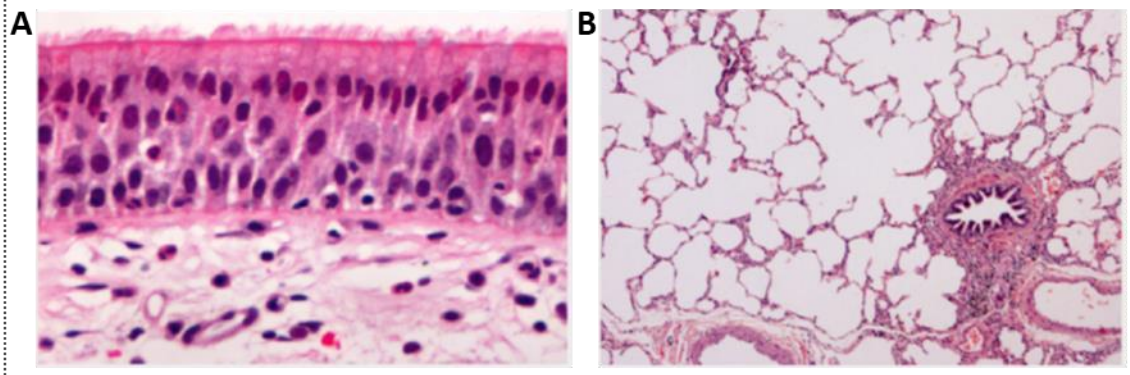

Figure 1.1.5. Differential organisation of the conducting and acinar airway. (A) The conducting airways are lined by a pseudostratified, columnar epithelium. The apical surface is lined with cilia and mucus, which protects the airway. The stem / progenitor cell for this epithelium, the BC, sit at the base of the epithelium, in contact with the basal lamina. Beneath this is a mixed population of mesenchymal cells. **(B)** By contrast, the acinar airways are lined with thin, squamous epithelium, which creates an extensive surface area for gas exchange. (Reproduced from ref. [23] with the permission of Elsevier)

Around two-four years after the birth, these developmental pathways will have enabled the generation of around 300 million alveolar units, creating a gas exchange surface of roughly 70 m^2 [22]. The development of the lung is a masterclass in inter-cellular communication, most notably between the mesenchymal mesoderm and epithelial endoderm. The crosstalk required to orchestrate this development continues to find prominence throughout an adults' life, contributing to both the maintenance of normal lung homeostasis, as well as co-ordinating the lungs response to injury.

1.1.2. Maintaining lung homeostasis

The processes of development generate a complex tree of respiratory airways. Broadly, these airways can be categorised into two regions, the conducting airways, involved in the movement of air, and the respiratory airways, involved in facilitating gas exchange **(*Figure* 1.1.5.)** [23]. The conducting airways begin at the trachea, which descends distally, undergoing around 23 generations of branching, giving rise to the bronchi, bronchioles and the terminal/transitional bronchioles. The respiratory airways consist of respiratory bronchioles, which combine conductance with gas exchange, alveolar ducts and alveolar sacs, where half of all alveolar units reside. Maintaining the function of these airways, even under a steady state, requires constant crosstalk. This section will set out to explore the mechanisms and cell-cell relationships that facilitate this.

1.1.2.1. The tracheobronchial airways

The dichotomy of roles in the airways is reflected in the differing cell types, and differing structure, of the conducting and respiratory regions of the lung. Regarding the epithelium, the proximal airways of the trachea and bronchi are populated by a thick, pseudostratified columnar layer composed of several cell types, all arising from developmental, *Sox2* expressing endodermal cells **(*Figure* 1.1.6.)** [24,25].

Mucosal cells

A crucial role of this epithelial layer is host defence. Mucin 5ac (*Muc5ac*) expressing mucosal (goblet) cells, along with forkhead box protein J1 (*Foxj1*) and tubulin β-6

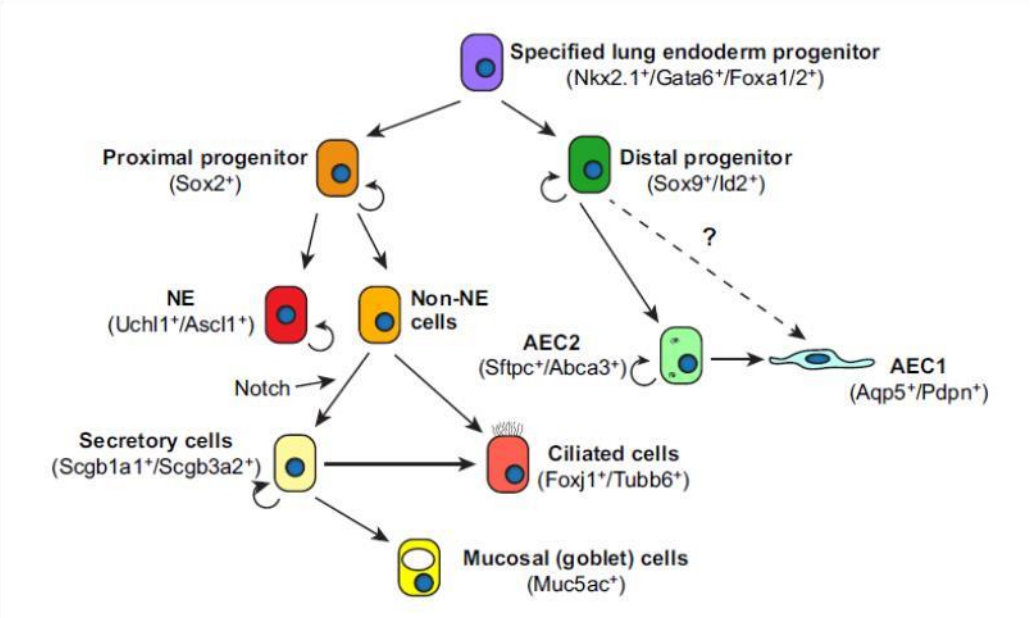

Figure 1.1.6. Hierarchy of lung epithelial cell progenitors and expression markers of their lineage. *Nkx2.1*$^{+}$ endoderm gives rise to proximal, *Sox2*$^{+}$, and distal, *Sox9*$^{+}$ / *Id2*$^{+}$ epithelial progenitors. Proximal progenitors give rise to all cell types of the upper airway, including neuroendocrine cells, secretory cells, mucosal and ciliated cells. Conversely, distal progenitors are restricted to giving rise to the type I and II alveolar epithelial cells. (Reproduced form ref. [25] with the permission of *Development*)

(*Tubb6*) expressing multiciliated cells are key to this. These two populations of cells make up the majority of the tracheobronchial epithelium. Mucosal cells are responsible for the elaboration of airway surface liquid (ASL), which coats the upper airways and protects the lungs from inhaled particles and micro-organisms. It also maintains immune homeostasis and can modulate macrophage function in response to infection [26]. The large glycoproteins, MUC5AC and MUC5B, are important ASL components and their diverse and extensive range of carbohydrate sequences acts to sequester dangerous inhalants [27]. Secretoglobin family 1A member 1 (*Scgb1a1*) expressing club cells, and secretory cells of the tracheal submucosal glands (SMG), are also important sources of mucin production [28,29].

Multiciliated cells

The removal of substances trapped in the ASL is achieved by its continuous transport out of the trachea and into the oesophagus. This can be elicited by cough but also the repetitive and co-ordinated beating of cilia, flagella-like projections situated on the apical surface of multiciliated cells. These cells have around 250 cilia each, which can beat at around 1,000 bpm. Cilia do not make contact with the viscous mucus and are instead bathed in a low viscosity, watery fluid called the periciliary liquid layer. This underlies the mucus layer and makes repetitive beating less energy demanding [30].

Immune-modulating cells

Other tracheobronchial cell types that are less numerous but also important in host defence include neuroendocrine cells and tuft cells. Pulmonary neuroendocrine cells are found in isolation or in groupings of cells called neuroepithelial bodies. These cells are part of the diffuse neuroendocrine system. Nervous innervation occurs at the base of these cells whilst, at the apical surface, they protrude microvilli into the luminal space. They can also secrete numerous amines and peptides that can co-ordinate the airway immune response [31]. Tuft cells (also known as brush cells) function as solitary chemosensory cells, responding particularly to secreted bacterial compounds, activating innate response to potential infection [32].

Basal cells

Underlying the pseudostratified epithelium, in a near continuous layer, is a population of basal cells (BCs). BCs are a multipotent stem cell characterised by the expression of transformation related protein-63 (*Trp63*), keratin-5 (*Krt5*) and, additionally in humans, nerve growth factor receptor (*NGFR*) and integrin subunit α6 (*ITGA6*). They make up roughly 20-30% of proximal airway cells, becoming less numerous and more disperse in a distal direction and they are also found at the base of SMGs in the upper trachea. BCs have the ability to maintain cell turnover in the steady state lung and also repopulate the airway in response to injury [33,34]. Within the BC population different subsets can also be defined [35]. For example, SMG-located BCs are able to give rise to duct and tubular cells, as well as airway epithelial cells [36]. Another subset of keratin-14 (*Krt14*) expressing BC also exist, which make up around 20% of the epithelial BC population [37]. These are a facultative progenitor that are unipotent in the normal epithelium, becoming activated and multipotent only in response to injury [38].

The mesenchyme

Below this epithelial surface is a population of fibroblasts and airway smooth muscle cells, believed to be primarily of a common CPP lineage, as well as nerve endings, vasculature and, in the trachea, cartilaginous rings. These cells provide structural as well as trophic support, an example of which is parabronchial smooth muscle cell secretion of FGF10 [39]. Roles such as this are an important facet of lung cell communication, and many more examples can be found in the proximal airways.

1.1.2.2. Maintaining the proximal airways

Maintenance of the steady state tracheobronchial airway requires careful co-ordination of inter-cellular communication, through both paracrine and autocrine signalling as well as cell-cell and cell-matrix interactions. Cell turnover in the lung is slow in comparison to other organs (although it does occur with consistency) and most cells can be found in a quiescent state [40].

Crosstalk is key to maintaining this quiescence and preventing unwanted differentiation (especially in progenitor cells) with several pathways regulating identified. 3dimensional (3D) tracheospheres, a model assay of the pseudostratified epithelium, demonstrate BMP4 signalling as key to regulating BC activity [41]. Mesenchymal BMP4 signalling acts as a brake on proliferation and maintains quiescence through elevation of epithelial phospho-Smad1/5/8. Similarly, the Yes-associated protein-1 (YAP) also regulates mouse BC activity. YAP is a transcriptional co-activator in the Hippo kinase cascade and its conditional deletion in *Trp63*$^{+}$ BCs leads to a loss of BC number through uncontrolled differentiation. YAP elicits this through functional interaction with TRP63 although the upstream mechanisms coordinating *Yap* expression are, however, yet to be elucidated [42].

Investigation of the BC transcriptome has revealed enrichment for genes involved in autocrine and paracrine signalling. Epidermal growth factor receptor (EGFR) family expression is enriched, indicating an importance of EGF signalling in BC function, and there is also enrichment for expression of the integrins *Itga6* and *Itgb6*, both of which are required for the spatially-restricted activation of latent transforming growth factorβ (TGF-β) [43]. TGF-β is an important factor throughout development, homeostasis, repair and disease. In a co-culture system of tracheal epithelial cells and mesenchymal fibroblasts, ITGB6 expressed on airway epithelial cells activates latent TGF-β. Active TGF-β can then act in a paracrine manner on fibroblasts leading to the suppression of hepatocyte growth factor (HGF) secretion that, in turn, maintains epithelial quiescence [44]. More recent investigations into HGF have further underpinned its role in epithelial function. In a lung colony forming assay, epithelial cells fail to form colonies when monocultured, however, co-culture with mesenchymal cells helps to achieve this. Further addition of recombinant FGF10 and HGF enhances the potential of these epithelial cells with synergistic effects. Conversely, addition of TGF-β1 and BMP-4 reduces colony growth, presumably through HGF suppression. Also, the mesenchymal cells in co-culture were found to wrap themselves around the epithelial cells, indicating that cell contact as well as paracrine communication is important in mediating this effect [45].

Hedgehog signalling also plays an important role in maintaining airway quiescence. SHH signals via its downstream target GLI family zinc finger-1 (GLI1). In mouse, SHH is expressed in proximal airway epithelial cells with *Gli1* expression found in corresponding mesenchymal cells, which express markers such as platelet derived growth factor receptor-α (*Pdgfra*), vimentin (*Vim*) and collagen type I, α-1 (*Col1a1*). Conditional knockout of *Shh* in epithelial cells leads to mesenchymal expansion. This signalling is bidirectional, with *in vitro* co-culture of epithelium and mesenchyme highlighting that SHH also promotes epithelial quiescence via a mesenchymal feedback-loop **(*Figure* 1.1.7.)** [46].

The small airways

As the airways descend to towards the alveolar bed their composition changes from a pseudostratified, columnar epithelium to a more simple, cuboidal one. In mice, these airways, termed bronchioles, have been well characterised and well-studied. The progenitor cell responsible for maintaining these airways is understood to be the *Scgb1*$^{+}$ Club cell. In humans, however this region of the respiratory tree is less well understood and observations in mouse may not directly relate to man.

1.1.2.3. The alveoli

The most distal regions of the lung airway, the alveoli, are however much better understood. They are comprised of just a few epithelial cell types, namely, AEC1 and AEC2, which arise from *Sox9*$^{+}$/*Id2*$^{+}$ expressing endoderm. Within the alveoli AEC1 constitute roughly 8% of all cells yet make up around 90% of the lungs surface area. AEC2 make up double the cell number yet cover only 7% of the alveolar surface. AEC1 are the largest by volume and surface area but they are extremely thin and share a fused basement membrane with the basolateral endothelia. These endothelial cells make up around 30% of all cells, second in number to the varying interstitial cells that comprise 37% of all alveolar cells [47,48].

Squamous AEC1s can be identified by *Pdpn*$^{+}$/*Hopx*$^{+}$ expression and function to allow gas exchange between the air and the circulating blood, the primary function of the lungs. To maintain the delicate structure of the alveoli and prevent collapse during breathing,

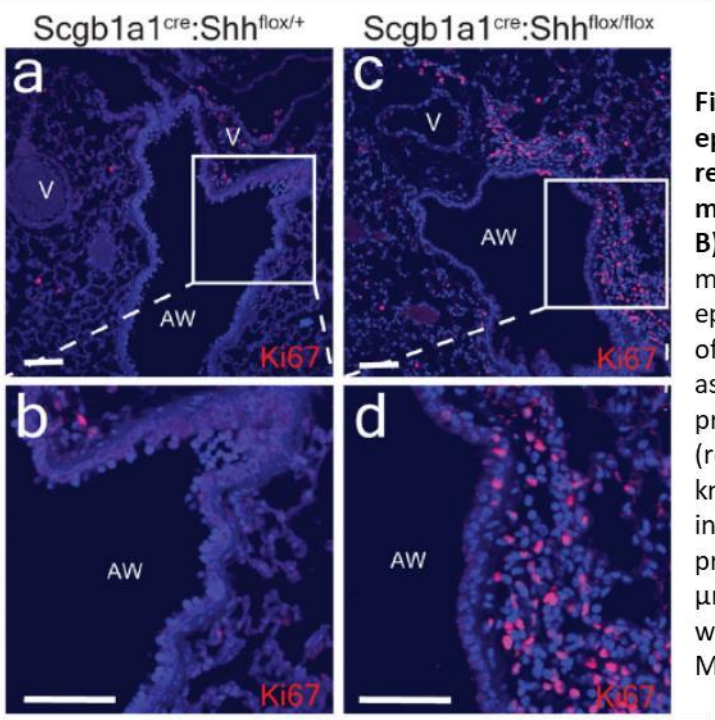

Figure 1.1.7. Postnatal, epithelial Shh signalling is required for maintaining mesenchymal quiescence. (A-B) When *Shh* is expressed by mouse proximal mouse epithelium there is a paucity of mesenchymal proliferation, as assessed by the proliferation marker Ki67 (red). **(C-D)** Conditional knockout of *Shh* causes an increase in mesenchymal Ki67 proliferation. Scale bar = 100 µm. (Reproduced from ref. [19] with the permission of Macmillan Publishers Ltd)

surfactant covers the air-surface interface. Surfactant is a product of AEC2s, which can be identified by expression of *Sftpc*. These cuboidal cells lie in the corners of alveoli atop a discontinuous basement membrane, which allows communication with the interstitium and forms the AEC2 niche **(*Figure* 1.1.8.)**. Lineage tracing studies in mouse have backed-up the long held understanding that AEC2 are a renewable source of AEC1, under both normal conditions and in response to injury [49,50]. Alveolar cell turnover is very low in the normal lung and only around 1% of AEC2 in the adult lung display stem cell function at any one time. Their replication is intermittent, with a population doubling time of roughly 40-days, and these factors contribute to an alveolar renewal rate of only 7% of alveoli per year [50]. The perceived paradigm regarding AEC1 is that they are terminally differentiated with limited, if any, proliferative capacity. Recent investigations in mouse, however, have begun to suggest that AEC1 have the plasticity to facilitate generation of both AEC1 and AEC2 cells, and that a bi-directional lineage relationship exists between the two populations. Jain *et al*. identified AEC1s via *Hopx* and *Pdpn* expression in adult mouse alveoli and used a 3D culture model of FACS sorted, single cells to show that AEC1 can form alveolar organoids [51].

Maintaining the alveoli

Trophic intercellular communication is important in maintaining function and homeostasis of the alveoli. In the lung, mesenchymal cells sit beneath AEC2s, with fenestrations in the basement membrane facilitating communication between the two [52]. Treatment of mono-cultured, rat AEC2 with concentrated fibroblast conditioned medium (CM) i*n vitro* promotes DNA synthesis and proliferation, facilitated by the mitogenic proteins HGF and keratinocyte growth factor (KGF) [53]. KGF also maintains the AEC2 phenotype by increasing activation of c-Jun and abrogating expression of the AEC1 marker, aquaporin-5 (*Aqp5*) [54]. Similarly, isolated AEC2s, cultured in 3D mono-culture, fail to proliferate, yet, when co-cultured with *Pdgfra* expressing mesenchymal cells, AEC2s are able to form differentiated, sphere-like colonies termed alveolospheres [49].

Likewise, epithelial-mesenchymal signalling is important for maintaining AEC1 function. In AEC1 and *Pdgfra*-expressing fibroblast co-culture, pharmacological inhibition of TGFβ signalling augments the ability of AEC1s to generate AEC1 and AEC2 organoids [51].

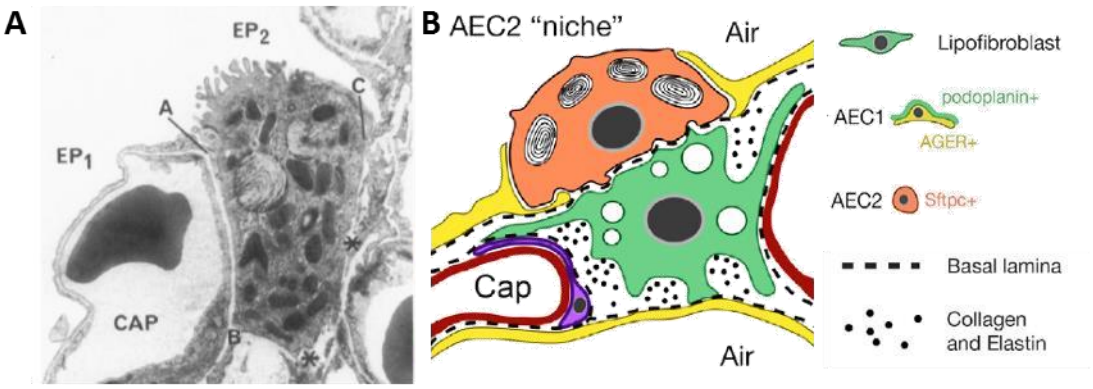

Figure 1.1.8. Structure and cell types of the AEC2 niche. (A) Electron microscopy image of alveoli in mouse lung. The capillary (CAP) is lined by an AEC1 (EP_1) that makes contact with the air. The AEC2 (EP_2) contains surfactant-filled granules and has an irregular basal surface (A – C). The AEC2 makes contact with fibroblasts via fenestrations in the basal lamina (*). (Reproduced from ref. [49] with the permission of Elsevier) **(B)** Graphical representation of this AEC2 niche. (Reproduced from ref. [23] with the permission of Elsevier)

Signalling in the alveoli is bi-directional. Not only do fibroblasts maintain epithelial cells but epithelial cells can determine fibroblast activity. AEC2s produce prostaglandin E_2 (PGE_2), which limits fibroblast proliferation and maintains quiescence in the uninjured lung. This acts as an important brake on fibroproliferation and conserves lung architecture [55]. The next section will describe how the lung responds when homeostasis is perturbed through injury.

1.1.3. Responding to Injury

The air we breathe contains a vast array of pathogens, pollutants and particulates, all of which can cause injury to the airways, disrupting established homeostatic niches. Due to the environmental abundance of such injurious stimuli, damage to the lung is common, and often accentuated by the consistent expansion and contraction of the airways with breathing. In order to appropriately respond to injury, epithelialmesenchymal crosstalk again plays an important role, facilitating both structural and functional repair. Epithelial and mesenchymal cells also communicate with the vasculature and the immune system, enabling angiogenesis and helping to limit infection, which forms another important aspect of secretory communication.

Though injury is common, the type and the severity can be extremely different depending on the offending stimuli and where it acts. For example, chemical injury with naphthalene in mouse leads to specific loss of bronchiolar, *Scgb1a1*$^+$ club cells, whereas bleomycin instillation exerts cytotoxic effects on AEC1s [55,56]. Conversely, mechanical injury can cause loss of both of these cell types whilst also resulting in destruction of the basement membrane, this activates an extensive reparative response.

1.1.3.1. Haemostasis and inflammation

Loss of epithelial and basement membrane integrity elicits a dynamic repair response in the lung. When the basement membrane is breached extravasation of the blood occurs initiating the process of haemostasis. Platelets become activated and undergo degranulation leading to the formation of a fibrillar clot. This functions not only to limit

the loss of blood but also acts as a major signalling event, alerting the immune response to possible pathogenic intrusion. The first immune cells to emigrate to the wound-site are neutrophils, a cell whose primary function is bacterial clearance. This process is mediated via reactive oxygen species (ROS)-dependent killing and mechanisms such as NETosis [57]. Neutrophils are found in the circulation and therefore initially enter the wound site passively, leaking out from damaged blood vessels. With platelet signalling they become actively recruited and infiltrate via diapedesis. Paradoxically, the recruitment and activity of these cells can act to exacerbate the damage in the airways [58]. Neutrophils are followed by resident macrophages, which phagocytose pathogens and other cellular debris whilst also having a huge impact on co-ordinating the repair process. Interestingly, intravital imaging of skin wounds has shown that macrophages may transiently enter the wound sites before neutrophils, departing and returning in two distinct waves [59]. Macrophages are drawn from the circulation, as monocytes, and also attracted from their resident niche in the airways. The macrophage phenotype can be diverse and the extremities of these phenotypes have been well characterised. When macrophages first arrive, they exhibit a pro-inflammatory phenotype. They up-regulate cytokines such as interleukin-6 (IL-6) and further contribute to the generation of an inflammatory environment containing high levels of CXC chemokine ligand-8 (CXCL8) [60]. This is coupled with a phenotype primed for bacterial clearance [61]. Depletion of macrophages populations at certain phases of repair has demonstrated that these early, inflammatory macrophages play a substantial role initiating repair [62,63]. They promote vascularisation by releasing vascular endothelial growth factor (VEGF) and also activate fibroblasts. This all leads to the formation of granulation tissue, a hallmark of the early phases of repair.

1.1.3.2. Activation of fibroblasts

Within the inflamed wound, the recruitment and activation of fibroblasts is an important process. The general understanding of their role is to repopulate damaged tissue and deposit a scaffold of ECM. This process allows mechanical and structural restitution of the damaged airway whilst also providing a platform for re-epithelialisation and regeneration. The migration of fibroblasts into the wound area is induced by numerous

stimuli from macrophages, epithelial cells and platelets. For example, in the skin, PDGFAA signalling is a key chemoattractant, inducing fibroblast migration towards the wound site [64]. Lineage tracing in skin has revealed that this migration is complex, occurring in two different waves from two differing subsets of dermal fibroblasts. These differing waves play alternative roles in repair and are responsive to different signalling pathways. In the first wave, fibroblasts from the lower dermis are stimulated via TGFβ1, which causes differentiation and matrix deposition, allowing structural restitution and subsequent re-epithelialisation. The second wave originates from the upper dermis and is mediated by SHH signalling. These cells facilitate regeneration of epithelial function [65].

In the lung, the origin of infiltrating fibroblasts is difficult to determine and it is not known if such differential recruitment occurs. In uninjured epithelium, SHH normally acts as a control on fibroblast proliferation, maintaining their quiescence. With injury it is understood that a loss of this signalling through epithelial destruction then enables mesenchymal proliferation to facilitate repair [46]. Regardless of the signalling mechanism, the recruitment of fibroblasts leads to their activation, part of which involves differentiation into a myofibroblast phenotype. In wound granulation tissue this can be observed by the transient expression of α-smooth muscle actin (αSMA), which endows the cells with contractile properties, enabling mechanical repair [66]. TGFβ1 is a key signalling mediator in eliciting this activation, functioning via phosphorylation of SMAD proteins 2 and 3 [67]. When this signal is sustained however scar formation occurs through the overproduction of matrix. Application of exogenous TGF-β1 to wounded, *Smad3*$^{-}$ mouse, or treatment with TGF-β1 neutralising antibodies, reduces this scar formation [68,69].

Regulated ECM secretion is, however, a crucial part of the fibroblast response. The production of provisional matrix is important for re-epithelialisation and also regulating fibroblast behaviour. Monomeric collagen that is secreted during early phases of repair further promotes fibroblast proliferation. In the latter stages of repair this collagen becomes polymerised via cross-linking, which then acts as a break on fibroblast growth

[70]. The instructive cues for this behaviour arise, in part, from the macrophages present in the granulation tissue, which themselves respond to wound-site signalling, particularly type2 immune signalling. This causes them to promote upregulation of the collagen cross-linking enzyme, lysyl hydroxylase-2 (LOXL2) in fibroblasts, reducing their proliferation and also enhancing scaffold formation [71]. As well as depositing matrix, fibroblast activation involves the up-regulation of secretory signalling factors that augment the initial inflammatory response and enhance the activity of neighbouring cell populations. For example, during viral influenza infection, crosstalk results in HGF and tumour necrosis factor-α (TNF-α) secretion that reciprocates on the epithelium, stimulating CXCL8 and granulocyte-macrophage colony-stimulating factor (GM-CSF) production, further attracting neutrophils [72]. Signalling via interleukin 1-β (IL1β) also induces further production of VEGF, PDGF and bFGF in fibroblasts as well as upregulation of KGF [73,74].

1.1.3.3. Re-epithelialisation

Such factors effect both the vasculature and the epithelium, which, when damaged and denuded, is required to undergo re-epithelialisation in order to facilitate the next phase of repair. The mitotic activity of the repairing epithelium only peaks after the completion of re-epithelialisation and the process is facilitated primarily by migration [75]. With a denuding of the tracheal epithelium rapid migration occurs giving rise to a continuous yet 'leaky' and poorly differentiated layer [76]. This initial migration is carried out by several rows of epithelial cells closest to the wound edge [75]. Whereas mesenchymal cells individually extend lamellipodia and filopodia to migrate, this only occurs in a few epithelial cells at the leading edge, and the entire epithelial sheet moves as one. The leading cells are connected along the wound edge by continuous actin stress fibres, which run parallel to the wound, creating mechanical tension **(*Figure* 1.1.9A.)** [77,78].

Further back from the wound edge the cells also play a substantial role in migration. Movement at the front is facilitated by down regulation of tight and adherens junctions

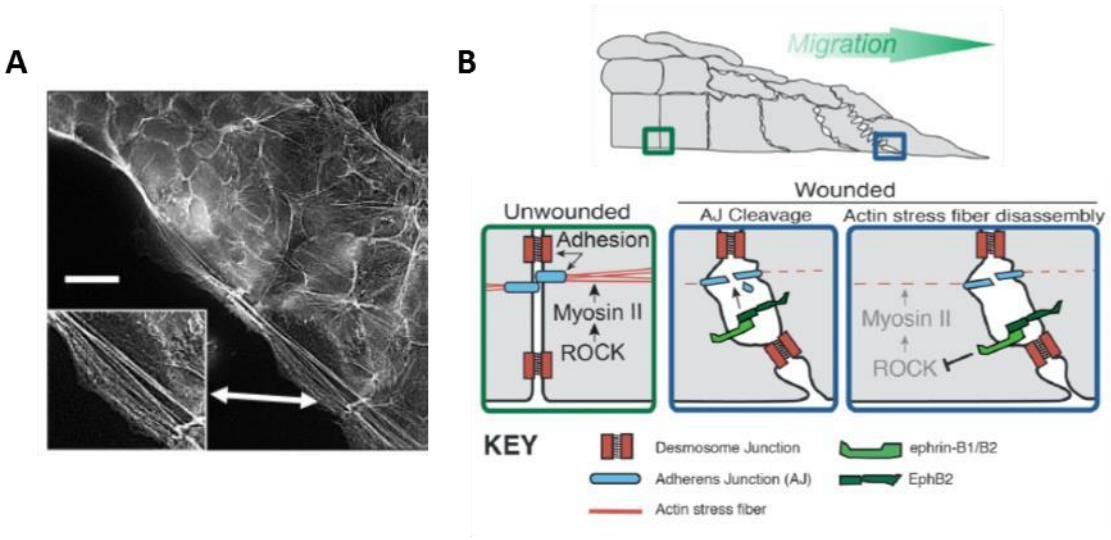

Figure 1.1.9. Mechanisms of re-epithelialisation in response to injury. (A) Immuno-staining of actin with rhodamine-phalloidin in migrating HBEC monolayers. Actin bundles form parallel to the leading edge, creating a continuous stress fibre. Scale bar = 20 µm. (Reproduced from ref. [77] with the permission of The American Physiological Society). **(B)** Graphical representation of the method by which epidermal cells spread to cover the wound void. Normal, unwounded epidermis forms tight junctions, with actomyosin stress fibres creating tension across the epithelium. Upon injury, migration is facilitated by the relaxation of this tension, a result of ephrin upregulation, which reduces actomyosin contraction. (Reproduced from ref [79], available under the Creative Commons Attribution License)

at the back. This allows the epithelial sheet to stretch and cover the wound. This is enabled via an upregulation of ephrin-B1 **(*Figure* 1.1.9B.)** [79]. Likewise, these cells also re-arrange their cytoskeleton to lie perpendicular to the wound edge, enabling a release in tension at the rear, facilitating leading edge migration [80]. Damage in the epithelium stimulates various signalling mechanisms that help create an environment amenable to repair. One of these is endongenous hydrogen peroxide (H_2O_2), which, in keratocytes, promotes migration, cytoprotection and resistance to apoptosis [81]. The activation of fibroblasts also assists in the re-epithelialisation process. HGF secretions enhance epithelial wound closure in both human bronchial epithelial cells (HBECs) and AEC2s [82,83].

1.1.3.4. Epithelial regeneration

With successful re-epithelialisation, epithelial regeneration is next required to restore function to the airway. In the trachea BCs take up the mantle of regeneration [34]. BCs implanted onto xenografts in denuded mouse trachea demonstrate that, once migration has created a continuous (yet leaky) basal cell epithelium, proliferation occurs. The BCs become multi-layered and form tight junctions [84]. This proliferation is mediated by diverse transcriptional changes in the epithelium, with upregulation of G2 and M phase genes [85], as well as signalling from the mesenchyme. BMP4 produced by fibroblasts normally maintains epithelial quiescence during homeostasis but, in response to injury the BMP4 antagonist Follistatin is upregulated, enabling proliferation [41]. Proliferation occurs in cells that are poorly differentiated. The process of restoring a fully differentiated airway occurs first with the extrusion and apoptosis of a number of these cells **(*Figure* 1.1.10.)** [41]. This precedes differentiation to the secretory and ciliated populations of the conducting airway, a process mediated by several signalling moieties. One such example is ROS. After injury BCs experience a flux change in ROS that activates Nrf2, altering *Notch* expression and shifting BCs to a reparative phenotype [86]. Intracellular Notch activation leads to BC lineage segregation, with two mutually exclusive sub-populations arising. One population displays Notch2 activation and commitment to a secretory lineage; the other, inhibition of Notch and upregulation of FOXJ1, committing cells to a ciliated lineage [87]. IL-6, produced by mesenchymal cells at

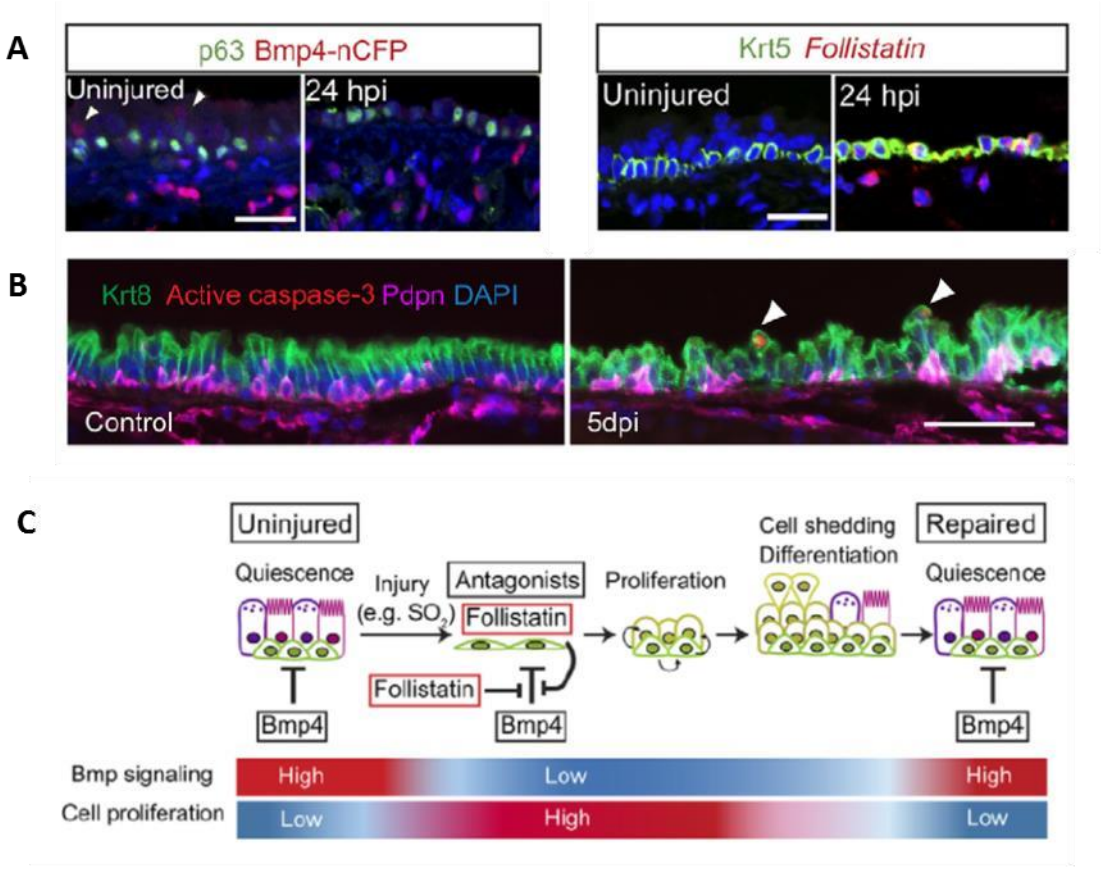

Figure 1.1.10. BMP4 signalling and epithelial dynamics in homeostasis and wound repair. (A) (left) In mouse trachea, *Trp63*$^{+}$ BCs (green) sit on top of *Bmp4*$^{+}$ mesenchyme (red), maintaining quiescence in uninjured lung. 24 hrs post-injury, BMP4 signal is diminished allowing proliferation. (right) This proliferation is enabled by upregulation of *Fst* (red) that is expressed in both mesenchyme and epithelium (green). Scale bar = 20 µm **(B)** 5 days post tracheal injury, arrowheads highlight *Casp3*$^{+}$ epithelial cells being excluded into the lumen and undergoing apoptosis. **(C)** Graphical representation of BMP4/Follistatin interactions in maintaining homeostasis and facilitating repair, with the role of cell shedding in allowing epithelial regeneration, preceding differentiation. (Reproduced from ref. [41], available under the Creative Commons CC-BY License)

the site of injury, facilitate this commitment. IL-6 signals via the signal transducer and activator of transcription-3 (STAT-3), which ultimately inhibits Notch pathway activation [88]. The balance between these pathways is clearly important for regenerating the full complement of airway epithelial cell types and BC lineage segregation is also tempered by the need for stem-cell self-renewal, which is achieved primarily by concurrent, asymmetric division [35].

In the alveoli, AEC2s are required for regeneration [49]. Loss of AEC1s causes them to proliferate and migrate, recovering the denuded basement membrane. The cessation of

this growth and the induction of differentiation to an AEC1 phenotype is dependent on the fibroblasts. The promotion of fibroblast expansion via epithelial cell death allows ECM deposition. When AEC2 respond to injury and migrate they eventually come into contact with this new matrix which promotes their differentiation [47]. Factors such as HGF and KGF are also important in this process although their roles are complex. For example, HGF stimulates repair at low concentrations *in vitro* but inhibits it when high [53,89].

1.1.3.5. Angiogenesis

With restoration of both epithelial integrity and function, a greater part of the repair response is complete. Throughout the process, it should be noted that angiogenesis also plays an important role, especially in the formation of granulation tissue, and it is key in resourcing the wound site with metabolites and immune cells. Endothelial cells also play a role in crosstalk between the differing cells of the wound site with regulation, in part, mediated by interactions with ECM deposited by active fibroblasts [90]. Angiogenesis is also key in the final stages of regeneration, restoring complete function and returning the tissue to normal.

Summary

A multitude of cytokines, chemokines and growth factors are required for repair, arising from numerous interactions between differing cell types. Such pathways are extremely relevant to embryonic growth and the maintenance of homeostasis, with epithelialmesenchymal crosstalk constituting a key relationship in these processes. When these mechanisms become defective though, and the relationship between epithelial and mesenchymal cells breaks down, there can be serious, detrimental effects on all these aspects of lung physiology. One potential consequence is the development of chronic respiratory disorders. The next section of this introduction will particularly focus on one such disorder: pulmonary fibrosis.

1.2 Pulmonary Fibrosis

1.2.1 Clinical Presentation and Epidemiological Significance

There are many forms of fibrotic lung disease **(*Figure* 1.2.1.)** [91]. Broadly, they are termed diffuse parenchymal lung diseases (DPLDs) and, what they share in common, is a remodelling of the pulmonary interstitium, in a process that leads to loss of respiratory function. Affected patients present with shortness of breath, arising often in an insidious manner, which continually worsens over time. Cough is common, and patients typically display reduced lung volume and impaired gas transfer, as well as a restrictive defect on spirometry. The presentation of these symptoms and early testing mean that a whole range of diseases could be at play. Occupational exposures can indicate asbestosis or silicosis. Concurrent signs of other diseases, such as rheumatoid arthritis, can indicate fibrosis due to systemic connective tissue disease. Or, other DPLDs may be involved, including granulomatous DPLD or drug-induced DPLDs. When patients have no known occupational or environmental exposures and they present with fine end-inspiratory crackles and signs of digital clubbing, the most likely form of DPLD present is one of the idiopathic interstitial pneumonias (IIPs).

1.2.1.1. Idiopathic interstitial pneumonias

So called because of their unknown aetiology, IIPs are the most common form of DPLD. They can be further divided into idiopathic pulmonary fibrosis (IPF) and non-IPF IIP. Of the latter group, there are also several subtypes. Distinguishing between IIPs and concluding the right diagnosis is exceptionally important. High-resolution computed tomography (HRCT) is key to achieving this and it can provide robust information without being invasive. In cases where more information is required, biopsy and histology can be performed, providing a gold-standard for diagnosis, which can be backed-up with bronchoscopy and analysis of broncho-alveolar lavage (BAL). Getting the diagnosis right is critical because, although sharing similarities in symptomology, prognosis and therapeutic options can differ widely. For example, with the non-IPF IIP, cryptogenic organising pneumonia, fibrosis can be completely resolved within 6-12

months using corticosteroid treatment. For IPF however, the prognosis is a continual decline in respiratory function leading to death within 3-5 years, an outcome that, as of yet, cannot be prevented with treatment, only delayed.

1.2.1.2. Idiopathic pulmonary fibrosis

The clinical diagnosis of IPF requires HRCT and, in around 50% of cases in the US, surgical biopsy, as well as exclusion of environmental causes [92]. Patients, typically presenting in their 60s and most commonly male, display a pattern of usual interstitial pneumonia (UIP). This patterning, whilst often heterogeneous, is typically found in the basal and peripheral regions of the lung. UIP is characterised by the presence of reticular opacities, a complex network of diffuse opacities where the ratio of gas to soft tissue has declined. Medium sized opacities, termed honeycombing, is common and a requirement for diagnosis. These honeycomb opacities are typically subpleural with well-defined walls. Smaller opacities, termed ground-glass opacities can also be observed, though they are not a requisite for diagnosis. Other key and prominent features are signs of traction bronchiectasis, a phenomenon in which contraction of fibrotic tissue around the small airways causes dilatation, and also a thickening of the interlobular septa **(*Figure* 1.2.2.)** [92].

If surgical biopsy is required, a UIP pattern can also be confirmed histologically **(*Figure* 1.2.3.)** [93]. In areas of honeycombing, there is a variable pattern of both fibrosis and seemingly non-affected lung. Where there is fibrosis, regions of the lung interstitium are distorted and thickened with an ablation of normal lung architecture. There are dense patches of fibroblast and myofibroblast expansion, coupled to thick depositions of ECM. When large in size and of a nodular appearance these patches are referred to as fibrotic foci. They are typically covered by a bronchiolar, cuboidal epithelium that is covered in mucus and inflammatory cells. More generally, infiltration of inflammatory lymphocytes is also observable but less consistently. AEC2 hyperplasia can also be seen [94]. Together these alterations dramatically inhibit lung function and impair gas exchange.

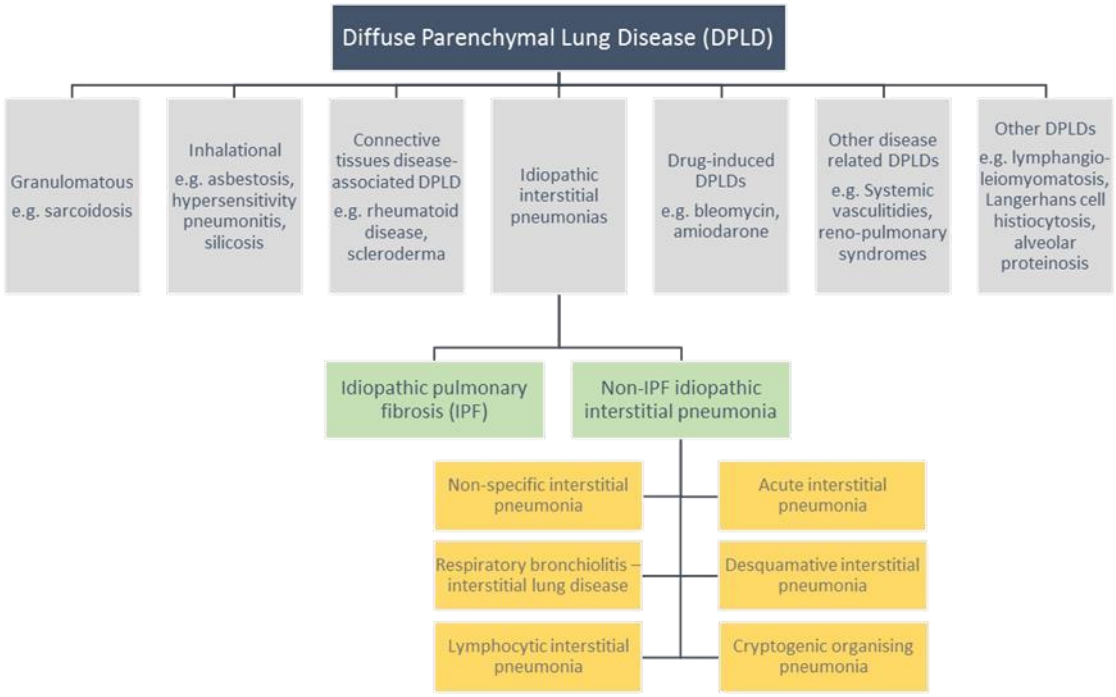

Figure 1.2.1. The general classification of the diffuse parenchymal lung disease. A graphical representation of the hierarchy of the DPLDs. IPF is just one of many DPLDs, categorised as an idiopathic interstitial pneumonia. Within this category it also represents one many other disease. (Adapted from ref. [91] with the permission of Elsevier)

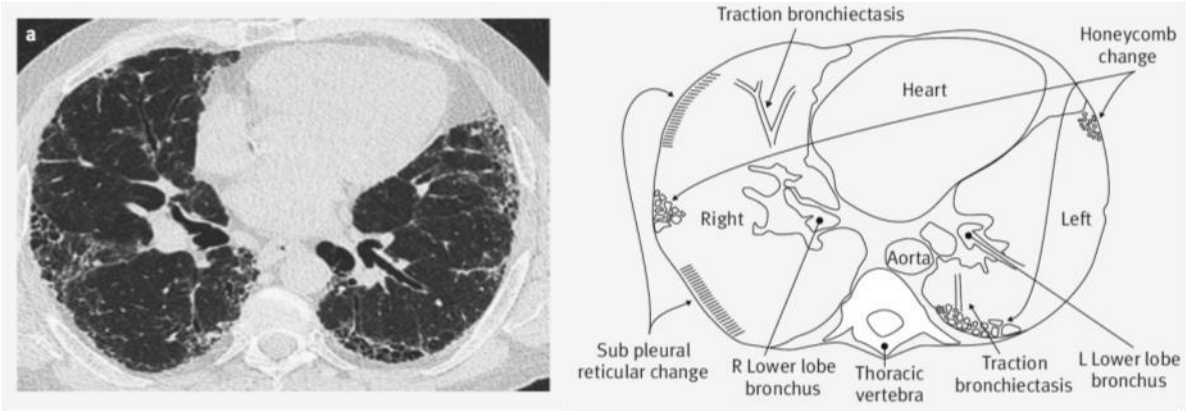

Figure 1.2.2. The pattern of UIP found under HRCT scan. An example of an IPF HRCT image from a 65 year old man, with additional diagrammatic representation. The scan shows bilateral, subpleural honeycomb change, traction bronchiectasis but minimal ground glass opacity. (Reproduced from ref. [91] with the permission of Elsevier)

1.2.1.3. Epidemiology

This destruction of normal lung architecture and subsequent loss of function presents a serious problem for patients and clinical practice. The disease has a poor prognosis and patients suffer a reduced quality of life. In the UK, IPF affects roughly 32,500 people. Around 6,000 new cases are diagnosed each year and, overall, 5,300 people die from the disease per year [95]. For patients, the outcome of the disease is made worse by the unpredictability of clinical progression. Markers for progression are starting to be validated and used but, from the point of diagnosis, a patient typically won't know if they'll experience a relatively slow decline in lung function, over 6-10 years, or a rapid decline, within periods of less than a year. Decline may also be intermittent, with patients experiencing relative periods of stability punctuated by short periods of acute exacerbation **(*Figure* 1.2.4A.)** [96]. The certainty of impending respiratory failure coupled with the uncertainty of progression are serious factors determining patient well-being and make disease management highly challenging.

From a clinical perspective, the problem of IPF is furthered by both the rising incidence of the disease and the increasing mortality arising from it **(*Figure* 1.2.4B.)** [97,98]. There are currently over 9,000 hospital admissions a year due to IPF accounting for up to 86,000 bed days. Respectively, this represents 1.3% of all admissions and 1.4% of all bed days due to lung disease. These figures are disproportional to the percentage of lung diseases that IPF actually accounts for, which is under 0.25% [95]. Also, 80% of those diagnosed with IPF are over the age of 75, making it a disease of old age. With an ever-ageing population and projections of the number of over 60 year-olds to reach 1.4 billion by 2050 this could create an even greater issue for healthcare [99].

1.2.2. Therapeutic Options

The epidemiological statistics attached to IPF ultimately highlight the reality of a disease for which there is no cure. In the past few years, there have been significant advances in treatment options, with two clinically licensed drugs now available, but neither drug, Nintedanib nor Pirfenidone, reverse pathology of disease. Likewise, their efficacy as

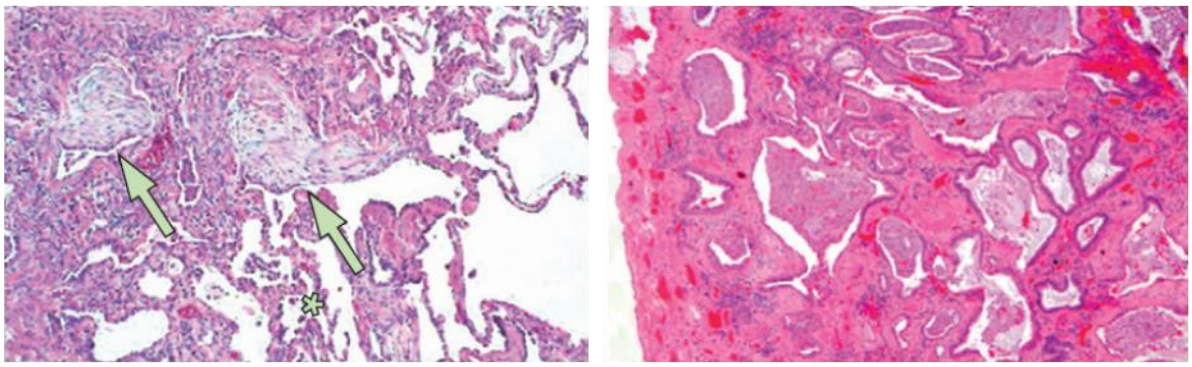

Figure 1.2.3. Histological identification of UIP. Haematoxylin and eosin staining of IPF tissue sections, derived from surgical biopsy. (left) The UIP pattern is heterogenous. The thickened regions of lung represent architectural destruction but there are also regions of relatively normal lung (*). The arrows point towards regions of fibroblastic foci, areas of fibroblast accumulation and matrix deposition. (right) Staining of a region of honeycomb cyst formation. Cystic fibrotic airspaces in the distal lung are lined with bronchiolar epithelium and filled with mucus. (Adapted from ref. [93] with the permission of Elsevier)

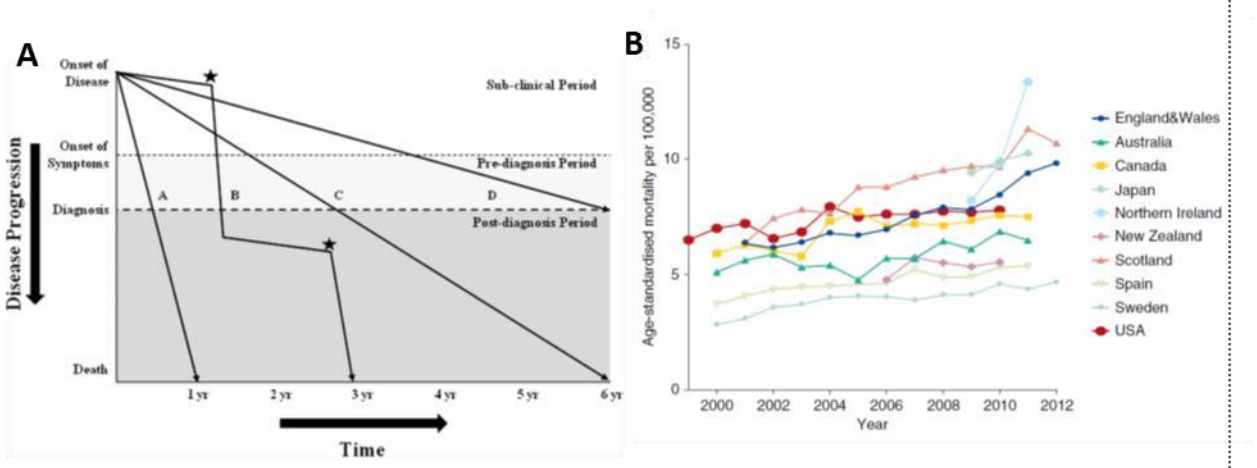

Figure 1.2.4. Epidemiological issues associated with IPF. (A) Disease progression among patients can be highly variable, with either rapid progression, exacerbation driven decline, or medium to long-term steady state decline. (Reproduced from ref. [96] with permission of The American Thoracic Society) **(B)** Age-associated mortality (per 100,000) is rising across the globe. From the 2000-2012 mortality increased in 10 countries. (Adapted from ref. [97] with permission of The American Thoracic Society)

determined by clinical trial endpoint, remains somewhat contentious, with arguments both for and against the utility of measures such as forced vital capacity (FVC) [100,101].

1.2.2.1. Nintedanib

Nintedanib is a tyrosine kinase inhibitor that targets multiple pathways, including VEGF, FGF and PDGF signalling, interfering with the processes of fibroblast proliferation,

migration, differentiation and ECM production *in vitro* [102]. The rationale for its application in clinic is therefore strong and it is a recommended therapy in accordance with the ATS/ERS/JRS/ALAT guidelines for IPF treatment [103]. In patients, Nintedanib's validity has been established through three randomised control trials (RCT). The first was a phase 2 safety and efficacy trial, which found that a 150mg, twice-daily treatment, reduced the percentage of patients experiencing >10% decline in FVC, although mortality rates did not change [104]. This RCT was followed up with two, phase 3, INPULSIS trials, using the same regimen across a total enrolment of 1,066 patients. The results (analysed collectively) found no significant benefit on mortality or acute exacerbation. There were however significantly less patients with a 10% decline in FVC. The report of non-serious adverse events was increased with treatment, as was report of diarrhoea and nausea [105].

1.2.2.2. Pirfenidone

Pirfenidone, like Nintedanib, has pleiotropic effects. *In vitro*, using a murine, macrophage-like cell line, it has inhibitory effects on inflammatory cytokine production, reducing TNFα production via a translational mechanism [106]. In BLM-induced mouse fibrosis, the drug attenuates collagen deposition and supresses levels of IL-1β, IL-6 and CC chemokine ligand-2 (CCL2), though an explicit mechanism of action remains poorly defined [107]. The CAPACITY and ASCEND RCTs have provided the best evidence for use of Pirfenidone [108,109]. Part of the CAPACITY trial found a reduction in FVC decline over a 72week treatment period versus placebo but there were, however, increased rates of vomiting, nausea, dyspepsia, anorexia, photosensitivity and rash. The ASCEND trial used the same high-dose regimen in a study of 555 patients. Like Nintedanib, Pirfenidone showed a significant reduction in the number of patients exhibiting more than a 10% decline in FVC, yet, like Nintedanib again, mortality was not impacted.

1.2.2.3. Other therapeutic candidates

Both Nintedanib and Pirfenidone, despite side-effects and seemingly no effect on mortality, represent major success stories in the field of IPF therapy. Many other promising treatment options have ended in disappointment at clinical trial. Most

recently, Simtuzumab, an antibody targeted against the collagen cross-linking enzyme LOXL2, disappointed at phase 2 trial [110]. The drug failed to reduce mortality or decline in FVC despite a strong rationale for success, generated *in vitro* and in mouse. Prior investigation had revealed an upregulation of collagen cross-linking at sites of fibrosis with inhibition of LOXL2 reducing scar formation and aberrant signalling by factors such as VEGF [111]. The reasons for trial failure were hypothesised to be either redundancy in fibroblast cross-linking capacity or failure of the drug to reach its target in the lungs. Candidate therapies such as Warfarin, Imatinib and N-acetylcysteine (as either monotherapy or in conjunction with Pirfenidone) have also failed to show a meaningful impact on disease progression [112–115]. However, by stratifying IPF patients into cohorts according to levels of circulating antibodies for type V collagen, Wilkes *et al.* have demonstrated efficacy of an immunotherapeutic (IW001) modulating the body's response to this auto-antigen. This therapy was used in a phase 1 trial over 24 weeks and, in the high-dose cohort, there was a trend towards stabilisation of FVC [116]. The preliminary success of this trial reflects the necessity for patient stratification. It also suggests that the classification of IPF may be too broad, representing a number of clinically distinct disease entities.

1.2.3. Biological Alterations in IPF

The changes in lung architecture seen clinically represent a plethora of biological alterations occurring at a cellular level within the lung, whilst the limited efficacy of treatment options reflects the unknown cause of the disease. Understanding the biological alterations that occur is typically approached using two models: the isolation of primary cells from IPF patients and their investigation *in vitro*, and the *in vivo* model of lung fibrosis, the bleomycin (BLM) mouse model. BLM is a chemotherapeutic agent often used in the treatment of testicular cancer. Treatment in mice, typically via intratracheal administration, leads to an inflammatory response followed by chronic tissue re-modelling that recapitulates many of the aspects of IPF. Both approaches have been key in identifying pertinent biological alterations in the IPF lung. One of the key effector cell types identified in this disease is the lung fibroblasts.

1.2.3.1. Lung fibroblasts in IPF

The macro and microscopic loss of pulmonary architecture in IPF is the result of interstitial, mesenchymal cell expansion and matrix deposition. Fibroblasts form a heterogenous population of varying cell subtypes that act in conjunction to destroy the normal lung. Within this population numerous pathological characteristics have been observed and these cells are understood to be the key effector cell of disease pathology.

Activation

Firstly, in IPF, fibroblasts appear to be aberrantly activated. In normal wound healing fibroblasts are activated in response to a loss of tissue homeostasis. Part of this reparative activation involves differentiation to a contractile, αSMA myofibroblast phenotype [117]. TGF-β1 is a key molecule in mediating the activation and, as well as being elevated in the IPF lung, it can robustly induce myofibroblast differentiation *in vitro* [67]. TGF-β1 induces production of H_2O_2 via members of the NADPH oxidase (NOX) family of enzymes in human lung fibroblasts (HLFs) [118] and one of these enzymes, NOX4, is critical in the fibroblast response to injury [119]. Coincidently, NOX4 is highly expressed in the fibrotic foci of IPF patients and, if *NOX4* is knocked down by siRNA, isolated IPF HLFs (FHLFs) are less able to differentiate and secrete collagen when treated with TGF-β1. When knockdown is elicited in concurrence with BLM instillation in the mouse, fibrosis is prevented [119]. Taken together, this indicates that a key alteration in FHLFs is an aberrant activation in response to injury-associated stimuli.

Proliferation

As well as being activated, FHLFs become excessively proliferative. Collagen that is crosslinked by active fibroblasts acts as a negative regulator of sustained proliferation [70]. The PI3K-AKT-S6K1 pathway facilitates this regulation and is responsive to PTEN activity.

PTEN activity is deficient in IPF derived cells cultured on polymerised collagen [120]. Similarly, AKT can further promote proliferation via phosphorylation and inactivation of forkhead box O3a (FOXO3A). Both FHLFs and IPF human tissue sections show the

presence yet the inactivity of FOXO3A [121]. These cells are therefore unable to respond to environmental cues and internally co-ordinate growth, subsequently leading to inappropriate proliferation.

Resistance to apoptosis

The continued accumulation of fibroblasts in IPF is thought to be related to their inability to respond to apoptotic signalling. Isolated FHLFs have an altered response to Fas signalling as well as an inability to respond to starvation signals [122,123]. When starved, FHLF display persistent activation of the mammalian target of Rapamycin (mTOR), a key kinase in nutrient sensing pathways and inducer of autophagy, the process of cellular self-eating. In prolonged response to nutrient depravation, normal HLFs (NHLFs) from aged patients transition through autophagy to apoptosis via the ultimate deactivation of mTOR. Conversely, FHLF elude this regulation and resist apoptosis [123].

Invasiveness

FHLFs also exhibit invasive properties that further contribute to the destruction of lung architecture. Hyaluronan (HA) is a non-sulphated glycosaminoglycan synthesised by mesenchymal cells via HA synthase enzymes (HAS). In the mouse model of lung fibrosis HA interacts with the mesenchymal marker CD44 and accumulates. Overexpression of *Has2* in *Acta2*$^{+}$ fibroblasts results in increased collagen deposition and worsened BLMinduced mouse fibrosis. This is, in part, attributed to an increased invasiveness; demonstrated by the isolation of *HAS2* overexpressing cells that display an increase in spontaneous invasion into Matrigel [124]. As well as HA-CD44 interactions, α_6-integrin B, a mechanosensing integrin subunit, promotes pericellular proteolysis of basement membrane collagen and subsequent myofibroblast invasiveness. The expression of this subunit is also higher in both FHLFs *in vivo* and when isolated *in vitro* **(*Figure* 1.2.5.)** [125]. Such invasive properties are attributed to a 'transcriptome-wide invasion signature'. This signature, identified through 3D invasion assays using murine lung fibroblasts, has highlighted the mechanisms of invasion, including PTEN downregulation and matrix metalloproteinase (MMP) upregulation, whilst also predicting and validating the upstream regulators of such action, elucidated as TGF-β1, FGF2, EFG and PDGF-BB [126].

The result of this phenotype is a loss of respiratory airway architecture, with fibroblasts disrupting the basement membrane and impairing epithelial function.

1.2.3.2. Lung epithelium in IPF

The IPF fibroblast gains pathological characteristics during the course of the disease and these characteristics come at the expense of the overlying epithelium, which also undergoes substantial biological alterations leading to a loss of normal function.

Alveolar cells

In IPF, necrosis and cell death occur in distal AEC1s [55,127]. Loss of these cells is observed alongside hyperplasia of both AEC2 and BCs. AEC2 normally constitute a small number of alveolar epithelial cells, acting as a quiescent progenitor population. Throughout the IPF lung, regions of AEC2 hyperplasia have been identified in which *SFTPC*$^{+}$ cells have proliferated to form a simple, cuboidal epithelium around regions of fibrosis [128]. In response to injury AEC2 differentiate to restore AEC1 loss, in IPF however they retain surfactant protein expression and fail to differentiate to AEC1s, furthering the loss of respiratory lung function. The phenotype of these AEC2 in patients also includes the accumulation of dysmorphic and dysfunctional mitochondria. This is understood to be the result of impaired mitophagy and elevated stress in the endoplasmic reticulum (ER). PTEN-induced putative kinase-1 (PINK1) is a regulator of mitochondrial function and, in IPF, its expression is low. Knockout of *Pink1* in mouse recapitulates a similar mitochondrial morphology with affected cells upregulating *Tgfb* and *Il6,* and mice suffering a more severe fibrotic response when challenged with BLM [129].

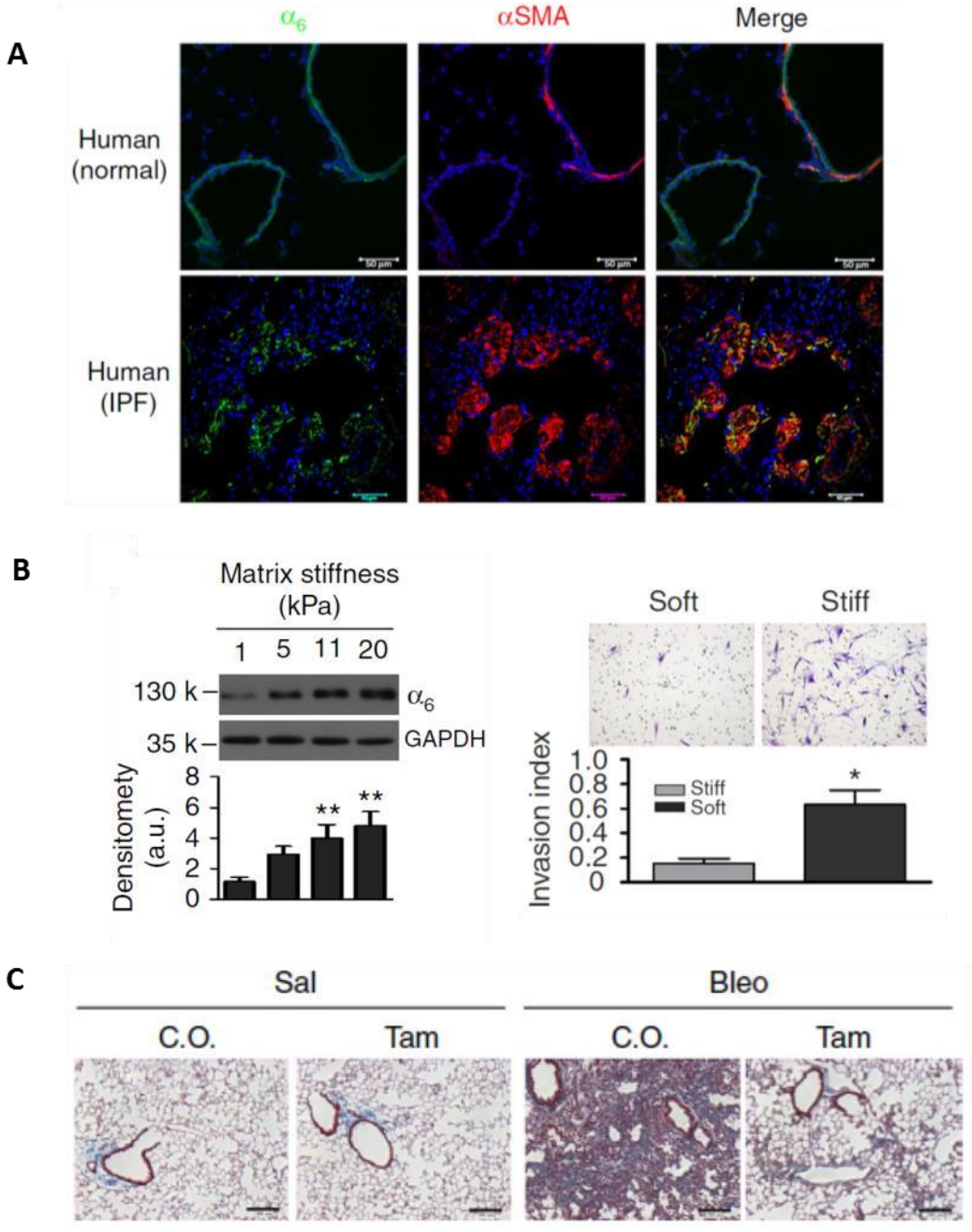

Figure 1.2.5. α_6 –integrin signalling on stiff ECM confers an invasive fibroblast phenotype and contributes to lung fibrosis. (A) Human lung tissue sections stained for α_6-integrin and αSMA. Immunofluorescent signal is greater in IPF samples. **(B)** (left) FHLFs cultured on progressively stiffer matrices display increased protein levels α_6-integrin, assessed via western blot. (right) Matrigel invasion assay indicated that FHLF cultured on stiff matrix are more invasive. **(C)** Representative images of collagen staining in BLM mouse. Conditional knockout of α_6-integrin via tamoxifen in BLM mouse reduces collagen deposition and fibrosis. (Reproduced from ref. [125], available under a Creative Commons CC-BY Licence)

Distal airway cells

A similar story of dysfunction is seen with BCs. Like AEC2s, BCs are a quiescent progenitor. Throughout the proximal, tracheobronchial airways they form a nearcontinuous layer at the base of a pseudostratified epithelium, becoming more dispersed in the distal airways. In the IPF lung however, the distal airways are populated by a continuous layer of densely packed BCs. This has been identified by TRP63 staining in a study that also found BC colonisation of the alveoli [130]. This bronchiolisation was coupled with honeycomb cyst formation in which regions of mucin filled airway become lined with ectopically differentiated mucosal and ciliated cells, typically infiltrated by inflammatory cells **(*Figure* 1.2.6.)** [128,131].

This description of an IPF epithelium in which there is hyperplasia, dysregulated differentiation and loss of proximal-distal patterning has recently been given more clarity via the method of single-cell RNA sequencing. Using distal lung from IPF patients and healthy controls, Xu *et al.* have shown with greater resolution the scale of epithelial change in IPF. Three distinct populations of epithelial cell were identified, all with gene expression patterns in keeping with conducting airway cells. These included *TP63*/*KRT5* expressing BCs as well as *MUC5AC/MUC5B* expressing goblet cells. Interestingly though the third type lacked an expression profile consistent with any classical epithelial cell type. These 'intermediate' cells expressed both the hallmarks of AEC2s, AEC1s and also the proximal airway. These cells also showed increased expression for VIM and, through gene enrichment analysis, showed significant alterations in TGF-β, PI3K/AKT and HIPPO/YAP signalling pathways. Upregulation of VIM confers a more mesenchymal phenotype on these cells, impairing their epithelial function and perturbations to these pathways disrupts epithelial mesenchymal crosstalk, disrupting homeostasis [132].

Other alterations

Though alterations in fibroblast and epithelial biology are critical in IPF many others have also been identified. Proteomic analysis of peripheral blood cells in IPF patients has revealed a profile in which regulation of repair responses are inhibited, there is a downregulation of pathways required for host defence and an increase in kinase

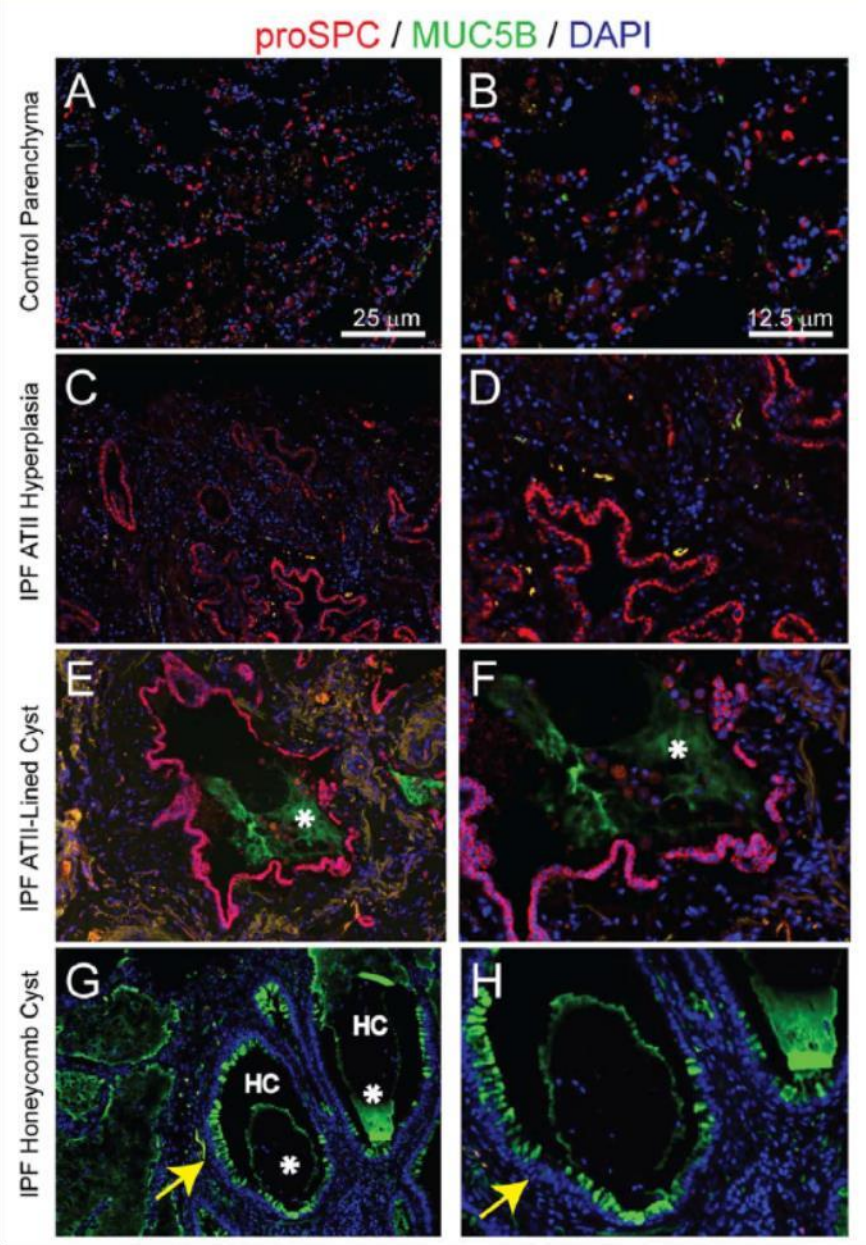

Figure. 1.2.6. Epithelial alterations in the parenchyma of IPF lungs. Merged immunofluorescent images staining for the AEC2 marker proSPC (red) and the mucus cell marker MUC5B (green) **(A-B)** Normal parenchyma shows a diffuse population of AEC2. **(C-D)** AEC2 hyperplasia in IPF. **(E-F)** Further AEC2 hyperplasia in IPF cyst. Cyst are also filled with mucus (*). **(G-H)** IPF honeycomb cyst (HC) lined with pseudostratified epithelium (arrows). Mucus producing cells line the luminal surface, filling the cyst with mucus (*). (Reproduced from ref. [128] available under a Creative Commons CC-BY Licence)

signalling proteins, most significantly VEGF [133]. The lung microbiota also appears altered, with an increased bacterial burden in BAL that can change composition during acute exacerbation [134,135].

1.2.4. Driving Forces in IPF

Though the end-state alterations that occur in IPF are well defined, the driving forces that lead to them and a possible cause of the disease remain to be fully understood. Epidemiological studies have thus far been unable to identify an environmental cause and, although disease progression can be predicted through additional co-morbidities, the initiating event in IPF remains elusive [136,137]. One issue that may contribute to this is the insidious onset of the disease. Patients presenting with symptoms may potentially have been victim to the disease for many years, with observations at clinic only representing the closing stages of pathology.

1.2.4.1. Genetic predisposition

Much research has gone into identifying genetic factors that may initiate and drive the disease. Initial findings were reported primarily in patients with the familial form of IPF (F-IPF), during small scale investigations, yet more recent studies have been able to utilise genome wide sequencing across much wider cohorts of patients with the sporadic form of the disease.

SFTPC

An early study in one family with F-IPF identified a common mutation in *SFTPC*. This mutation resulted in exon skipping and production of an altered SFTPC pro-protein. The result was identified as an inability of *SFTPC*$^{+}$ epithelial cells to transport the pro-protein within the cell, leading to defective processing, secretion and ER stress, as evidenced by a lack of mature protein in patient BAL [138]. A further study, in which SFTPC was sequenced in 89 patients with UIP, found only 10 single nucleotide polymorphisms, of which only one caused a change in amino acid sequence and protein alteration [139]. This study, coupled with another, conducted in 35 IPF patients, found *SFPTC* mutations to be a rare cause of the sporadic disease [140].

MUC5B

MUC5B is a mucin that plays an important role in host defence of the conducting airway. Genome wide sequencing, in a study that included 492 patients with IPF, identified a common variant in the promoter region of *MUC5B* , a finding corroborated in two further, independent cohorts [128,141]. The suggestion from these studies was that enhanced activity in the *MUC5B* promoter creates too much of the protein. This alters the balance of mucins in the airway and impairs host defence by impeding mucus clearance. Seibold *et al*. identified this clearly relevant polymorphism in 38% of their study cohort. A more recent study in 115 Dutch patients also found *MUC5B* mutation to associate with IPF, however, though this mutation predisposes patients to IPF, it does not influence or predict survival [142].

TERT

Telomerase reverse transcriptase (TERT) is an enzyme that maintains telomere length. Telomeres cap the end of chromosomes and are degraded with each replication of the cell, activating a process of cell cycle arrest. Telomere maintenance is important for maintaining proliferative activity and TERT functions alongside TERC, the RNA component of the enzyme. Unlike SFTPC and MUC5B, TERT and TERC function throughout all cell types of the body and are not restricted to the lungs. Investigations into both F-IPF and the sporadic form identified mutations in *TERT* and *TERC* [143,144]. A further study also found mutations but these were rare, detected in only 1 in 100 patients [145].

AKAP13

A recent study by Allen *et al.* has identified a novel genome-wide association between the SNP rs62025270 and susceptibility to IPF. This polymorphism is understood to regulate expression of A-Kinase Anchoring Protein 13 (AKAP13), a scaffold protein that functions as a Rho guanine nucleotide exchange factor, activating RHOA in response to G-protein signalling. The protein is understood to contribute to thrombin mediated activation of TGF-β in the epithelium and is therefore thought to modulate the

epithelium's response to injury. Targeting this pathway may be an attractive approach for future therapeutics [146].

Current thinking suggests that these mutations, found across familial and sporadic cases of IPF, indicate a blurring of the distinction between the two diseases, suggesting that they reflect two ends of a spectrum of genetic predisposition [147]. However, a large proportion of patients do not appear to have significant mutations and, in those that do but who experience late onset of the disease, the mutations are not the sole drivers of the disease. Therefore, it is more likely that defects in genes such as *SFTPC, MUC5B* and *TERT* coalesce with environmental factors to create a lung environment permissive for the development of IPF.

1.2.4.2. Dysfunctional epithelial-mesenchymal crosstalk

As discussed previously, communication between the epithelium and the mesenchyme is crucial for numerous processes, including embryonic development, maintenance of homeostasis and repair. Evidence suggests that, on top of a permissive genetic background, a breakdown in epithelial mesenchymal-crosstalk could play a critical role in driving the pathology of IPF.

Matrix interactions

As well as secretory communication, the relationship between a cell and its' surrounding matrix are also key in regulating behaviour. Dysregulated interactions with the ECM have been consistently observed in FHLFs and have been thought to contribute to their pathological phenotype. As well as promoting proliferation, matrix stiffness can cause differentiation to an *ACTA2* expressing, myofibroblast phenotype and promote migration [148,149]. Transcriptional proteins of the Hippo pathway, YAP and the transcriptional coactivator with PDZ-binding Motif (TAZ), are highly expressed in fibrotic regions of IPF lung. They are key in responding to the ECM environment and regulate cell activation and matrix production, in part through targeting plasminogen activator inhibitor-1 (PAI-1). *In vitro*, knockdown of YAP/TAZ reduces pro-fibrotic fibroblast activity [150]. Likewise, the matrix produced by FHLFs creates a positive feedback loop that

sustains fibrotic activity. FHLFs cultured on non-IPF derived ECM show little translational differences when compared to NHLFs in the same conditions. When cultured on IPFderived ECM however, there is an upregulation of ECM production, which also recapitulates the composition of that found in IPF tissue [151].

Developmental signalling

It has become well established that a potentially critical driver in the pathology of IPF is an aberrant reactivation of the signalling pathways found in development. The growth and patterning of the embryonic lung, as previously eluded to, requires complex interactions between numerous cell types, with many of the signalling molecules continuing to play roles in maintaining adult homeostasis. In IPF it appears that there is an inappropriate activation of these pathways, with developmental and homeostatic factors driving pathological activity. Strong evidence for this has been derived from the gene expression profiles of mesenchymal stromal cells in the terminal airways and alveoli. The profile of these cells has revealed an IPF-specific enrichment for genes required in branching morphogenesis and tissue patterning. Most notably an upregulation of SHH and TGF-β pathways has been identified, coupled with a downregulation of FGF-10 [152]. As well as this, much evidence has been gathered to implicate WNT signalling as playing an aberrant role in IPF.

Hedgehogs

SHH facilitates myofibroblast differentiation and matrix deposition in the developing lung. This is also true for isolated, adult HLFs. SHH can function through GLI transcription factors and, in the BLM-injured mouse, there is an observed induction of SHH and GLI activity [153]. Likewise, in an injury-induced model of interstitial renal fibrosis, SHH is induced causing a fibrotic response in *Gli1*$^{+}$ cells [154]. The activation of these pathways has also been identified in IPF lung tissue, where SHH is expressed in the epithelium with its responsive element, GLI1, in the mesenchyme. As well as differentiation and ECM production, recombinant SHH also promotes fibroblast migration and resistance to apoptosis [155]. Inhibition of GLI transcription factors, via blocking their DNA binding domains, reduces BLM-induced fibrosis decreasing lung collagen content, RNA levels of

myofibroblast markers and creates a less inflammatory environment by reducing expression of factors such as *Vegfa, Pai1* and *Il1b* [156].

WNTs

There are numerous members of the WNT family of signalling proteins and many of them are both elevated and functionally relevant in IPF. In human tissue, the signalling molecules, as well as their receptors and intracellular signal transducers, are increased in IPF, localised primarily to the alveolar and bronchiolar epithelium. *In vitro*, treatment with recombinant WNT ligands induces epithelial proliferation and also myofibroblast activation [157]. A member of the WNT signalling pathway, the WNT1-inducible signalling protein-1 (WISP1) is elevated in patient and mouse AEC2s. Treatment of normal AEC2 with the recombinant protein increases proliferation, as well as markers of epithelialmesenchymal transition (EMT). Subsequent targeting of this protein in the BLM mouse model with neutralising antibodies improves lung function and survival [158]. Similarly, molecular inhibition of β-catenin, the nuclear effector of WNT-targeted gene expression, attenuates fibrosis, when given in concurrence with BLM in the mouse [159]. One of the WNT family members, WNT3A, up-regulates transcription and production of IL-1β and IL-6 in human AEC2s, an outcome that also occurs with WNT3A treatment in mouse. This protein is also elevated in human, fibrotic alveolar epithelium as well as in human BAL [160].

Growth factor signalling

Such developmental signalling pathways form an integrated network and subsequently other growth factors can interact and influence their activity. For example, TGF-β activates WNT signalling via decreasing expression of the antagonist to the canonical signalling pathway, Dickkopf-1 (DKK1). This occurs in a p38 mitogen-activated protein kinase (MAPK)-dependent manner and, in human IPF tissue, a paucity of DKK1 expression is observed in comparison to normal lung. Overexpression of DKK1 ameliorates dermal fibrosis, highlighting the capacity of TGF-β to mediate fibrosis via WNT [161]. Likewise, the upregulation of TGF-β and SHH signalling in IPF patients, stratified according to disease progression, has an effect on other developmental pathways,

including those of FGF-10 and BMP-4, which are downregulated. This is most noticeable in fibrotic foci where there is a downregulation of FGF-10 signalling [152]. Isolated mesenchymal stromal cells also lose their epithelial-supportive capacity, a function related to FGF-10 activity, which can be reinstated with TGF-β inhibition [162]. Deletion of the TGF-β receptor (type 2) in mouse epithelium is protective against BLM induced fibrosis, although emphysema also develops spontaneously in these mice after birth [163].

1.2.4.3. Dysfunctional repair

As well as reactivation of developmental signalling, one of the most enduring paradigms concerning IPF initiation and progression revolves around the hypothesis that recurrent injury in the lung leads to a progressive inability of the epithelium to repair. This epithelial deficiency is coupled with an over-activation of mesenchymal repair responses, compounding the issue and leading to fibrosis [164]. The specific source of injury in IPF remains elusive. The lungs, however, are exposed to a diverse range of potentially damaging stimuli and, after many decades of exposure, a tipping point may be reached in which the airways can no longer adequately respond. The lungs of IPF patients also exhibit all the relevant hallmarks of injury and excessive repair.

Hallmarks of injury and repair

With injury, blood loss is limited by haemostasis, a process involving activation of the coagulation cascade. This process is under exceptionally tight regulation to prevent inappropriate blood clotting. The expression of a key member of this cascade, Factor Xa, is increased in IPF alveolar and bronchiolar epithelium, signifying airway injury. This factor also has potent effects on initiating mesenchymal repair processes and eliciting fibroblast differentiation [165]. With injury also comes immune cell infiltration and a temporal increase in inflammatory signalling. CXCL8 and CCL2 are key members of this inflammatory repertoire and both are elevated in the BAL fluid of IPF patients [60,166]. Likewise, both IL-6 and CXCL8 are also elevated in the blood of patients experiencing an acute exacerbation, an elevation predictive of increased mortality [167]. The presence of increased numbers of myofibroblasts also points towards an attempted repair response. These cells are only transiently increased in the facilitation of repair and their

persistence reflects a protracted upregulation of damage signals expressed in the IPF lung [66,155,156]. A loss of AEC1s, concurrent with AEC2 and BC migration and hyperplasia, also signify a failed repair response. AEC2s and BCs are typically maintained in a state of quiescence, becoming active upon loss of airway cells [33,49]. Their hyperactive nature in IPF suggests continuous airway damage.

Consequences of recurrent injury

Though a causative agent remains unidentified, the increase of these hallmarks of injury and repair in the IPF lung creates a strong impression that recurrent injury is the key initiator of the disease. More direct evidence to substantiate this hypothesis can be found in murine models of lung injury.

During investigation of the progenitor functions of AEC2s, Barkauskas *et al.* employed a protocol of targeted AEC2 ablation. They found that the specific deletion of AEC2s, occurring in around 50% of the cellular population, once every two weeks simply led to efficient re-epithelialisation with no fibrosis. Daily ablation however led to parenchymal fibrosis, hypothesised to be the result of persistent denudation of the basal lamina and disruption of epithelial mesenchymal crosstalk [49]. As well as this, Cao *et al.* observed the effects of recurrent BLM on fibrosis establishment. With their model of mouse fibrosis, in which they injected BLM at 12 day intervals, they found that with each treatment there was a loss of gas exchange function, as assessed via measuring blood oxygen levels. With the first three treatments, however, function recovered to normal within the recovery interval. *Aqpn5*$^{+}$/*Pdpn*$^{+}$ AEC1s were destroyed with each BLM injection but alveolar function was restored by *Sftpc*$^{+}$ AEC2 re-epithelialisation. The mesenchyme also appeared to appropriately respond in transient fashion. Single BLM treatment led to an increase in *Acta2* and *Col1a1* expression that abated 35-days post-injury. With the continuation of treatment though there was a continual decline in lung function. After the sixth treatment, the AEC2 response failed and there was a loss of alveolar structure.

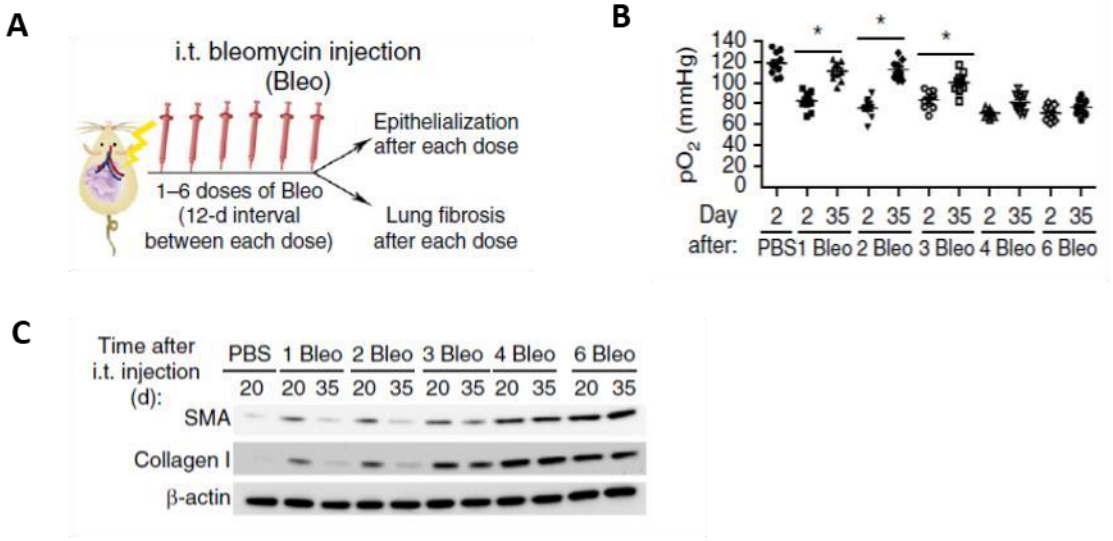

Figure 1.2.7. Recurrent injury establishes long lasting fibrosis. (A) A graphical overview of the experimental process adopted by Cao *et al.* BLM was injected into mouse up to 6 times, with a 12-day interval between each does. **(B)** Blood oxygen levels in mice 2 and 35 days after each BLM injection. By the fourth injection, levels failed to recover. **(C)** αSMA western blot image highlighting a transient increase in protein levels with early treatments that, with recurrent injury, becomes more intense and longer lasting. (Reproduced from ref. [167] with the permission of Macmillan Publishers Ltd)

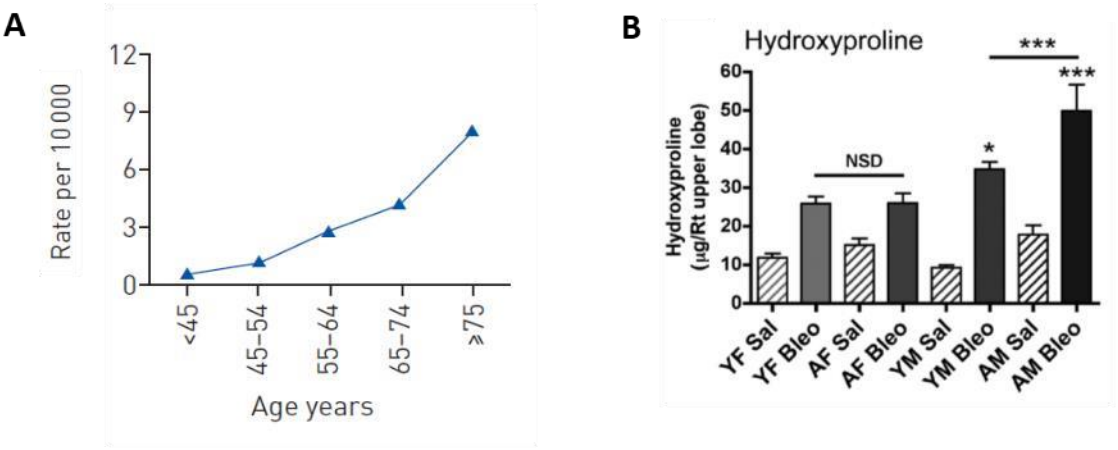

Figure 1.2.8. Age as a driving factor in IPF. (A) The incidence rate (per 10,000) of IPF with increasing age. Below the age of 45 IPF is exceptionally rare. The greatest incidence occurs in those over 75, with a steady incidence increase occurring between 45 and 75 (Reproduced from ref. [168] with the permission of the ERS) **(B)** Lung collagen content (as measured via hydroxyproline) was measured in young (Y) and aged (A) female (F) and male (M) mice following BLM installation. Lung collagen is significantly higher in AM mice compared to YM. The effect of age, however, is only significant in males. (Reproduced from ref. [171] with the permission of The American Physiological Society).

This was paralleled by a sustained elevation of markers of mesenchymal fibrosis and histologically persistent scarring **(*Figure* 1.2.7.)** [168].

1.2.4.4. Age

The list of driving forces in IPF also includes age, a process associated with a progressive decline in homeostasis throughout the body. The rate of incidence of IPF increases with age and the majority of patients are over the age of 75 **(*Figure* 1.2.8A.)** [95,169]. Therefore, the changes associated with age are thought to be key in the pathology of the disease.

The congenital disorder Dyskeratosis congenita (DKC) is a condition characterised by a premature shortening of telomeres, manifesting in symptoms similar to progeria. Interestingly, despite no environmental exposure, an investigation found that two DKC patients developed sporadic UIP and went on to die from respiratory failure [170]. Similarly, short telomeres are a risk factor for IPF and mutations in telomere regulators have been detected in IPF patients [143,171]. Mice that have been naturally aged suffer a more severe response to BLM, with worsened fibrosis and elevated BAL levels of TGF-β, IL-17A and CXCL1 when compared to young counterparts **(*Figure* 1.2.8B.)** [172]. Part of the changes that occur with age revolve around inflammation. The nuclear factor (NF)-□B is a critical, systemic regulator in the inflammatory process, regulating transcription of numerous proteins such as TNF-α, IL-1β, IL-6 and CXCL1. Numerous pathways can induce its activity, including the ERK and p38 MAPK pathways [173]. The activity of NF-□B is thought to be important in driving the process of ageing. There are numerous subunits of NF-□B, which can dimerise in differential configurations to either promote or suppress inflammation. In a transgenic mouse, with the suppressive components knocked out, there is chronic and progressive, low-grade inflammation. This inflammation drives premature ageing and impairs the regenerative processes in liver and gut [174]. Likewise, inhibition of NF-□B attenuates skeletal muscle loss in aged mice and prevents bone loss in models of osteoporosis [175]. Another feature of ageing, that is likely to be important in IPF, is stem cell exhaustion. With age the ability of stem cells to repair and maintain their resident tissue declines. For example, in geriatric mouse muscle, the resident stem cells, the satellite cells, lose their ability to activate upon injury and proliferate to promote

muscle repair [176]. Inflammation is again implicated in driving this decline in function. Hair follicle stem cells in the skin lose their functionality with age. This is associated with an age-related increase in local environmental cytokine signalling, which hyperactivates STAT-3, a transcription factor functioning downstream of Janus kinases (JAKs). JAKs respond to external cytokine signalling and JAK knockout decreases STAT3 phosphorylation, promoting stem cell function [177].

The biological changes that occur in ageing, which may cause or allow IPF development, have, however, yet to be fully elucidated. Understanding the biological landscape of the aged lung may better reveal the context within which IPF occurs and better direct therapeutic intervention.

Summary

Taken together, the evidence regarding persistent injury and aberrant repair are compelling. With the addition of genetic alterations, aberrant developmental signalling and a background of age, these features constitute the predominating characteristics of IPF. Importantly, these characteristics are not disparate, and epithelial-mesenchymal crosstalk is one feature involved throughout. Another phenomenon, one that perhaps unifies all these characteristics in IPF, is that of cellular senescence. The final section of this introduction will explore the cellular phenotype of senescence and discuss its role in the pathology of IPF.

1.3 Cellular Senescence

Senescence has a pleiotropic role in human biology. It can be both beneficial, limiting cancer development, and detrimental, driving the ageing process. This antagonistic pleiotropy makes understanding its role in disease complex. Not only this, but there are numerous pathways leading to senescence, the selection of which can dramatically alter the role of the senescent cell.

1.3.1. What is Senescence?

Senescence is a complex program of cell-cycle arrest, coupled with extensive phenotypic changes, including changes to morphology, metabolism and secretome. The term senescence derives from the Latin *senex*, meaning older man, and was first described by Leonard Hayflick in 1965 after the observation that primary fibroblasts in culture have a finite proliferative lifespan with serial passage [178]. Following on from this, much research into senescence has focused on its role in cancer biology.

In young organisms, senescence plays a crucial role in tumour suppression. Tumourigenesis occurs with the activation of oncogenes and the inactivation of tumour suppressor genes. A key suppressor is p53, a nuclear protein that responds to DNA damage and cell, stress signals; inhibiting proliferation to allow time for repair, or inducing apoptosis when damage is too great. Loss of p53 function is common in many types of cancer and its restoration can lead to tumour regression [179]. This occurs due to induction of cellular senescence, which halts tumour growth and stimulates the immune system [180,181]. Tumour suppression, however, represents just one facet of the numerous roles of senescence.

1.3.1.1. Inducing stimuli

Numerous stimuli can induce senescence. Broadly, senescence can be categorised into two forms, replicative and cellular **(*Figure* 1.3.1)** [182]. The senescence observed by Hayflick was replicative senescence, the result of a loss of stability in chromosomal

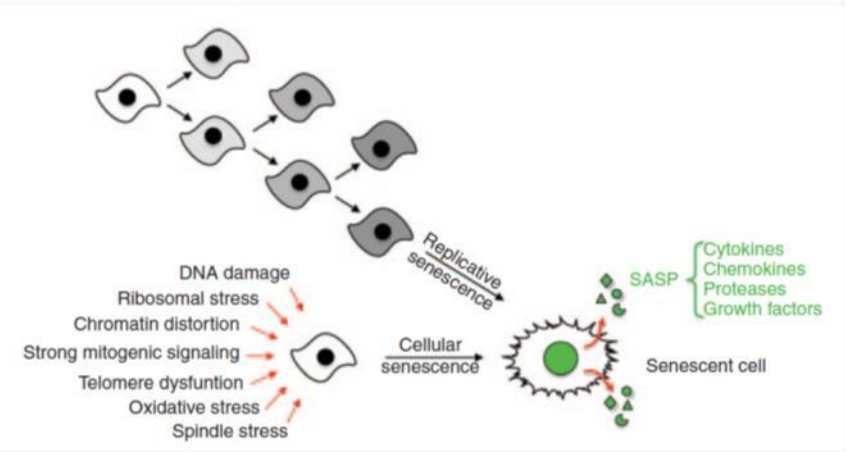

Figure 1.3.1. The origins of senescent cells. Senescence can be categorised as either replicative or cellular. Replicative senescence occurs with multiple cell divisions and was first identified by Hayflick. This limit on proliferation is term the Hayflick limit. Cellular senescence can be caused by numerous external stimuli at any stage of a cells proliferative lifespan. When a cell becomes senescent it acquires a secretory phenotype termed SASP. This results in production on various cytokines, chemokines, proteases and growth factors. (Reproduced from ref. [181] with the permission of John Wiley and Sons)

telomeres, a form of senescence results from intrinsic cell events [183]. With each replicative cycle of a cell telomere degradation occurs, ultimately disrupting chromosomal integrity and activating a DNA-damage response (DDR). This causes p53 phosphorylation and activation of cyclin dependent kinase (CDK) inhibitors, preventing progression through the cell cycle and inhibiting growth. This is important in limiting tumourigenesis as, with continued mitotic divisions, the possibility of DNA mutations increases. By preventing proliferation, the risk of oncogenic mutation is decreased.

Cellular senescence results from extrinsic stimuli and it can occur at any point of a cells replicative lifespan, irrespective of telomere integrity. Substantial DNA damage occurring in any chromosomal region activates the same pathways as replicative senescence. A DDR response is activated with downstream activation of the CDK inhibitor p21 [184]. Oncogenic signalling can induce cellular senescence, as can several other stimuli. ROS can cause senescence in a p38 dependent manner as can environmental cytokine signalling [185–188]. Both neighbouring senescent cells and developmental pathways, functioning via TGF-β and SMAD, are also able to induce senescence as well as mitochondrial dysfunction [189–194].

1.3.1.2. Senescence pathways

All senescence pathways converge on the inhibition of Retinoblastoma protein (RB) phosphorylation, which prevents cell cycle progression by restricting transcription of E2F genes. RB inhibition is the result of upstream inhibition of numerous other cyclins and CDKs, facilitated by two main pathways, the p53-p21 and p16-pRB pathways. The p53p21 pathway, activated in response to DDR, ROS and oncogenic stimulation, is regulated by alternative-reading-frame (ARF) proteins, which inhibit the activity of E3 ubiquitinprotein ligase (MDM2), an enzyme that degrades p53 [195]. This induces p21 activity, which inhibits cyclinE-CDK2 activity. The p16-pRB pathway can be directly activated by oncogenic RAS signalling, or p38-mediated ROS signalling, and appears to function secondary to the p53-p21 pathway [196]. Active p16 inhibits proliferation via inactivation of cyclinD-CDK4/CDK6 **(*Figure* 1.3.2.)** [197].

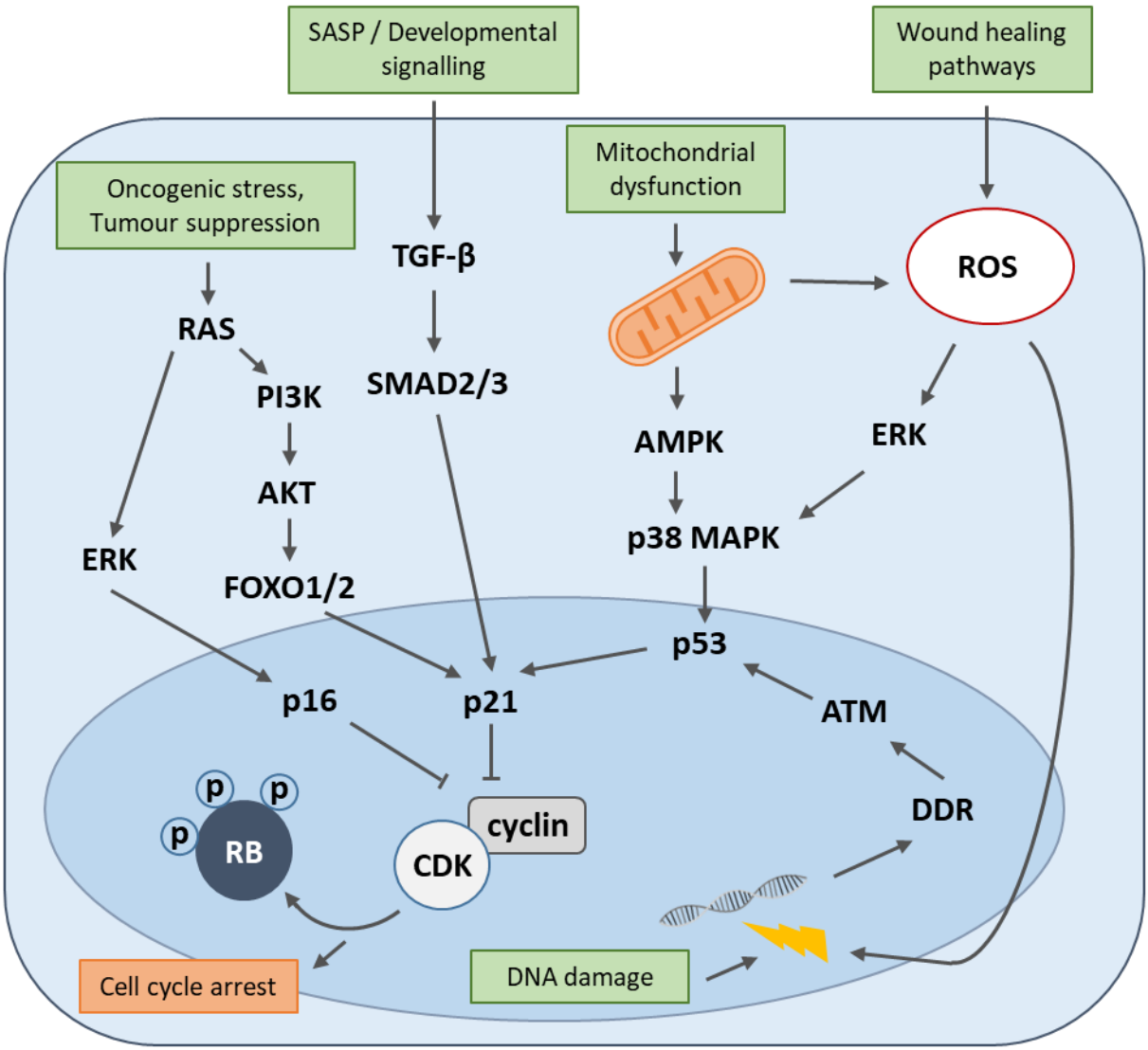

Figure 1.3.2. Pathways to establish senescence. The numerous stimuli that induce cellular senescence also function through differing pathways and employ differing cell cycle inhibitors. All of these signalling cascades converge on inhibition of cyclin and CDKs, leading to an inhibition of RB phosphorylation and subsequent cell cycle arrest.

These pathways can be transiently induced in response to minor damage and deactivated upon repair, allowing a cell can revert to a proliferative state. It is only with sustained activation of these pathways that senescence is induced. For example, after irradiation induced DNA damage, cells recover via transient p53 expression. Pharmacologically sustained p53 expression however leads to differential gene expression and senescence [198]. Likewise, the long-term activation of *CDKN1A* (which encodes for p21) by DDR leads to p38 and TGF-β signalling that causes mitochondrial dysfunction. Such dysfunction reduces oxidative phosphorylation, increasing the production of ROS (such as H_2O_2). This ROS consequently reinforces the senescence

pathways by creating further DNA damage, further activating the p16-pRB pathway. This process can be averted via the complete depletion of cellular mitochondrial content, achieved by PINK1 mediated targeting of the ubiquitin ligase, Parkin, to the mitochondria, promoting mitophagy [199]. That elimination of mitochondria prevents senescence induction heavily implicates this heterogenous population of organelles in both establishing and maintaining this phenotype [200,201].

1.3.1.3. Cellular changes

The entrance of a cell into a permanent state of senescence is coupled with a diverse range of phenotypic changes. These arise from extensive chromatin remodelling events. Early remodelling occurs in satellite heterochromatin, located in the peri-/centromeric regions of the chromosomes. These regions undergo striking decondensation (in response to both senescence inducing pathways) in a process termed senescenceassociated distension of satellites (SADS) [202]. These changes are followed by chromatin condensation in numerous other regions of the chromosome. The accumulation of these distinctly patterned, senescence-associated heterochromatic foci (SAHFs) act to sequester transcription of numerous genes, most notably those required for cell cycle control, including E2F genes [203,204]. The regulation of these changes is controlled by lamin B1, which is downregulated to facilitate these changes [205,206].

These alterations subsequently introduce a plethora of changes to a senescent cells transcriptome. Interestingly, the pattern of transcriptional differentiation varies substantially between cell types, despite induction via common pathways [207]. Microarray analysis of fibroblasts in a state of replicative senescence reveals upregulation of mRNA for *PAI*- 1 and 2, *CCL2*, *CXCL1* and *MMP*- 1 and 2. Concomitantly, there is down-regulation of cyclooxygenase-1 (COX1) and MMP3. Conversely, in retinal epithelial cells, Follistatin (*FST*) and prostaglandin D synthase (*PTGDS*) are upregulated without significant changes to inflammatory genes[208].

There are also alterations in cell morphology and metabolism, as well as alteration to the mitochondrial phenotype [209,210]. With senescence there is an enlargement of

mitochondrial mass, and increases in mitochondrial volume fraction, organelle number and the copy number of mitochondrial DNA (mtDNA) [201]. Similarly, then is an increase in the ratio of mtDNA/total cell protein [211]. However, these changes represent just some of the alterations that have been identified in senescent cells.

The most significant changes to cell behaviour arise from an upregulation of genes encoding an array of secretory cytokines, chemokines, protease and growth factors, collectively termed the senescence-associated secretory phenotype (SASP). This phenotype does not arise in cases of transient DNA damage and p53 is not required to maintain it, instead persistent DDR signalling elicits both its activation and its maintenance [212]. Analysis of the secretome of irradiated fibroblasts shows that SASP is composed of a broad range of proteins. These include factors such as: IL-6, CXCL1, CXCL8, GM-CSF, IL-7, Osteoprotegerin and HGF, though many others are also typically produced [213]. Overall, the SASP is dominated by inflammatory cytokines, immune modulators and growth factors **(*Figure* 1.3.3.)**.

Activation of the NF-□B pathway is an important upstream regulator of SASP induction, with activation leading to an up-regulation of *IL1A* and *IL1B* gene expression [214]. They are produced as pro-proteins and their function is facilitated by the inflammasome, a multiprotein complex required for driving inflammation. Through stimulation of caspase-1 it can promote the processing of the precursor proteins of IL-1β and IL-1α, as well as IL-18 and IL-33, via a non-canonical protein processing pathway [215,216]. The

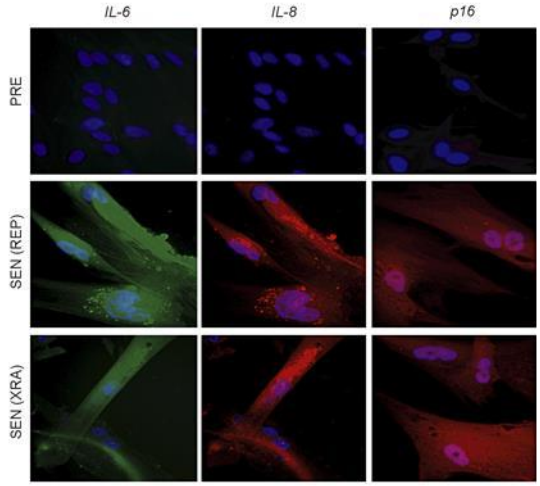

Figure 1.3.3. Key components of the senescence associated secretory phenotype in fibroblasts. Senescence (SEN) was induced in fibroblasts via γ-irradiation or repeated passage. The CM was analysed by antibody array revealing elevation of numerous factors that constitute the SASP. Key factors included IL-6 and CXCL8. Elevation was validated via immunofluorescent staining. The marker of senescence, p16, was also stained for. (Reproduced from ref. [212] available under a Creative Commons CC-BY Licence)

inflammasome is heavily implicated in oncogene-induced senescence (OIS), with an increase in production of the mature forms of IL-1β and IL-1α. These cytokines are critical in inducing SASP, with inhibition of processing or inhibition of activity blunting SASP secretion, decreasing levels of IL-6 and CXCL8 [191,217].

1.3.1.4. Impact on the local environment

Senescent cells exert their effect on the local environment via this secretory phenotype and such effects can be dramatic. SASP can facilitate and maintain senescence, with secretory factors such as IL-6, CXCL8 and WNT16B acting in an autocrine manner to establish persistent growth arrest [218,219]. Not only this, but the components of SASP can induce senescence in neighbouring cells. Co-culturing normal epithelial cells with senescent fibroblasts can induce epithelial senescence, an event attributed to the properties of secretory proteins that can be recapitulated with senescent cell CM. Quantitative proteomics has revealed that VEGF signalling and the TGF-β pathway are be key in mediating this paracrine effect [191].

Therefore, cellular senescence can be induced in response to numerous stimuli that, if sustained, create a stable form of cell-cycle arrest and the acquisition of an inflammatory secretory phenotype. But, aside from limiting tumourigenesis, what role does senescence play?

1.3.2. The Homeostatic Roles of Senescence

The context in which a cell becomes senescent is crucial in determining the role that SASP plays. In the young organism senescence plays numerous homeostatic functions that are carefully controlled to benefit organism fitness. As previously discussed, cellular senescence can occur at any stage of a cells proliferative lifespan, in response to not only DNA damage and oncogenic signalling, but also developmental pathways and cytokine signalling.

1.3.2.1 Embryonic development

Senescence plays an important role from the earliest stages of an organism's lifespan. In the embryonic mouse, senescence has been observed at numerous sites, including: the closing neural tube, apical ectodermal ridge (AER), interdigital webs, mesonephric tubules and endolymphatic sac **(*Figure* 1.3.4.)** [190,192].

The AER is found at the distal tip of the nascent limb bud, marking the dorso-ventral boundary, and forming a signalling centre that facilitates both tissue growth and patterning. This is achieved by reciprocal signalling with a region of underlying, distal mesenchyme that forms the progress zone (PZ). In mice, at embryonic day 11, staining reveals AER-specific positivity for p21 and the classical senescence marker, senescenceassociated β-galactosidase (SA-βgal), as well as evidence of growth arrest. Interestingly, p53 signalling is absent, indicating senescence induction through a unique pathway. PZ mesenchymal signalling maintains this AER senescence by pERK signalling and in turn senescence promotes mesenchymal growth **(*Figure* 1.3.5.)** [190]. In the kidney, organ development requires the involution of early forming mesonephric tubules, facilitating transition to a stage of metanephric development and establishment of the adult kidney. During early growth of the mesonephric tubules, the luminal epithelial cells express proliferation markers. As development continues this transitions to markers of senescence. This again occurs in a p53-independent manner, controlled by p21, and activated by TGF-β, Hedgehog and WNT pathways [192]. Importantly, in both instances of senescence induction, immune infiltration occurs at the end stage of development and senescence markers decline. These investigations revealed a transient role of senescence in development, highlighting another example of epithelial-mesenchymal crosstalk in development and eluding to the role of developmental signals in regulating senescence.

1.3.2.2. Wound repair

Wound repair is characterised by the phases of haemostasis, inflammation, granulation tissue formation, re-epithelialisation and regeneration. In young mice, senescence has been identified as an important component of this process.

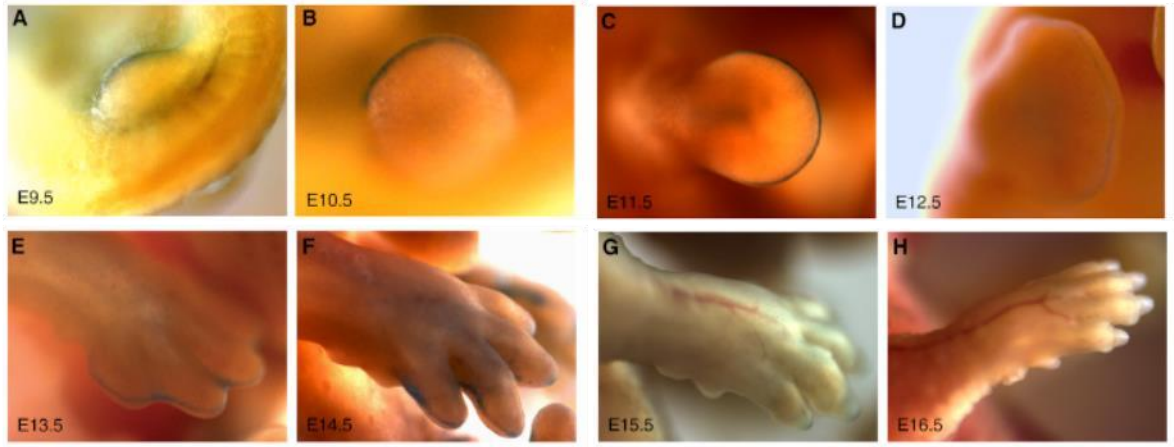

Figure 1.3.4. Presence of senescent cells over the course of forelimb development in mouse. SAβ-Gal staining (blue) of whole mount embryos at different embryonic days. **(A-D)** Prominent staining in the AER across the ridge of the nascent forelimb at days E10.5 – 11.5, reducing in strength by E12.5. **(E-F)** Positive staining during interdigitation at E13.5 – 14.5. **(G-I)** Weak staining at the tips of the digits at E15.5 which has subsided by E17.5. (Reproduced from ref. [189] with the permission of Elsevier)

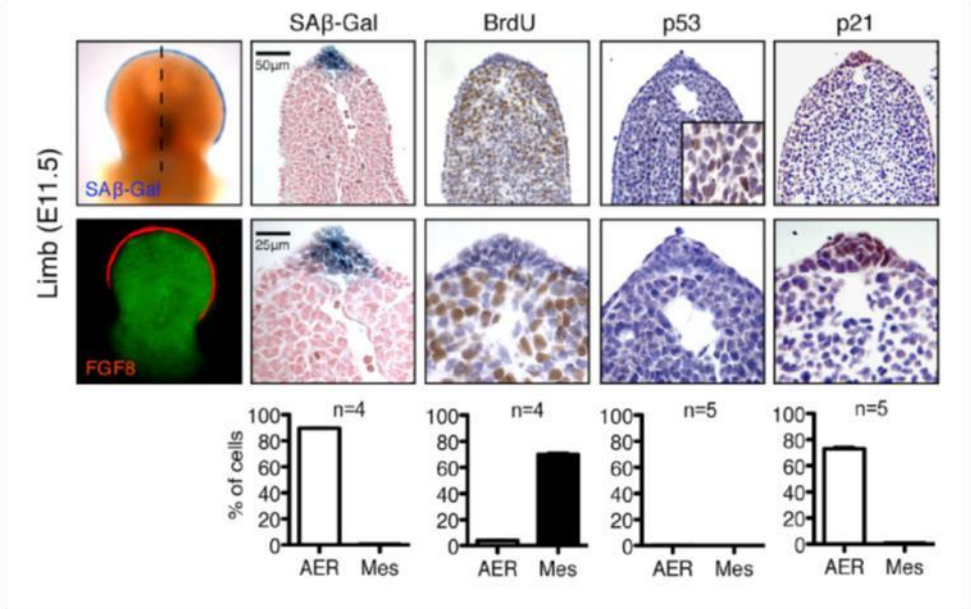

Figure 1.3.5. Senescent cells in AER of the developing mouse forelimb. At E11.5 the forelimb was stained for SAβ-Gal, BrdU incorporation and p53 and p21 by immunohistochemistry, with corresponding quantification shown beneath. In there AER there is a cohort of senescent cells, sustained by p21 in a p53-independent manner. (Reproduced from ref. [189] with the permission of Elsevier)

Using a mouse model that reports the presence of senescent cells via luminescence, and that can be pharmacologically treated to cause selective removal of these cells, the role

of senescence in repair has been better elucidated. Upon full-thickness, dermal punchbiopsy, a transient induction of senescent cells is observed, arising around day-3 postinjury and peaking at day-6, prior to returning to baseline. Depletion of senescent cells during this time-course leads to an impairment of re-epithelialisation, as well as a loss of angiogenesis and collagen deposition. Senescence is induced in local fibroblasts and endothelial cells, which upregulate production of PDGF-AA and VEGF at the early stages of induction. These senescent cells further recruit fibroblasts and promote their differentiation to myofibroblasts, enabling efficient wound repair **(*Figure* 1.3.6.)** [220]. A key inducer of fibroblast wound-site senescence has been identified as the matricellular protein, CCN1. CCN1 binds to integrin $\alpha_6\beta_1$ and heparin sulphate proteoglycans, activating a DDR and ROS generation, leading to p16-pRB induced senescence. In the skin wounds of mice, and over a time-course of several days, the presence of CCN1mediated senescent cells causes an increase in gene expression of matrix degrading MMPs and limits the fibrogenic response in granulation tissue formation [221].

1.3.2.3. Tissue regeneration

Senescence also promotes tissue regeneration. New-born, primary mouse keratinocytes (PMKs) are able to regenerate skin when transplanted into tissue biopsy wounds, expressing numerous stem-cell markers. A short-term (2-day) incubation of PMKs with the CM of OIS cells enhances the expression of these markers, increasing colony-forming capacity *in vitro* and augmenting regeneration in skin grafts [222]. These results indicated that a transient exposure to SASP can enhance the plasticity and regenerative potential of cells in the local environment, further implicating senescence as a beneficial, homeostatic process.

Similarly, a key roadblock to the full regeneration of tissue is the development of fibrosis. In the liver, senescence has been found to limit fibrosis, enabling regeneration. Using a mouse model of cirrhosis, in which young mice are treated with CCl_4 causing tissue

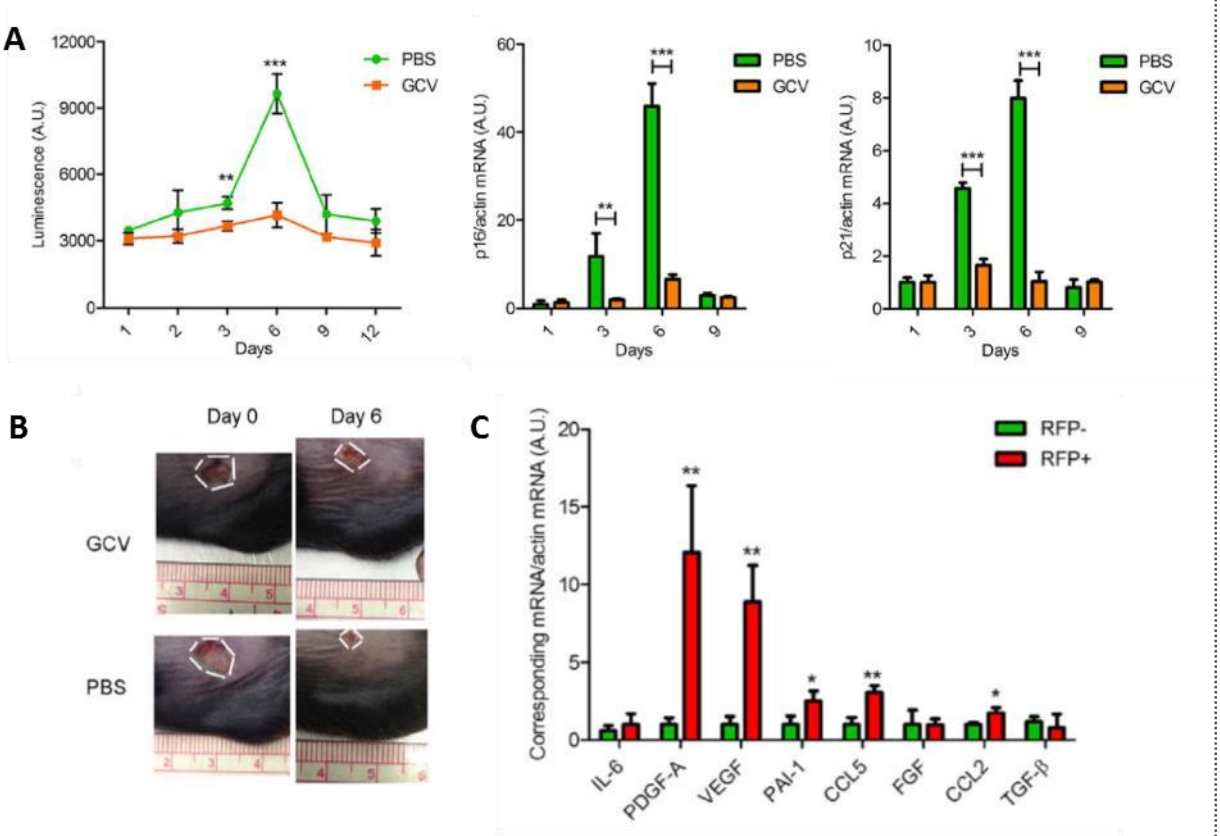

Figure 1.3.6. Senescence promotes wound healing in young mice. (A) Punch biopsy of a transgenic mouse, in which senescent cells fluoresce but can also be cleared by GCV treatment, revealed a transient increase in senescent cells at the wound site 6 days post injury. This was further validated by elevated mRNA levels of *CDKN1A* and *CDKN2A* in PBS treated mice. **(B)** The presence of these senescent cells was found to promote healing, with smaller wound diameters at 6 days in PBS treated mice. **(C)** Red fluorescent protein (RFP) positive senescent cells were isolated and found to express elevated levels of *PDGFA, VEGF, PAI1, CCL5* and *CCL2*. PDGF-A was subsequently found to promote wound healing. (Reproduced from ref. [217] with the permission of Elsevier)

damage, fibrosis occurs, mediated by activated hepatic stellate cells (HSCs). Concomitant with the onset of fibrosis regression and tissue regeneration is the accumulation of senescent HSCs in regions of fibrosis. In this disease model, but in mice with a double knock-out of *Tp53* and *Cdkn2a*, senescence is impeded and subsequently there is an increase HSC proliferation, an increase in ECM deposition and persistent, non-resolving fibrosis [223]. Similarly, in a mouse model of kidney fibrosis, p16 is significantly elevated post-injury injury. However, in a *Cdkn2a*$^{-}$ mouse, injury results in increased interstitial proliferation and subsequent fibrosis [224]. Likewise, using an aortic constriction model of cardiac fibrosis in a *Tp53*$^{-}$/*Cdkn2a*$^{-}$ mouse, senescence is decreased

corresponding to an increase in fibrosis. Inducing senescence can increase fibroblast senescence and reduce fibrosis [225]. Importantly, however, studies in the cirrhotic mouse liver revealed that this homeostatic function of senescence is under strict, temporal regulation, with natural killer (NK) cell recruitment in the wild-type mouse leading to the selective clearance of senescent cells [223].

1.3.3. The Detrimental Roles of Senescence with Age

The benefits of senescence come when its induction is transient and tightly controlled. This so called 'acute' senescence is what facilitates embryonic development, wound repair and tissue regeneration in young organisms. When senescent cells persist, however, through either a lack of clearance or an accumulation, they become detrimental to tissue function. These 'chronic' senescent cells naturally accumulate in aged organisms and are now thought to be the central contributors to age-related tissue dysfunction and disease.

1.3.3.1. The driving force in ageing

In mammals senescent cells accumulate with age [226,227]. The significance of this and the causal link between senescence and ageing has been described in two key investigations, both utilising the BubR1 mouse. This mouse has a hypomorphic mutation in the BubR1 protein, a key mitotic checkpoint protein, which creates a progeroid phenotype, with shortened life-span, sarcopenia and impaired wound healing. By crossing this mouse with a *Cdkn2a* knockout, it was found that, with the subsequent absence of senescence, BubR1 lifespan was increased and muscle loss decreased [228]. Further evidence was found after establishment of the *INK-ATTAC* mouse. This mouse, with a *BubR1*^{hypo} background, has a reporter for p16, allowing for identification, but also a selective clearance of *Cdkn2a* expressing cells. Expression of *CDKN2A* coincides with expression of an apoptosis inducing element that can be activated upon pharmacological intervention. Investigation revealed that age-related phenotypes arise due to senescence cell accumulation and that clearance in older mice is able to delay the progression of several age-related changes, although reversal is not possible [229]. In conjunction with the

concept of senescence driving ageing, mice strains that demonstrate sustained regulation of gene splicing display reduced markers of senescence and are longer-lived [230].

1.3.3.2. Promoting tumourigenesis

The studies by Baker *et al.* demonstrated that senescence drives the ageing process. Encompassed within this though are numerous other detrimental effects of senescence. Almost paradoxically, the tumour suppression mechanism of senescence creates an environment, via SASP, that promotes tumourigenesis in neighbouring cells. Co-culture of senescent fibroblasts and pre-malignant mammary epithelial cells causes them to become invasive and undergo full malignant transformation [231]. Senescent CM also induces upregulation of EMT markers in mammary, alveolar epithelial cells, evidenced by reduction in tight junction and adherens proteins and an increase in *VIM* expression. Key mediators of this are IL-6 and CXCL8 and neutralising antibodies towards these can reduce epithelial membrane invasion [213]. As well as this, reduction of *IL1A* translation, by treatment with Rapamycin, reduces SASP and suppresses the ability of senescent fibroblasts to promote prostate tumour growth in mice [232].

1.3.3.3. Impairing regeneration

The transient exposure of SASP CM to progenitor cells enhances their stem-cell properties and regenerative capacity [222]. However, in this same study, prolonged and repeated exposure to SASP lead to the impairment of regeneration, due, in part, to the effect of paracrine senescence. Chronic senescence in the liver also leads to failed regeneration and fibrosis. In mouse models of liver cirrhosis, senescence is transiently induced to limit fibrosis, with cells subsequently cleared by the immune system [223]. This immune-mediated clearance is achieved by granule exocytosis, another form of secretory communication. Blocking this process leads to the persistent accumulation of senescent liver cells that leads to fibrosis [233]. This implicates an important role of the immune system in facilitating acute senescence. Implantation of senescent cells into mice leads to the recruitment of innate immune cells, particularly macrophages. Insertion embedded within alginate beads allows secretory communication but prevents

immune-mediated senescent cell destruction. By studying the cells that accumulate around these beads it has been found that exposure to the senescent microenvironment leads to macrophages transiently entering a state of senescence themselves. The hypothesis was put forward that, with age, innate immune cell dysfunction causes chronic immune senescence, impairing clearance of other senescent cells and further impairing regeneration [234].

Senescence therefore represents a cellular protocol that, though initiated under the pretences of limiting cancer, facilitating development and assisting repair, becomes a hazard to human health when unnecessarily sustained. This persistence occurs with age, the fault, in part, of a declining immune system, and within this setting, senescence ultimately impedes the processes of repair, a result that is followed by a decline in tissue function.

1.3.3.4. Targeting senescence

The deleterious effects of senescence in age have led to the development of numerous strategies aimed at targeting senescent cells and alleviating their effects. These strategies range from senescence reprogramming, to dampening SASP, or to the targeted apoptosis of senescent cells.

Reprogramming of aged cells is complex. A recent study by Ocampo *et al.* used shortterm induction of the classical, pluripotency inducing transcription factors: *Oct4, Sox2, Klf4* and *cMyc* (OSKM) to ameliorate the hallmarks of ageing in mice. The genetic background of these mice meant that they prematurely aged and were able to express OSKM upon doxycycline treatment. Treatment extended mouse lifespan and reduced the hallmarks of ageing, an effect that was, in part, achieved by a systemic reduction in DNA damage, p53 activity and a downregulation of *Cdkn1a* and *Cdkn2a*, as well as expression of *IL6* [235]. Viable therapies for humans, however, cannot as easily rely on genetic modulation, therefore pharmacological therapies are attractive. Selfmaintenance of senescence involves autocrine IL-6 signalling [218]. IL-6 binds to cytokine receptors on the cell surface leading to trans-phosphorylation of JAK 1 and 2. JAKs phosphorylate STAT3, which

translocates to the nucleus and regulates transcription of numerous genes, including those required for SASP. Molecular inhibition of JAK signalling inhibits this process and reduces production of numerous SASP proteins. Treatment in aged mice decreases systemic inflammation and is able to alleviate frailty [236]. The selective clearance of senescent cells from chronologically aged and progeroid mice also delays the onset of age-related pathology and extends healthspan [237]. This has been achieved with the Bcr-Abl and Src family tyrosine kinase inhibitor Dasatinib (D) and the flavonoid Quercetin (Q), which, when used in combination, create what is termed a 'senolytic' therapy. Similar senolytic strategies have been achieved using an inhibitor of anti-apoptotic proteins (BCL-2 and BCL-xL), ABT263, with which treatment in both prematurely and naturally aged mice rejuvenated muscle and haematopoietic stem cell populations [238]. Most recently, targeted apoptosis of senescent cells has been achieved with a small peptide that blocks the interaction of p53 and FOXO4. This prevents p53 nuclear localisation and subsequently causes nuclear exclusion, leading to cell intrinsic apoptosis via caspase-3/7 [235]. Interestingly, the authors of this paper were unable to reproduce the selectivity of D+Q *in vitro* and ABT263 was found to influence control cells at low concentrations. Regardless, senescence is becoming well established as a viable therapeutic target, with clearance facilitating numerous beneficial effects across several animal models.

1.3.4. Evidence for Senescence in IPF

What, however, is the relevance of senescence to IPF? Does it play an important role in the disease and could it also be targeted? Thus far, there is compelling evidence to suggest that the answer is yes.

Firstly, one of the driving forces in IPF is an aberrant reactivation of developmental signalling pathways, including signalling via WNTs, Hedgehogs and TGF-β **(Intro 2.4.2.)** Acute senescence plays a role in development and these pathways are important in establishing the phenotype [190–192]. In particular, TGF-β can induce embryonic senescence

and WNT signalling can maintain senescence in an autocrine fashion. Therefore, if these pathways are persistently reactivated in IPF it could lead to the induction of senescence. Secondly, IPF is characterised by recurrent injury and an impaired wound healing response **(Intro 1.2.4.3.)**. Though acute senescence in young animals is known to promote wound healing [220], its role in the context of age is hazardous, with chronic senescence understood to impair regeneration [222]. Repeated injury could therefore cause persistent senescence that ultimately leads to the impairment of airway regeneration observed in IPF. Thirdly, IPF is a disease of ageing **(Intro 1.2.4.4.)**. Age is the greatest risk factor for IPF and 80% of patients with the disease are over 75 [169]. With age there is an increase in the burden of senescent cells, cells that are causal in driving both the process itself and numerous other age-related pathologies [228,229]. These cells go unchecked by a faltering immune system and accumulate to become chronically senescent and damaging to the local environment [234]. This aged background subsequently provides fertile ground for the induction of senescence and its chronic activation. Taken together, this provides the rationale for the conception of a paradigm in which the acute signalling of developmental and repair pathways become chronically activated in the IPF lung, leading to the accumulation of senescent cells that further contribute to impaired regeneration and fibrosis. Direct evidence for such a paradigm does exist and recent publications have made the pathological role of senescence in IPF considerably more salient.

1.3.4.1. Senescence in IPF

Up until recently there has been little *in vivo* evidence of fibroblast senescence in IPF. Isolated FHLFs display the characteristics of senescence *in vitro* but the understanding was that there was a detrimental absence of senescence in this disease [239,240]. Subsequently, strategies were employed to induce senescence with the aim of using it as a brake on excessive fibroplasia. HAS2, known to be a potent inducer of fibroblast differentiation and invasiveness, is more significantly expressed in the IPF lung and its overexpression in mouse leads to a more severe response to BLM [124]. By depleting HAS2, senescence can be induced in mouse fibroblasts and it was subsequently suggested that the pathological phenotype conferred by HAS2 prevents senescence and therefore

prevents wound resolution. HAS2 was subsequently proposed as a target to promote resolution of fibrosis [240]. Furthering this, a study investigating the micro RNA, miR-34a, found that it was upregulated in FHLFs. However, mice deficient in this miRNA developed a worsening of BLM-induced fibrosis. miR-34a induces HLF senescence, suggesting that it acts in a negative feedback loop, inducing senescence in response to fibroplasia, limiting fibrosis. Restoring this feedback was therefore suggested to help resolve fibrosis [241].

Other studies have, however, focused on the detriment of an excessive senescence burden in IPF. In young mice BLM-induced fibrosis can resolve over time (although this is not a universal finding). However, in aged mice fibrosis does not resolve. This is associated with an increase in the burden of senescent fibroblasts. Both young and aged mice accumulate senescent fibroblasts in response to injury. In the young though, their existence is transient whereas in the aged these cells persist. This chronic accumulation was found to impair resolution and promote fibrosis [242]. Likewise, shortening of telomeres is associated with a poorer prognosis in IPF. Telomere specific dysfunction in AEC2s causes them to become senescent and lose their regenerative capacity. This causes subsequent lethality upon BLM instillation [145]. A consequence of telomere dysfunction in AEC2s is an increase in production of pro-inflammatory cytokines, creating an environment of low-grade, sterile inflammation, analogous to ageing. The occurrence of this in the lung is able to contribute to myofibroblast differentiation [243].
Cellular senescence has also been identified in the epithelial cells of IPF lung tissue. *In vitro,* TGF-β1 induces senescence in primary HBECs, causing them to produce elevated levels of IL-1β, which subsequently causes fibroblast differentiation [244]. Protecting AECs from senescence by knocking out expression of the protein caveolin-1, reduces senescence and also attenuates fibrosis [245]. Senescence markers have been found in AEC2s within IPF tissue. This is understood to be the result of an elevation of the senescence-associated micro-RNAs, miR-34a-c [246].

Finally, senescence has most recently been identified in both the epithelium and the mesenchyme of IPF patient tissue, in a study investigating the targeted clearance of

senescent cells **(*Figure* 1.3.7.)**. Expression of p16 was found to be increased with increasing disease severity and the senescence secretome is complicit in fibrogenesis. Transgenic ablation and treatment with the senolytic combination of D+Q was found to selectively clear senescent cells. The effect of this was an improvement in pulmonary function and overall health after BLM instillation [247]. This study provides the best evidence so far that senescence plays a critical role in IPF and that senescent cells are a viable target for therapeutic intervention.

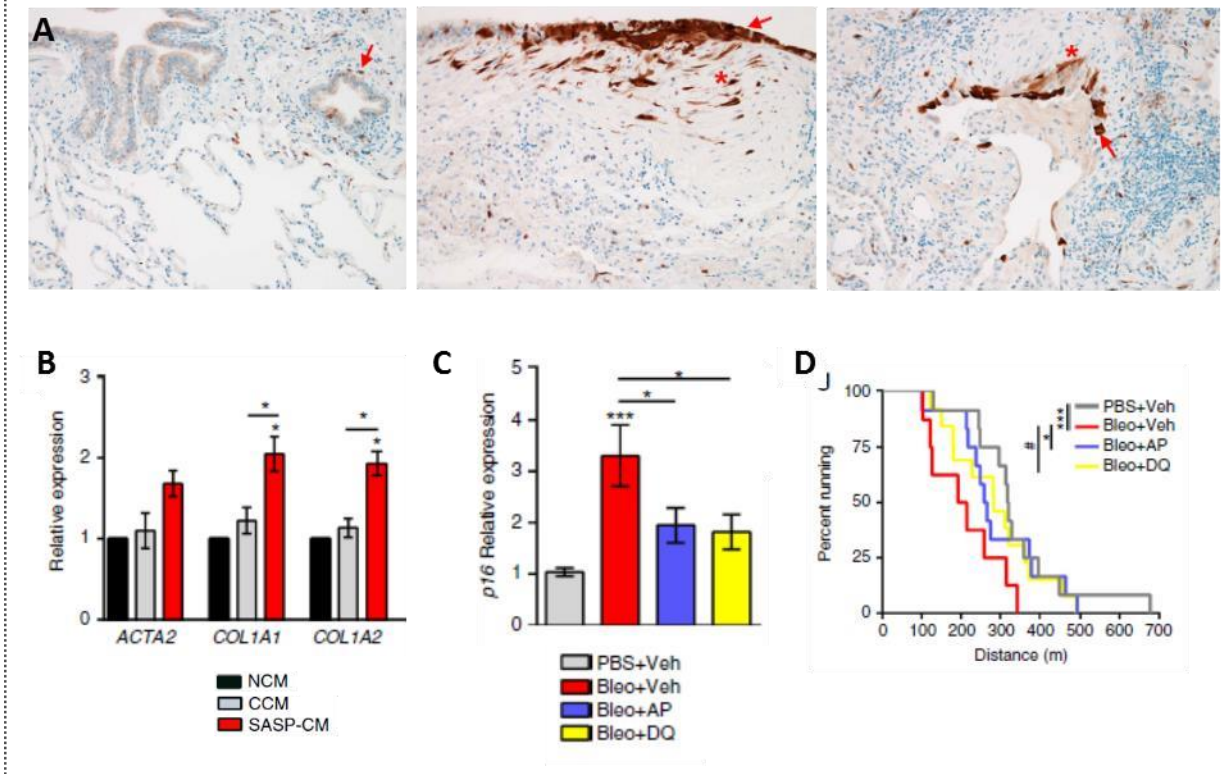

Figure 1.3.7. Cellular senescence is evident in IPF and clearance of senescent cells can improve health. (A) Immunohistochemistry of lung tissue sections stained for p16 from (left) control samples, (middle) honeycomb lung, and (right) fibroblastic foci. Arrows highlight p16-positive epithelium. (*) Indicate p16-positive fibroblasts. **(B)** SASP is fibrogenic *in* vitro. A fibroblast cell line was treated for 72 hrs with CM from either normal cells (NCM), sham-irradiated cells (CCM), or irradiated and senescent cells (SASP-CM). SASP CM promoted an increase in RNA levels of *COL1A1* and *COL1A2*. **(C)** BLM induces lung senescence via an increase in p16. Selective clearance of senescent cells in *INK-ATTAC* mouse (AP) reduces the senescence burden, as does treatment with D+Q (DQ). **(D)** Mice with these treatments performed a run to exhaustion to test exercise capacity. Clearance of senescent cells by either AP or DQ significantly improves exercise capacity. (Reproduced from ref. [246] available under a Creative Commons CC-BY Licence)

1.4 Summary and Thesis Aims

This introduction has attempted to cover a diverse range of biological concepts and research, encompassing the current understanding of epithelial-mesenchymal crosstalk, IPF and cellular senescence. The aim of this introduction has been to impress the importance of communication between cell types, highlighting the importance of these processes in both health and disease. More specifically it has aimed to identify examples of crosstalk within normal lung physiology, discuss how this goes wrong in the pathology of IPF and observe how it participates in the phenomenon of senescence. Subsequently, the importance of the fibroblast phenotype in mediating crosstalk (through

inflammatory signalling) has been highlighted. Ultimately this introduction has aimed to demonstrate that the driving forces of IPF are interconnected with the processes of cellular senescence, a connection enabled by secretory crosstalk between the epithelium and the mesenchyme.

Consequently, the overarching experimental aim of this thesis was to understand more about the biology of IPF-derived fibroblasts, uncovering new insight into their pathological properties, with a particular focus on their roles in inflammation and senescence. The hypothesis of this work was that a breakdown in epithelialmesenchymal crosstalk is a key driver of IPF, with the senescent fibroblast acting as a critical orchestrator of this process and a viable therapeutic target.

Specifically, the aims of this project were broken down into:

1. The isolation of primary HLFs and their phenotypic characterisation *in vitro.*
2. The establishment of an *in vitro* model of secretory crosstalk, allowing investigation of epithelial-mesenchymal crosstalk.
3. Determining the effect of FHLF co-culture on the ability of the epithelium to respond to injury.
4. The induction of senescence in NHLF to create a benchmark cell phenotype with which to compare FHLFs.
5. Pharmacological modulation of secretory crosstalk *in vitro*.

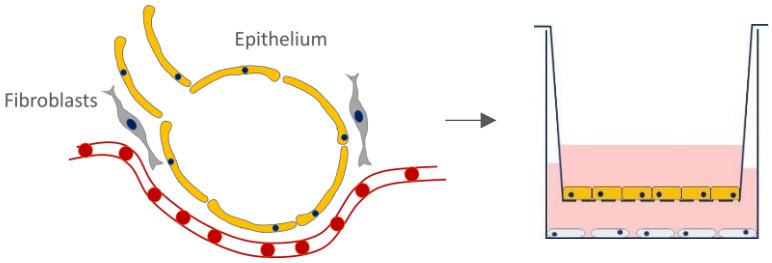
Epithelium
Fibroblasts

2.1 Cell Culture

2.1.1. General plastic ware and chemical reagents

Cells were propagated in sterile tissue culture flasks, (Thermo Scientific, USA) or (Greiner Bio-one, Austria). Experiments were performed on Nunc cell-culture treated multidishes (Thermo Scientific, USA). Cell suspensions and other tissue culture reagents were handled in 15 ml (Thermo Scientific, USA) and 50 ml (Greiner Bio-one, Austria) centrifuge tubes and transferred with serological pipettes: 5 ml, 10 ml, 25 ml (Fisherbrand, USA). Sterile micro-centrifuge tubes (0.6 ml and 1.5 ml) were purchased from (Thermo Scientific, USA). Cell culture grade, endotoxin free ddH_2O and phosphate-buffered saline (PBS) were also purchased from (Thermo Scientific, USA). Tris-buffered saline (TBS) was made using tris-base (Fisher Bioreagents, USA), sodium chloride (Fisher Bioreagents, USA), ddH_2O (purified by a PURELAB-Ultra system) (Elga, USA), and hydrochloric acid (Fisher Bioreagents, USA).

2.1.2. Cell culture conditions and general practice

Cell Culture

All cells were cultured at 37 ^oC, 5% CO_2, under atmospheric levels of O_2. Cells were routinely passaged before reaching confluency. Passage consisted of: removal of the culture media, a brief wash with serum-free media, trypsinisation (Gibco, UK), neutralisation with media containing 10% foetal bovine serum (FBS) (Gibco, UK) and transfer into a fresh flask. For the seeding of cells into experimental plates, cells were counted after neutralisation using a haemocytometer. The suspension of cells was then pelleted via centrifugation at 200*g* for 4 mins, the supernatant aspirated, and the pellet re-suspended in 1ml of media. The proportion of cells was then aliquoted and seeded as required.

Long-term storage

For long-term storage, cells were trypsinised and pelleted as previously described. Cells would then be re-suspended in cryo-media, a mixture of 50% media, 40% FBS and 10% dimethyl sulfoxide (DMSO) (Sigma Aldrich, UK). Cells in cryo-media suspension would then be aliquoted into cryogenic storage vials (1 ml/vial) (Thermo Scientific, USA) and stored at -80 ^{o}C in a Mr. Frosty (Thermo Scientific, USA). The Mr. Frosty, containing isopropanol (Fisher BioReagents, USA), facilitated a cooling rate of ≈1 ^{o}C/min. Cells were stored for a minimum of 24 hrs at -80 ^{o}C prior to long-term storage in liquid nitrogen (LN_2).

Defrosting cells

Cells were defrosted from LN_2 storage by the addition of pre-warmed media. 1 ml of media would be added to each vial and gently mixed by repetitive pipetting. The defrosted cells would then be transferred to a T75 flask with 20 ml media, to dilute the DMSO. After overnight adherence, the media was replaced.

2.1.3. Cell lines

To model the lung airway epithelium, the 16HBE14o- (HBECs) transformed cell line was used. This line has been immortalised via transfection with SV40 T-antigen encoding DNA. The cells form tight junctions, become polarised and display vectorial ion transport, making them appropriate for airway modelling [248]. Though other lines were available (such as BEAS-2B or A549), this line was chosen as distal bronchiolisation is evident in IPF and represent an interesting aspect of IPF pathology **(Intro. 2.3.2.)**. HBECs were a kind gift from Dr Jo Porter (University College London) and were cultured in alpha-minimum essential medium (αMEM) (w/ L-glutamine and penicillin-streptomycin) (Lonza, Switzerland), with 10% FBS.

2.1.4. Primary fibroblast isolation

Primary human lung fibroblasts (HLFs) were isolated from patient tissue via a standard method of explantation. This process started with the surgical removal of lung tissue by the Cardiothoracic surgery team at the Royal Devon & Exeter Hospital (RD&E). Tissue that was surplus to requirements for diagnostic purposes was stored on ice and transport to the lab. Tissue sections were further dissected into 1 mm^3 pieces. These explants were recessed into 10 cm^2 tissue culture dishes and covered in a minimal volume of Dulbecco's modified eagle medium (DMEM) (Gibco, UK), 20% FBS with Amphotericin-B (2.5 μg/ml) (VWR, UK). Plates were incubated for 24 hrs prior to the addition of more media, submerging the explants. These plates were cultured for a further 3–5 weeks to allow cell outgrowth, without media change but with Amphotericin-B addition every 3-4 days. When good outgrowth had occurred, plates were washed in serum-free media, trypsinised and passaged into T175 flasks.
Confirmation of the successful isolation of a fibroblastic population of cells was achieved by positive immunofluorescent staining for the mesenchymal marker vimentin and the absence of staining for the epithelial marker cadherin (CDH1). Cells were then available for use in experiments or for population expansion.

2.1.5. Primary HLFs and continuous culture

Of the cells derived by this process during this project, seven were normal HLF lines (NHLFs). These cells were derived from the marginal tissue surrounding a tumour resection, tissue was free of any obvious pathology. Of the seven, five were from males, two from females and the average age of donor was 72 years-old.

Fibrotic HLFs (FHLFs) were derived in-house from one patient during this project; three other primary FHLF lines (BR001-3) were provided as a gift from Professor Ann Millar (University of Bristol). All IPF tissue was obtained by video-assisted, thoracic surgical biopsy and was used to assist with the diagnosis of IPF via histological identification of a

UIP pattern. All donors were subsequently confirmed to have IPF. Donor information for explanted HLFs is provided in **(*Table*.2.1.1.)** with cells ascribed a donor ID as stipulated by the RD&E. All HLFs were cultured in DMEM (w/ high glucose, L-glutamine, phenol red, penicillin-streptomycin; and w/o sodium pyruvate and HEPES) 10% FBS, the amphotericin used in the early stages of explantation was not used during continuous culture.

All primary cells were used in experiments between passage 3 and 11. Population doublings were not consistently accounted for, but the passage range was used under the assumption from previous work in this lab that significant phenotypic changes do not occur within this range, and that the observable behaviour of a primary cell line at p11 should reflect, with equivalence, the behaviour at p3.

Donor ID	Normal / Fibrotic	GENDER	AGE
TB0908	Fibrotic	M	74
TB0912	Normal	F	75
TB0916	Normal	M	63
TB0917	Normal	M	66
TB0918	Normal	M	76
TB0921	Normal	F	79
TB0932	Normal	M	68

Table 2.1.1. Human lung fibroblast cell donor information.

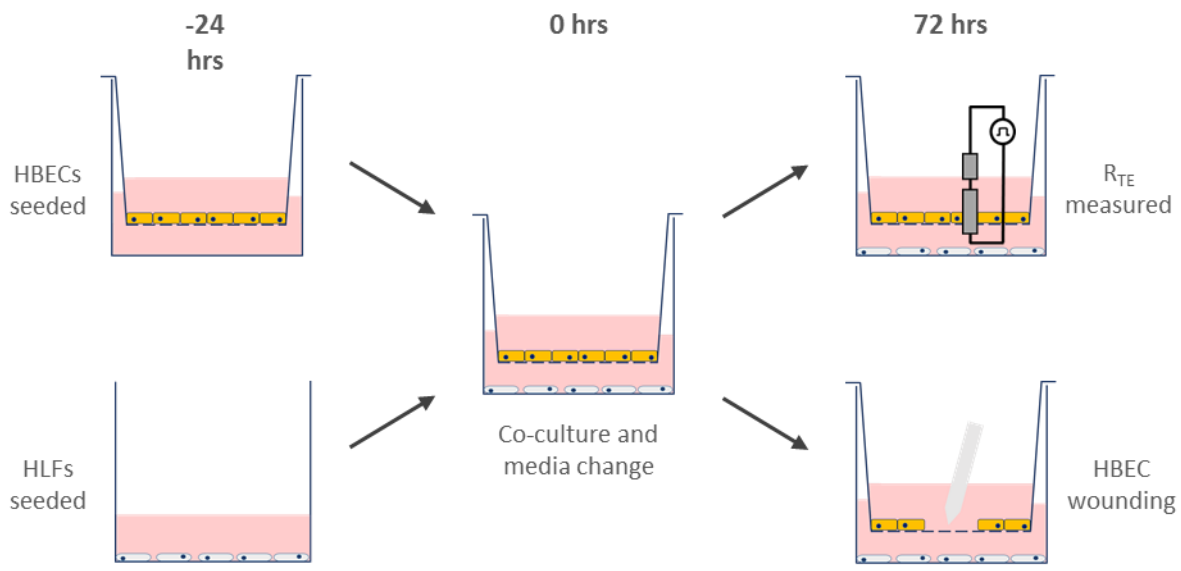

Figure 2.1.1. Schematic representation of co-culture set-up and experimental protocol. HBECs (22,000 cells/insert) and HLFs (12,000 cells/well) were seeded separately at -24 hrs and then transferred to co-culture at 0 hrs, when the media was changed. Co-cultures were maintained for 72 hrs. R_{TE} was measured and wound healing assays performed.

2.1.6. Co-culture systems

Experimentation in co-culture required the use of transwell, hanging inserts (Greiner Bio-One, Austria). A 24-well size was used with a culture area of 33.6 mm^2. Inserts had a

transparent PET membrane with 0.4µm diameter pores, at a density of $2x10^6$ cm^{-2}. The membrane was suitable for HBEC culture, allowing secretory component exchange. The inserts do not come into contact with cells co-cultured basolaterally and do not cause cell damage or prevent growth. For co-culture experiments, at -24 hrs, HLFs were seeded at a density of 12,000 cells/well (unless stated otherwise) in an experimental, 24-well plate. HLFs were cultured in DMEM 10% FBS and not seeded into the outer wells of experimental plates, these were filled with media, maintaining humidity in co-culture experiments. HBECs were concurrently seeded at a density of 22,000 cells/well in transwell inserts in a separate plate, with αMEM-/10% FBS. 24 hrs later, at 0 hr, the inserts were transferred into co-culture with HLFs. This coincided with media change to a 1:1 mix of DMEM /-αMEM 10% FBS. Media was not changed again for the duration of the experiment **(*Figure* 2.1.1)**. Though serum was used throughout all experiments it is appreciated that the array of different factors within potentially add an unnecessary level complexity to the co-culture system. The conditions for co-culture experiments, including cell number, time-course and the media used was previously optimised, with the most robust set up used throughout this investigation.

2.1.7. Stress-induced premature senescence (SIPS)

For the investigation of senescence in NHLFs, SIPS was induced in NHLFs using H_2O_2 (H_2O_2; 30% w/w [= 9.79 M] in H_2O, Sigma Aldrich). Reproducing a consistent and equal burden of senescence across experiments was extremely difficult to achieve; different NHLF lines responded differently to H_2O_2 treatment with large variations in toxicity that were unexpected. Consequently, the protocol was individually tailored to each cell isolate to achieve reproducible senescence across donors. Quantification of the percentage of senescent cells was performed and this displayed along with the experimental data. What follows is a generalised form of the SIPS protocol.

NHLFs were seeded at $1.0x10^6$ cells / T75 flask and allowed to adhere overnight under normal conditions. For the following 5 days flasks were treated with 200 (±100) µM H_2O_2 daily (am). On day 6 flasks were passaged 1 in 3 (±1) and allowed to adhere overnight.

On day 7 the media was changed, and cells allowed to recover for up to a further 6 days. On day 13 cells were passaged, counted and seeded for experiments.

2.2 Cell-based Assays

2.2.1. Trans-epithelial electrical resistance measurements

Trans-epithelial electrical resistance (R_{TE}) provides a measure of ionic permeability, indicative of cell monolayer development. The EVOM2, Epithelial Volt/Ohm Meter (World Precision Instruments, USA) was used to measure R_{TE}. This instrument uses an STX2 chopstick electrode to apply an AC current across the epithelial layer via two silver coated electrodes. The voltage is measured and resistance in Ohms calculated. R_{TE} data are expressed in KΩ cm^2. The average Ω reading across a blank insert membrane was 450 Ω (n = 5, SEM = 13 Ω). The culture surface of each insert was 3.36 mm^2. R_{TE} was calculated by: *((reading – blank reading) / surface area) / 1,000*.

2.2.2. Wound healing assays

Wound healing assays were performed throughout this investigation to identify the capacity of HBECs to re-epithelialise after injury. For all wound healing assays, HBECs were cultured on transwell inserts for 72 hrs without media change. Inserts were then removed and placed in a 12-well plate. Using a p200 pipette tip, a scratch was drawn down the centre of the insert, wounding the cells. Without media change, inserts were then returned to their respective culture conditions. Immediately after wounding (0 hrs) cells were imaged using an EVOS XL Core cell imaging system (Invitrogen, UK). Images were taken again at various timepoints up to 9 hrs. Quantification of the percentage wound closure was performed using ImageJ. For each wounded HBEC culture, the wound void was demarcated on ImageJ, allowing calculation of the percentage area of the wound. The macro used on ImageJ was:

```
run("Fill", "slice");
run("Clear Outside");
run("Make Binary");
run("Measure");
```

The percentage wound closure was calculated by finding the percentage by which each wound void had decreased in area at each timepoint.

2.2.3. SA-βgal activity staining

SA-βgal staining works on the principal that, due to an excess accumulation of damaged organelles and macro-molecules during senescence, there is a significant increase in lysosomal β-D-galactosidase activity, enough to be detectable at a sub-optimal pH of 6.0 [249]. This activity has been robustly identified as a characteristic unique to senescent cells, although some cells maintained at confluence can also display this activity. The protocol used to detect SA-βgal activity was taken directly from ref. [249], following the chromogenic assay method.

Staining

The composition of 1 ml of X-gal staining solution was achieved according to **(*Table*.2.2.1)**. The reagents used were made up in dH_2O and included: 100mM citric acid solution, $C_6H_8O_7.H_2O$; 200 mM sodium phosphate (dibasic) solution, $NaH_2PO_4.H_2O$; 100 mM potassium hexacyano-ferrate (II) trihydrate solution, $K_4[Fe(CN)_6]$ $3H_2O$; 100 mM Potassium hexacyano-ferrate (III) solution, $K_3[Fe(CN)_6]$; 5 M sodium chloride, NaCl; 1 M magnesium chloride hexahydrate solution, $MgCl_2.6H_2O$; 20 mg/ml 5-Bromo-4-chloro-3indolyl β-D-galactosidase (X-gal), made up in N,N-dimethylformamide. All reagents were purchased from Sigma Aldrich, UK. Each component of the solution was made in advance and stored at 4 ^oC. The final solution was made on the day of staining.

Cells, cultured for at least 24 hrs post seeding, were washed with PBS 3x for 10 sec then fixed for 20 min at RT in 4% paraformaldehyde (PFA) (Fisher Bioreagents, USA). This was followed by a 3x 5 min PBS wash at RT. Staining solution was then added, and PBS added to any remaining empty wells (to maintain humidity). The plate was then sealed in parafilm and incubated at 37 ^oC overnight. After incubation, cells were washed 1x 1 min

in PBS at RT prior to imaging using an EVOS XL Core cell imaging system (Invitrogen, UK) SA-βgal activity was highlighted in cells via a blue chromogenic stain.

Reagent	Final Concentration	Volume
Citric acid / sodium phosphate buffer (pH 6.0)	200 mM	200 µl
$K_4[Fe(CN)_6]$ $3H_2O$	100 mM	50 µl
$K_3[Fe(CN)_6]$	100 mM	50 µl
NaCl	5 M	30 µl
$MgCl_2.6H_2O$	1 M	2 µl
X-gal	20 mg/ml	50 µl
Cell culture grade H_2O	1x	618 µl
	Total Volume	1,000 µl

Table 2.2.1. Reagents used for 1 ml of X-gal SA-βgal stain.

SA-βgal quantification

SA-βgal activity was quantified using ImageJ. Images of cells were taken (at 10x magnification: 400 μm scale bar) and the total number of cells, and the number of blue staining cells, were counted using the ImageJ cell counter. This allowed percentage positivity to be calculated.

2.2.4. Mitochondrial membrane potential measurements

2,000 cells/well were seeded into clear 96-well plates and allowed to adhere overnight under normal culture conditions. Tetramethylrhodamine, ethyl ester (TMRE) (Sigma Aldrich, UK) and carbonyl cyanide-4-(trifluoromethoxy)phenylhydrazone (FCCP) (Sigma Aldrich, UK) were diluted from stock in normal media. FCCP was added to the media of each relevant well and incubated for 10 min. The media was removed and replaced with a dilution of TMRE. The plate was then incubated for 15 min followed by 2x 30sec wash with PBS. PBS was then replaced with normal media. The plate was then read using a SpectraMax M2e microplate reader (VWR, UK). A bottom read at excitation/emission 548/575 nm was performed. Data are presented as fluorescence intensity.

2.2.5. Cell viability and cell counting assays

Cell viability was assessed using the ReadyProbes Cell Viability Imaging Kit (Invitrogen, UK). This kit comprises of a NucBlue Live reagent and NucGreen Dead reagent. NucBlue stains the nuclei of all cells, with an excitation/emission maxima of 360/460 nm. This staining was visible with the EVOS FL cell imaging system DAPI filter. NucGreen stains dead cells that have compromised cell membranes. Excitation/emission maxima of 504/523 nm allow visualisation with the GFP filter. For live cell staining, 2 drops/ml of each reagent was added to the cell media. Cells were then incubated under normal conditions for 30 min and then viewed by fluorescence microscopy. To count all cells, images were taken and analysed using the ImageJ 3D objects counter plugin. This identified all cells with NucBlue staining. Cells also staining for NucGreen were counted manually.

Alamar blue (Sigma Aldrich, UK) was also used to quantify cell number. The reducing environment of live cells allows the conversion of resazurin, the active component of Alamar blue, from a non-fluorescent, blue compound to resorufin, a highly fluorescent, red compound. Resazurin is non-toxic and cell permeable. For each cell line assessed, a serial dilution of seeding densities was plated and allowed to adhere overnight. Alamar blue was then diluted 1:10 into the cell media and incubated under normal conditions for 2 hr 30 min. The resulting fluorescence was measured using a SpectraMax M2e microplate reader. Fluorescence intensity was plotted against cell seeding density, and linear regression analysis performed, giving a standard curve. This protocol was repeated for proliferation experiments. The number of cells in experimental conditions was calculated using the standard curve.

Cell number was further quantified in several experiments using a haemocytometer. HLFs, seeded in a co- or mono-culture format at 12,000 cells / well (in a 24-well plate), were washed and trypsinised with 100 µl of trypsin. After 2 mins, this was neutralised by addition of 100 µl of media (w/ 10% FBS) and mixed via pipetting. 8 µl of cell suspension was then transferred to a window of a haemocytometer and the cells were counted across 5 grids. This was repeated with a second aliquot of suspension and the total number of cells divided by the number of grids used, giving an average. This was used to calculate the number of cells per well.

2.3 Molecular Assays

2.3.1. Reverse transcription – quantitative polymerase chain reaction (RT-qPCR)

RNA isolation

Working areas (fume-hood, work bench) and pipettes were cleaned with RNAse Away spray (Thermo Scientific, USA). Cell culture media was removed from tissue culture plates and TRI reagent (Sigma Aldrich, UK) added in a fume-hood. Using a pipette tip,

the surface of each plate was scraped and the reagent repetitively mixed. Samples were then transferred into 1.5 ml micro-centrifuge tubes and stored at -20 ^{o}C until subsequent use.

From -20 ^{o}C, samples were returned to a clean fume-hood and allowed to defrost and stand at RT for 5 min. 200 µl molecular biology grade chloroform (Thermo Scientific, USA) was then added (per 1 ml TRI reagent) and samples were vortexed for 8 sec. Samples were incubated at RT for 10 min prior to centrifugation at 4 ^{o}C, 14,000 *g* for 15 min. This created three phases: a lower phase = organic protein (pink), intermediate phase = DNA (white) and an upper phase = aqueous, RNA (clear). The aqueous phase was carefully removed from each tube, taking care not to contaminate with protein or DNA, and transferred to a fresh micro-centrifuge tube on ice. 500 µl molecular biology grade isopropanol (Thermo Scientific, USA) was then added (per 1 ml TRI reagent) and 1 µl Glycoblue RNA co-precipitant (15mg/ml; Ambion, UK). Isopropanol facilitates RNA precipitation and Glycoblue gives the RNA a blue colouration. Samples were inverted to mix and allowed to stand at RT for 10 min prior to centrifugation at 4 ^{o}C, 13,000 *g* for 12 min. This centrifugation created a blue RNA pellet. On ice, the supernatant was removed by vacuum pump and the pellet was washed via addition of 500 µl ice-cold 75% ethanol – made up in 0.1% diethyl pyrocarbonate (DEPC) ddH_2O (Sigma Aldrich, UK). The samples were inverted to detach the pellet and aid the ethanol washing. Samples were then centrifuged again at 4 ^{o}C, 10,000 *g* for 8 min, returned to ice and the supernatant aspirated. After aspiration, with the micro-centrifuge lids left open, the samples were left at RT to dry. The pellets were then re-suspended in 11 µl ice-cold, nuclease-free H_2O (Ambion, UK) via repetitive, but gentle, pipetting. Samples could then be stored at -20 ^{o}C until required.

To quantify sample RNA content, 1 µl of sample was analysed using a NanoDrop 8000 spectrophotometer (Thermo Scientific, USA). Prior to this the machine was calibrated and blanked (with nuclease-free H_2O). RNA concentration was measured in ng/µl. Protein contamination was also measured via the A_{260}/A_{280} ratio. A ratio of 2.00 was considered optimal, samples with a ratio below 1.70 were discounted for further use.

DNAse treatment

To eliminate any genomic DNA contamination, samples were treated with a DNAse kit. 1.2 µl 10X Precision DNAse reaction buffer (Primerdesign, UK) was added to samples on ice, along with 0.5 µl Precision DNAse enzyme (Primerdesign, UK), per 10 µl sample. Samples were briefly vortexed and pulse-spun. Using a thermocycling heat-block, samples were then incubated at 30 ^{o}C for 10 min (to activate the enzyme), followed by incubation at 55 ^{o}C for 5 min (to deactivate the enzyme). Samples were then returned to 4 ^{o}C.

cDNA synthesis

RNA samples were diluted to equivalent concentrations with nuclease-free H_2O. Samples were then briefly vortexed and pulse-spun. qScript reagents were defrosted on ice, vortexed and pulse-spun. A cDNA synthesis reaction mix was created according to ***Table*.2.3.1a** using qScript 5X Reaction Mix (Quanta Biosciences, UK) and qScript Reverse Transcriptase (Quanta Biosciences, UK). cDNA synthesis reaction mixes were briefly vortexed and pulse-spun prior to an incubation protocol of: 22 ^{o}C for 5 min, 42 ^{o}C for 30 min, 85 ^{o}C for 5min and a final hold at 4 ^{o}C. cDNA samples were then diluted 1:2 with nuclease-free H_2O. Samples could then be stored at -20 ^{o}C, until required.

Reference genes

The reference genes *GAPDH* and *B2M* were used for all RT-qPCR experiments. The validity of these reference genes was confirmed using a GeNorm Reference gene kit (Primerdesign, UK). This kit comprises of 11 housekeeping genes (*CYC1, ACTB, SDHA, TOP1, ATP5B, GAPDH, RPL13A, EIF4A2, UBC, B2M* and *YWHAZ*) which were tested on HLF samples from NHLF or FHLF mono-cultures, either 24 or 144 hrs post-seeding, or cocultures, 144 hrs post-seeding. The resulting Ct values were analysed using qBASE+ software. The average expression stability of reference targets was analysed to give a GeNorm M value, of which values <0.50 were considered stable for reference gene use. For the experimental conditions described, *GAPDH* had an M value <0.40 and *B2M* a value <0.34.

RT-qPCR reaction

For the RT-qPCR reaction, 20X TaqMan Gene Expression Assay (Thermo Scientific, USA), including genes of interest and reference genes, PrecisionPLUS Master Mix (Primerdesign, UK) and cDNA samples were defrosted on ice, vortexed and pulse-spun. RT-qPCR reaction mixes were made according to ***Table*.2.3.1b**. 8 µl of each mix was dispensed into the relevant well of an RT-qPCR 96-well plate (Primerdesign, UK). This was followed by 2 µl of cDNA. Technical duplications of each reaction were not performed. An optical adhesive seal (Primerdesign, UK) was then firmly applied and the reaction plate spun for 1 min in a plate centrifuge. The plate was then run on a Roche LightCyler96 RT-qPCR machine (Roche, UK). The PCR reaction was setup as follows: 1x pre-incubation (95 ^{o}C for 120 sec), followed by, 40x 2-step amplification (95 ^{o}C for 10 sec, 60 ^{o}C for 30 sec), ending with 1x cooling (37 ^{o}C for 30 sec). For the TaqMan primers used, the reaction was measured on the FAM channel. The TaqMan primers used were predesigned, with an amplification efficiency of 100% (±10%), according to the manufacturer. A list of primers used can be found in ***Table*.2.3.2**.

Relative quantification analysis

Ct values were obtained for each reaction using the LightCycler96 software. A Ct value is described as the cycle at which the fluorescence of a sample rises above the background fluorescence and is pre-determined by the software. The geometric mean of reference gene Ct values was calculated for each experimental sample. This value was

A

Reagent	Volume per Reaction
qScript 5X Reaction Mix	4.0 µl
qScript Reverse Transcriptase	1.0 µl
RNA sample	10 pg – 1µg total RNA
Nuclease-free H_2O	Up to 20.0 µl
Total Volume	20.0 µl

B

Reagent	Volume per Reaction
20X TaqMan Primer	0.5 µl
PrecisionPLUS Master mix	5 µl
Nuclease free water	2.5 µl
Total Volume	8.0 µl

C

Reagent	Volume per Reaction
PrecisionPLUS Master mix SYBR	6.25 µl
Primer Mix	0.5 µl
DNA Sample	1 - 100ng DNA
Nuclease free water	Up to 12.5µl
Total Volume	12.5 µl

Table 2.3.1. RT-qPCR reaction mixes. (A) cDNA synthesis reaction mix **(B)** RT-qPCR reaction mix for TaqMan primers **(C)** RT-qPCR reaction mix for mtDNA copy number quantification.

Target Gene	Dye	Assay ID	Supplier
B2M	TaqMan FAM-MGB	Hs00187842_m1	Thermo Scientific, UK
CDH1	TaqMan FAM-MGB	Hs01023895_m1	Thermo Scientific, UK
CDKN1A	TaqMan FAM-MGB	Hs00355782_m1	Thermo Scientific, UK
CDKN2A	TaqMan FAM-MGB	Hs00923894_m1	Thermo Scientific, UK
CSF3	TaqMan FAM-MGB	Hs00738432_g1	Thermo Scientific, UK
CXCL1	TaqMan FAM-MGB	Hs00236937_m1	Thermo Scientific, UK
CXCL8	TaqMan FAM-MGB	Hs00174103_m1	Thermo Scientific, UK
DNM1L	TaqMan FAM-MGB	Hs01552605_m1	Thermo Scientific, UK
FGF7	TaqMan FAM-MGB	Hs00940253_m1	Thermo Scientific, UK
GAPDH	TaqMan FAM-MGB	Hs02758991_g1	Thermo Scientific, UK
HGF	TaqMan FAM-MGB	Hs00300159_m1	Thermo Scientific, UK
IL1A	TaqMan FAM-MGB	Hs00174092_m1	Thermo Scientific, UK
IL1B	TaqMan FAM-MGB	Hs01555410_m1	Thermo Scientific, UK
IL33	TaqMan FAM-MGB	Hs00369211_m1	Thermo Scientific, UK
IL6	TaqMan FAM-MGB	Hs00985639_m1	Thermo Scientific, UK
KRT5	TaqMan FAM-MGB	Hs00361185_m1	Thermo Scientific, UK
MFN1	TaqMan FAM-MGB	Hs00966851_m1	Thermo Scientific, UK
PINK1	TaqMan FAM-MGB	Hs00260868_m1	Thermo Scientific, UK
TNFA	TaqMan FAM-MGB	Hs01113624_g1	Thermo Scientific, UK
VIM	TaqMan FAM-MGB	Hs00958111_m1	Thermo Scientific, UK
WNT3A	TaqMan FAM-MGB	Hs00263977_m1	Thermo Scientific, UK

Table 2.3.2. Table of RT-qPCR primers used. Primers used throughout experiments are listed along with their respective assay ID from Thermo Scientific, UK.

then subtracted from the Ct value of each corresponding gene of interest, giving a ΔCt value. The average ΔCt value for experimental controls was calculated, giving a calibrator value. This was subsequently subtracted from all ΔCt values to give a ΔΔCt value. All

statistical analyses were performed using ΔΔCt values. RT-qPCR data is shown using average fold change values. Fold change was calculated by finding the antilogarithmic value of each logarithmic ΔΔCt value.

Limitations of analysis

Though a standard approach for analysing and presenting qPCR data, this approach is caveated by that fact that individual genes are calibrated and normalised to themselves. This approach means that the relative quantity of other genes assessed is not reflected in the fold change value. Therefore, a gene of interest may display a 4-fold increase under experimental conditions, appearing to be an extremely significant result when compared to a 2-fold increase for an alternate gene, however the quantity of RNA measured may extremely small and the differences of no real biological impact. This issue can be overcome by calibrating results to the controls of all genes analysed. This can better display the relationship between RNA levels for the different genes analysed. Though useful, however, this approach is also flawed due the experiments in this investigation utilising various panels of transcripts. Having different genes means that the relative change between experiments is not comparable, as a the addition of a certain gene could vastly skew the observable relative quantity. If the same gene set was used each time, with genes known to affect each other's expression and regulation, whole gene-set calibration would be useful. Therefore, with these considerations in mind, the ΔΔCt method with graphs plotting fold change was used throughout.

2.3.2. Relative mtDNA Copy Number Analysis

The 16-kilobase mitochondrial genome (mtDNA) encodes 13 mitochondrial proteins required for the electron transport chain. There are many copies of this genome throughout a cell, with their replication occurring independently of the cell cycle. The copy number of mtDNA can be indicative of cell health and mitochondrial function. The human mtDNA monitoring primer set quantifies the relative mtDNA copy number by amplifying two regions of mtDNA (*SCLO2B1* and *SERPINA1*) and two regions of nuclear

DNA (nDNA) (*ND1* and *ND5*). nDNA content is used as a reference for mtDNA and the difference in Ct values is used to calculate mtDNA copy number.

DNA preparation

DNA was isolated using the PureLink genomic DNA mini kit, which comprised of: proteinase-K, RNase-A, genomic lysis/binding buffer, spin columns, collection tubes, wash buffer-1, wash buffer-2, and genomic elution buffer (Invitrogen, UK). Adherent cells were trypsinised and centrifuged (4 min, 200 *g*). The supernatant was then removed and the cellular pellet re-suspended in 200 µl PBS. 20 µl of proteinase-K and 20 µl of RNase-A were added and the sample briefly vortexed. Sample was then incubated at RT for 2 min. 200 µl genomic lysis/binding buffer was added, the sample briefly vortexed and then incubated in a waterbath for 10 min at 55 ^{o}C. 200 µl of 100% ethanol (Sigma Aldrich, UK) was added and the sample briefly vortexed. The 640 µl lysate was then transferred to a spin column (with collection tube) and centrifuged at 10,000 *g* for 1 min. The collection tube was changed, 500 µl wash buffer-1 added and the sample centrifuged again at 10,000 *g* for 1 min. This step was repeated using wash buffer-2, with centrifugation at 22,000 *g* for 3 min. 50 µl of genomic elution buffer was then added to the spin column and it was incubated for 1 min at RT. The spin column, with fresh collection tube, was then spun at 10,000 *g* for 1 min. The elution buffer was taken from the collection tube and re-added to the spin column. It was then centrifuged at 22,000 *g* for 2 mins. The eluted genomic DNA was then transferred to a fresh micro-centrifuge tube and stored at -20 ^{o}C.

RT-qPCR

DNA samples and RT-qPCR reagents were defrosted on ice. DNA content was measured using a NanoDrop 8000 spectrophotometer (Thermo Scientific, USA) and samples diluted to equivalent concentrations with nuclease-free H_2O (Ambion, UK). The reaction mix was formulated according to ***Table*.2.3.1c** using Human mitochondrial DNA monitoring primer set (Clontech, USA) and PrecisionPLUS Master Mix w/ SYBR green (Primerdesign, UK). A mix of nuclease-free H_2O and PrecisionPLUS master mix was first added to a RT-qPCR 96-well plate (Primerdesign, UK), followed by DNA samples, then

the relevant primers. The plate was sealed with an optical adhesive seal (Primerdesign, UK) and spun for 1min. The reaction was then performed on a Roche LightCyler96 RTqPCR machine (Roche, UK). The PCR reaction was setup as follows: 1x pre-incubation (95 ^{o}C for 120 sec), followed by, 40x 2-step amplification (95 ^{o}C for 10 sec, 60 ^{o}C for 45 sec), ending with 1x melting (65 ^{o}C for 60 sec, 95 ^{o}C for 10 sec and 97 ^{o}C for 1 sec). For the primers used, the reaction was measured on the SYBR green channel.

Analysis

To calculate mtDNA relative copy number, two ΔCt values were calculated, from the difference in Ct values of *ND1* and *SCLO2B1*, and *ND5* and *SERPINA1*. These values were converted to $2^{\Delta Ct}$ and averaged, giving a mean copy number of mtDNA for each sample.

2.3.3. Western blotting

Protein preparation

The media of cells in culture was removed and the cells washed twice in PBS. Tissue culture plates were kept on ice for 5min prior to PBS aspiration and addition of ice-cold RIPA buffer, (10ml): 100 µl IGEPAL CA-630 (Sigma Aldrich, UK), 0.05 g sodium deoxycholate (Fisher BioReagents, USA), 100 µl 10% sodium dodecyl sulphate (SDS) (Fisher BioReagents, USA), 1x tablet Complete Mini Protease Inhibitor Cocktail (Roche, UK); 9.8 ml PBS. For investigation into phosphorylated protein expression, PhosphoSafe Extraction reagent (Millipore, UK) was used, which better preserves protein phosphorylation status. Using a pipette tip, cells in buffer were scraped and then transferred to micro-centrifuge tubes. These were then stored at -80 ^{o}C for later use. Samples were defrosted on ice and centrifuged at 4 ^{o}C, 20,000 *g* for 5 min. The supernatant was then transferred to fresh micro-centrifuge tubes on ice.

For protein quantification, the Pierce BCA protein assay kit (Pierce, USA) was used. A serial dilution of known protein standards (starting from a solution of 2 mg/ml bovine serum albumin (BSA - Millipore, UK)) was made in a 96-well plate as a standard curve. 10 µl of each protein sample was added to a well, followed by 100 µl BCA solution. Plates

were covered and then incubated for 15-30 min at 37 ^{o}C. Plates were analysed using a FLUOstar microplate reader (BMG Labtech, Germany). Using MARS software, a standard curve was generated from the BSA standards and sample protein concentration was calculated. Samples were diluted in ddH_2O to give equivalent protein concentrations.

Gel loading and transfer

On ice, protein samples were prepared for gel loading according to ***Table*.2.3.3** using 4x Bolt LDS sample buffer (Invitrogen, UK) and 10x Bolt sample reducing agent (Invitrogen, UK). Samples were then incubated at 70 ^{o}C for 10 min. A Bolt Mini Gel Tank (Invitrogen, UK) was then assembled and half filled with running buffer, (500 ml): 20 ml 20x Bolt MOPS SDS running buffer (Invitrogen, UK) and 480 ml ddH_2O. Bolt 4-12% Bis-Tris Plus gels (Invitrogen, UK) were used and 1 µl of SeeBlue Plus2 pre-stained protein standard (Invitrogen, UK) was added to the left-hand well of each gel. 35 µl of each protein sample was then added to the adjacent wells. The remaining running buffer was added to the tank and the gel run at 200 V for 22 min (or for 35 min when investigating zonula occludens-1 (ZO-1) protein expression).

After running, gels were removed from their cassette and incubated in transfer buffer, (1L): 3.03 g tris base (Fisher BioReagents, USA); 14.4 g glycine (Fisher BioReagents, USA); 200 ml methanol (Fisher BioReagents, USA) and 800 ml ddH_2O, for 15 min at RT. 3MM chromatography filter papers (Whatman, USA) were also soaked in transfer buffer. An Immobilon-FL PVDF membrane (Millipore, UK) was first wet in methanol then soaked in transfer buffer. Transfer sandwiches were then made according to the following order: electrode, sponge, 4x filter paper, gel, membrane, 4x filter paper, sponge, electrode. Sandwiches were placed in a wet transfer tank with an ice pack and magnetic stirrer, this was then filled with transfer buffer. Proteins were transferred for 1 hr at 100 V, changing the ice pack every 30 min (ZO-1 transfer was performed over 1 hr 30 min).

Reagent	Reduced Sample
Sample	x µl (equal concentration)
LDS Sample Buffer (4x)	10 µl
Reducing Agent (10x)	4 µl
Deionised Water	up to 26 µl
Total Volume	**40 µl**

Table 2.3.3. Western blot protein reduction sample mix.

Antibody staining

After transfer, membranes were removed and washed, 3x for 5 min in TBS. They were then incubated in blocking buffer (3% BSA – TBS) for 1 hr at RT. This was followed by a 3x 5 min wash in TBST, made using TBS and Tween20 (Sigma Aldrich, UK). The primary antibody of interest and β-actin mouse mAb loading control (Sigma Aldrich, UK) were diluted in antibody dilution buffer (3% BSA – TBST). The antibodies used can be found in ***Table*2.3.4**. Membranes were incubated for 1hr at RT. A 3x 5min wash in TBST followed and membranes were then incubated with the secondary antibodies, goat anti-mouse IgG-HRP (Santa Cruz, USA) and goat anti-rabbit IgG-HRP (Santa Cruz, USA), made up in antibody dilution buffer. A final 3x 5min TBST wash was performed.

Imaging and densitometric analysis

Blots were imaged via chemiluminescence. A 500 µl chemiluminescence reaction mix was made per blot. This consisted of 200 µl each of parts A and B SuperSignal West Pico chemiluminescent substrate (Thermo Scientific, USA), and 50 µl each of parts A and B

Antibody	Raised in	Supplier	Application	Dilution used
Anti-p21	Rabbit monoclonal	Abcam, UK	IMF WB	IMF 1:500 WB 1:500
Anti-Phospho-Stat3 (Try705)	Rabbit monoclonal	Cell Signalling, USA	WB	1:1,500
Anti-Stat3	Mouse monoclonal	Cell Signalling, USA	WB	1:750
Anti-β-actin	Mouse monoclonal	Sigma Aldrich, UK	WB	1:25,000
Anti-ATPB	Mouse monoclonal	Abcam, UK	IMF	1:500
Anti-ZO-1	Mouse monoclonal	Invitrogen, UK	IMF WB	IMF 1:500 WB 1:750
Texas Red-X Phalloidin	-	Invitrogen, UK	IMF	1:1,000
Alexa Fluor 488	Goat anti-mouse	Invitrogen, UK	IMF	1:500
Alexa Fluor 595	Goat anti-rabbit	Invitrogen, UK	IMF	1:500
IgG-HRP	Goat anti-mouse	Santa Cruz, USA	WB	1:5,000
IgG-HRP	Goat anti-rabbit	Santa Cruz, USA	WB	1:2,500

Table 2.3.4. Table of primary and secondary antibodies used.

SuperSignal West Femto chemiluminescent substrate (Thermo Scientific, USA). This mix was added to each blot prior to imaging via an Azure c600 blot imaging system (Cambridge Biosciences, UK). Densitometric analysis was performed using the ImageJ Gel Analyser plugin. The optical density of each band was normalised to its loading control (β-actin) and calibrated to the experimental control, giving a relative density.

2.3.4. Immunofluorescence (IMF) staining

Protocol and imaging

For IMF, cells were seeded onto Lab-Tek Chamber Slide system (Thermo Scientific, USA) and cultured for at least 24 hrs prior to washing and fixation with 4% PFA, clarified with NaOH. For HBECs cultured on transwell inserts, inserts were transferred to a fresh plate for the IMF staining process. IMF was performed in accordance with the protocol in ***Table.*2.3.5** using: Triton X-100 (Sigma Aldrich, UK); BSA (Millipore, UK); Goat serum (Sigma Aldrich); DAPI (Sigma Aldrich); and ProLong Gold Antifade mountant (Invitrogen, UK). The antibodies used can be found in ***Table*.2.3.4**. For insert-cultured HBECS, mounting was achieved by dissecting the basal membrane from the inserts with a scalpel. This was then transferred to a glass microscopy slide, with mountant and cover slide then added. After slides were cured in mountant, imaging was performed using an EVOS FL cell imaging system (Invitrogen, UK).

Process	Reagent	Concentration	Time	Repeats	Temp
Wash	TBS	1x	10 sec	3x	RT
Fix	PFA	4%	20 min	1x	RT
Wash	TBS	1x	5 min	3x	RT
Permeabilise	Triton X-100 in 3% BSA- 1x TBS	0.2%	10 min	1x	RT
Wash	TBS	1x	5 min	3x	RT
Block	Goat serum in 3% BSA- 1x TBS	5%	10 min	1x	RT
Primary Ab	Ab in 3% BSA- 1x TBS	Ab specific	Overnight / 1hr	1x	4 °C / RT
Wash	TBS	1x	5 min	3x	RT
Secondary Ab + DAPI	Goat anti-mouse 488 Goat anti-rabbit 595 DAPI 300µM in 3% BSA- 1x TBS	1:500 1:500 1:1000	1 hr	1x	RT in dark
Mounting	Prolong Gold anti-fade	1x	Overnight	1x	RT in dark

Table 2.3.5. Protocol for immunofluorescence staining. Tabular representation of the steps used for IMF staining, highlighting the reagents used, at what concentration, for how long, the number of process repetitions and under what conditions. This protocol was used for all IMF staining.

2.3.5. Analysis of mitochondrial morphology

IMF images were taken of HLFs stained with anti-ATP5B antibody, which binds to a subunit of mitochondrial specific adenosine triphosphate (ATP) synthase. IMF imaging provided a structural outline of the mitochondria and their morphology could be analysed via ImageJ. The following macro was used:

```
run("Subtract Background...",
"rolling=75");
setOption("BlackBackground", false);
run("Make Binary"); run("Erode");
run("Skeletonize");
```

The macro converts Alexa Fluor 488 (bound to ATP5B) signal into skeletonised image. This image represents signal as particles. Thickness is not factored into this process, only the presence of continuous signal, thereby creating a pixilated network of representative mitochondria. This allows quantification of various structural parameters. The particle networks generated could be counted and measured, giving an indication of the number of distinct mitochondria within a cell and the area they occupy. Furthermore, the individual mitochondria themselves could be assessed, providing information on parameters such as the average size of mitochondria within a cell and how the morphologies differ. An example of this analysis is shown in ***Figure* 2.3.1**.

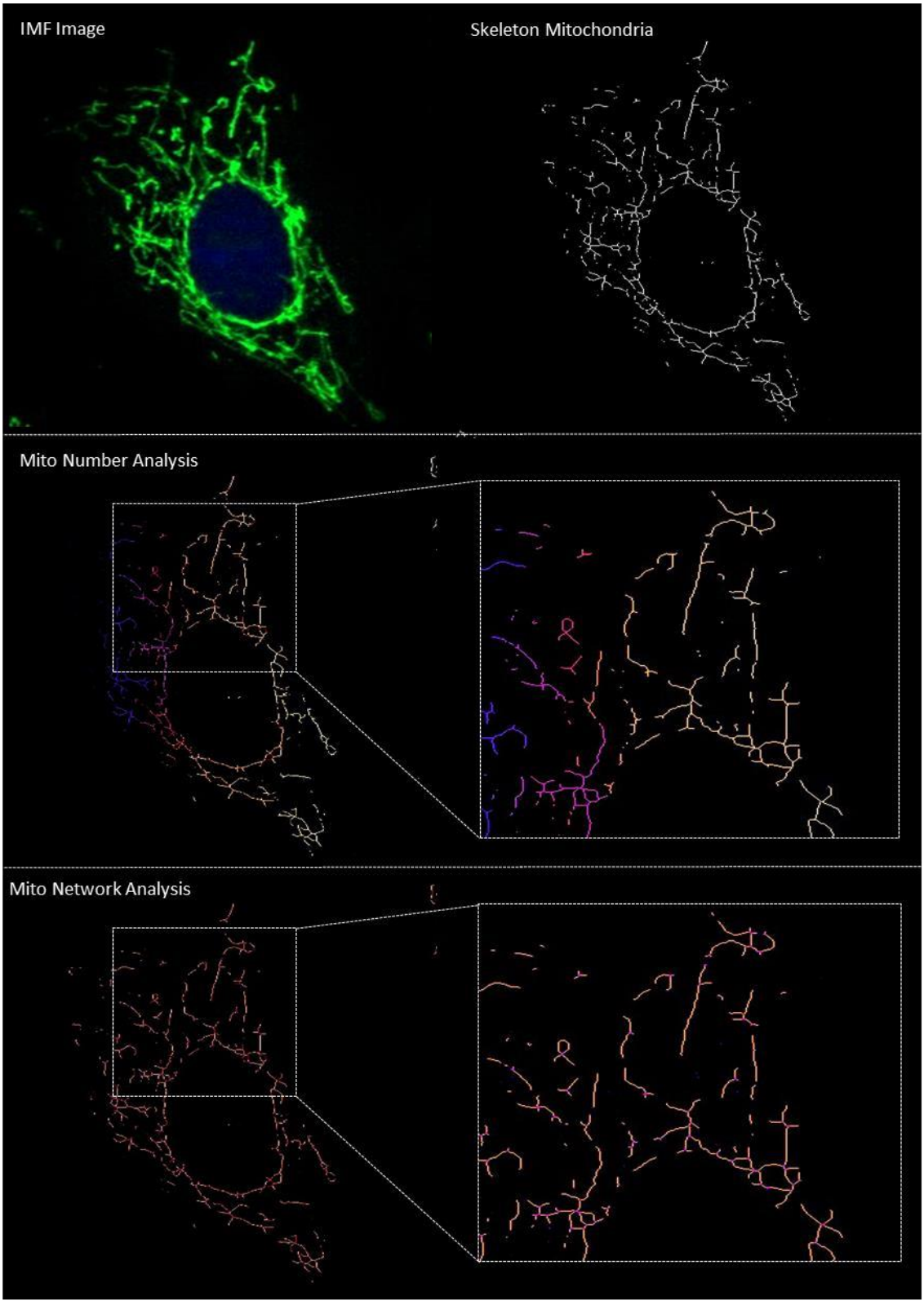

Figure 2.3.1. Representative analyses of mitochondrial morphology. (A) (right) Mitochondrial were stained for ATP5B. (left) Secondary Alexa Fluor 488 signal was converted to a skeletonised image using ImageJ. **(B)** A combination of skeleton and particle analysis allowed measurement of mitochondrial number, area and average size. Images shows distinction of individual mitochondria by colour. **(C)** Network analysis was performed with image showing branches in orange and junctions in pink. **(D)** Parameter values for example, NHLF.

2.3.6. IL-33 enzyme-linked immunosorbent assays (ELISA)

Assay protocol

Samples of basolateral CM, collected from 72 hr mono- or co-cultures, were defrosted on ice after storage at -80 ^{o}C. ELISA was performed using the Human IL-33 DuoSet ELISA (R&D Systems, USA), which contained: human IL-33 capture antibody; human IL-33 detection antibody; human IL-33 standard and streptavidin-HRP. These reagents were used in addition to the DuoSet Ancillary Reagent Kit 2 (R&D Systems, USA), containing: ELISA plate-coating buffer; reagent diluent, stop solution (2N sulfuric acid); colour reagent A (hydrogen peroxide); colour reagent B (tetramethylbenzidine); wash buffer; clear microplates and an ELISA plate sealer. Firstly, capture antibody was diluted to a working concentration in PBS and 100 µl added to a 96-well plate. This plate was incubated overnight at RT. The plate was then washed with 400 µl wash buffer 3x and blocked, via addition of 300 µl reagent diluent to each well. The plate was incubated for 1 hr at RT. A further 3x washes were performed. 100 µl of standards (in reagent diluent) and 100 µl of sample CM was then added to the relevant wells, the plate covered and incubated for 2 hr at RT. 3x washes were performed. 100 µl of detection antibody was then added with another 2hr RT incubation. After a further 3x washes, 100 µl of streptavidin-HRP was added to each well and the plate incubated at RT for 20 min, in the dark. The plate was washed 3x and 100 µl of substrate solution added to each well. Another 20 min incubation at RT in the dark was performed followed by the final addition of 50 µl stop solution to each well. The plate was gently tapped to mix and the optical density (OD) read using a SpectraMax M2e microplate reader (VWR, UK), set to 450 nm and 540 nm.

Analysis

The 540 nm OD readings were subtracted from the 450 nm reading for each well, correcting for optical imperfections in the plate. A standard curve was constructed by plotting the log of human IL-33 standard concentrations against the log of OD values. Regression analysis provided an equation for the subsequent calculation of CM sample IL-33 concentrations.

2.3.7. Multiplex ELISA (Luminex)

Multiplex ELISA assays were performed using a MAGPIX analyser (Millipore, UK). The MAGPIX analyser uses Luminex xMAP technology to perform ELISA-based assays for numerous analytes at one time. Luminex technology utilises sets of 6.45 µm magnetic microspheres, coated with a capture antibody, to detect a range of proteins in a given sample. Each set of beads has a specific proportion of red and infrared fluorophores, creating a unique detection signature. Target proteins bind to the beads, a biotinylated detection antibody is then introduced and the sample is incubated with reporter molecule (streptavidin-phycoerythrin (strep-PE) conjugate). Red and greed LEDs interrogate each bead, which is identified with CCD camera. The 532 nm green 'assay' laser excites the strep-PE conjugate, determining analyte concentration, whilst the 635 nm red 'classify' laser excites the internal fluorophores, identifying the analyte and enabling doublet discrimination by light scatter.

Preparation of reagents

Having been stored at -80 ^{o}C, 500 µl CM samples, obtained from the basolateral compartment of 72 hr mono- or co-cultures, were defrosted on ice. MILLIPLEX Map Kit (Millipore, UK) reagents were reconstituted (if required) and allowed to warm to RT. These reagents included: human cytokine/chemokine standard; human cytokine quality controls 1 and 2; 96-well plat with sealers; assay buffer; 10x wash buffer; human cytokine detection antibodies – premixed 38-plex beads; strep-PE conjugate and bead diluent. Antibody beads were sonicated for 30 sec and vortexed for 1 min prior to use. Quality controls 1 and 2 were reconstituted in dH_2O, inverted to mix and briefly vortexed. The human cytokine/chemokine standard was reconstituted in dH_2O, giving a 10,000 pg/ml concentration standard for all 38 analytes. Standards were created via a 1:5 dilution down to a concentration of 3.2pg/ml. CM samples were also allowed to warm to room temperature.

Immunoassay procedure

Prior to assay running, the Luminex MAGPIX analyser (Millipore, UK) analyser was calibrated. Then, 200 µl of wash buffer was added to each well of the Map Kit, 96-well plate. The plate was shaken for 10min at RT and the buffer removed. 25 µl standard / control was added to the relevant wells, 25 µl of assay buffer was added to sample wells and then 25 µl of matrix solution (non-CM) to all wells. 25 µl of CM samples was added to sample wells and 25 µl of antibody beads to each well. The plate was incubated overnight at 4 ^{o}C. The beads were captured using a handheld magnetic separator block (Millipore, UK) and the plate washed 2x with 200 µl wash buffer. 25 µl of detection antibodies was added to each well, the plate was sealed and then incubated for 1 hr at RT on a plate shaker. 25 µl of strep-PE was added to each well, the plate incubated for 30 min at RT and then washed, as previous. 150 µl Drive fluid 4PK (Millipore, UK) was added to each well and the beads re-suspended for 5 min on a plate shaker. The plate was then run on the MAGPIX analyser.

Analysis

Data was analysed using xPONENT software. Median fluorescent intensity (MFI) data was analysed using a 5-parameter logistic method, allowing calculation of cytokine/chemokine concentrations in each sample. Standard curves for each analyte are displayed in **Appendix 1. (*Figure* 6.1.1.)** along with minimum detection ranges **(*Figure* 6.1.2.)**.

2.4 Statistical Analyses

Biological replication

Throughout this work n numbers were generated using a combination of repeated, independent experiments using cells from a single patient donor and experiments using the cells from different patient donors. Independently repeated experiments were deemed to constitute a biologically distinct repetition due to: differing passage, culture and experimentation at differing times, and cells populations being expanded from

differing subsets of originally expanded tissue explant material. Such combinations of n number are highlighted in figure legends whereby the n number is denoted along with the patient donor identification and the number of times such donor was used.

Statistical testing

Regarding all statistical analysis, despite small sample sizes used throughout experimentation, parametric tests were utilised under the assumption that data had a normal distribution, and this was preferred to the use of non-parametric tests. All data are presented as mean values. All error bars are representative of standard error of mean (SEM). All statistical analysis was performed using GraphPad Prism 5. Analysis between two groups was performed using a student's t-test. Analysis between multiple groups was performed using either 1-way ANOVA, with Tukey's multiple comparisons, or 2-way ANOVA, with Bonferroni multiple comparisons. For analysis between multiple groups with repeated measures over time, 2-way RM ANOVA, with Bonferroni multiple comparisons was used. A difference between groups was deemed statistically significant when the p value for each relevant test was <0.05.

3. Results

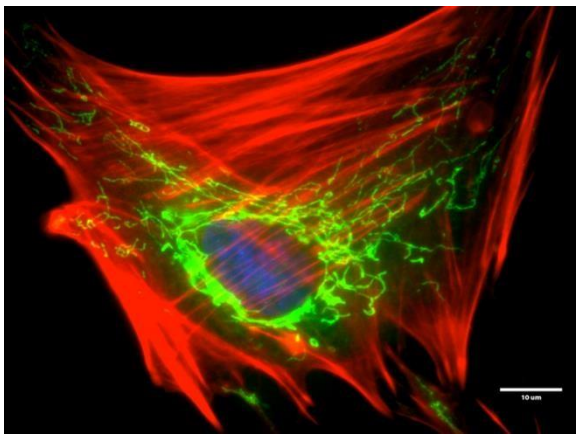

3.1 Phenotypic characterisation of normal and fibrotic human lung fibroblasts in mono-culture

3.1.1. Introduction

FHLFs: drivers of IPF pathology

The FHLF is understood to be the primary mediator of fibrotic remodelling in IPF. This heterogeneous population of cells proliferate in the interstitium, differentiate into myofibroblasts and deposit excessive amounts of ECM, destroying normal lung architecture. Numerous pathogenic characteristics of FHLFs have been identified **(Intro.2.3.1.)**. They are aberrantly over-activated in response to injury-associated and pro-fibrotic stimuli [119,250], circumvent proliferation-suppressing signalling [251], display a spontaneous, invasive phenotype [252], and an intransigence to pro-apoptotic stimuli [123]. Therefore, investigating this population of cells is important to further understanding the cellular mechanisms involved in IPF.

Inflammatory wound signals

FHLFs drive fibrosis in a lung environment subjected to recurrent injury and the lungs response to injury involves a diverse range of inflammatory signalling. IL-6 and CXCL8 are secreted proinflammatory signalling molecules that play an important role in the early response to injury. They are elevated in the early wound site and enhance the infiltration of leukocytes, as well as promoting endothelial migration and angiogenesis,

contributing to the formation of granulation tissue [60,253]. Increased expression of these factors is indicative of injury and associated with IPF [167].

Regulation of IL-6 and CXCL8 production can be mediated by members of the IL-1 cytokine family. IL-1α and IL-1β are the archetypal family members but another nine members also exist, including IL-33. IL-1α is constitutively expressed at low levels in all cells and can function in both its pro-protein, immature form and its cleaved, mature form. IL-1α, as well as IL-33, are dual function cytokines, with the ability to function as classical, secretory cytokines as well as an ability to function as direct transcription factors. Both cytokines function as 'alarmins', damage associated markers that can activate the immune response. This occurs when they are released into the local environment by injury-induced cell necrosis [254]. IL-1α release from damaged epithelial cells induces upregulation of IL-6 and CXCL8 [255]. IL-1β is an inducible cytokine that is not constitutively expressed in normal cells. Along with IL-33, it is activated by the inflammasome [256]. Production and activation can be stimulated by numerous stimuli, but predominantly by bacterial signalling. Along with TGF-β, IL-1α and IL-1β are also important in stimulating fibroblast collagen deposition at the wound site.

CXCL1 and G-CSF are two additional proteins that are elevated in response to injury. The CXCL1 chemokine is a long-acting, long-range attractant for neutrophils, the first type of leukocyte to infiltrate the wound-site [257]. G-CSF plays a similar role. It is a pleiotropic cytokine that functions as an attractant and growth factor for neutrophils in the wound site [258]. Collectively these cytokines and chemokines form part of a wider inflammatory signalling network that is important in early wound inflammation. Although numerous cell types can produce these factors, in the lung fibroblasts also play an important role as immune mediators [259,260]. As IPF is a disease of recurrent injury it was hypothesised that levels of these proteins would be elevated in the HLFs derived from patients with IPF, indicative of sustained wounding.

Inflammation and senescence

Though the factors discussed are important in wound inflammation, they also find prominence in ageing and senescence. With age there is development of a systemic background of the low-grade, sterile inflammation, regulated by the NF-□B pathway [174]. This pathway can promote cellular senescence and upregulate expression of *IL1A* and *IL1B* [214]. This again increases cytokine and chemokine production, both of which can reinforce the state of senescence and cause other non-cell autonomous effects [213,218,261]. Likewise, chronic senescence results in increased secretion of IL-6, CXCL8, CXCL1 and CCL2 [201]. Therefore, elevation of these proteins in FHLFs could also be indicative of a background of age and senescence, both of which are implicated in IPF.

Regulators of senescence

To understand if senescence is a characteristic of FHLFs, investigating the pathways that regulate this process is also important. Senescence is established via induction of two main pathways, the p53-p21 and p16-pRB pathways **(Intro.3.1.2.)**. Both p21 (encoded by *CDKN1A*) and p16 (encoded by *CDKN2A*) are established markers of senescence. *CDKN2A* however, also encodes several different transcript variants, which produce at least two different proteins. Both ultimately regulate progression through the cell-cycle but by different means: p16, inhibits CDK4 and 6, preventing RB phosphorylation, and is referred to as $p16^{Ink4a}$, $p14^{Arf}$, which is specified by an alternate reading frame (ARF), sequesters MDM2, preventing degradation of p53 and promoting cell cycle arrest. It was hypothesised that if FHLFs have a senescent phenotype, RNA levels of *CDKN1A* and *CDKN2A* would be elevated.

Mitochondrial phenotype in senescence and IPF

Mitochondrial phenotype is another facet of fibroblast biology that is linked to senescence and IPF. Hyperplasic AEC2s derived from IPF honeycomb lesions and senescent fibroblasts display a high mitochondrial content and these mitochondrial are enlarged, dysmorphic and with an increased surface area. mtDNA copy number is also increased and there is impaired activity in complex I and IV of the electron transport chain [129,200]. Senescent fibroblasts produce more superoxide and peroxides, due to a

decrease in mitochondrial membrane potential and an increase in proton leak, whilst mitochondrial changes in IPF AEC2s coincide with ER stress. In these epithelial cells this phenotype is due to a lack of mitophagy, the upregulation of which can alleviate senescence [201]. Altered fission/fusion dynamics also play a role. Mitochondria form a heterogenous population of organelles within a cell (referred to as heteroplasmy) that can form extensive networks by fusion or become more punctate by fission. The epithelium of aged mice and senescent fibroblasts display a preference for fusion, with downregulation of the fission protein DNM1L and upregulation of the fusion proteins OPA1 and MFN1 [262]. PINK1 is an important regulator of both mitochondrial dynamics and mitophagy. It is downregulated in IPF and *PINK1* knockout in an epithelial cell line leads to upregulation of *TGFB* and *IL6.* Likewise, *PINK1* knockout mice are more vulnerable to pulmonary fibrosis [129]. Though the significance in IPF fibroblasts has yet to be fully investigated, an altered mitochondrial phenotype, and altered mitochondrial regulation, in isolated FHLFs could provide evidence for a senescent-like phenotype in these cells, which may contribute to the fibrotic process.

In summary, the hallmarks of wound-associated inflammation, senescence and ageing, as well as mitochondrial phenotype, are inter-linked. Investigating these aspects in FHLFs has not yet been explored in detail, therefore, initial experiments set out to understand these characteristics in isolated FHLFs and question whether they are different when compared to NHLFs.

Hypotheses

1. FHLFs will display an inflammatory phenotype in comparison with NHLFs, with elevated expression of senescence-associated cytokines and chemokines.
2. FHLFs will exhibit dysfunctional mitochondrial content resulting from altered expression of key genes involved with mitochondrial homeostasis.

3.1.2. Results

3.1.2.1. FHLFs in mono-culture display limited hallmarks of inflammation and senescence.

To investigate whether FHLFs are more inflammatory when compared to NHLFs, cells were first isolated from patient samples, obtained from the RD&E. FHLFs were derived from patients undergoing surgical biopsy for IPF diagnosis and NHLFs were derived from the marginal tissue of lung tumour resections, via a method of explantation. HLF populations were expanded under normal culture conditions on plastic. Cells were seeded at a density of 30,000 cells/well of a 12-well plate and maintained under normal conditions for a period of 24 hrs prior to the extraction of RNA. Via RT-qPCR, RNA levels were measured, assessing levels of:

Wound inflammatory genes: *IL6, CXCL8, IL1A, IL1B, CXCL1, CSF3, TNFA*
Senescence regulatory genes: *CDKN1A, CDKN2A*

The results are displayed as an average fold change, relative to the expression of the reference genes *GAPDH* and *B2M* and calibrated to the levels found in NHLFs **(*Figure* 3.1.1)**. *CDKN2A* RNA levels were significantly elevated in FHLFs but levels of *CDKN1A* did not significantly differ. The results also showed a tendency towards an increase in *IL6, CXCL8, IL1A* and *IL1B*, and a decrease in *IL-33* but these results did not reach statistical significance. Both *CXCL1* and *CSF3* were reliably expressed in some, but not all, donor lines. In FHLFs, the average expression of *IL1A* was 8.26-fold greater than NHLFs, but the standard deviation (SD) was 10.91, indicative of a high variability between the donors used. Indeed, with the exception of *CDKN2A* levels, the average SD for FHLF fold change was 2.52, compared to 0.48 in NHLFs.

Despite the limited variations at an RNA level, the importance of the FHLF phenotype and the potential role of a much broader range of immune-modulating factors in IPF led to further investigation of the FHLF phenotype at the secretory protein level. Protein

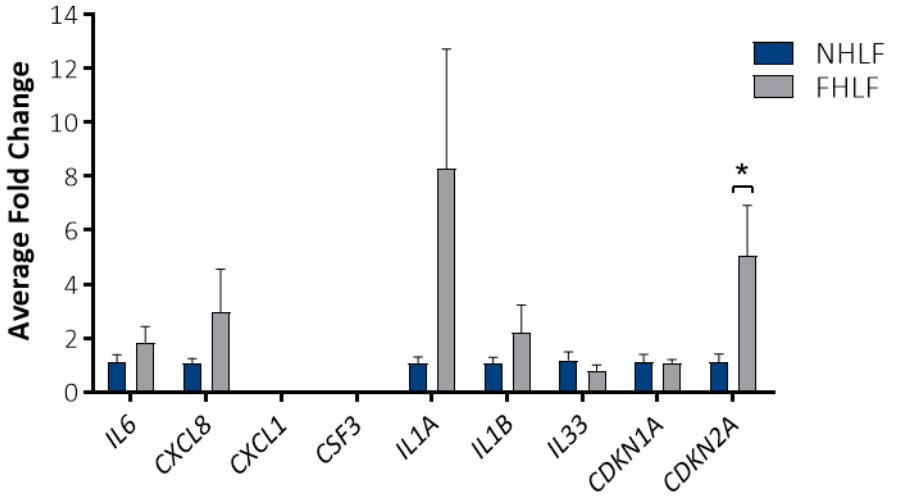

Figure 3.1.1. RT-qPCR comparing RNA levels in NHLFs and FHLFs after 24 hrs of mono-culture. HLFs were seeded 24 hr prior to media change with DMEM/αMEM (1:1) 10% FBS. Cells were then cultured for 24 hrs. RT-qPCR was performed with genes of interest normalised to the reference genes *B2M* and *GAPDH.* FHLF RNA levels were calibrated to NHLF levels and the data is shown as an average fold change. *CXCL1* and *CSF3* were not reliably expressed. RNA levels of *CDKN2A* were significantly greater in FHLFs. NHLF n = 4 (3x donors: TB0917, TB0918, TB0932 [2]), FHLF n = 6 (5x donors: BR001, BR002, BR003 [2], TB0908 [2]). * $p < 0.05$. Two-tailed, unpaired t-test performed on ddCt values.

concentrations in the CM, collected after a 72 hr incubation period in mono-culture, was assessed via Multiplex ELISA (or, in the case of IL-33, by standard ELISA) and a range of 39 immune-modulating cytokines, chemokines and growth factors were analysed **(*Figure* 3.1.2.).** The panel of analytes assessed were not specific to wound inflammation or senescence but did include a multitude of factors associated with both. All analytes were detectable but, for 29 of them, protein concentration was below 20 pg/ml. Concentrations of IL-1α, IL-1β and IL-33 were exceptionally low in the CM (>10 pg/ml), as too was the concentration of the pro-inflammatory cytokine TNF-α. The antiinflammatory cytokines, IL-4, IL-10 and IL-13 were also detected at exceptionally low concentrations. Nine of the measured factors were detected at concentrations greater than 50 pg/ml, of which CCL2 and CXCL10 were found at high concentrations >750 pg/ml. Of these nine analytes, there were only significant differences between NHLF and FHLF for two of them. GM-CSF and CXCL10 were both significantly elevated in FHLFs. Taken together, this suggests that, in mono-culture, FHLFs are not substantially more pro-inflammatory than NHLFs.

3.1.2.2. Regulation of FHLF mitochondrial phenotype is not altered at an RNA level and FHLFs do not have an altered copy number of mtDNA.

PINK1 is a major homeostatic regulator of mitochondrial homeostasis, playing a key role in the clearance of defective mitochondria by mitophagy. Mitochondrial fission and fusion events are regulated by proteins such as DNM1L and MFN1, respectively. The RNA levels of these genes were assessed via RT-qPCR in NHLFs and FHLFs, monocultured for 24 hrs **(*Figure* 3.1.3A.)**. There were no significant differences in RNA levels between any of these transcripts, implying that regulation of mitochondrial phenotype is equivalent in NHLFs and FHLFs. mtDNA copy number was also assessed via RT-qPCR. Only two FHLF lines were assessed but their mean copy number fell within the range of NHLF mtDNA copy number **(*Figure* 3.1.3B.)**. This non-significant difference in copy number indicated equivalent mitochondrial heteroplasmy between cell types.

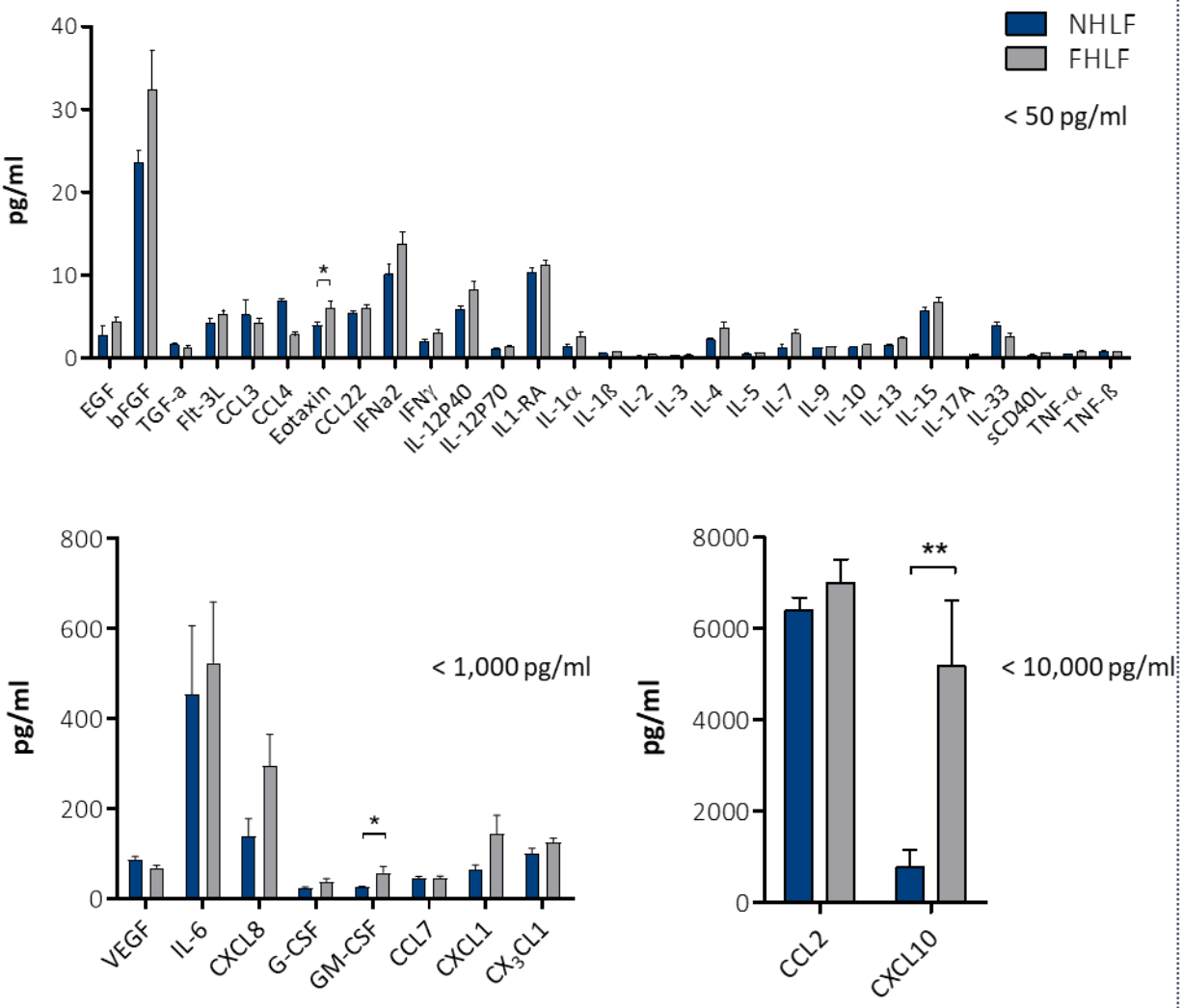

Figure 3.1.2. Multiplex cytokine array comparing NHLF and FHLF CM, after 72 hrs of mono-culture. HLF were seeded 24 hr prior to media change with DMEM/αMEM (1:1) 10% FBS. Cells were then cultured for 72 hrs and the basolateral media collected and stored at -80 °C. After thawing, conditioned media were analysed via Luminex Multiplex array, screening for immuno-modulating cytokines, chemokines and growth factors. Results are shown across 3 graphs of differing y-axis scales. All results show non-significant results with exception of Eotaxin, GM-CSF and CXCL10, which are at a significantly higher concentration in FHLF. NHLF n = 12 (4x donors: TB0912 [3], TB0917 [3], TB0932 [3], TB0918 [3]). FHLF n = 12 (4x donors: BR001 [3], BR002 [3], BR003 [3], TB0908 [3]). * $p < 0.05$, ** $p < 0.01$, two-tail, unpaired t-test.

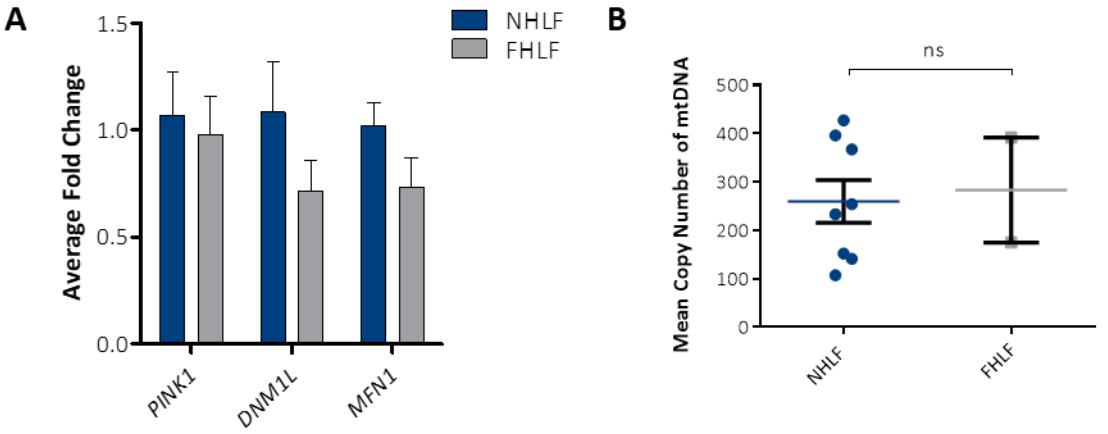

Figure 3.1.3. RNA levels of regulators of mitochondrial phenotype and average mtDNA copy number in NHLFs and FHLFs. (A) HLFs were seeded 24 hr prior to media change with DMEM/αMEM (1:1) 10% FBS. Cells were then cultured for 72 hrs. RT-qPCR was performed with genes of interest normalised to the reference genes *B2M* and *GAPDH.* FHLF RNA levels were calibrated to NHLF levels and the data is shown as an average fold change. NHLF n = 4 (3x donors: TB0917, TB0918, TB0932 [2]), FHLF n = 6 (5x donors: BR001, BR002, BR003 [2], TB0908 [2]). * $p < 0.05$. Two-tailed, unpaired t-test performed on ddCt values. **(B)** DNA was isolated from 24 hr mono-cultured NHLFs and FHLFs. RT-qPCR was performed with the nDNA primers *ND1* and *ND5,* and the mtDNA primers *SCLO2B1* and *SERPINA1*. *ND1* and *ND5* were used as reference genes. The relative number of mtDNA copies was determined by the difference in Ct values between nuclear and mitochondrial DNA. There was no significant difference between NHLF and FHLF. NHLF n = 8 (TB0912, TB0916, TB0917 [2], TB0918 [2], TB0921, TB0932). FHLF n = 2 (2x donors: BR002, BR003) . Two-tailed, unpaired t-test.

3.1.2.3. FHLFs in mono-culture do not have an altered mitochondrial membrane potential but do display an altered mitochondrial morphology.

Mitochondrial dysfunction, which encompasses mitochondrial membrane depolarisation, drives cellular senescence and is associated with IPF. Mitochondrial membrane potential ($\Delta\psi m$) represents a component of the proton motive force (Δp), the force that drives protons into the mitochondrial matrix after exclusion by the electron transport chain. A high proton motive force is indicative of high mitochondrial energy output via adenosine ATP synthase, which uses protons to generate ATP. $\Delta\psi m$ can be measured with various lipophilic, cationic dyes, including JC-1 and TMRE. These dyes accumulate in the mitochondrial membrane matrix in an inverse proportion to $\Delta\psi m$, with more dye accruing in a more negatively polarised membrane. $\Delta\psi m$ can be reduced by treatment with uncoupling proteins, such as FCCP, which causes protons to pass freely

across the inner mitochondrial membrane. FCCP is typically used as a positive control when investigating $\Delta_{\psi m}$.

TMRE was used to assess the membrane potential of NHLFs and FHLFs under normal conditions in mono-culture. Firstly, an appropriate experimental concentration of TMRE was established using NHLFs **(*Figure* 3.1.4A)**. Cells were seeded at a density of 2,000 cells/well in 96-well plates and cultured for 24 hrs prior to treatment with TMRE across a range of concentrations, either with or without 20 µm FCCP. Fluorescence was then measured via a plate reader. The background intensity was high at 0 nM TMRE/TMRE + FCCP but there was a linear, concentration-dependent increase in fluorescence intensity with increasing TMRE concentration. Uncoupling was not significantly observable at 200 nM TMRE but was at higher concentrations, with the greatest difference at 800 nM. This concentration was used in subsequent experiments. To try and further accentuate the uncoupling effect, 30 µM FCCP was trialled with NHLFs **(*Figure* 3.1.4B)**. A significant difference in $\Delta_{\psi m}$ was found with this concentration and it was chosen for further experiments. When comparing $\Delta_{\psi m}$ in NHFL and FHLF there was no significant difference in coupled potential **(*Figure* 3.1.4C)**.

To investigate mitochondrial morphology, NHLFs and FHLFs were cultured in chamber slides (10,000 cells/chamber) under normal conditions for 24 hrs prior to fixation and IMF staining for ATP5B, a subunit protein of ATP synthase. To better understand the mitochondrial morphology, IMF images were analysed by converting the fluorescent signal to a skeletonised image using ImageJ **(*Figure* 3.1.5.)**. Imaging demonstrated that the mitochondria of NHLFs form a complex and interconnected network of large organelles. Conversely, though the cells themselves were also bigger, FHLF mitochondria were substantially smaller, more punctate and less interconnected. In this form, it was possible to quantify numerous parameters of mitochondrial morphology via ImageJ, assigning an arbitrary unit of particle size to the mitochondrial signal **(*Figure* 3.1.6.)**. Compared to NHLFs, the average number of mitochondria per FHLF was significantly higher. The average mitochondrial areas were the same, although the average size of each mitochondrion was significantly less in FHLFs. Likewise, the average number of

branches each mitochondrion had was decreased in FHLFs. There was no difference in the average length of mitochondrion branches, but the average, maximum branch length per cell was less. The average number of junctions made by each mitochondrion was also less in FHLFs. These results highlight significant changes in mitochondrial morphology, with an apparent fragmentation of the mitochondrial network in FHLFs.

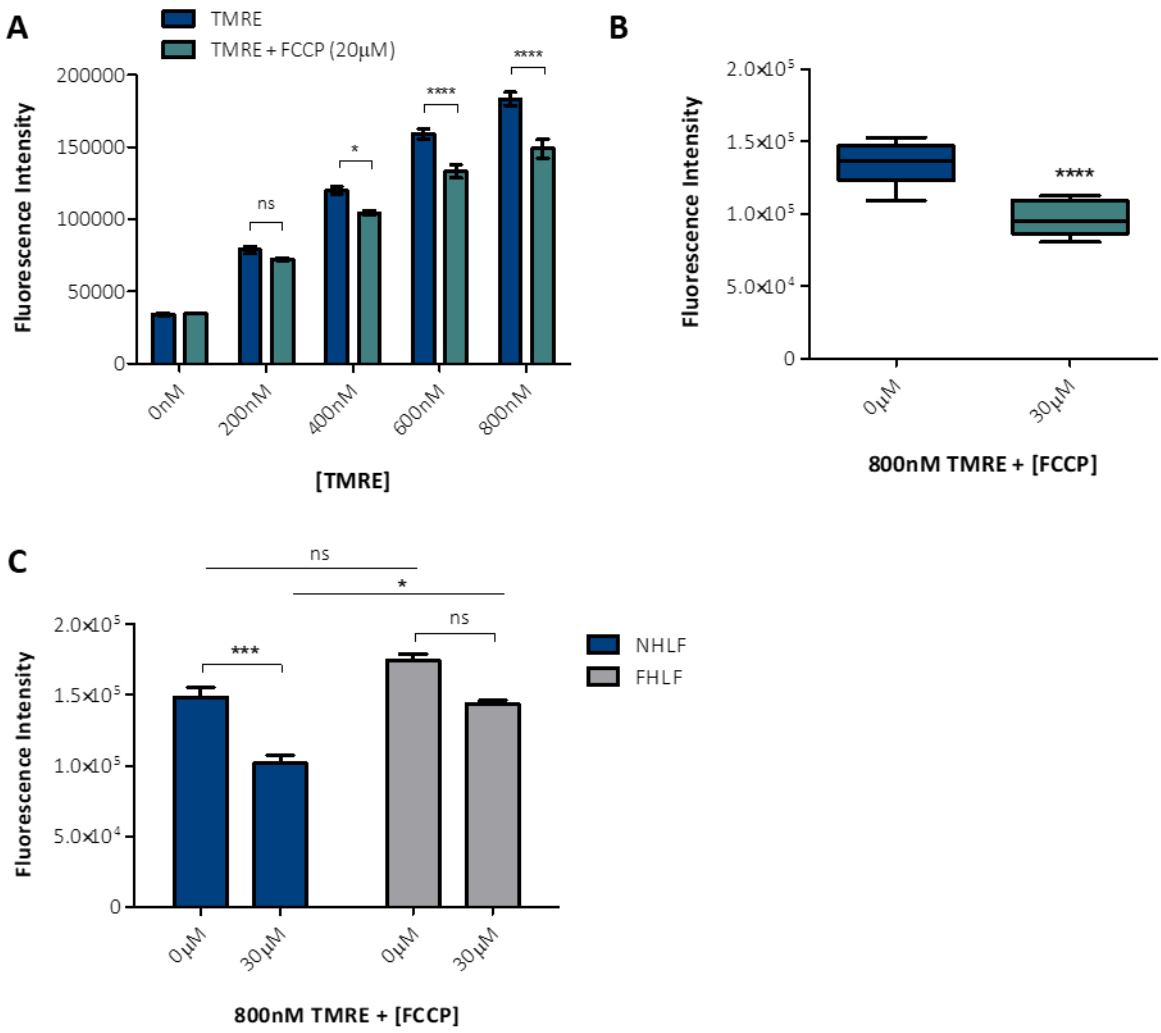

Figure 3.1.4. Assessment of mitochondrial membrane potential between mono-cultured NHLFs and FHLFs. (A) Establishment of appropriate TMRE concentration for fluorescent measurement in NHLFs, 24 hrs post-seeding with 20 µM of the mitochondrial uncoupling agent FCCP. n = 4 (1x donor: TB0932 [4]). **(B)** Effect of 30µM FCCP on membrane potential in NHLFs, 24 hrs post-seeding. n = 3 (1x donor: TB0932 [3]). **** $p < 0.0001$, two-tailed, unpaired t-test. **(C)** Comparison of NHLF and FHLF membrane potential 24 hrs post-seeding with 800 nM TMRE and 30 µM FCCP. FCCP significantly decreased membrane potential in NHLFs but not FHLFs. There was no difference in normal potential between NHLFs and FHLFs but a difference in uncoupled potential. NHLF n = 4 (4x donors: TB0912, TB0917, TB0918, TB0932), FHLF n = 5 (2x donors: BR002 [3], BR003 [2]). *** $p < 0.001$, * $p < 0.05$. 2-way ANOVA, Bonferroni multiple comparison.

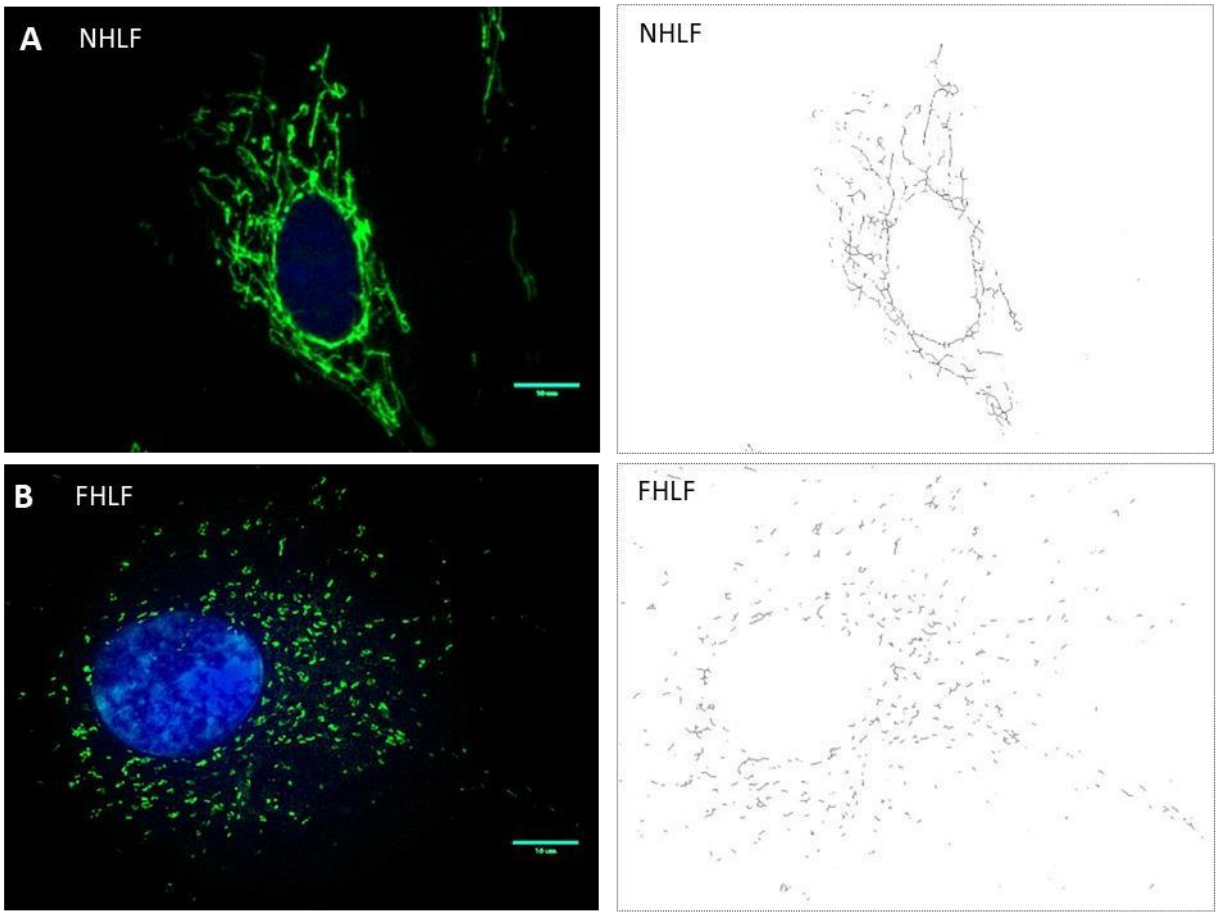

Figure 3.1.5. Representative immunofluorescent imaging of mono-cultured HLF mitochondria. 24 hrs post-seeding NHLF were fixed and stained for ATP5B (green) with additional DAPI (blue) nuclear staining. **(A)** (left) IMF image. (right) Corresponding skeletonised image. NHLF image donor ID: TB0932. Scale bar = 10 µM. **(B)** Representative images of FHLFs. FHLF image donor ID: BR002.

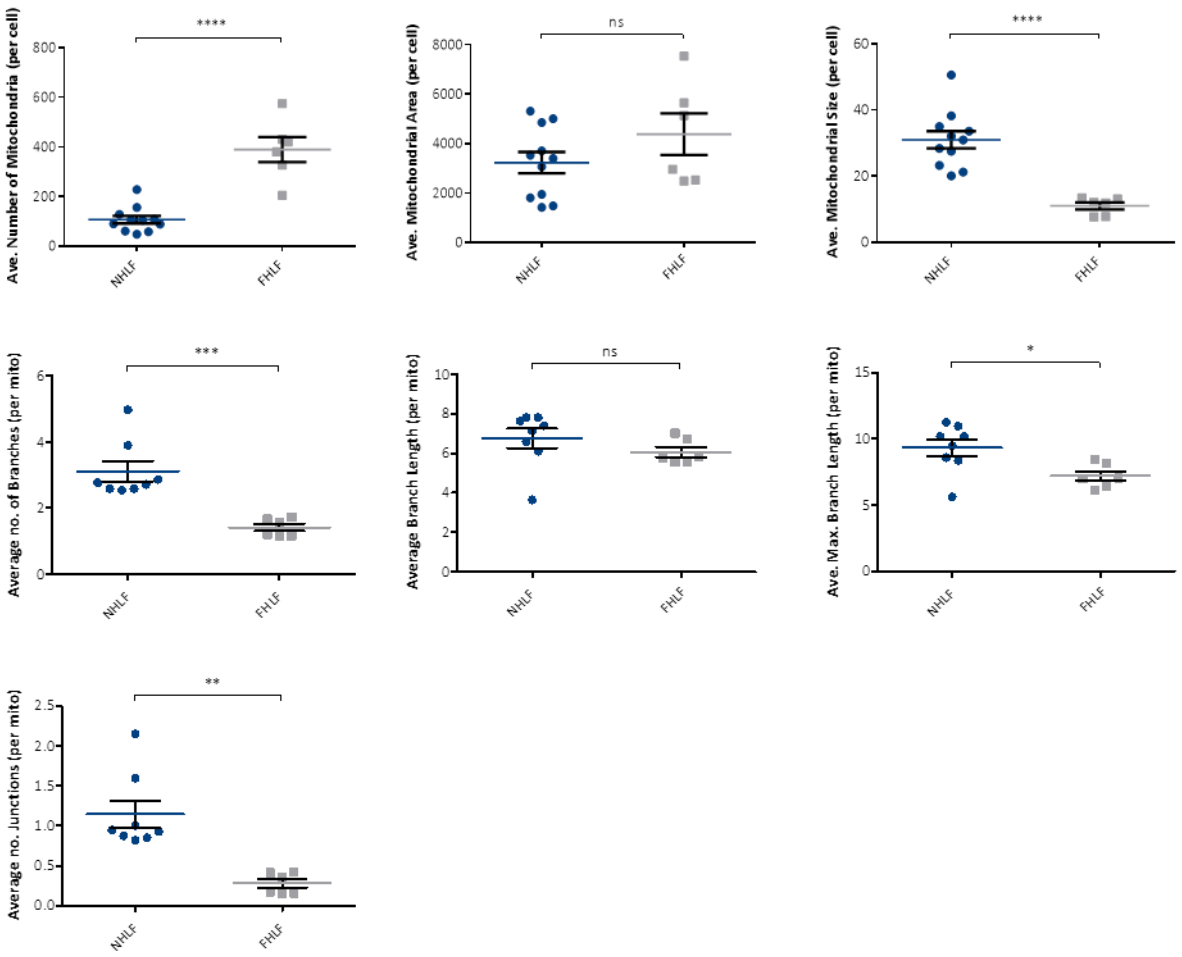

Figure 3.1.6. Quantification of mitochondrial morphology in NHLFs and FHLFs. Skeletonised, immunofluorescent ATP5B signal was quantified via ImageJ. Within cells, the average number of mitochondria per cell was higher in FHLFs yet the total area was not significantly different. Average size was decreased in FHLFs. Within mitochondria, the number of branches was decreased. There was no difference in average branch length but the maximum number of branches per mitochondria and average number of junctions was significantly decreased. Data points are the average of 3 cells within an independent experiment. NHLF n = 8 (4x donors: TB0912 [2], TB0916 [2], TB0918 [2], TB0921 [2]). FHLF n = 6 (3x donors: TB0908 [3], BR002, BR003 [2]). **** $p < 0.0001$, *** $p < 0.001$, ** $p < 0.01$, * $p < 0.05$. Two-tailed, unpaired t-test.

3.1.3. Discussion

This section set out to investigate the intrinsic, pathological characteristics of FHLFs, assessing expression of inflammatory and senescence-associated markers, as well as the mitochondrial phenotype. This was achieved by isolating FHLFs from patients with confirmed IPF and comparing them to NHLFs from patients without fibrosis. Importantly, all HLFs were derived from aged patients, therefore, any differences between cell types were less likely due to age-related changes and more reflective of pathology. Not only

this but the detrimental cellular changes that occur with age, including increases in inflammation, changes to mitochondrial homeostasis and an increased predisposition to become senescent are likely to affect both FHLFs and the control cells. Via RT-qPCR and multiplex ELISA, it was found that mono-cultured FHLFs do not express significantly higher levels of inflammatory proteins, with the exception of GM-CSF and CXCL10. There were however significant differences in mitochondrial morphology, but this was not coupled to altered mtDNA copy number or mitochondrial membrane potential.

Inflammation and senescence markers

Genes relating to wound-associated inflammation and senescence were investigated at the RNA level, with the hypothesis that, due to recurrent injury in IPF these markers would be elevated. *IL6, CXCL8, IL1A, 1IL1B, IL33, CDKN1A* and *CDKN2A* were expressed in both cell types. There was inconsistent expression however of *CSF3* and *CXCL1,* despite detection of these proteins at concentrations >50 pg/ml in CM. Typically, these proteins are not normally expressed and expression is induced in response to signalling from stimuli such as IL-17, lipopolysaccharide (LPS) and/or TNF-α [263,264]. IL-17 and TNFα secretory protein concentrations were very low (<10 pg/ml), suggesting an absence of the paracrine signalling required to drive their expression. RNA was also collected after 24 hrs of culture, whereas CM was collected after 72 hrs. It is therefore possible that any differences were down to a temporal variation in expression, a variation that could be checked by assessing RNA levels after 72hrs of culture. *IL1A* and *IL33* are also not normally expressed in HLFs and are induced in response to inflammasome activation.

The trend towards *IL1A* RNA increase may point towards inflammasomal activation in FHLFs, suggesting a more inflammatory phenotype. Conversely, *IL6, CXCL8* and *IL1B* are typically expressed in fibroblasts. Though FHLFs displayed a greater average fold change for these transcripts, there was no significant difference compared with NHLFs. Taken together, this suggests that at an RNA level FHLFs do not have a more inflammatory phenotype. An important feature of the RNA data however was the variability in FHLF fold change, with data showing a broad range and large standard deviation. For all genes analysed, at least one FHLF cell line displayed a decrease in fold change when compared to NHLFs. This potentially reflects the heterogeneity of lung fibroblasts within IPF,

highlighting that, even within regions of fibrosis, some cells may not display the pathological characteristics associated with this disease and explaining the lack of RNA differences. However, these results may also have been indicative of pathological differences between cell types at a protein level.

Consequently, a broad range of immune-modulating proteins were analysed in HLF CM. For 28 of these proteins, concentrations were below 50 pg/ml. Such a small concentration was considered to be non-physiologically relevant and few conclusions can be drawn from those results. Despite strong expression at an RNA level (relative to reference genes), neither IL-1α, IL-1β or IL-33 were highly expressed in HLF CM. This might be expected however as these proteins typically function intracellularly, being released only in instances of necrosis or on appropriate activation of the inflammasome. To understand their relevance in HLF mono-culture, protein expression would need to be assessed by ELISA of cell-lysate or by western blotting, an experiment that could be performed in future studies. Though not assessed at an RNA level, there was a significant difference in protein concentrations of CXCL10, a chemokine associated with the early wound response. CXCL10 expression is typically induced by IFN-γ signalling, which in the HLF CM was produced at extremely low concentrations (<10 pg/ml). Interestingly, CXCL10 is also considered to be an antifibrotic chemokine. Exogenous CXCL10 treatment is protective against BLM-induced lung injury in mice and *CXCL10*$^{-/-}$ mice suffer more severe fibrosis [265–267]. CXCL10 is postulated to inhibit fibroblast migration, thereby reducing accumulation and matrix deposition in the airway, yet fibroblasts lack the receptor for this chemokine, CXCR3, and consequently the mechanism by which this occurs is unclear. Likewise, these effects have been evidenced using mice treated with BLM in the context of an acute, non-infectious injury and the role of CXCL10 in established fibrosis remains uncertain. It is difficult to interpret why this potentially antifibrotic protein is elevated in mono-cultured FHLFs, yet CXCL10 is also a key woundassociated chemokine, important in post-wound immune cell recruitment [253]. It may therefore be that its upregulation reflects a propensity of FHLFs to generate an injuryassociated environment in culture. However, aside from this chemokine, the overall picture created by HLF RNA and protein assessment is that there is little intrinsic

difference between the two and that FHLFs are simply more variable than NHLFs. This could indicate that, in the absence of relevant stimuli, FHLFs are not inherently pathogenic, although there are other possibilities. Many of the proteins assessed in this work are expressed in different isoforms, with variations in splicing playing an important role. For example, the ratio of VEGF splice isoforms can alter the lung microenvironment to be either anti- or pro-fibrotic [268]. Whether differing isoforms of such proteins were expressed by normal and fibrotic HLFs was not assessed but could be performed in future.

Mitochondrial phenotype

The results from investigating mitochondrial phenotype were also of interest. There was no difference at an RNA level of the regulatory genes *PINK1, DNM1L* and *MFN1*, suggesting that mitochondrial homeostasis and the balance between fusion and fission is not differentially regulated between NHLF and FHLF. This fails to corroborate previous literature suggesting a loss of homeostatic regulation in IPF, ageing and senescence, and a cellular preference towards mitochondrial fusion. Likewise, in senescent cells and aged AEC2s there is an increase in mtDNA copy number [129,201]. This was also not observed in FHLFs. However, there was limited access to IPF tissue in this study and it would be interesting to repeat these experiments with more donor lines and better expand on these results in the future. It was also expected that FHLFs would have more depolarised mitochondrial membranes, as depolarisation leads to increased ROS production, important in both myofibroblast differentiation and induction of senescence [119,200]. This was not evident. There was no significant difference between FHLF and NHLF $\Delta\psi m$, indicating that the mitochondria do not have an altered polarisation status. This could begin to suggest an equivalence in mitochondrial function between NHLFs and FHLFs, with no difference in mitochondrial ROS production. However, TMRE is just one measure of mitochondrial function and mitochondrial ROS production was not directly measured. JC-1 fluorescence could also have been assessed, further elucidating $\Delta\psi m$, and ROS production could have been measured by dyes such as MitoSox. These dyes could be used following the same experimental design as TMRE experiments but, as well as measuring fluorescence via plate reader, could be assessed by microscopy. For example,

when using JC-1, an increase in membrane potential leads to increased dye accumulation. This causes a shift in fluorescence emission from green (529nm) to red (590nm), which can be observed via microscopy. If the results of TMRE were truly reflective of membrane potential in NHLFs and FHLFs it would be expected that both cell types would display an equivalent ratio of red/green fluorescence signal, further suggesting equivalent mitochondrial health and activity.

The analysis of mitochondrial morphology was achieved by establishing a new, quantitative methodology, which has thus far been unreported. This method was useful for allowing statistical analysis from IMF images. Analysis revealed that FHLFs, although having equivalent mitochondrial content, had significantly smaller and more punctate mitochondria, which were also more numerous. These changes would suggest the occurrence of more fission events, leading to fragmentation of the mitochondria. It was therefore surprising that *DNM1L* was not upregulated in FHLFs, although this was not assessed at the protein level (something that could be assessed via western blot). Though there were significant differences in morphology via this methodology there were limitations to this approach. The images captured and analysed were in 2D, overlooking the complex, 3D mitochondrial network within a cell and only one antibody type was used (more confidence could be gained through use of a different mitochondrial antibody such as TOM20). Similarly, it remains unknown how these potential differences relate to function and ultimately few conclusions can be drawn. This is also true for the experiments with TMRE and mtDNA copy number. Ideally, mitochondrial function would be assessed via an extracellular flux analyser, which provides data on cell metabolism by analysing glycolytic function and mitochondrial respiration. This would provide a more complete picture of the mitochondrial phenotype and will be a focus of future investigations.

Importance of micro-environment

In summary, these results suggest that, in terms of inflammation, senescence and mitochondrial phenotype, there is little difference between HLFs isolated from IPF patients and normal controls. Though evidenced by investigation using a small

repertoire of genes, it may be that these aspects are not important to IPF pathology. However, as previously discussed, there is strong evidence to suggest that they are. It may then be that the conditions in which these cells were investigated was inappropriate. Mono-culture on plastic differs vastly from the 3-dimensional, multi-cell type environment of the lung. Indeed, a study by Parker *et al.*, in which NHLFs and FHLFs were also isolated, found that the environment the cells were cultured on was more important to the establishment of pathological characteristics than the intrinsic differences of the cells themselves [151]. HLFs in this investigation were not stimulated and they were cultured under standard culture conditions. They were therefore not exposed to stimuli found in either the normal or the IPF lung. Furthermore, recent global gene expression analysis into the profile of HLFs has suggested that the differential profile of NHLFs and FHLFs is lost once the cells have adapted to an *in vitro* environment. The authors proposed that the IPF environment is key to differential activity, not the intrinsic propensity of the FHLF itself [269]. Together, it is therefore likely that HLFs in 2D monoculture are simply not subjected to an environment relevant enough and require more physiological stimuli to expose any pathological differences. The subsequent sections of this thesis will present work aimed at better recapitulating the lung micro-environment, in an attempt to further understand the role of FHLFs in IPF pathology.

3.2 Modelling Secretory Communication *in vitro*

3.2.1. Introduction

To better recapitulate the lung micro-environment, it was decided to establish a model of co-culture, in which HLFs were cultured with epithelial cells. By culturing these two cell types together, it was thought that secretory communication between them would create more physiologically relevant stimuli for the HLFs, enabling a better investigation of their role in health and disease.

The importance of epithelial-mesenchymal crosstalk

As well as evoking a more physiological response in fibroblasts, establishing a model of crosstalk *in vitro* could also allow a recapitulation of the secretory communication found in the airways. Epithelial-mesenchymal crosstalk is fundamental to the development of the embryonic lung, crucial in maintaining homeostasis of the adult airways, and important in facilitating wound repair. Importantly, aberration of these processes is key to the pathology of IPF. Therefore, by modelling secretory communication *in vitro*, these facets could also be investigated, at first in the context of normal physiology and then in the context of disease.

Co-culture

Methods involving the co-culture of epithelial and mesenchymal cells have been utilised before in the investigation of numerous aspects of lung biology, focused primarily within the context of normal lung function. The effect of mesenchymal cells on the epithelium has been investigated, using cells isolated from young mice, showing that co-culture allows epithelial progenitors to form mixed-lineage, tracheobronchial colonies [162] and AEC2s to proliferate and form alveolospheres [49]. Similarly, co-culture allows a bronchial epithelial cell line to differentiate, establish ionic impermeability and better respond to injury [83]. Co-culture also has reciprocating effects on the mesenchyme. Using immortalised cells, IL-1α release from damaged epithelial cells induces the release of IL6 and CXCL8 from fibroblasts [270] and isolated rat epithelial cells can control fibroblast proliferation, with co-culture reducing their growth [55]. However, the effects of coculture using primary human cells within the context of IPF continues to offer opportunity for further investigation.

In methods of co-culture, both secretory communication and cell-cell contact are important in mediating beneficial, physiological effects and previous co-culture methods have included: culturing epithelial and mesenchymal cells together, culturing epithelial and mesenchymal cells on opposing sides of a permeable membrane, or culturing mesenchymal cells in a basolateral compartment, with epithelial cells cultured apically on a semi-permeable membrane. Though all feasible, the latter of these methods was

chosen in this investigation. To understand changes in inflammatory wound signalling and senescence-associated secretion from HLFs, it was chosen as it allows easy interrogation of signalling proteins in the media. When cells are cultured either side of a membrane secretory factors can be trapped between cell types and therefore go undetected. Similarly, when co-cultured cells are seeded together and intermixed, it becomes difficult to isolate RNA from the respective cell types. In this study a method was therefore optimised in which HLFs were cultured with epithelial cells in a system allowing secretory communication, whilst preventing direct cell contact between these two compartments.

16HBE14o-

HLFs were co-cultured with the human bronchial epithelial cell line 16HBE14o- (HBEC), a transformed cell line that retains many of the characteristics of differentiated bronchial epithelium *in vitro*. In submerged culture, HBECs have many of the characteristics of BCs, the progenitor cells of the tracheobronchial airway that are key to facilitating both airway development and responding to injury. HBECs have a classical, cobblestone morphology, form tight junctions and, after formation of a confluent monolayer, become polarised with a reduction in ionic permeability [248,271]. Though primary HBECs would more faithfully recapitulate the lung airway, this cell line was chosen to provide better consistency and greater experimental control, allowing interrogation of the impact of crosstalk with primary HLFs.

Methodology

HLFs were routinely cultured in DMEM and HBECs in αMEM. All co-culture experiments were subsequently optimised with cells cultured in a 1:1 mix of these two media types, thereby including all necessary growth factors for each cell type. HBECs were cultured in transwell inserts with a semi-permeable membrane (0.4 µm pore size). After seeding, inserts were placed into a standard culture plate, in which NHLFs had previously been seeded. Co-cultures were maintained for 72 hrs without media change **(*Figure* 2.1.1.)**. Initial experiments were performed using NHLFs, with the aim of developing an understanding of the model for subsequent use with FHLFs.

Hypotheses

1. Co-culture with NHLFs would promote HBEC development and repair in response to injury.

3.2.2. Results

3.2.2.1. Co-culturing NHLFs with HBECs decreases NHLF proliferation, changes RNA levels and alters secretory phenotype.

Initial investigations focused on the effect of co-culture on NHLF behaviour. Firstly, NHLF proliferation was measured over a 72 hr culture period **(*Figure* 3.2.1)**. NHLFs were seeded in equal densities at -24 hrs and transferred to experimental conditions at 0 hrs. NHLFs were transferred to either co-culture with HBECs or kept in mono-culture **(*Figure* 2.1.1.)**. At 24 hr intervals, cell numbers were counted using a haemocytometer and a relative cell number (RCN) calculated from the initial seeding density. By 72 hrs, RCN was significantly lower in co-cultured NHLFs when compared to mono-culture NHLFs. To investigate this further, and uncover whether the reduced RCN in co-culture was due to a lack of cell viability, NHLFs were incubated with ReadyProbes Cell Viability reagents and imaged via fluorescent microscopy, after 72 hrs of mono- or co-culture **(*Figure* 3.2.2A)**. Under fluorescent excitation, these reagents highlight viable cell nuclei in blue and non-viable nuclei in green. Images were taken and quantified via ImageJ. In both mono- and co-cultured cells there was an exceptionally low number of non-viable cells **(*Figure* 3.2.2B)**. The number of viable cell nuclei in mono-cultured NHLFs was significantly higher than in co-culture. These results suggest that HBECs influence NHLF cell number. This could be the result of a change in proliferation, with an increase in competition for resources in the media or signalling from the epithelium. The normal lungs have a low rate of proliferation and epithelial cells are known to maintain fibroblast quiescence as part of normal homeostasis. A similar phenomenon may be occurring in co-culture.

Wound inflammatory and senescence associated RNA levels were also assessed via RTqPCR **(*Figure* 3.2.3.)**. RNA was isolated from NHLFs in either mono- or co-culture, after 72 hrs of culture. There was a significant increase in RNA levels of *IL6, CXCL8, IL1A, IL1B* and *CXCL1* following co-culture. Levels of *CDKN1A, CDKN2A* and *PINK1* were significantly decreased and there was no change in levels of *IL33* and *CSF3*. Interestingly, whereas at

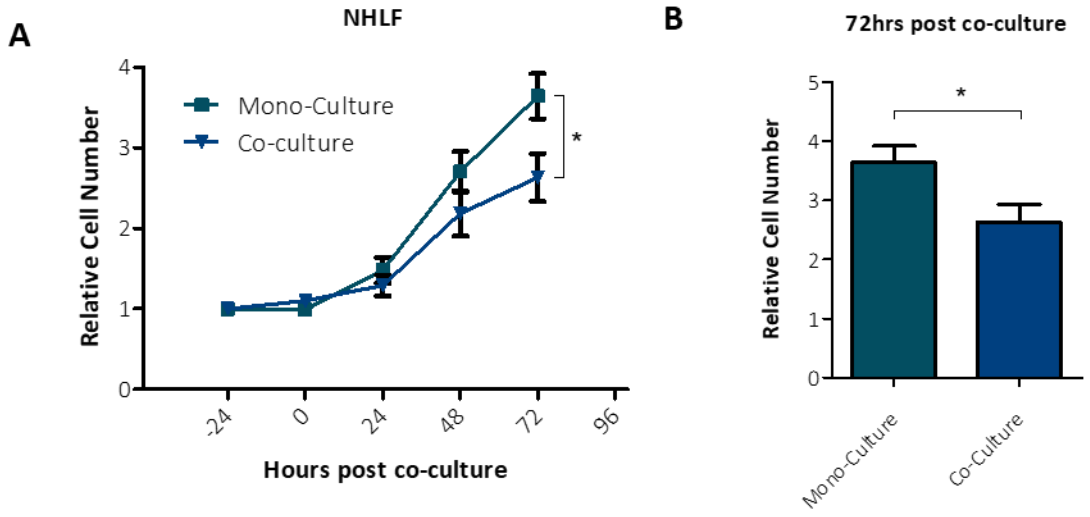

Figure 3.2.1. NHLF cell number over 72 hrs in mono-culture or HBEC co-culture. (A) NHLFs were seeded at 12,000 cells/well at -24 hrs in DMEM 10% FBS. At 0 hrs media were changed for DMEM / αMEM (+/-) 10% FBS and cells were either left in mono-culture or co-culture with HBEC. At 24 hr intervals, over 72 hrs, NHLF cell numbers were counted using a haemocytometer. Cell numbers are shown relative to the initial seeding density. **(B)** Relative cell number of (A) at 72 hrs post co-culture. There was a significant increase in mono-culture cell number compared to co-culture. NHLF n = 9 (3x donors: TB0917 [3], TB0916 [3], TB0932 [3]). *** $p < 0.001$, * $p < 0.05$. 1-way ANOVA, Tukey's multiple comparisons.

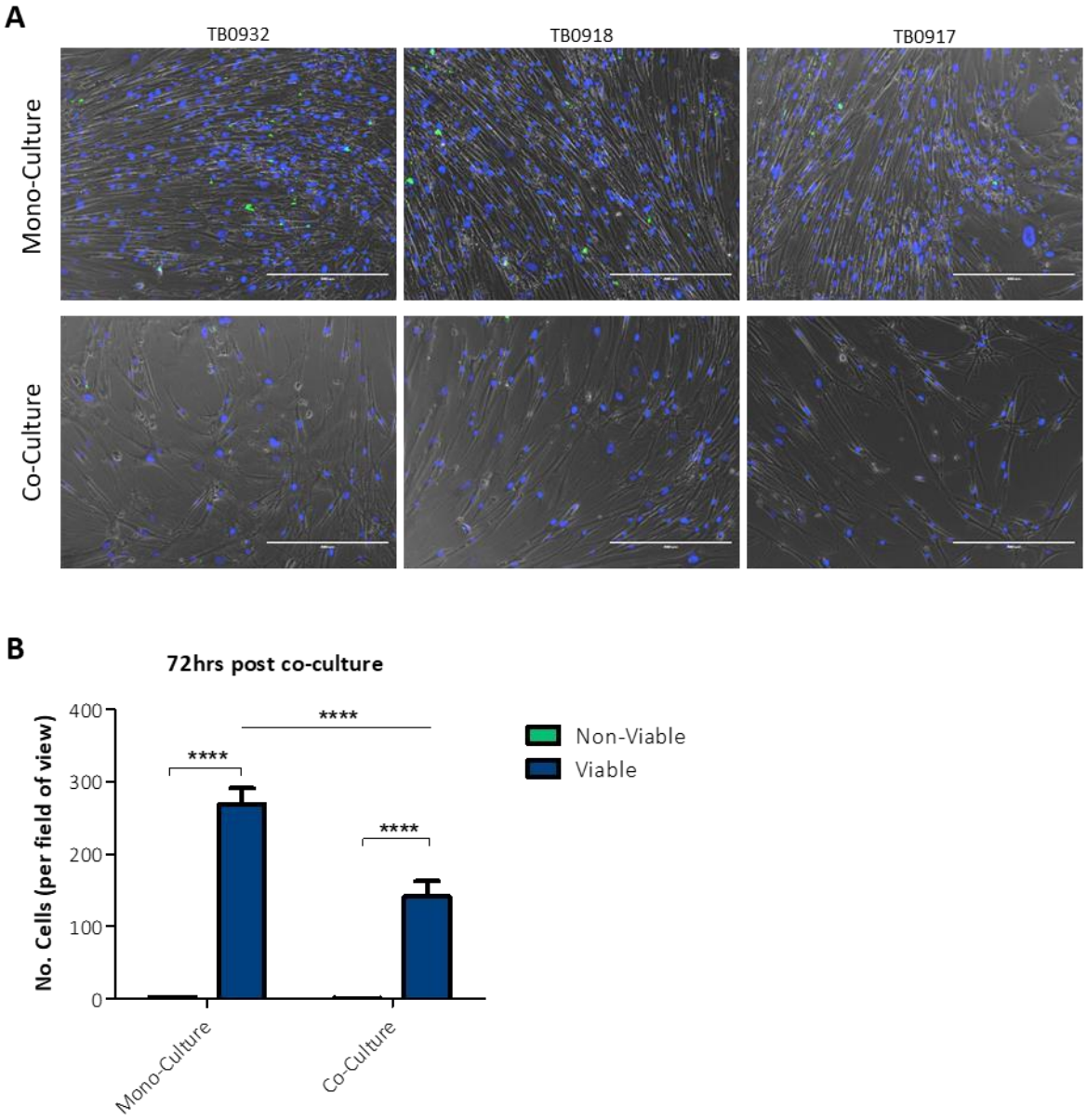

Figure 3.2.2. NHLF cell viability after 72 hrs of mono- or co-culture. (A) After 72 hrs, NHLFs were incubated with ReadyProbes Cell Viability Kit. IMF images were then taken providing a nuclear stain for viable cells (blue) and non-viable cells (green). Images are shown overlaid onto corresponding phase contrast images. Scale bar = 400 µm. NHLF image donor ID: TB0932 **(B)** Via ImageJ 3D objects counter, non-viable and viable cells were counted. In both mono- and co-culture, less that 1% of cells were non-viable and there were significantly less viable cells in co-culture compared to mono-culture. NHLF mono-culture n = 7 (3x donors: TB0917 [2], TB0918 [2], TB0932 [3]), co-culture n = 6 (3x donors:TB0917 [2], TB0918 [2], TB0932 [2]). **** $p < 0.0001$. 2-way ANOVA, Bonferroni multiple comparisons.

24 hrs *CXCL1* and *CSF3* were not reliably expressed at 72 hrs they were, suggesting that they may be under temporal regulation. The developmental signalling protein WNT3A and the inflammatory protein TNF-α were not reliably expressed. However, the

interesting implication was that, in co-culture, NHLFs are more pro-inflammatory whilst also less likely to be entering a state of senescence.

Protein concentrations in the CM after 72 hrs of culture also significantly differed between mono- and co-culture. Using Multiplex and standard ELISA, immunemodulating proteins were measured in the basolateral CM of NHLF mono-cultures, NHLF co-cultures and HBEC mono-cultures **(*Figure* 3.2.4.)**. As previously, all 39 analytes were detectable but again the majority were at low concentrations, <100 pg/ml, including concentrations of IL-1α, IL-1β and IL-33. Of those detected at concentrations >100 pg/ml, all were significantly elevated in co-cultured NHLFs. For VEGF, G-CSF, GM-CSF, CX_3CL1, CXCL10, IL-6 and CXCL8, co-culture concentrations were significantly higher than either NHLF or HBEC mono-cultures; no differences were observed between monocultured NHLF and HBECs. In the case of CCL7 and CCL2, there was an increase with coculture, but production by mono-cultured HBECs was extremely low, highlighting that these two factors are likely to be exclusively produced by the NHLFs, an interesting result considering that in LPS-challenged mice CCL2 is localised exclusively to epithelial cells [272]. Conversely, NHLF mono-culture CM contained extremely low concentrations of TNFα and CXCL1, with significantly higher concentrations in HBEC mono-culture. In the case of CXCL1 co-culture did not change protein concentration but, for TNF-α, co-culture significantly reduced levels in the CM, suggesting that TNF-α is predominantly derived from the epithelium and that co-culture can reduce its expression. One important consideration to make is that only the basolateral CM of co-cultures was analysed. As HBECs form a functioning epithelial layer they become polarised, this polarity means that secretion can be directed exclusively in either a basolateral or an apical direction. Therefore, the effect of co-culture may cause significant changes in apical HBEC secretion that will not have been observed with these experiments. However, these results do reaffirm those found at an RNA level, indicating a more inflammatory environment in co-culture, influenced by secretory signalling.

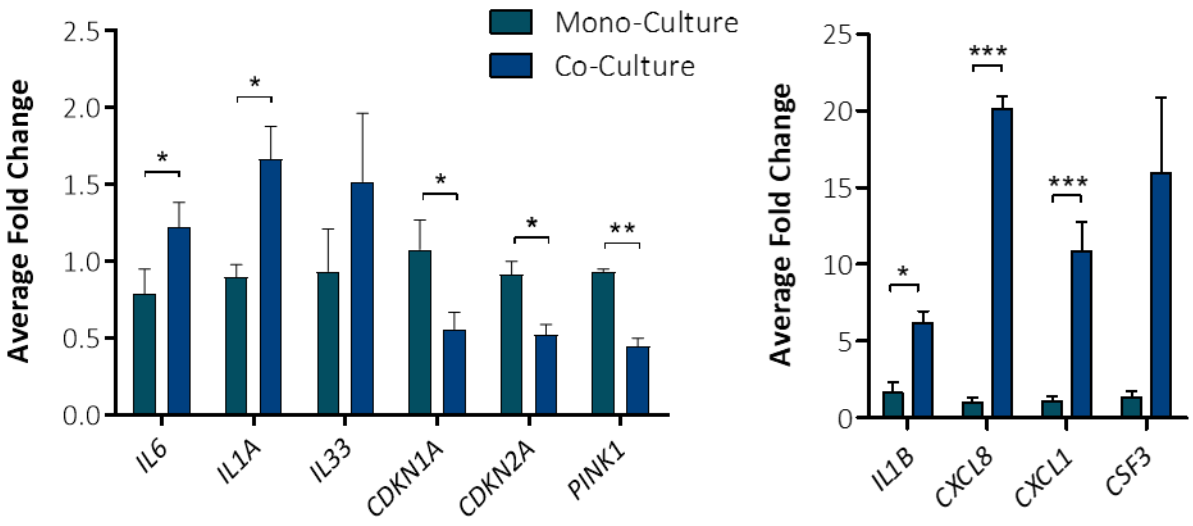

Figure 3.2.3. Comparison of NHLF RNA levels after 72 hrs of mono- or co-culture. RT-qPCR was performed with genes of interest normalised to the reference genes *B2M* and *GAPDH.* NHLF co-culture RNA levels were calibrated to mono-culture levels and the data is shown as an average fold change. Data is shown across 2 graphs of differing y-axis. *IL6*, *IL1A*, *IL1B, CXCL8* and *CXCL1* RNA levels are all significantly elevated in co-culture whereas *CDKN1A*, *CDKN2A*, *MPST*, *CTH, CBS* and *PINK1* are all significantly decreased. *TNFA* and *WNT3A* were not reliable expressed. NHLF n = 5 (3x donors: TB0917 [2], TB0918 [2], TB0932). *** $p < 0.001$, ** $p < 0.01$, * $p < 0.05$. Two-tailed, paired t-test, performed on ddCt values.

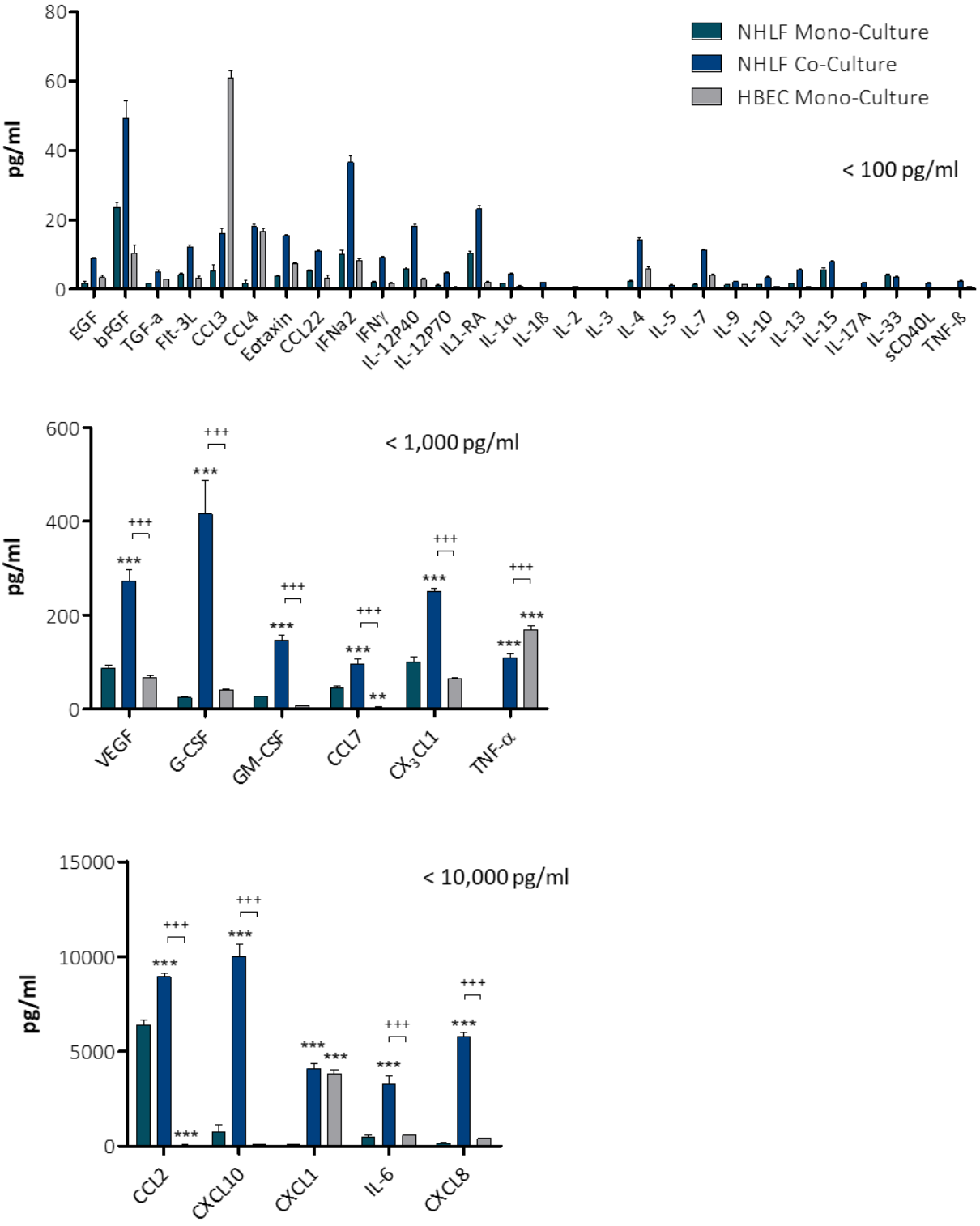

Figure 3.2.4. Multiplex cytokine array comparing NHLF mono-cultured, NHLF co-cultured and HBEC mono-cultured CM, 72 hrs post co-culture. Basolateral media were collected and stored at -80 °C. After thawing, conditioned media were analysed via Luminex Multiplex array, screening for immuno-modulating cytokines, chemokines and growth factors. Results are shown across 3 graphs of differing y-axis scales. Across all analytes detected at a concentration >100 pg/ml there was a significant increase in concentration for NHLF in co-culture. Likewise, co-culture concentrations were all significantly higher when compared to mono-cultured HBEC with the exception of CXCL1, in which there was no significant difference, and TNF-α, in which concentrations were higher in HBEC mono-culture. NHLF n = 12 (4x donors: TB0912 [3], TB0917 [3], TB0932 [3], TB0918 [3]). **** $p < 0.0001$, ** $p < 0.01$ (vs NHLF mono), +++ $p < 0.001$ (vs NHLF co). 1-way ANOVA, Tukey's multiple comparison.

3.2.2.2. NHLF co-culture enhances epithelial development via bi-directional secretory communication.

The effect that NHLF co-culture had on the epithelial cells phenotypes was next considered, using the same experimental conditions and in the context of epithelial development - a process reliant on crosstalk and implicated in IPF. Firstly, ionic permeability, considered as a function of development, was quantified by measuring trans-epithelial electrical resistance (R_{TE}). This was achieved using a chopstick electrode voltohmeter. As ionic permeability decreases, electrical resistance is increased and this quantitative increase is taken as qualitative increase in epithelial barrier integrity and function, a process that occurs in the developing lung. R_{TE} was measured at 24 hr intervals, up to 72 hrs, in mono- or co-cultures. With each day, R_{TE} increased in both culture types **(*Figure* 3.2.5A.)**, however from 24 hrs onwards, there was a significant increase in R_{TE} when HBECs were co-cultured with NHLFs. At 72 hrs this difference remained significant **(*Figure* 3.2.5B.)**.

This augmentation of R_{TE} in co-culture was achieved with an initial NHLF seeding density of 12,000 cells/well. To see if this effect was a function of basolateral cell number, the experiments were repeated across a range of NHLF seeding densities **(*Figure* 3.2.6A.)**. After 72 hrs of co-culture it was found that, with either half or double the seeding density, R_{TE} was still increased compared to mono-culture and that there was no significant difference in R_{TE} between differing seeding densities **(*Figure* 3.2.6B.)**. There is therefore a large tolerance in this system for cell number and it would be interesting to further investigate just how few HLFs are required to mediate an increase in R_{TE}.

The setup of the transwell co-culture is designed to prevent epithelial-mesenchymal contact. To test whether the increase in R_{TE} was the result of exclusively secretory communication, R_{TE} was measured over 72 hrs in mono-cultured HBECs treated with the CM from either an NHLF-HBEC co-culture, or the CM from an NHLF mono-culture **(*Figure* 3.2.7A.)**. The CM was derived from a previous 72 hr culture and transferred directly to mono-cultured HBECs at 0 hrs. By 72 hrs, co-culture and both CM treatments had

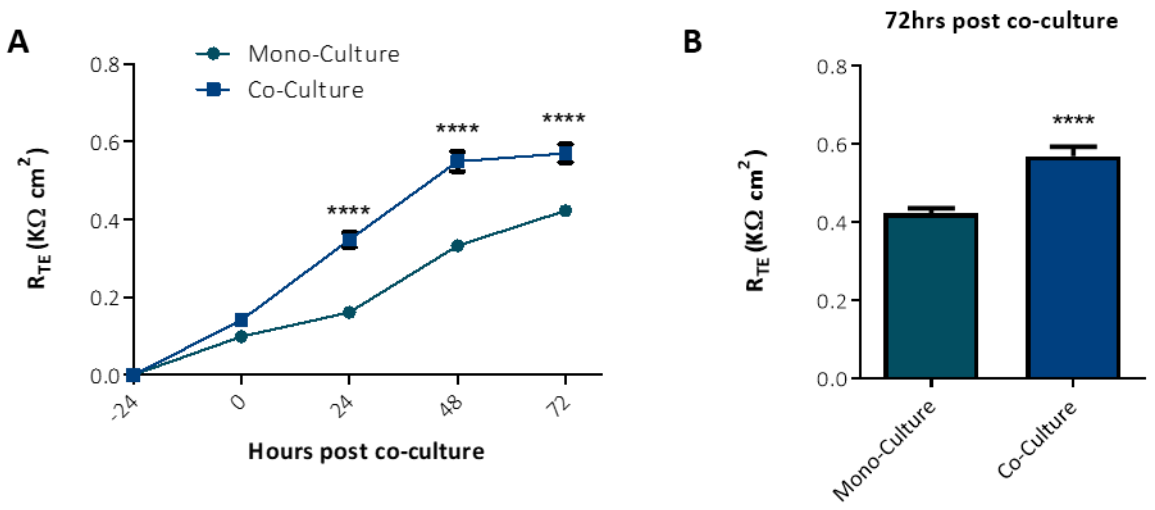

Figure 3.2.5. Comparison of R_{TE} over 72 hrs between HBEC in mono-culture or in co-culture with NHLFs. (A) At -24 hrs NHLFs were seeded in 24-well plates (DMEM 10% FBS [12,000 cells/well]) and HBEC were seeded in transwell inserts (αMEM 10% FBS [22,000 cells/insert). At 0 hrs the media for both cell types was changed to a 1:1 mix of DMEM / αMEM (10% FBS) and HBEC inserts were transferred to either mono-culture or to co-culture, with basolateral NHLF. R_{TE} was measured every 24 hrs up to 72 hrs. NHLF co-culture significantly increase R_{TE} over this time course. **(B)** Average R_{TE} values at 72 hrs post co-culture from (A). NHLF n = 9 (6x donors: TB0912 [2], TB0916 [2], TB0918 [2], TB0917, TB0916, TB0932), HBEC n = 9. **** $p < 0.0001$. 2-way RM ANOVA, Bonferroni multiple comparisons.

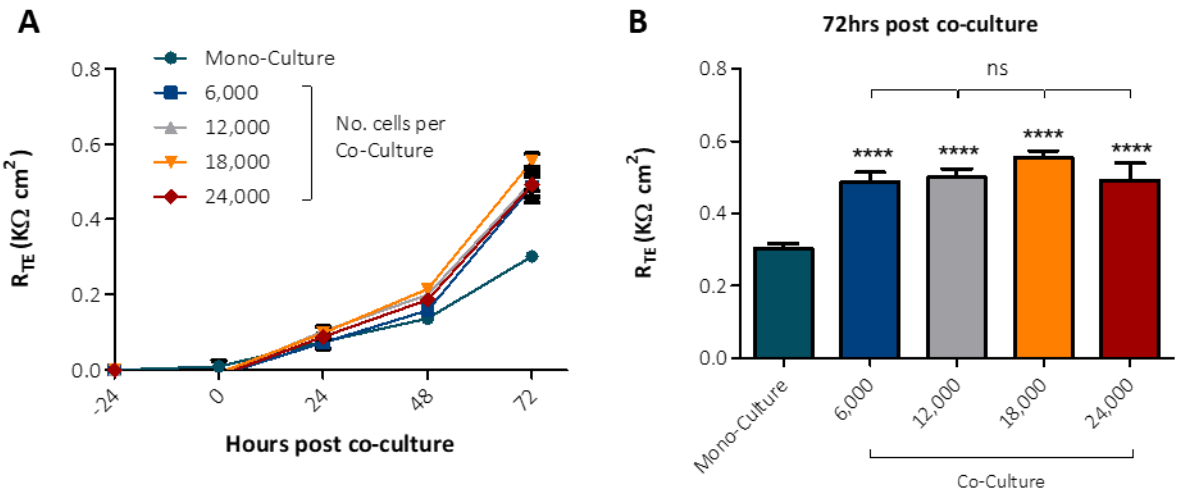

Figure 3.2.6. Effect of the number of co-cultured NHLFs on R_{TE} over 72 hrs. (A) R_{TE} was measured over 72 hrs of mono-culture or co-culture, with a range of NHLF co-culture seeding densities used at -24 hrs. **(B)** Average R_{TE} values at 72 hrs post co-culture. There was no significant difference in R_{TE} between the different NHLF seeding densities. NHLF n = 6 (3x donors: TB0916 [2], TB0921 [2], TB0912 [2]), HBEC n = 6. **** $p < 0.0001$. 2-way RM ANOVA, Bonferroni multiple comparisons.

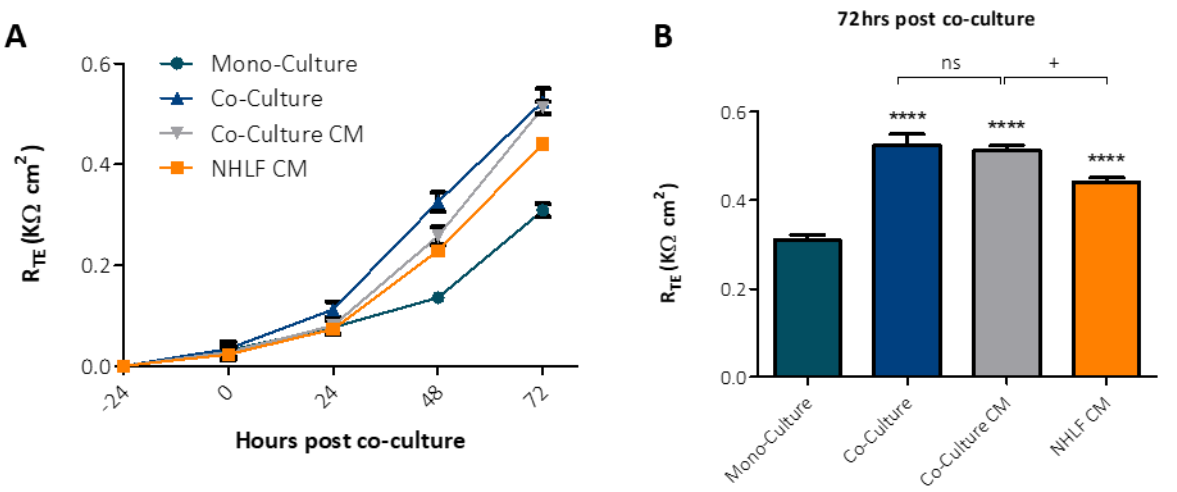

Figure 3.2.7. Effect of NHLF co-culture and NHLF mono-culture CM on R_{TE} over 72 hrs. (A) R_{TE} was measured over 72 hrs of mono-culture or NHLF co-culture. R_{TE} was also measured in HBEC mono-culture treated with CM from either: the basolateral compartment of a 72 hr NHLF co-culture, or a 72 hr NHLF mono-culture. All CM treatments were donor matched. **(B)** Average R_{TE} values at 72 hrs post co-culture. Co-culture and CM treatments all significantly increased R_{TE} at 72 hrs. There was no significant difference between co-culture and treatment with co-culture CM but co-culture CM significantly increased R_{TE} when compared to NHLF mono-culture CM treatment. NHLF n = 9 (3x donors: TB0917 [3], TB0916 [2], TB0918 [2]), HBEC n = 9. **** $p < 0.0001$, + $p < 0.05$. 2-way RM ANOVA, Bonferroni multiple comparisons.

significantly increased R_{TE} compared to HBEC mono-culture. Co-culture and treatment with co-culture-derived CM equally elevated R_{TE} and there was no significant difference between them. The elevation from NHLF mono-culture-derived CM was, however, significantly less potent than that of the two co-culture treatments, indicating that a bidirectional relationship exists between the cell types and that signalling from the epithelium may be required to promote the secretion of trophic factors by NHLFs **(*Figure* 3.2.7B.)**.

The effect of co-culture on HBEC cell number was also considered. Cell number was counted using a haemocytometer and RCN calculated at 24 hr intervals **(*Figure* 3.2.8A.)**. At 72 hrs, RCN was significantly lower in co-culture than in mono-culture **(*Figure* 3.2.8B.)**, indicating that co-culture reduces both NHLF and HBEC cell number. To understand the relationship between RCN and R_{TE}, R_{TE} was measured at 72 hrs just prior to cell counting. By plotting the values of RCN against corresponding R_{TE}, an inverse relationship between cell number and R_{TE} was found, where the greater the RCN, the lower the R_{TE} **(*Figure* 3.2.9.)**. Since increased cell number was therefore not required for increased $R_{TE,}$ this further raised the question of how does co-culture promote epithelial barrier development?

Tight junction formation is a requisite of HBEC function and enables establishment of an epithelial barrier that is both impermeable to macromolecules and ions. It was hypothesised that the increase in R_{TE} elicited by co-culture could be the result of increased tight junction formation. ZO-1 is an archetypal tight junction protein expressed in numerous epithelial cell types. The presence of ZO-1 was examined in HBECs cultured over 72 hrs by IMF **(*Figure* 3.2.10A.)**. The protein was expressed predominantly at the periphery of each cell where it formed junctions. This was evident in both culture conditions. Epithelial layer thickness and an undulating contour meant that any one plane of focus under microscopy could not show all cellular junctions and, *prima facie*, there was no observable difference in protein expression. Therefore, western blotting was performed on protein lysates **(*Figure* 3.2.10B.)**. By analysing the relative density of chemiluminescent banding, no significant difference in ZO-1 protein

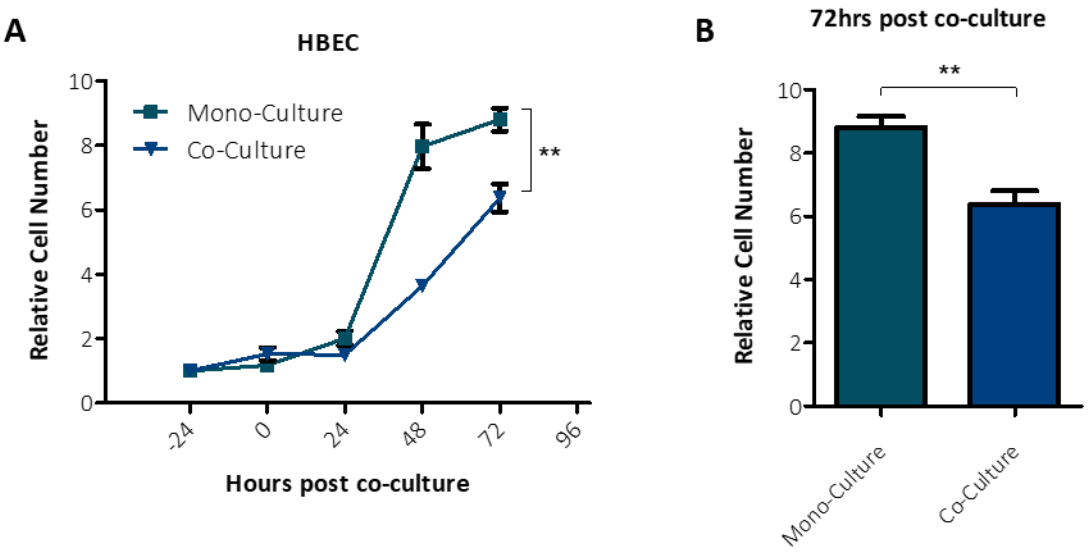

Figure 3.2.8. HBEC cell number over 72 hrs in mono-culture or NHLF co-culture. (A) HBECs were seeded at 22,000 cells/insert at -24 hrs in αMEM 10% FBS. At 0 hrs media were changed for DMEM / αMEM 10% FBS and cells were either left in mono-culture or transferred to co-culture with NHLFs. At 24 hr intervals, over 72 hrs, HBEC cell numbers were counted using a haemocytometer. Cell numbers are shown relative to the initial seeding density. **(B)** Relative cell number 72 hrs post co-culture. Cell number was significantly greater in mono-culture than co-culture. HBEC with NHLF co-culture n = 3 (3x donors: TB0917, TB0918, TB0932), HBEC mono-culture n = 4. ** $p < 0.01$, * $p < 0.05$. 1-way ANOVA, Tukey's multiple comparisons.

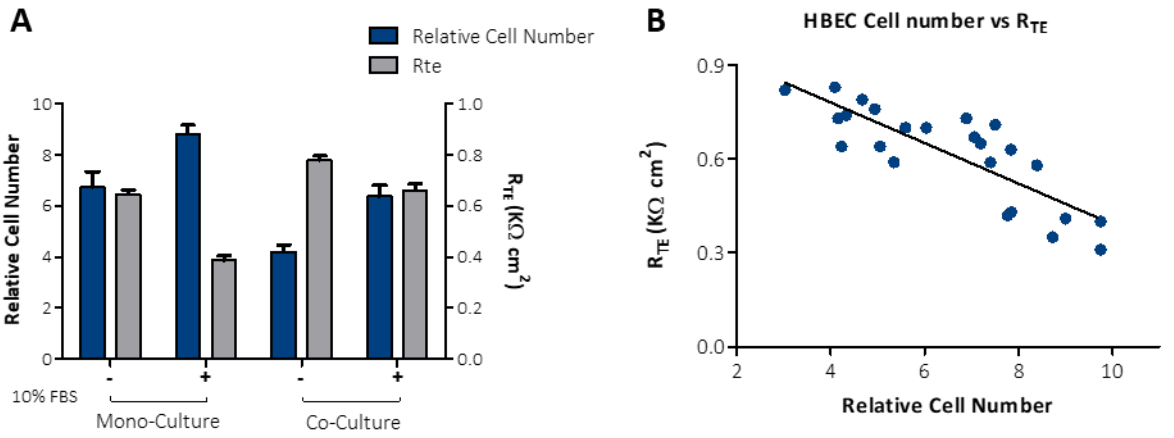

Figure 3.2.9. Relationship between the HBEC cell number and corresponding R_{TE}. (A) Comparison of relative HBEC cell number (blue) to R_{TE} (grey) in mono- or co-culture with or without 10% FBS. In mono-culture with + 10% FBS the cell number is high and the corresponding R_{TE} low. In co-culture with (- 10%) FBS this pattern is reversed. **(B)** HBEC R_{TE} can be plotted against HBEC cell number showing a negative correlation. Each point represents 1x insert. $R^2 = 0.684$, linear regression.

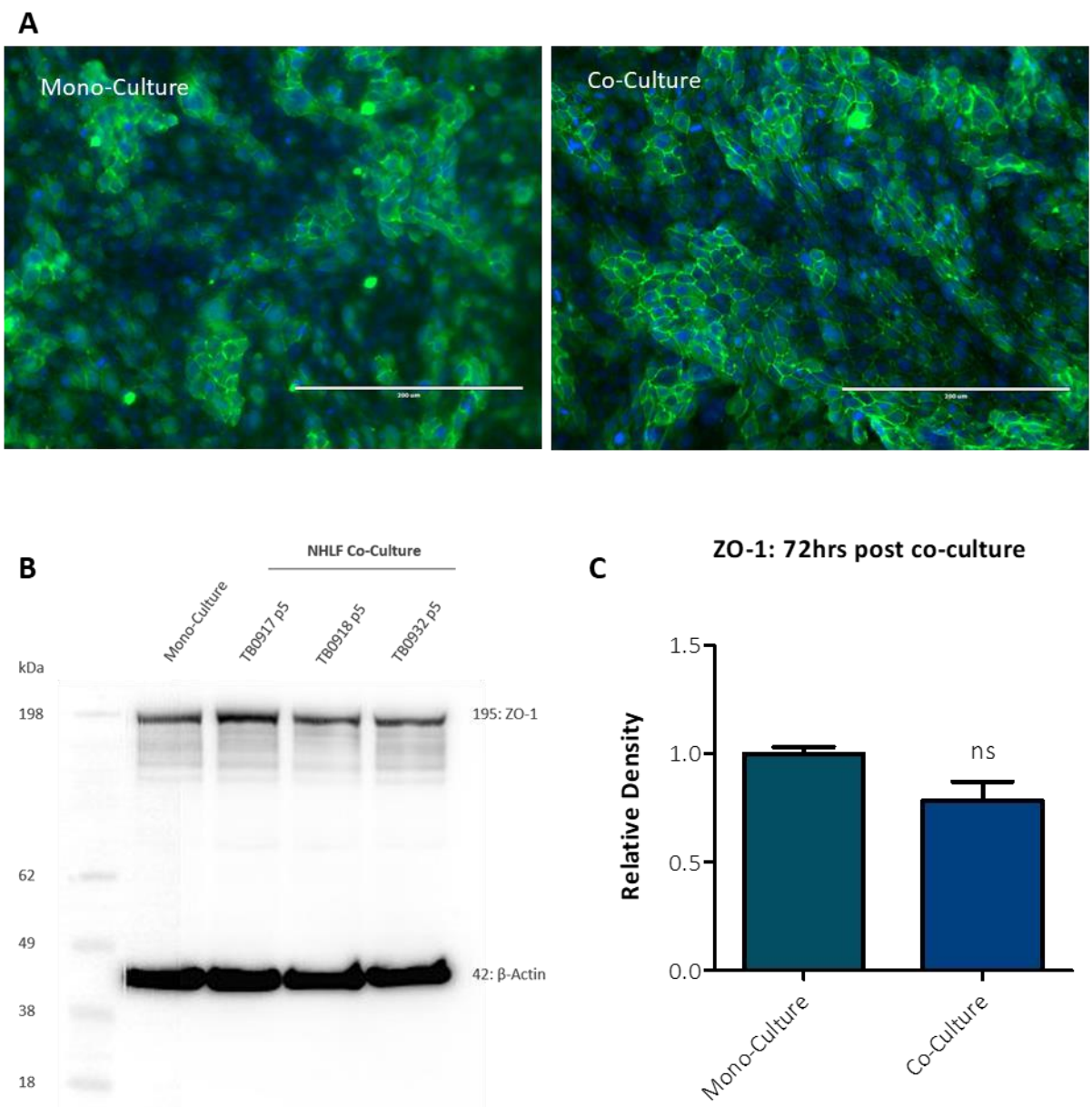

Figure 3.2.10. IMF imaging and western blot quantification of ZO-1 protein in HBECs, comparing mono- and co-culture. (A) HBECs stained for ZO-1 tight junction protein (green) and DAPI 72 hrs after either mono- or co-culture. Representative images from 9x co-culture and 3x mono-culture experiments. Co-culture image produced from experiment using TB0917. Scale bar = 200µM. **(B)** 72 hrs post culture, HBEC protein was extracted and western blot performed for ZO-1 (198kDa) with β-actin (42kDa) as a loading control. Representative blot image (1 of 3) shown for 1x mono-culture and 3x co-culture across 3 donors. **(C)** Relative band density as quantified via ImageJ Gel analysis (relative to mono-culture). There is no significant difference in ZO-1 band density between mono- and co-culture. NHLF n = 9 (3x donors: TB0917 [3], TB0918 [3], TB0932 [3]), HBEC n = 3. Two-tailed, unpaired t-test.

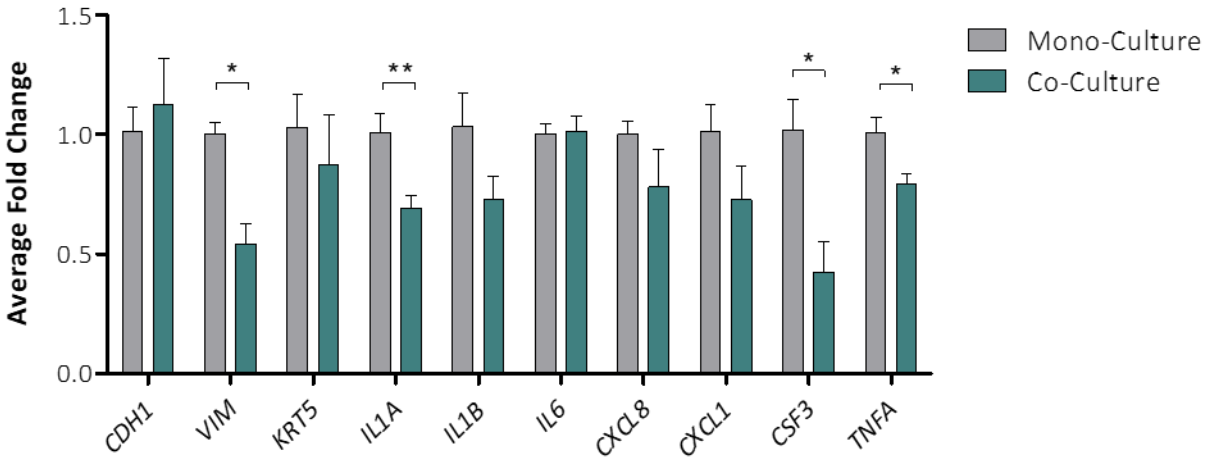

Figure 3.2.11. Comparison of HBEC RNA levels after 72 hrs of mono- or co-culture. RT-qPCR was performed with genes of interest normalised to the reference genes *B2M* and *GAPDH.* HBEC co-culture RNA levels were calibrated to mono-culture levels and the data is shown as an average fold change. RNA levels of *VIM*, *IL1A, CSF3* and *TNFA* were all significantly decreased in co-culture. There was no significant change in other genes of interest. NHLF co-culture n = 7 (3x donors: TB0917 [2], TB0918 [2], TB0932 [3]), HBEC mono-culture n = 4. ** $p < 0.01$, * $p < 0.05$. Two-tailed, unpaired t-test performed on ddCt values.

expression was quantifiable between mono- and co-culture, indicating the R_{TE} improvements are not related to expression level or localisation of this tight junction protein **(*Figure* 3.2.10C.)**. It may be that a distinction could be found by assessing expression of other types of tight junction protein, such as E-cadherin - an experiment that could be performed in the future.

HBEC RNA levels were also measured, 72 hrs after culture. As well as the repertoire of inflammatory signals previously analysed, the epithelial marker *CDH1* and the mesenchymal marker *VIM* were also assessed, as well as the BC marker *KRT5* and the epithelial inflammatory cytokine *TNFA* **(*Figure* 3.2.11.)**. *CDH1* and *KRT5* were both reliably expressed but levels did not change under differing culture conditions. *VIM* was also expressed and levels decreased in co-culture, suggesting a shift towards a more epithelial phenotype. Regarding inflammatory markers, *IL1A*, *CSF3* and *TNFA* levels were all decreased in co-culture, whereas other transcript levels remained the same. The decrease in *TNFA* levels were consistent with the reduced CM protein levels previously observed. The decrease in inflammatory markers was contrary to results found in cocultured NHLFs, suggesting that the co-cultured epithelium is less inflamed despite functioning in a seemingly more pro-inflammatory micro-environment.

3.2.2.3. NHLF co-culture enhances HBEC re-epithelialisation after injury.

Crosstalk facilitates epithelial repair and epithelial injury is implicated as a driving force in IPF; therefore, to begin to understand the dynamics of wound repair in the model of crosstalk, HBECs in mono- or co-culture, were wounded, allowing investigation of the role of secretory communication in re-epithelialisation. HBECs were cultured for 72 hrs then mechanically wounded by drawing a scratch down the centre of the monolayer with a 200 µl pipette tip. The inserts were then returned to their respective culture environment and incubated for a further 9 hrs, with phase contrast images taken at 3 hr intervals. With these images the percentage of wound closure was calculated. Briefly, using ImageJ, for each phase contrast image the wound void was demarcated, allowing conversion to a binary image. The area of the image covered by wound void could then

be calculated at each subsequent time interval. By calculating subsequent wound areas as a percentage of the starting area, the percentage by which the wound had closed over time could be gauged. For example, in the HBEC mono-culture wound shown in **(*Figure* 3.2.12.)**, at 0 hr wound closure was 0%, at 3 hrs the void had decreased in size by 5.33% and by 9 hrs it had decreased by 51.07%. Analysis was performed as a percentage of starting wound due to the variability of starting wound size. The images in ***Figure* 3.2.12.** represent the images and analyses generated when comparing reepithelialisation between mono- and NHLF co-cultured HBECs over 9 hrs **(*Figure* 3.2.13A.)**. After 9 hrs, the percentage wound closure in co-culture was significantly higher than mono-culture, with a mean of 66.16% closure versus 40.33% **(*Figure* 3.2.13B.)**. Therefore, co-culture promotes re-epithelialisation.

When looking at phase-contrast images it was difficult to understand how reepithelialisation was taking place. To gain a better understanding, 9 hrs post-wounding HBECs were fixed and stained for actin, using Texas Red-conjugated phalloidin and IMF images taken. At a lower magnification, representative mono-culture images show a region of open wound and a region of closing wound **(*Figure* 3.2.14A-B.)**. In both, there was actin present around the periphery of cells, and also in fibres, which ran across multiple cells. At a higher magnification **(*Figure* 3.2.14C-D.)**, these stress fibres were found to orientate parallel to the leading edge. Further back from this front, orientation was re-configured, with fibres running perpendicular to the leading edge. The fluorescent signal arising from these fibres at the leading edge was very strong, however, at certain intervals this signal was interrupted by single cells extending broad lamellipodia into the wound void. The frequency of these salient cells was seemingly random. Images taken at the highest magnification **(*Figure* 3.2.14E-F.)**, further highlight the organisation of parallel stress fibres at the leading edge. Differentiating the organisation between mono- and co-culture was not possible. However, these images describe a mode of migration in which adherent HBECs move in unity, led by individual cells on the leading edge that determine directionality by extending processes into the wound void. The continuous leading edge is maintained by parallel actin stress fibres but, further back, actin is re-orientated to enable the stretch of the epithelial sheet over

the wound void. The 9 hr time-course of these experiments limited the effect of HBEC proliferation and this understanding of sheet migration is concurrent with previous literature **(Intro.1.1.3.3.)** [77,78]. It could therefore be postulated that the microenvironment created in co-culture accelerates migration, possibly via the fibroblastmediated secretion of chemotactic proteins in response to epithelial injury,

Finally, the effect that epithelial wounding and the re-epithelialisation process had on the RNA levels of NHLF inflammatory wound signals was assessed by RT-qPCR. NHLF RNA was extracted 72 hrs after co-culture, either before wounding (0 hrs) or 9 hrs after wounding. It was unclear if 9 hrs would be long enough to have significant transcriptional effects on inflammatory markers but it was hypothesised that with wounding they would be increased. Though senescence is important in wound healing, literature evidence would suggest that this response occurs later in repair and that the senescence phenotype takes many days to develop *in vitro*. Therefore, levels of CDK inhibitors were not expected to change. The growth factors HGF and KGF (encoded by *FGF7*) were also assessed, as they are known to be important in promoting epithelial repair, and it was thought that they would be elevated [83,273]. The results found levels of *CXCL8, IL1B* and *CXCL1* to be significantly elevated, however levels of *IL6, IL1A* and *IL33* were unchanged. Levels of *HGF* and *CDKN1A* were both significantly decreased and there was no change in levels of *FGF7* or *CDKN2A* **(*Figure* 3.2.15.)**. The results suggest a limited increase in inflammatory signalling with wounding yet an ability of the damaged epithelium to signal to basolateral fibroblasts and alter their behaviour.

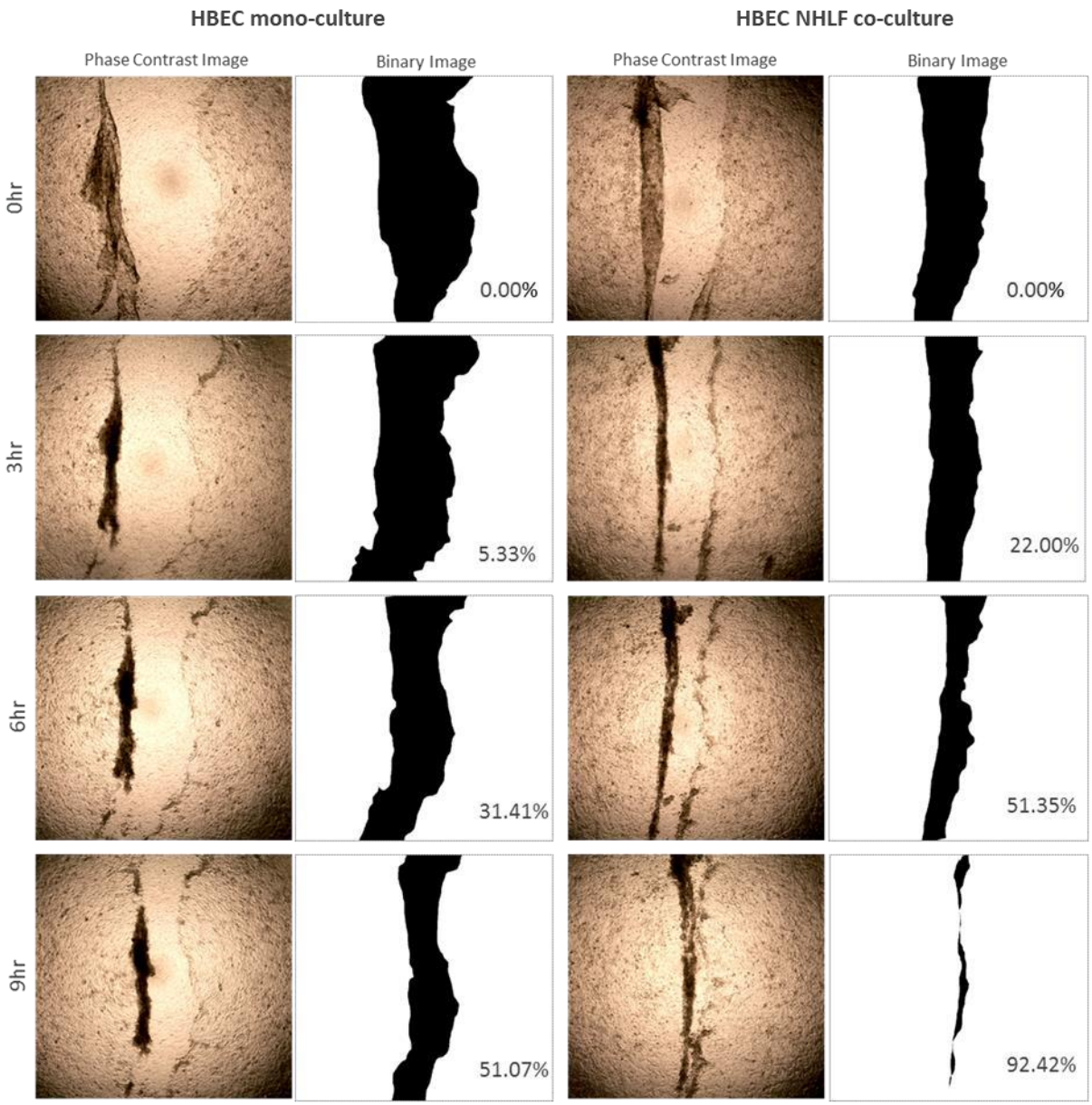

Figure 3.2.12. Representative images of HBEC mono-culture and co-culture wound closure over 9 hrs with ImageJ quantification. After 72 hrs were mechanically wounded by pipette scratch. Phase-contrast images were taken and the percentage size of the wound quantified on ImageJ by making a binary image. Wound closure was calculated as a percentage of the starting wound size. Images representative of 8x experiments. Co-culture image produced from experiment using TB0932.

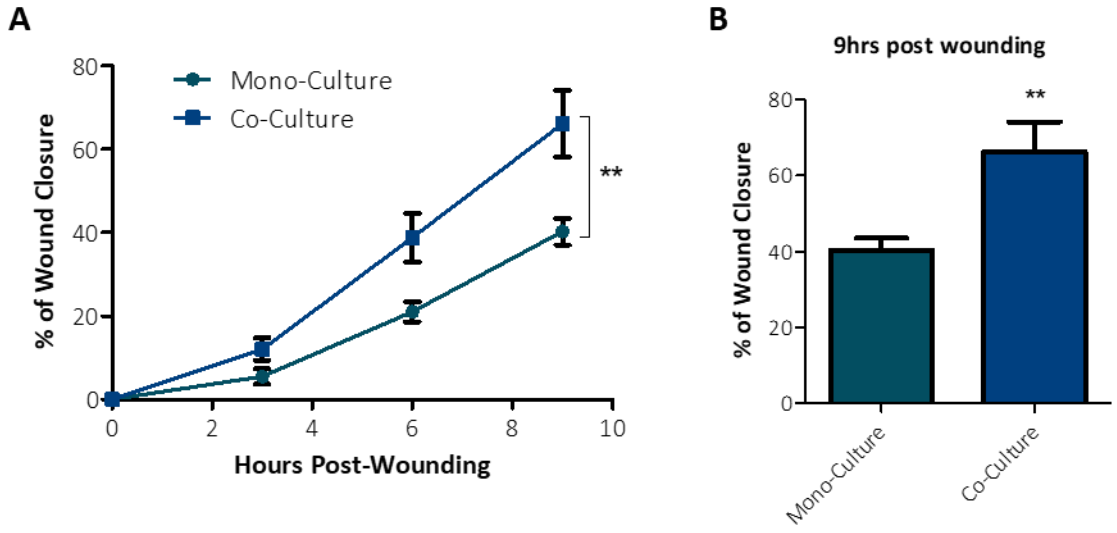

Figure 3.2.13. Comparison of HBEC wound closure between mono- and NHLF co-culture. (A) After 72 hrs of either mono- or co-culture, HBECs, seeded on transwell inserts, were wounded by scratching down the centre of the insert with a p200 pipette. HBECs were then kept in their respective culture conditions for 9 hrs with phase-contrast images taken every 3hrs. Results are shown as a percentage size of the starting wound. **(B)** Percentage of wound closure at 9 hrs. NHLF co-culture corresponds to a significant increase in the percentage of wound closure at 9 hrs. NHLF n = 8 (4x donors: TB0916, TB0917 [2], TB0918 [2], TB0932 [3]), HBEC n = 4. ** $p < 0.01$. 2-way RM ANOVA, Bonferroni multiple comparisons.

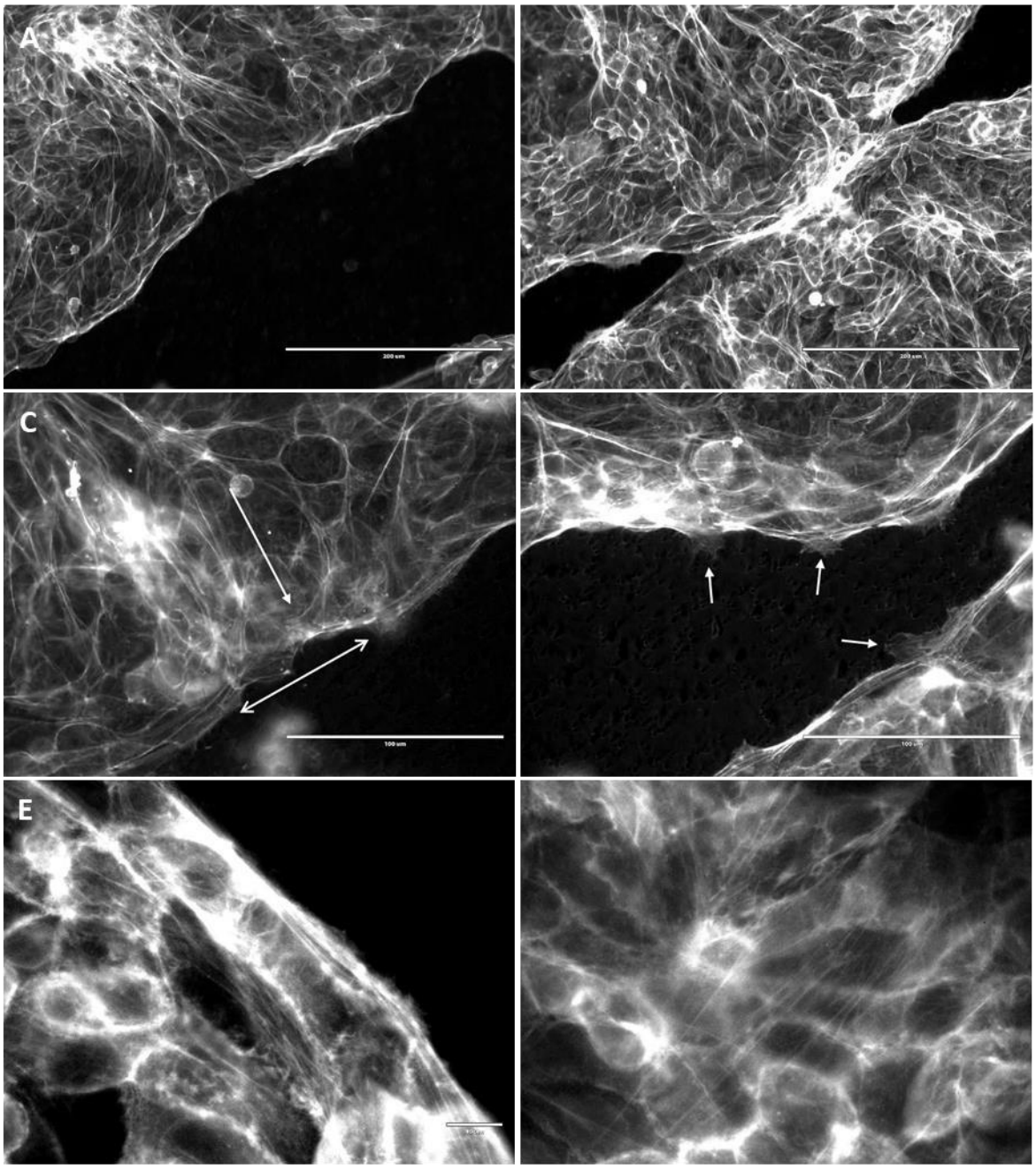

Figure 3.2.14. Representative IMF images of mono-cultured HBEC actin 9 hrs post-wounding. HBECs were fixed and stained with TexasRed conjugated Phalloidin. Images representative of 4x experiments **(A-B)** Scale bar = 200µM. **(A)** A region of unclosed wound. **(B)** Region of wound closure. **(C-D)** Scale bar = 100µM. **(C)** Bi-directional arrow running parallel to the wound edge highlights the actin organisation co-ordinated at the very edge of the migrating epithelial front. Arrow perpendicular to wound edge highlights similar, perpendicular actin organisation directed towards the epithelial front. **(D)** Arrows point towards actin organisation highlighting particular cells along the wound edge that forming protruding filopodia and lamellipodia. **(E-F)** Scale bar = 10µM. **(E)** Magnification of wound edge further highlighting the perpendicular actin structures directly at the leading edge. Further back from the front actin is less organised. **(F)** Image of cells within the migrating sheet showing actin organisation running towards the leading edge.

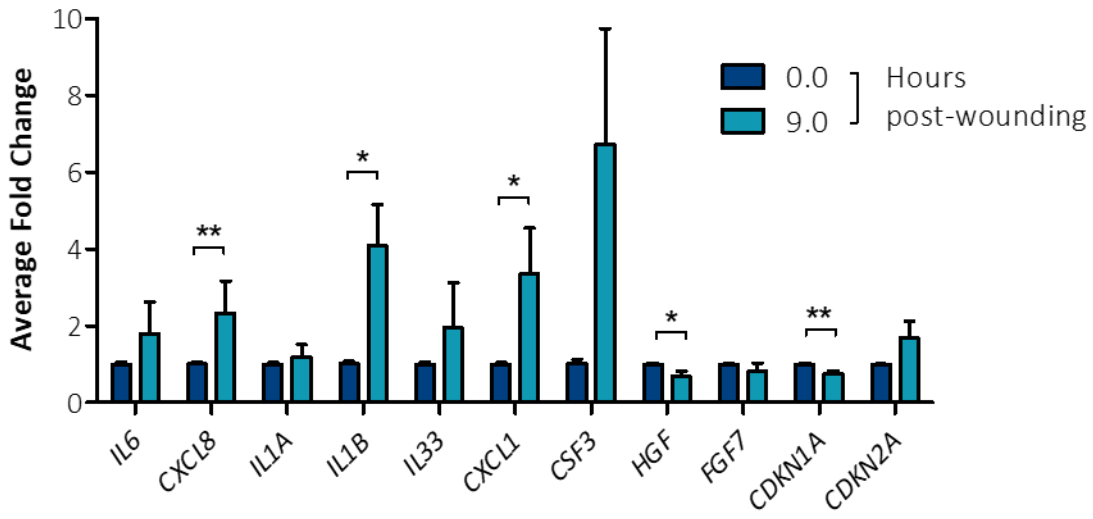

Figure 3.2.15. NHLF RNA levels at 0 and 9 hrs post-wounding, after 72 hrs in co-culture. RNA was isolated from NHLFs, quantified, DNAse treated and cDNA was synthesised. RT-qPCR was performed with genes of interest normalised to the reference genes *B2M* and *GAPDH.* 9.0 hr wound RNA levels were calibrated to 0.0 hr levels and the data is shown as an average fold change. There were significant increases in *CXCL8, IL1B* and *CXCL1* RNA levels and significant decreases in levels of *HGF* and *CDKN1A*. NHLF n = 7 (3x donors: TB0917, TB0918 [3], TB0932 [3]). ** $p < 0.01$, * $p < 0.05$. Two-way, unpaired t-test performed on ddCt values.

3.2.3. Discussion

This section set out to investigate the effect of co-culturing NHLFs with HBECs, with the aim of establishing a model of secretory crosstalk that could be used to uncover the role of FHLFs in IPF. NHLFs in co-culture have a lower cell number and display a more inflammatory phenotype. They do however promote HBEC development and reepithelisation. This is concomitant with reduced HBEC proliferation and decreased inflammatory gene expression. Taken together this suggest that, though more inflammatory than mono-culture, co-culture is nevertheless beneficial to HBEC function.

Maintaining homeostasis?

An aim of establishing this model was to recapitulate the secretory communication found in the lung airways. Epithelial-mesenchymal crosstalk plays an important role in maintaining homeostasis in the adult lung and therefore the reduction in cell number could be viewed as a reflection of homeostatic maintenance, a process that goes wrong in IPF. However, all other aspects of the results produced in this section would point towards much more active and dynamic processes occurring in co-culture. Therefore, though proliferation results are consistent with the idea of homeostasis, it is more likely that the model of crosstalk actually recapitulates processes of development and repair.

Epithelial development or an epithelial response to injury?

One of the important measurements employed in this investigation was R_{TE}. Initially, measurements of R_{TE} were seen as indicative of epithelial development, a measure of the processes that occur to establish the adult airways and processes that are also pertinent to the pathology of IPF. However, this investigation was not able to fully appreciate the role of developmental pathways in co-culture. *WNT3A* expression was assessed at an RNA level but found to be unreliably expressed and other key signalling proteins such as FGF10 and BMP4 were not investigated. This could be investigated in future experiments, initially by assessing RNA levels of developmental genes (including the broad range of other WNT genes) and then by measuring protein concentrations in the CM. This would add another dimension to this investigation and it would be

hypothesised that, as IPF is characterised by an aberrant reactivation of developmental signalling pathways, that these proteins would be elevated when investigating FHLFs in co-culture. Instead however, due to the focus of this study, these experiments found the co-culture microenvironment to be dominated by pro-inflammatory, wound-associated signalling mediators.

Inflammatory micro-environment

This pro-inflammatory micro-environment was of interest, potentially reflecting a more injury-associated environment. However, the proteins upregulated were also strongly associated with the SASP and NHLFs in co-culture were also less proliferative. This suggested that more cells could be beginning to enter a state of senescence. Morphologically though, these cells appeared normal and, at an RNA level, there was a decrease in expression of senescence regulators, making this possibility unlikely. Therefore, viewing the increase in inflammation from the perspective of wound healing was deemed to make more sense. At 0 hrs, when HBECs were introduced into coculture, the cells were not confluent; they were dispersed in colonies across the insert membrane **Appendix (*Figure* 6.1.3)**. This starting point may itself recapitulate a wounding event in the lung. Numerous forms of lung injury can occur that result in a denuding of the epithelial basement membrane and, though the stimulus of epithelial cell death was not present in this system, in essence, HBECs were put into a system in which they were required to repopulate a denuded membrane. Arguably this recapitulates injury and would begin to explain the increase in inflammatory signalling from the underlying fibroblasts. Therefore, in this study, it is more suitable to view R_{TE} experiments in the context of epithelial injury.

Epithelial regeneration

When viewing the co-culture system as a response to injury, R_{TE}, instead of a measure of development, can be described as a useful measure of the latter stages of epithelial regeneration. Airway denudation leads to epithelial migration and proliferation, which forms a permeable epithelial layer. This ‘leaky’ epithelium becomes more impermeable

with time. R_{TE} quantifies ionic permeability and can therefore be used to describe the process of HBEC regeneration in co-culture.

Arguably, regeneration elicits the use of many of the signalling pathways found in development, and it is a limitation of this study that they were not fully investigated, with a focus instead on immune-modulating signalling factors. However, the results from this section can support the concept of an epithelial response to injury, whereby the factors upregulated throughout this response are elevated. Understanding how coculture increases R_{TE} does remain partially unclear and, although HBECs express receptors for many of the signalling factors investigated, to gain a better understanding of how co-culture promotes regeneration, interrogation of regenerative growth factors, such as HGF and KGF, in the basolateral CM could be performed. This isn't without complication however as a simple increase in growth factors may not identify the cause of increased R_{TE}. In co-culture, HBECs proliferate less, which is related to an increase in R_{TE}. Therefore, co-culture is not beneficial due simply to an increase in growth factorinduced proliferation. Instead crosstalk is modulating HBEC phenotype and functionality in other ways, perhaps by enhancing differentiation.

The decrease in HBEC *VIM* expression could suggest this and the possibility of increased differentiation could be measured by staining for various differentiation markers such as *KRT5, MUC5AC* and *FOXJ1*. Preliminary experiments were previously performed using confocal microscopy, which allowed 3D assessment of the relatively thick, pseudostratified epithelial layer, and some of these markers were investigated in monocultured HBECs **(Appendix *Figure* 6.1.4.)**. These experiments could be repeated after coculture. However, it is unlikely that full differentiation to mucosal and multi-ciliated cell types would be observed by 72 hrs. Previous investigations have extended cultures up to 28 days in order to evaluate this effect and cells were cultured without apical media, exposing them to the air [274]. Therefore, co-culture experiments would have to be similarly extended and adjusted. However, it would be hypothesised that secretory factors produced by these cells would enhance differentiation of HBECs, resulting in

observation of increased numbers of mucosal and multi-ciliated cells via confocal microscopy.

Better understanding this HLF secretory signalling could also be achieved by taking a more global approach to NHLF gene expression. HLFs could be isolated 72hrs post mono or co-culture and microarray experiments performed, allowing gene expression profiling. By utilising gene ontology, enrichment for specific secretory pathways could be identified. It would be hypothesised that co-culture would result in enrichment for pathways relating to regeneration / development, the end products of which could be targeted via neutralising antibodies, attenuating improvements in R_{TE}. Similarly, factors up-regulated in co-culture but not mono-culture could be exogenously applied to monoculture in the form of recombinant proteins, subsequently enhancing R_{TE}.

Epithelial repair

If measurements of R_{TE} represent the latter stages of airway repair, then wound healing assays represent those stages at the start. These assays investigated re-epithelialisation, the process that precedes regeneration and NHLF co-culture was again found to be more beneficial. This is important within the context of IPF, in which there is recurrent injury to the lung. Interestingly, how HBECs respond to recurrent injury remains unknown and it could be interesting to perform multiple scratch assays on the same epithelium, comparing changes in percentage closure with recurrent injury. However, the immortalised HBEC cell line may not be perturbed by repeated injury and it would therefore be useful to investigate using primary epithelial cells or an *in vivo* model, in which aspects such as progenitor cell exhaustion may become important and lead to a decline in repair with repeated injury. Also, by investigating the morphology of the migrating HBECs it was not possible to discern a reason for these observed improvements but it would appear that factors in the micro-environment could accelerate migration. NHLFs further upregulated several inflammatory mediators but, interestingly, factors such as HGF and KGF were downregulated or unchanged. The enhancement of HBEC repair may be due to a whole range of other secretory factors not investigated thus far.

In conclusion, the co-culture of NHLFs and HBECs promotes the ability of HBECs to function in response to injury. The felicity of co-culture, however, remains to be underpinned by a more thorough, mechanistic understanding. Despite this, this investigation has established a series of useful assays and endpoints for future investigation into the nature of FHLF-mediated wound repair in the lung airway, which may further uncover the role of these cells in IPF.

3.3 Fibrotic Human Lung Fibroblasts in a Model of Crosstalk

3.3.1. Introduction

With the establishment of an *in vitro* model of epithelial-mesenchymal crosstalk, and an understanding of the behaviour of NHLFs and HBECs in this system, the next step was to utilise FHLFs in this model. When investigating FHLFs in mono-culture, the differences in RNA and secretory protein levels were minimal. NHLF co-culture experiments have, however, highlighted that the presence of an overlying epithelium can significant alter fibroblast behaviour. This system better recapitulates how HLFs function in their native, airway environment and demonstrates how they can interpret signals from a regenerating or wounded epithelium to reciprocate signalling via protein secretion. Since NHLFs promote epithelial regeneration and promote re-epithelialisation after wounding, the following investigations aimed to understand how FHLFs perform in these assays.

As evidenced from both the literature and the previous co-culture experiments with NHLFs, crosstalk is extremely important for epithelial repair and regeneration. Fibroblast secretions accelerate wound closure, in both AECs and HBECs, and also co-ordinate the regenerative process [41,82,83]. IPF, however, is characterised by an aberrant repair response, in which there is a breakdown of the relationships governing these processes [275]. Though inflammation is critical for repair, in IPF there is evidence for an elevated background of inflammation [166]. This may contribute to a defective repair process by altering the epithelial response to injury. It was therefore envisaged that co-culture with FHLFs may reveal an altered microenvironment, in which there is increased inflammation that impairs epithelial repair.

FHLFs in co-culture

There have been previous investigations into the role of epithelial-mesenchymal crosstalk in IPF. Primarily these have focused on the role of the epithelium in influencing fibroblast expansion and matrix deposition. For example, after mechanical epithelial

injury to cells isolated from healthy guinea-pig, fibroblast to myofibroblast differentiation and collagen deposition are observed *in vitro* [276]. Similarly, experiments have been performed to investigate the effect of epithelial-associated protein signalling on fibroblasts in mono-culture. The healthy epithelium produces PGE_2, which has antifibrotic effects, inhibiting fibroblasts proliferation and matrix deposition [277,278]. Receptors for this ligand are, however, downregulated in isolated primary FHLFs and the cells are refractory to this signalling in mono-culture [279]. This would suggest that FHLFs in a model crosstalk would be highly proliferative, ignoring direct epithelial signalling. Investigating this in co-culture with primary FHLFs has yet to be performed.

Likewise, little research has been conducted on the effect that IPF fibroblasts have on epithelial function however. Epithelial cell death co-localises with aberrant fibroblast expansion in IPF tissue sections and treatment of an alveolar, transformed epithelial cell line with the CM from isolated FHLFs decreases cell number and the quantity of recoverable AEC DNA after 20 hrs [127,280]. Likewise, TGF-β stimulated primary FHLFs produce H_2O_2 in a NOX4 dependent manner, which induces co-cultured, primary epithelial cell death [281]. Exogenously applied H_2O_2 also inhibits AEC wound repair [282]. How FHLFs facilitate epithelial re-epithelialisation and regeneration via secretion in coculture has yet to be established. Therefore, this study aims to provide a novel understanding of the role that FHLFs can play in the epithelial response to injury.

Hypotheses:

1. FHLFs in co-culture would create a micro-environment that fails to recapitulate the augmentation of epithelial regeneration and re-epithelialisation observed with NHLF co-culture.

3.3.2. Results

3.3.2.1. FHLFs show reduced cell number in co-culture, altered morphology and express higher levels of inflammatory signalling factors.

NHLFs in co-culture show attenuated cell number over 72 hrs, as measured by cell counting and viability staining, a characteristic that could be attributed to resource competition or epithelial signalling that impedes growth. IPF is a disease dominated by fibroproliferation and therefore it could be hypothesised that FHLFs in co-culture would proliferate significantly more than NHLFs and have a greater cell count. However, this was not evident. After 72 hrs, co-cultured FHLF RCN was calculated and compared to NHLF RCN. The RCN of FHLFs in co-culture was less than 1.00 and significantly lower than NHLFs, suggestive of proliferative arrest **(*Figure* 3.3.1A.)**. Interestingly, this was complicit with prior morphological and proliferative characteristics observed in these cells under normal conditions. NHLFs had an archetypal, spindle morphology when cultured on plastic and population doublings occurred in around 3-4 days. Anecdotally, FHLFs under the same conditions often displayed a much larger, flattened morphology, population doubling was slower. When assessed via β-galactosidase staining, many of the cells displayed markers of proliferative arrest **(*Figure* 3.3.1B.)**.

In a separate series of experiments and after 72 hrs of co-culture, FHLF and NHLF RNA levels were measured via RT-qPCR. FHLF fold changes were calibrated against NHLF values and a significant elevation in FHLF levels of *CXCL8* was observed **(*Figure* 3.3.2.)**. There were no significant differences between levels of other transcripts, but there was a trend towards an increase in *IL1B*. At the protein level, however, the differences were much more dynamic. The CM from NHLF and FHLF co-culture was collected at 72 hrs and analysed via multiplex ELISA **(*Figure* 3.3.3.)**. As in previous experiments, a broad range of immune-modulating cytokines, chemokines and growth factors were detected. 11 analytes were detected at concentrations of greater than 100 pg/ml and of these, six were quantified at significantly higher concentrations in FHLF CM compared with NHLF CM. Protein concentrations of VEGF, GM-CSF, IL-6, CXCL8, CXCL1 and G-CSF were all

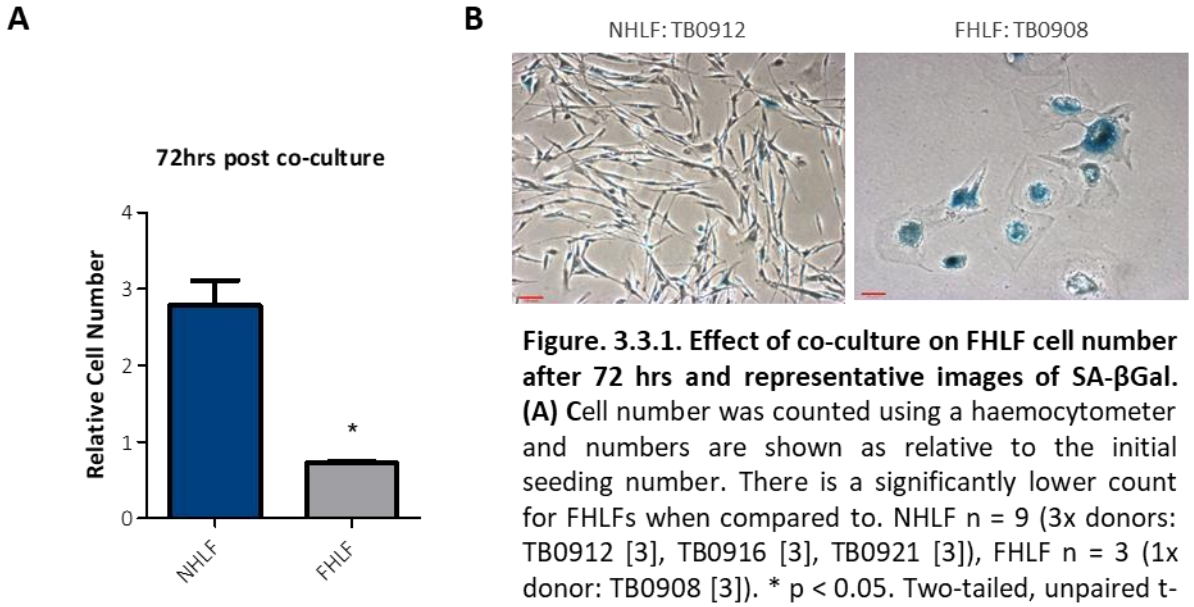

Figure. 3.3.1. Effect of co-culture on FHLF cell number after 72 hrs and representative images of SA-βGal. (A) Cell number was counted using a haemocytometer and numbers are shown as relative to the initial seeding number. There is a significantly lower count for FHLFs when compared to. NHLF n = 9 (3x donors: TB0912 [3], TB0916 [3], TB0921 [3]), FHLF n = 3 (1x donor: TB0908 [3]). * $p < 0.05$. Two-tailed, unpaired t-test. **(B)** NHLFs and FHLFs were fixed and stained for SA-βGal activity after 24 hrs mono-culture. Representative images of 1x experiment shown.

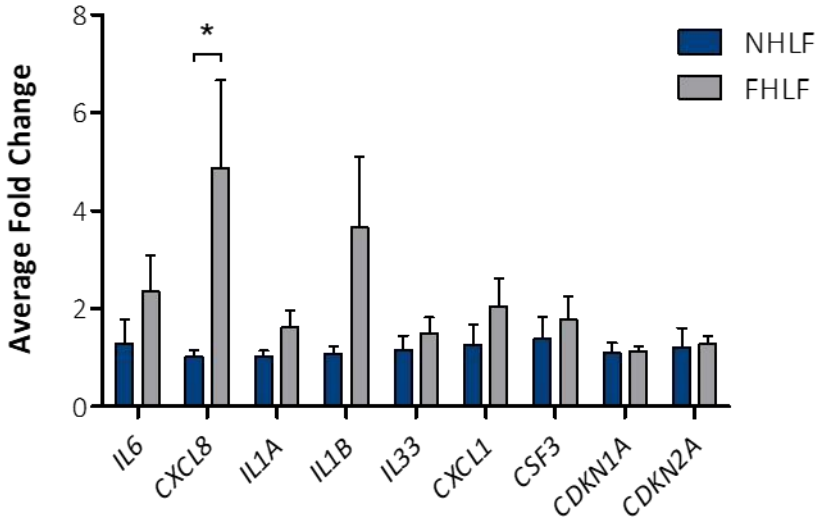

Figure 3.3.2. Comparison of NHLF and FHLF RNA levels after 72 hrs of co-culture. NHLFs and FHLFs were co-cultured in DMEM/αMEM 10% FBS. RT-qPCR was performed with genes of interest normalised to the reference genes *B2M* and *GAPDH.* FHLF co-culture RNA levels were calibrated to NHLF co-culture levels and the data is shown as an average fold change. There was no significant difference between NHLFs and FHLFs except for a significant increase in *CXCL8* RNA levels. NHLF n = 6 (3x donors: TB0917 [2], TB0918 [2], TB0932 [2]), FHLF n = 6 (2x donors: BR002 [3], BR003 [3]). * $p < 0.05$. Two-tailed, unpaired t-test performed on ddCt values.

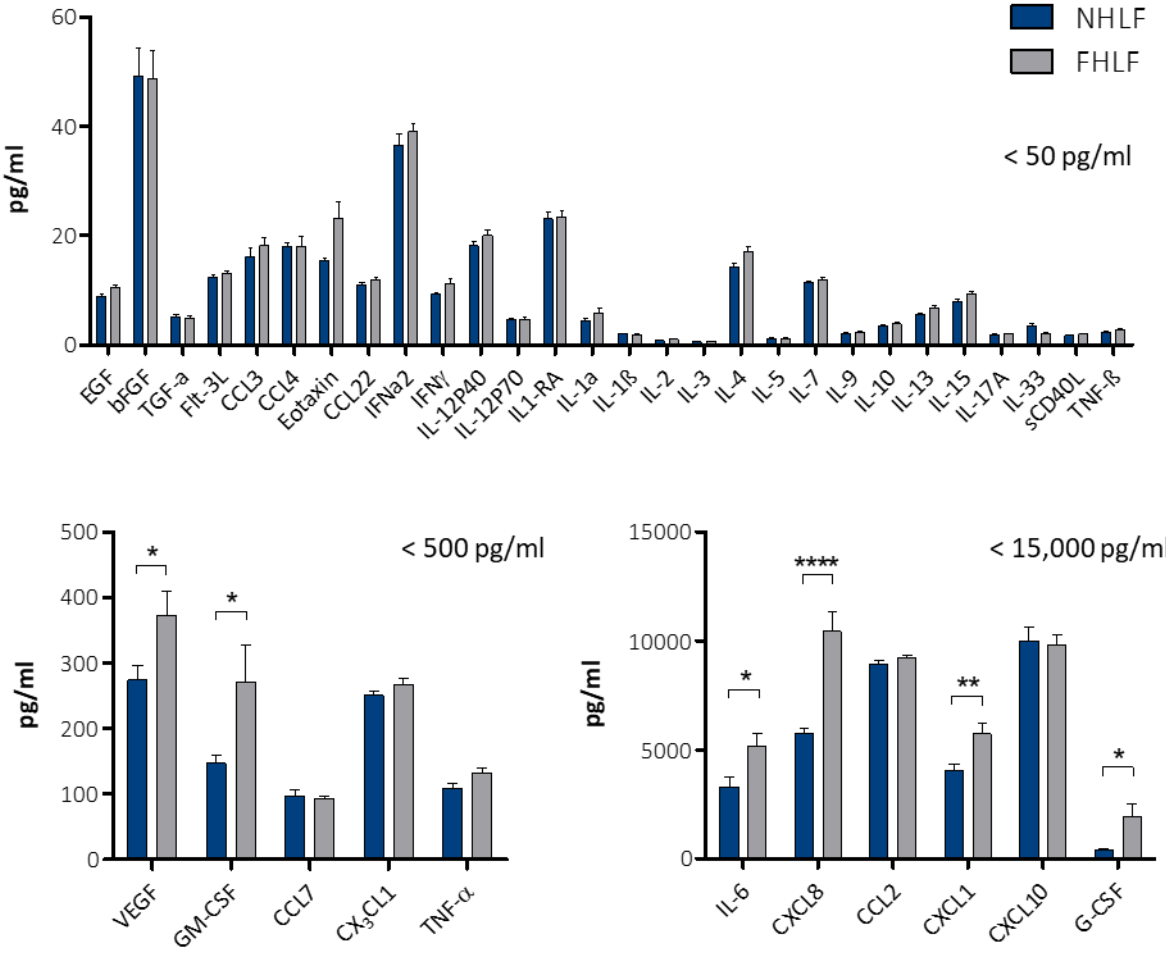

Figure 3.3.3. Multiplex cytokine array comparing NHLF and FHLF CM, 72 hrs after co-culture. Basolateral media were collected and stored at -80°c. After thawing, conditioned media were analysed via Luminex Multiplex array, screening for immuno-modulating cytokines, chemokines and growth factors. Results are shown across 3 graphs of differing y-axis scales. Across all analytes detected at a concentration >100 pg/ml there were significant increases in concentrations of VEGF, GM-CSF, IL-6, IL-8, CXCL1 and G-CSF in FHLF co-culture CM. NHLF n = 12 (4x donors: TB0912 [3], TB0917 [3], TB0932 [3], TB0918 [3]). FHLF n = 12 (4x donors: BR001 [3], BR002 [3], BR003 [3], TB0908 [3]). **** $p < 0.0001$, ** $p < 0.01$, * $p < 0.05$. Two-tail, unpaired t-test.

significantly greater in FHLF co-culture CM. CCL7, CX_3CL1, TNF-α, CCL2 and CXCL10 were also detected at concentrations >100 pg/ml but there no significant differences between co-culture conditions. This indicates that, though not necessarily evident at an RNA level, FHLFs upregulate a series of inflammatory secretory proteins that alter the composition of the co-culture micro-environment.

3.3.2.2. FHLFs in co-culture impair re-epithelialisation and do not enhance epithelial barrier regeneration.

The next steps in this investigation were to evaluate what effect this altered microenvironment had on epithelial function in co-culture. NHLF and FHLF co-cultures were maintained over 72 hrs, along with HBEC mono-cultures, and, at 0 hrs, mechanically wounded via pipette scratch. Phase contrast images were taken across a 9 hr time window and percentage wound closure quantified **(*Figure* 3.3.4A.)**. Representative images of 0 and 9 hr wound sizes, with corresponding binary images, are also shown **(*Figure* 3.3.4B.)**. 9 hrs post-wounding, HBEC re-epithelialisation was significantly less in co-cultures with FHLFs than in NHLF co-culture or HBEC mono-culture **(*Figure* 3.3.4C.)**. Unlike in prior experiments **(*Figure* 3.2.13.)**, there was no difference in closure between NHLF co-culture and HBEC mono-culture, with closure averaging at 80.24% and 77.64% respectively. However, it was concluded that the environment created by FHLFs, and the relationships between these cells and the HBECs, is detrimental to re-epithelialisation, with closure averaging only 66.11%.

The second aspect of epithelial function to be investigated was the development of epithelial ionic barrier integrity, as assessed by R_{TE}. Cells were seeded at -24 hrs and brought into their respective cultures at 0 hrs. R_{TE} was measured at 24 hr intervals from 0 to 72 hrs **(*Figure* 3.3.5A.)**. There were no significant differences in resistance at 0 and 24 hrs. The mean increase in R_{TE} across all culture types between these timepoints was 0.036 $K\Omega cm^2$. At 48 hrs there were significant differences between the mean R_{TE} of each culture type, with resistance in NHLF co-culture significantly higher than FHLF co-culture ($p<0.01$, 2-way RM ANOVA). By 72 hrs, NHLF co-culture R_{TE} was still significantly greater than HBEC mono-culture and FHLF co-culture **(*Figure* 3.3.5B.)**. At this timepoint however, there was now no significant difference in resistance between FHLF co-culture and HBEC mono-culture, averaging at 0.43 and 0.57 $K\Omega cm^2$ respectively. The mean resistance for NHLF co-culture was 0.90 $K\Omega cm^2$. NHLFs augment HBEC regeneration over 72 hrs. FHLFs, although not detrimental to HBEC regeneration, fail to recapitulate this benefit.

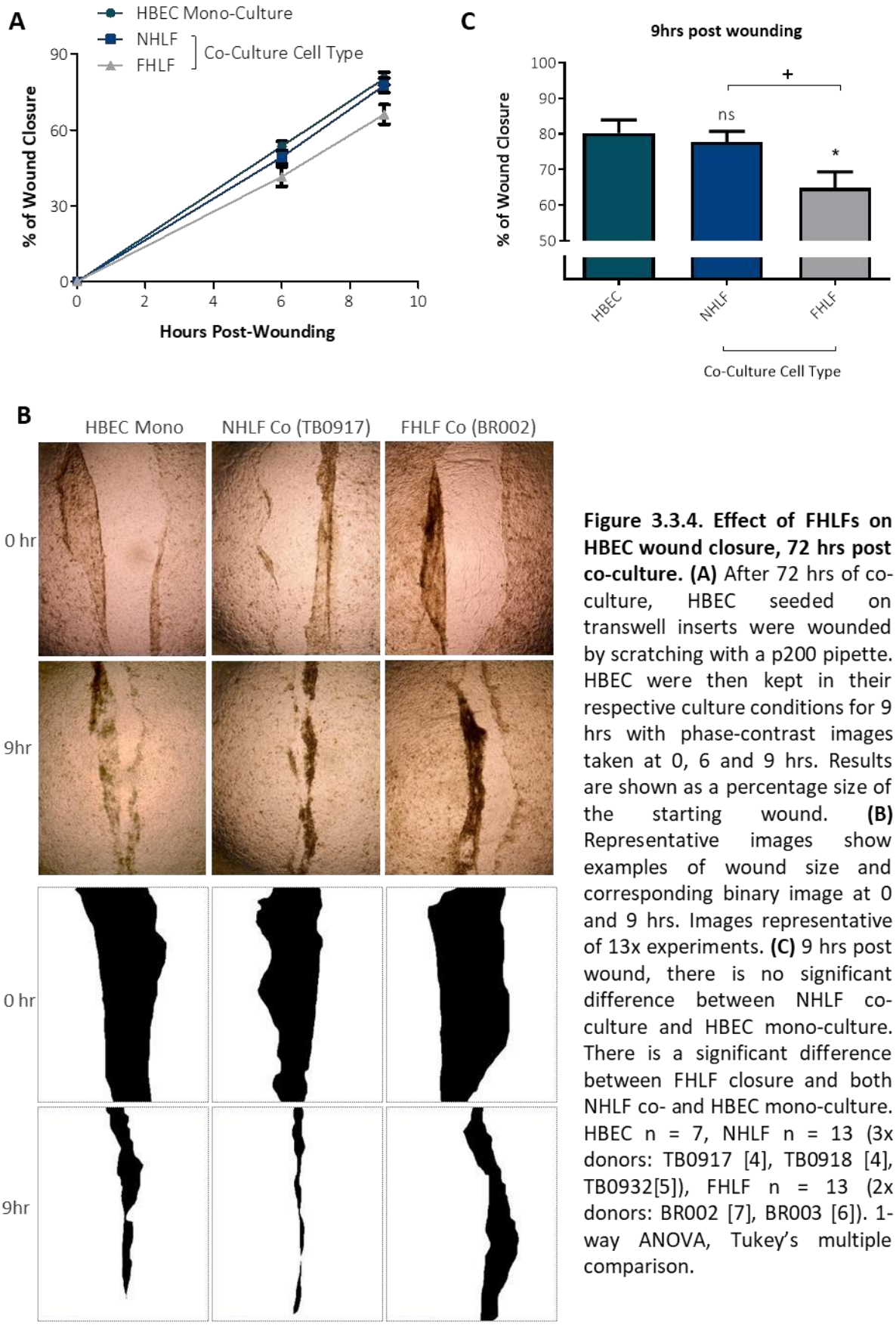

Figure 3.3.4. Effect of FHLFs on HBEC wound closure, 72 hrs post co-culture. (A) After 72 hrs of co-culture, HBEC seeded on transwell inserts were wounded by scratching with a p200 pipette. HBEC were then kept in their respective culture conditions for 9 hrs with phase-contrast images taken at 0, 6 and 9 hrs. Results are shown as a percentage size of the starting wound. **(B)** Representative images show examples of wound size and corresponding binary image at 0 and 9 hrs. Images representative of 13x experiments. **(C)** 9 hrs post wound, there is no significant difference between NHLF co-culture and HBEC mono-culture. There is a significant difference between FHLF closure and both NHLF co- and HBEC mono-culture. HBEC n = 7, NHLF n = 13 (3x donors: TB0917 [4], TB0918 [4], TB0932[5]), FHLF n = 13 (2x donors: BR002 [7], BR003 [6]). 1-way ANOVA, Tukey's multiple comparison.

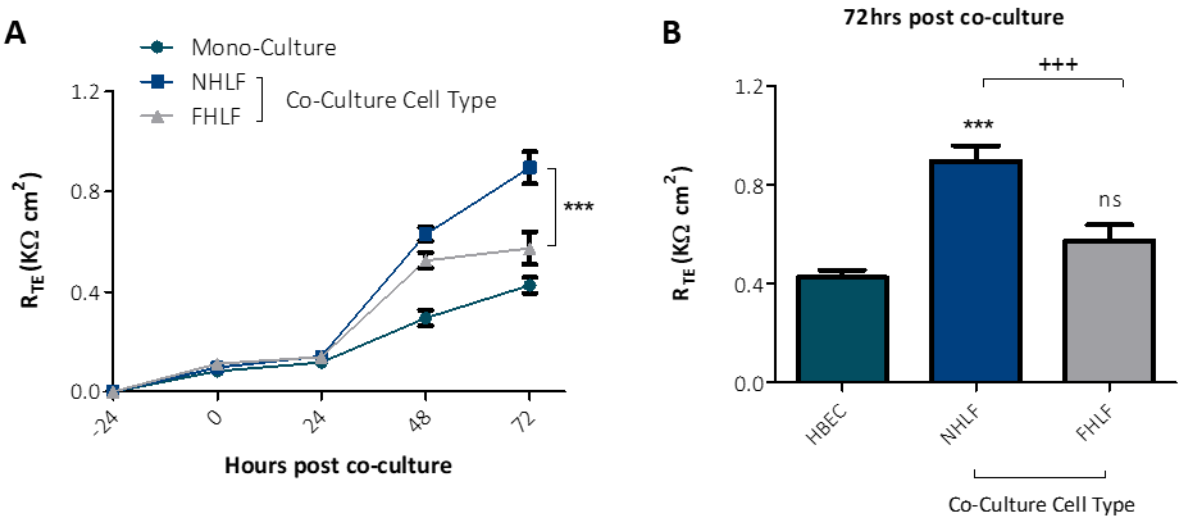

Figure 3.3.5. Effect of FHLF co-culture on HBEC R_{TE} over 72 hrs. (A) NHLFs and FHLFs were seeded in equal densities at -24 hrs and co-cultured in DMEM/αMEM 10% for 72 hrs. R_{TE} was measured every 24 hrs hours. **(B)** At 72 hrs R_{TE} are significantly higher for NHLF co-culture compared to HBEC mono-culture. There is no significant difference between FHLF co-culture and HBEC mono-culture but a significant difference between NHLF co-culture. HBEC n = 4, NHLF n = 4 (4x donors TB0912, TB0916, TB0917, TB0921), FHLF n = 4 (4x donors: TB0908, BR001, BR002, BR003). *** $p < 0.001$ (vs HBEC), +++ $p < 0.001$ (vs NHLF). 1-way ANOVA, Tukey's multiple comparison.

3.3.3. Discussion

This series of experiments aimed to investigate FHLFs in an *in vitro* model of secretory crosstalk; investigating their behaviour in co-culture, the micro-environment they contribute to, and their effect on HBEC repair. FHLFs do not proliferate in co-culture and create a more pro-inflammatory environment, which concomitantly impairs reepithelialisation and fails to promote epithelial regeneration. This highlights the pathological attributes of this cell type and re-affirms their importance in the pathology of IPF.

FHLF phenotype

It was interesting that FHLFs had a lower cell count in co-culture. IPF is a disease characterised by excess proliferation and it would be expected that this would be observed *in vitro* with an increased RCN [120]. That it wasn't may reflect the dynamics of disease progression with time. Patients presenting with symptoms are likely to demonstrate a pathology that has been in action for many years, a period in which such proliferation predominates. The cells isolated from patients may display proliferative arrest due to isolation at later stages of the disease, when other characteristics of IPF become more salient. The strong signal does however corroborate the RCN results, suggesting that FHLFs were non-proliferative. It was also consistent with previous findings in mouse, in which the active regions of disease pathology, the fibrotic foci, have a non-proliferative core when investigated in aged mice, challenged with BLM [242]. Though proliferation could be more accurately investigated with Ki67 or BrdU staining, taken together these results add to an overall picture of the FHLF phenotype *in vitro* in which they are characterised by a lack of proliferation.

The results from RT-qPCR and multiplex ELISA showed that FHLFs could contribute to a more inflammatory micro-environment. However, the differences in RNA levels between 24 hr mono-culture and 72 hr co-culture were intriguing. The differences in time-point and culture type mean that these results were not directly comparable but it was interesting that *IL1A* levels were not increased (on average) and that there was no

statistical difference between levels of *CDKN2A* **(*Figure* 3.1.1.)**. There are several possibilities for this. The loss of difference in *CDKN2A* could be due to NHLFs becoming more senescent in co-culture after 72 hrs, with increased expression of *CDKN2A*. Conversely, FHLF expression at an RNA level may be under temporal regulation, with levels at 72 hrs becoming less elevated when compared to normal cells. Not only this, but in terms of methodology, the primer used to assess *CDKN2A* **(Table 2.3.3.)** probed for the full complement of gene products. As the p16 protein was most pertinent to this investigation, it may perhaps be more appropriate to probe for this specific transcript. Likewise, experiments at an RNA level potentially miss the important effects of translational regulation of proteins, a mechanism of control that is important in the pathological characteristics of IPF fibroblasts [283]. Consequently, a more robust approach to investing expression of this senescence marker would be to perform experiments at the protein level, performing western blot and immunostaining for p16. This could be achieved in future studies.

Though not always reflected at an RNA level, there were significant increases in production of several pro-inflammatory proteins in the CM of FHLF co-cultures. These experiments were performed using all available cell lines. It remains difficult to delineate the cellular origin of proteins in the basolateral compartment, and the changes could be the result of increased HBEC production. Regardless, these results demonstrate that coculture with epithelial cells can expose significant differences in inflammatory protein production between NHLFs and FHLFs, results that were not obtained in mono-culture. This further highlights the importance of recapitulating elements of cell-cell signalling *in vitro* environment. It also raises questions about what other secretory factors could be differentially produced in this system and what would happen if additional stimuli were utilised, such as co-culture with immune cells or exposing the epithelium to the air.

Impact on the epithelium

However, in this system, the result of the environment created by FHLFs was that HBEC re-epithelialisation was impaired and that there was an attenuation of the regenerative benefits of NHLF co-culture. IPF is a disease characterised by an aberrant and

dysfunctional wound healing response, linked to epithelial dysfunction and fibroproliferative activation of a heterogenous population of fibroblasts. These results begin to implicate that, as well as the interstitial destruction described in the literature, FHLFs also mediate the loss of epithelial function, an ability elicited by the creation of a pro-inflammatory micro-environment that impairs their ability to respond to injury. That FHLFs can contribute to both of these disease characteristics further points towards the heterogeneity of this population, suggesting that different subsets of fibroblasts may elicit different pathological activities. This understanding firmly places the FHLF at the heart of IPF pathology, identifying them as the key orchestrator of disease progression.

FHLFs and senescence

One of the interesting features of the inflammatory environment generated by FHLFs in co-culture is its strong resemblance to the SASP, the key hallmark of senescence. IL-6, CXCL8, CXCL1, GM-CSF and VEGF are all core SASP components [213] and all were elevated with FHLFs. Growth arrest and SA-βgal activity have also been identified in FHLFs, as well as in increase in *CDKN2A* expression when mono-cultured. These features collectively imply a senescent, or at least a senescent-like / pre-senescent, phenotype in FHLFs, which is associated with impaired epithelial function.

There is much evidence for a role of senescence in the pathology of IPF. It is implicated in all of the driving forces of IPF, playing a role in developmental signalling, wound repair and ageing. Fibroblasts from IPF patients have previously been found to display senescent characteristics *in vitro* and there is evidence for senescence in the IPF epithelium *in vivo* [239,246]. Most recently, research has shown that senescent cells accumulate in mice treated with BLM and that the selective clearance of these cells reduces fibrosis-associated physiological impairments [247]. Likewise, mice treated with ionising radiation develop fibrosis over the course of several weeks. This fibrosis is understood to be mediated by senescence, which, after treatment with the senolytic compound ABT263, can be resolved via the specific clearance of senescent cells [284]. Therefore, the results from this section, coupled with current literature, suggest that

FHLFs are important in the pathology of IPF through a propensity to acquire a senescentlike phenotype that alters epithelial-mesenchymal crosstalk.

How senescence is mediated in FHLFs is thus far unclear. However, the elevation in *CDKN2A* expression in mono-cultured FHLFs would suggest mediation through the p16pRB pathway. This pathway is most strongly associated with OIS and ROS-induced senescence [197]. A role for ROS-induced senescence would comply with previous evidence highlighting a ROS imbalance in FHLFs that contributes to aberrant fibroblast activity in IPF [119]. Better understanding of senescence in epithelial-mesenchymal crosstalk and its relevance to FHLFs will require further investigation and will be the focus of the next section of this work.

In conclusion, FHLFs display a senescent-like phenotype in culture, associated with the generation of a more pro-inflammatory micro-environment. The detriment of this phenotype is evidence by a concomitant impairment of HBEC re-epithelialisation and an impairment of epithelial regeneration, further implicating the FHLF as a key mediator of the pathology of IPF.

3.4 Stress Induced Premature Senescence in Normal Human Lung Fibroblasts

3.4.1. Introduction

Senescence in IPF

FHLFs impair epithelial function, a result associated with increased production of several core SASP proteins. As well as an altered morphology, FHLF also display a poor proliferative capacity. Taken together, this points towards a senescent-like phenotype in these cells. In aged mice, senescence inhibits the resolution of BLM-induced mouse fibrosis, with senescent fibroblasts chronically accumulating in the lung [242]. Within fibroblastic foci of these aged mice, a combination of staining for p16, p21, Ki67 and αSMA, along with TUNEL staining, reveals a largely non-proliferative, myofibroblastic

core, positive for markers of senescence. On the periphery, there are regions of fibroblast proliferation and the foci are covered by a highly apoptotic epithelium. Elevated Nox4 activity in isolated FHLFs drives increased H_2O_2 production and its inhibition reduces SA-βgal activity. Coupled with a deficiency in fibroblast Nrf2 activity, an intrinsic redox imbalance in aged mice leads to this senescence and non-resolving fibrosis [242]. Crucially, senescence can be observed in the HLFs of IPF tissue sections and the clearance of senescent cells can alleviate many of the detrimental effects of BLMinduced fibrosis in mouse [247]. It is therefore conceivable that in the lungs of IPF patients there is an increased burden of senescent cells. The relationship between senescent fibroblasts and the epithelium in the context of IPF has yet to be elucidated.

Stress induced premature senescence

To better explore the impact of fibroblast senescence on the epithelium, and to establish a benchmark for the senescent-like FHLFs (whereby the degree to which they conform to the archetypal senescence phenotype could be compared), it was appropriate to generate a model of senescence *in vitro*. Senescence can be induced via numerous methods. As reported by Leonard Hayflick many decades ago, serial passage can induce senescence and this replicative senescence has been utilised in a wide range of published studies. The constitutive activation of oncogenic pathways, such as Kras, typically via viral transfection, can also induce senescence, a form of senescence termed OIS (oncogene-induced senescence). As well as this, stress, in varying guises, can be used to induce cellular senescence. This stress-induced, premature senescence (SIPS) can be caused by genotoxic agents such as ionising radiation, high glucose or H_2O_2. All three of these agents cause DNA damage [285–288].

DNA damage that causes double-strand breaks (DSBs) leads to ataxia telangiectasia mutated (ATM) activation and signal transduction, phosphorylating H2AX and p53 as part of a DDR. H2AX transitions to γH2AX, a classical marker of DNA damage, which promotes the recruitment of several DNA repair factors. p53 is stabilised via its phosphorylation, and cell cycle progression is inhibited. When DNA damage cannot be resolved, senescence is induced by activation of CDK inhibitors [289]. p21 is upregulated,

promoting both growth arrest and also inhibiting apoptosis, via pleiotropic activity in which mitochondrial cytochrome c release and caspase-9 activation is prevented [290]. Oxidative stress caused by genotoxic agents also leads to phosphorylation of p38 MAPK. $p38^{MAPK}$ causes TGF-β1 and caveolin-1 transcriptional upregulation [291,292]. Caveolin-1 is a scaffold protein that can promote cell cycle arrest via activation of the p21-p53 pathway [293]. TGF-β1 induces mitochondrial dysfunction that results in the endogenous production of H_2O_2, creating more oxidative stress and causing further DNA damage [200]. All of these pathways create a cyclical feedback loop, in which exogenous genotoxic insults, oxidative stress and mitochondrial dysfunction coalesce to either initiate or maintain commitment to a programme of cellular senescence.

To prematurely induce senescence in NHLFs it was decided to use exogenous treatments of sub-lethal concentrations of H_2O_2. SIPS was favoured over replicative senescence due to the ability of it to be induced at any stage of the NHLFs replicative lifespan, speeding the process of induction and enlarging the pool of cells that could be made senescent. It could be argued that because IPF is a disease of old age and that because the senescent cells in fibrotic foci are likely to have been previously involved in excessive proliferation, replicative senescence is more relative to the disease. However, there is also a strong rationale for utilising SIPS, especially via induction with H_2O_2. IPF is characterised by recurrent injury and with epithelial injury there is H_2O_2 release [81]. In the exhaled breath condensate of IPF patients there are elevated concentrations of H_2O_2 and isolated FHLFs display increased NOX4 activity, which produces H_2O_2 [118,294]. There is also increased TGF-β1 activity that can cause mitochondrial H_2O_2 production and induce senescence [93,295]. Therefore, exogenous, sub-lethal H_2O_2 treatment may in fact begin to recapitulate the environmental exposures relevant to the IPF lung.

Phenotypic changes in SIPS

The changes associated with SIPS *in vitro* are diverse and irreversible. The most obvious changes are those to morphology, with cells becoming flattened and enlarged [296]. This occurs in concurrence with growth arrest, in which DNA synthesis is inhibited and cells fail to respond to exogenous growth factor signalling. These irreversible changes are,

however, not associated with loss of cell viability [297]. The arrest in growth is mediated by classical senescence pathways, with a transient increase in p53 and long-term elevation of p21, which can be assessed by western blotting and IMF. Cells are arrested at the G1 phase of the cell cycle, which can be analysed via flow cytometry [298]. The most widely used marker for senescence induction is an increase in SA-βgal activity [299]. In both replicative and cellular senescence, there is an increase in lysosomal activity, occurring as part of a compensatory mechanism, elicited to assist the degradation of damaged organelles in secondary lysosomes [300]. *GLB1*, a gene encoding lysosomal β-Dgalactosidase, is upregulated and the resultant enzymatic activity can be detected by Xgal, a chromogenic substrate that produces a blue compound when enzymatically cleaved [301]. Lysosomal enzymes optimally function in acidic conditions (pH 4.0). The significantly greater lysosomal activity in senescence, however, allows detection at a sub-optimal pH of 6.0. By using a citric acid/sodium phosphate buffer at pH 6.0, SA-βgal activity can be distinguished from normal lysosomal β-gal activity [249]. SA-βgal has been robustly established as a marker of senescence, with activity limited to only senescent cells, not quiescent, proliferative or terminally differentiated cells. Finally, another key alteration that can be detected in SIPS is the establishment of SASP. SASP encompasses a broad range of cytokines, chemokines and growth factors, which can differ between cell types. For fibroblast SIPS, the core SASP repertoire consists of IL-6, CXCL8, CXCL1, CCL2 and GM-CSF [212,213]. Elevation of these factors is widely used as evidence of senescence induction, especially IL-6 and CXCL8 **(*Figure* 1.3.3.)**.

SIPS in co-culture

The effect of fibroblast SIPS in co-culture have been investigated before, although not in the context of IPF. Senescent tracheal HLFs, co-cultured with HBECs (the BEAS-2B cell line), promote EMT in the presence of the carcinogen, hexavalent chromium. After 4 weeks of transwell co-culture, almost 80% of HBECs display enlarged nuclei, a loss of cobblestone morphology and a fusiform morphological alteration, as well as a significant increase in vimentin expression. This is indicative of malignant transformation, part of the initial stages of tumourigenesis [302]. Other studies, using different approaches to paracrine signalling, have also found senescent lung fibroblasts to promote malignant

epithelial growth [303,304]. Interestingly, the epithelium of honeycomb lesions and cysts in IPF is also characterised by a hyperplastic epithelium, suggesting a similar mechanism could be at play. Using Matrigel-coated transwell inserts, the secretome of senescent fibroblasts promotes epithelial invasion, evidenced in both breast mammary epithelium and pancreatic cancer cells [231,305]. An inability to differentiate also occurs under the influence of SASP but the establishment of epithelial barrier integrity, as measured by R_{TE}, has yet to be assessed. Likewise, though studies have investigated the role of senescence in wound healing via other methodologies, how the secretory factors of senescent cells impact re-epithelialisation remains to be elucidated.

Taking all these aspects into consideration, the following experiments set out to establish a robust method of SIPS induction, utilising classical senescence markers. An understanding of how these cells function in co-culture and their effect on the overlying epithelium was also a principal aim, achieved by assessing re-epithelialisation and ionic permeability. The rationale for these experiments was that SIPS cells would represent the extremity of the FHLF phenotype, acting as a positive control for their behaviour in co-culture.

Hypotheses

1. Sub-lethal treatment with H_2O_2 will induce SIPS in NHLFs, leading to numerous phenotypic changes.
2. HBEC co-cultures with SIPS will fail to promote R_{TE} and impair re-epithelialisation.

3.4.2. Results

3.4.2.1. H_2O_2 treatment can prematurely induce senescence in NHLFs.

As previously discussed, treatment with sub-lethal concentrations of H_2O_2 can induce senescence via irreparable DNA damage. The concentration of peroxide is extremely important as too much can cause cell death and too little can have no effect. Various concentrations of H_2O_2 have been used in prior studies [295,298] and ultimately trial and error was adopted to identify a concentration suitable for this investigation. The literary nuance regarding SIPS protocols was further complicated by the heterogenous response of different NHLF lines to equivalent treatment regimes. For example, treating the NHLF line TB0917 for 5-days with 200 µM H_2O_2 resulted in 90% cell death, the same treatment in the line TB0932 however resulted in cells reaching confluence. Accommodating for these discrepancies was complicated but, through tailoring treatment protocols to each cell line, a uniform induction of senescence was achieved. The best suited concentration was found to be 200 (±100) µM peroxide, given recurrently over 5 days to NHLFs seeded at an initial density of 1.0 x10^6 cells/T75 flask. After treatment, the key step to achieving senescence was passage and recovery. On day 6, 1 day after final treatment, cells were passaged and left to recover for a further 6 days. During this time cells acquired the classical senescence morphology, in what appeared to be a time-dependent process. In total, 12 days was deemed to be a suitable period for senescence induction, offering robust increases in SA-βgal activity alongside morphological changes. This SIPS protocol was used throughout the following experiments.

The SIPS protocol and the assessment of senescence hallmarks was achieved in monoculture. After protocol completion, H_2O_2-treated NHLFs had undergone extensive morphological changes, as assessed by IMF **(*Figure* 3.4.1.)**. NHLFs have a typical fibroblast morphology, with an oblong or triangular shape and size (length) of around 100 µm. Cytoskeletal actin was present, with a strong signal, and it was observable in its polymerised form, with stress fibres running throughout the cells. SIPS displayed striking morphological alterations with many of the cells displaying an enlarged morphology.

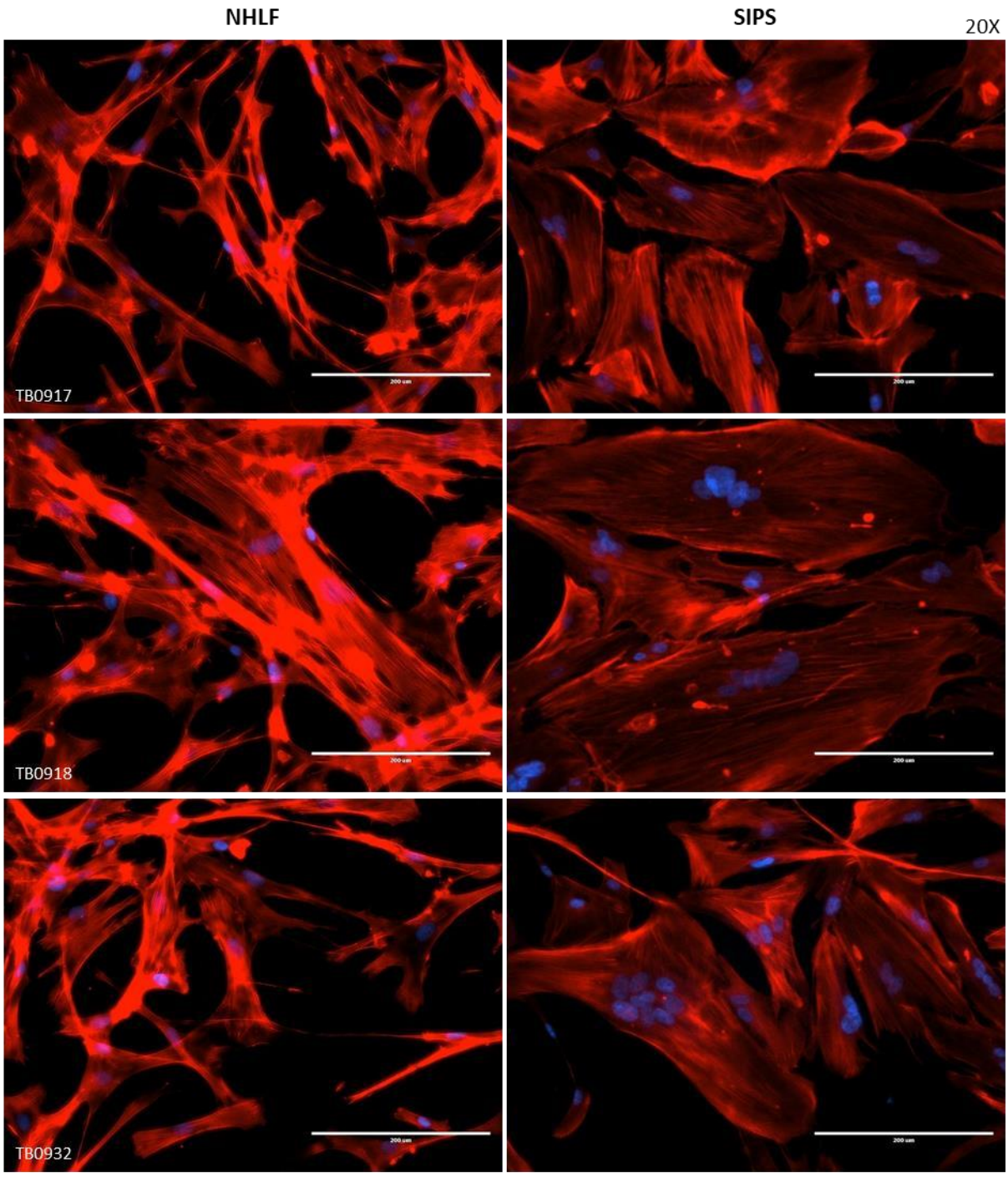

Figure 3.4.1. Representative NHLF and SIPS IMF imaging of actin and cell morphology. NHLFs and SIPS were cultured on chamber slides for 72 hrs prior to fixation and staining with DAPI and Texas-Red Phalloidin conjugate. In comparison to NHLFs, SIPS have a broadened morphology and are much bigger. SIPS also display multinucleation in some instances (arrows). Images representative of 6x experiments. Scale bar = 200µM.

There was still heterogeneity within these populations but in general there was a frequent enlargement, with cells reaching widths of 400 µm in some instances. Polymerised actin was still present in these cells, again forming stress fibres, yet, due to

the increase in size, these fibres were more dispersed. The nuclei themselves were also of interest. With the exception of cells such as megakaryocytes and tuberculosisassociated giant cells, cells do not routinely have multi-nucleation. Across multiple cell lines however, numerous SIPS cells displayed a multi-nucleated phenotype as seen via DAPI. This was not observed in NHLFs.

H_2O_2 treatment also robustly increased senescence associated lysosomal activity, as evidenced by chromogenic staining for SA-βgal activity. After the SIPS protocol, cells seeded at 30,000 cells/well of a 12-wall plate and allowed to adhere overnight. They were then fixed in 4% PFA and stained overnight with X-gal staining solution. Phasecontrast images were then taken revealing extensive SA-βgal activity in SIPS, but not NHLFs **(*Figure* 3.4.2.)**. Donor matched images are shown, with the majority of SIPS displaying a blue staining, located primarily around the nucleus. This was concomitant with the morphological changes previously seen although, interestingly, even cells that were not enlarged also stained positive for SA-βgal, suggesting that either senescence can be induced independently of morphological alterations or that SA-βgal precedes these changes, with fixation occurring before they had time to develop.

To elucidate the pathway that was facilitating these changes and establishing senescence, p21 protein expression was assessed. NHLFs and SIPS seeded at a density of 45,000 cells/well of a 6-well plate and culture for 72hrs. Cells were then lysed with RIPA buffer and the protein content quantified via BSA assay. Equal concentrations of protein were loaded onto a gel and run with subsequent antibody staining for p21 and the loading control β-actin **(*Figure* 3.4.3A.)**. p21 banding was considerably more intense in SIPS than NHLFs. Relative densitometric analysis quantified this intensity, highlighting a significant increase in p21 expression in SIPS **(*Figure* 3.4.3B.)**. To further corroborate this finding and identify the intracellular location of p21 activity, NHLFs and SIPS were stained for p21 and imaged by IMF **(*Figure* 3.4.4.)**. In NHLFs there was exceptionally little

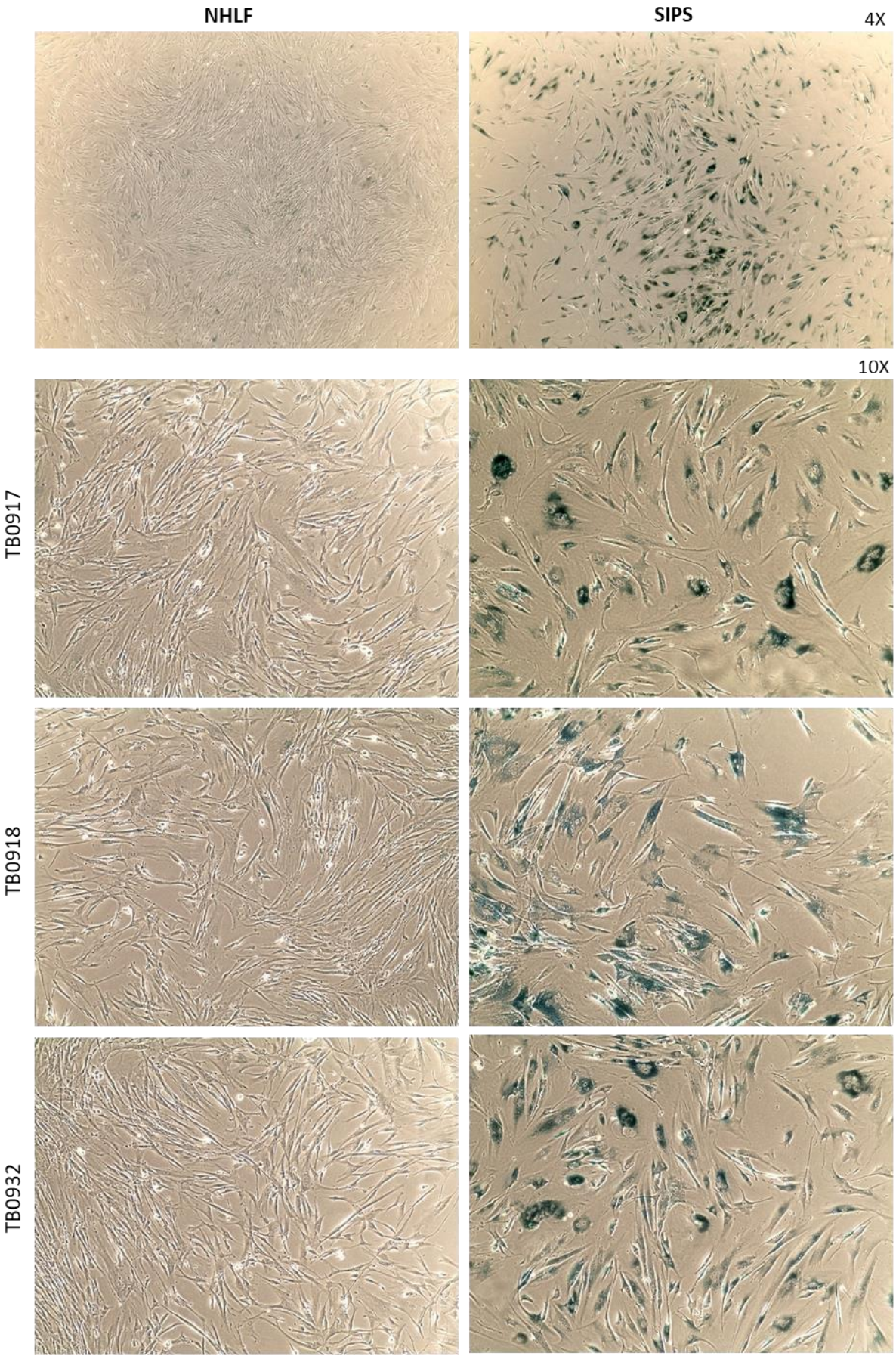

Figure 3.4.2. Representative images of SIPS β-galactosidase activity. NHLFs in mono-culture were treated with recurrent, sub-lethal concentrations of H_2O_2 (200 ±100 μM) over 5 days. Cells were then passaged and allowed to recover for a further 6 days, generating SIPS. NHLFs and SIPS were fixed and stained for β-galactosidase activity (blue). Representative, phase-contrast images from 3 NHLF donors are shown at 10x magnification.

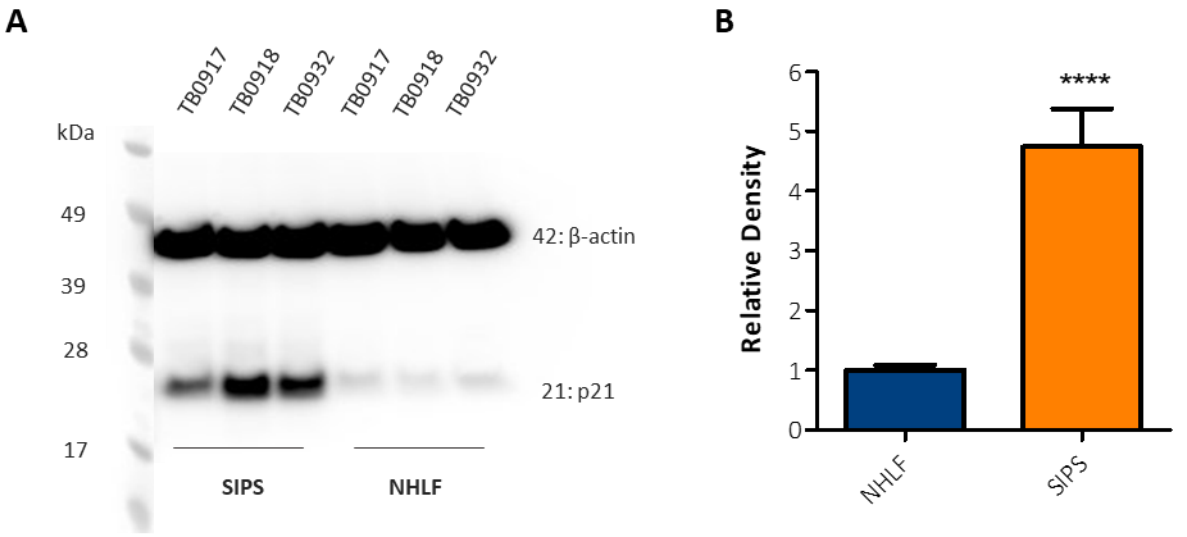

Figure 3.4.3. SIPS p21 western blot analysis. (A) Representative western blot image (1 of 4) stained for the protein of interest, p21, and the loading control β-actin. NHLFs and SIPS were cultured for 72 hrs prior to protein isolation and gel loading. HRP conjugated secondary antibodies were used for chemiluminescent imaging. **(B)** Analysis of relative band density using ImageJ Gel Analysis. The relative band density of SIPS p21 is significantly greater than NHLFs. NHLF n = 12 (3x donors: TB0917 [3], TB0918 [3], TB0932 [3]), SIPS n = 12 (3x donors: TB0917 [3], TB0918 [3], TB0932 [3]). **** $p < 0.0001$. Two-tail, unpaired t-test.

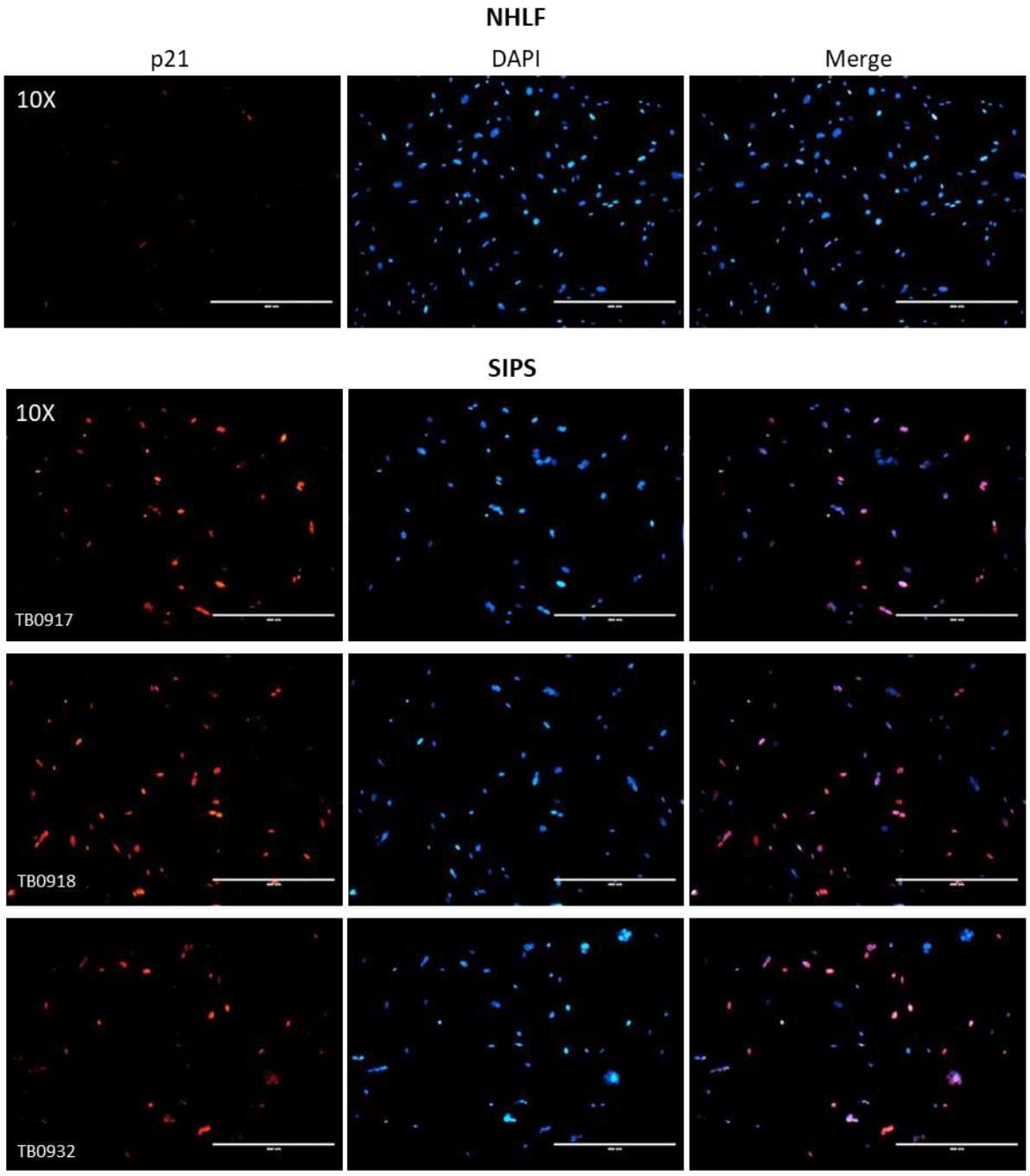

Figure 3.4.4. Representative images of NHLF and SIPS p21/DAPI IMF. NHLFs and SIPS were cultured on chamber slides for 72 hrs prior to fixation and staining with DAPI and p21 (red). Images from 3x SIPS donors are shown, representative of 6x experiments. Scale bar = 200µM.

p21 expression but in SIPS, p21 was observable in numerous cells. By merging p21 and DAPI signal this expression was found to be localised within the nuclei, consistent with physiological p21 activity. p53 was not investigated but, given the strong expression of p21, it could be postulated that the senescence induced by peroxide treatment is

mediated through the p21-p53 pathway, consistent with other evidence regarding DNAdamage induced senescence.

Changes in RNA levels were also assessed via RT-qPCR. After the SIPS protocol, cells were seeded at a density of 30,000 cells/well of a 12-well plate, in mono-culture and cultured for 24 hrs prior to RNA isolation. RNA levels for a range of senescence associated proteins were assessed, as well as *CDKN1A*, the gene encoding p21. As expected from the western blot and IMF analysis, *CDKN1A* levels were significantly higher in SIPS than in NHLFs **(*Figure* 3.4.5.)**. This was also evident for levels of *CXCL8*, *IL1A*, *IL1B* and *HGF*, genes upregulated in senescence and indicative of cellular stress. *IL6, IL33, CXCL1, FGF7* and *CDKN2A* were also expected to be elevated but were not and, as in previous experiments, *CSF3* was not reliably expressed at this timepoint. The lack of *CDKN2A* transcript elevation begins to suggest that the p16-pRB pathway is not heavily involved in this form of senescence or not involved at this stage of the induction process, in contrast to FHLFs, which display elevated *CDKN2A* RNA levels **(*Figure* 3.1.1.)**.

These results ostensibly highlight a robust induction of senescence upon recurrent treatment with sub-lethal concentrations of H_2O_2, evidenced by classical morphological alterations, increased SA-βgal activity and p21 expression, and an elevation of RNA levels encoding for several genes relating to senescence.

3.4.2.2. SIPS in mono-culture produce altered concentrations of secretory proteins.

To assess the secretory factors produced by SIPS and how their composition changes in relation to NHLFs, the CM of mono-cultured cells was analysed via Multiplex ELISA. Cells were mono-cultured for 72 hrs prior to CM collection. In this experiment the percentage of SA-βgal positivity differed between cultures. By quantifying the percentage positivity,

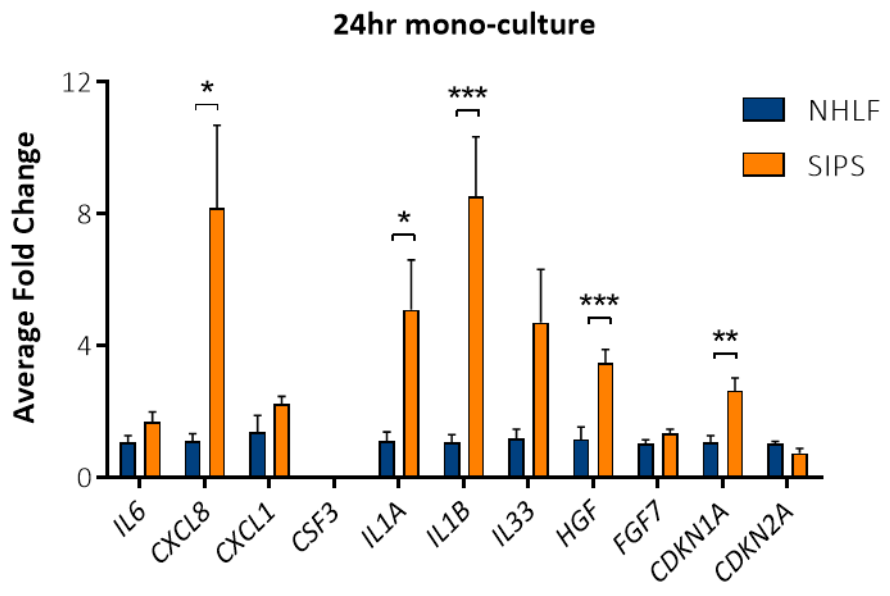

Figure 3.4.5. Comparison of NHLF and SIPS RNA levels after 24 hrs of mono-culture. NHLFs and SIPS were mono-cultured in DMEM/αMEM 10% FBS. RT-qPCR was performed with genes of interest normalised to the reference genes *B2M* and *GAPDH.* SIPS RNA levels were calibrated to NHLF levels and the data is shown as an average fold change. There was a significant increase in levels of *CXCL8, IL1A, IL1B, HGF* and *CDKN1A*. *CSF3* was not reliably expressed. NHLF n = 4 (3x donors: TB0917, TB0918, TB0932 [2]), SIPS n = 8 (3x donors: TB0917 [3], TB0918 [2], TB0932 [3]). Two-tailed, unpaired t-test performed on ddCt values.

two SIPS populations were identified: a low burden population, with a mean positivity of 39%, and a high burden population, with a mean of 85% **(*Figure* 3.4.6.)**. The secretory factors produced by these populations were detected at differing concentrations **(*Figure* 3.4.7.)**. As with previous multiplex ELISA experiments, many secretory proteins were detected yet only a select few were found at meaningful concentrations. Of these proteins, the pattern of concentration can be broadly grouped into four categories: (1) with a low burden of senescence there is no elevation of protein concentration, but when high there is significant elevation. This was evident for the factors: CX_3CL1, CXCL1, CXCL10, IL-6 and CXCL8. (2) Both low and high burdens of senescence resulted in elevated protein concentrations, evident in bFGF and CCL3 concentrations. (3) Both populations of senescent cells produced decreased protein levels compared to NHLFs, evident only for CCL2. (4) A low burden of senescence resulted in a significantly decreased protein concentration but at a high burden, concentrations were significantly elevated. This was evident in concentrations of VEGF, INFα2, G-CSF and GM-CSF. Therefore, the percentage burden of senescence is important for determining the local micro-environment.

3.4.2.3. SIPS have an altered mitochondrial morphology and increased mitochondrial membrane potential.

Mitochondrial function and membrane potential are important components in the pathways mediating senescence and, in IPF, dysmorphic mitochondria can promote the process of fibrosis. Therefore, as with FHLFs, experiments designed to elucidate mitochondrial phenotype were performed in SIPS. NHLFs and SIPS were mono-cultured prior to fixation and IMF staining for ATP5B **(*Figure* 3.4.8A.)**. As previously, using ImageJ the ATP5B signal was converted to a skeletonised image, allowing quantification of mitochondrial morphology **(*Figure* 3.4.8B.)**. NHLFs showed a highly-interconnected network of mitochondria. SIPS in contrast, as well as being much larger, showed a more extensive mitochondrial network with more numerous mitochondria. This network was less well connected, and the mitochondria were typically smaller and more isolated within the cytosol. Analysing these images by ImageJ quantified these differences

A

	NHLF	Low	High
Minimum	0.00	29.49	77.78
25% Percentile	0.00	35.11	80.20
Median	0.25	37.92	85.86
75% Percentile	0.91	42.58	88.31
Maximum	1.00	49.07	90.24
Mean	0.39	38.56	84.72
Std. Deviation	0.45	5.13	4.61
Std. Error	0.16	1.48	1.63

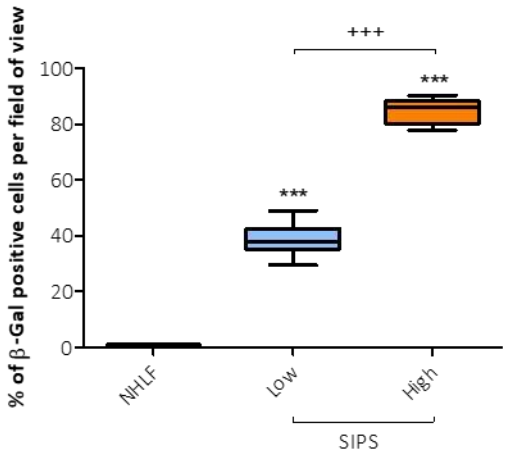

B

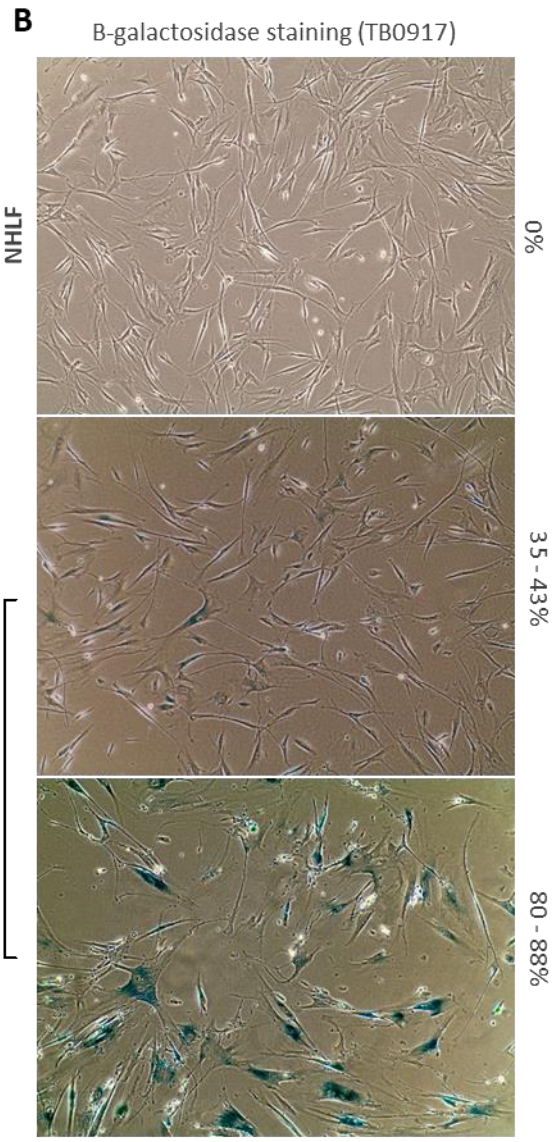

Figure 3.4.6. Stratification of SIPS (by percentage burden of β-galactosidase positivity) for CM protein analysis. (A) NHLFs in mono-culture were treated with recurrent, sub-lethal concentrations of H_2O_2 over 5 days. Cells were then passaged and allowed to recover for a further 6 days, generating SIPS. SIPS and NHLFs were mono-cultured for 72 hrs with subsequent CM collected. Cells were then fixed and stained for β-galactosidase activity (blue). Phase contrast images were taken and the percentage of β-gal positive cells per field of view quantified. 2 populations were identified: a low burden population, with a mean of 39% senescence, and a high burden population, with a mean of 85%. Percentage of β-gal positivity is an average of 2 images per n number. NHLF n = 4 (2x donors: TB0917 [2], TB0918 [2]), SIPS n = 3 (3x donors: TB0917, TB0918, TB0932). *** $p < 0.001$, +++ $p < 0.001$. 1-way ANOVA, Tukey's multiple comparison. **(B)** Representative images of β-gal staining with corresponding interquartile range for senescence burden.

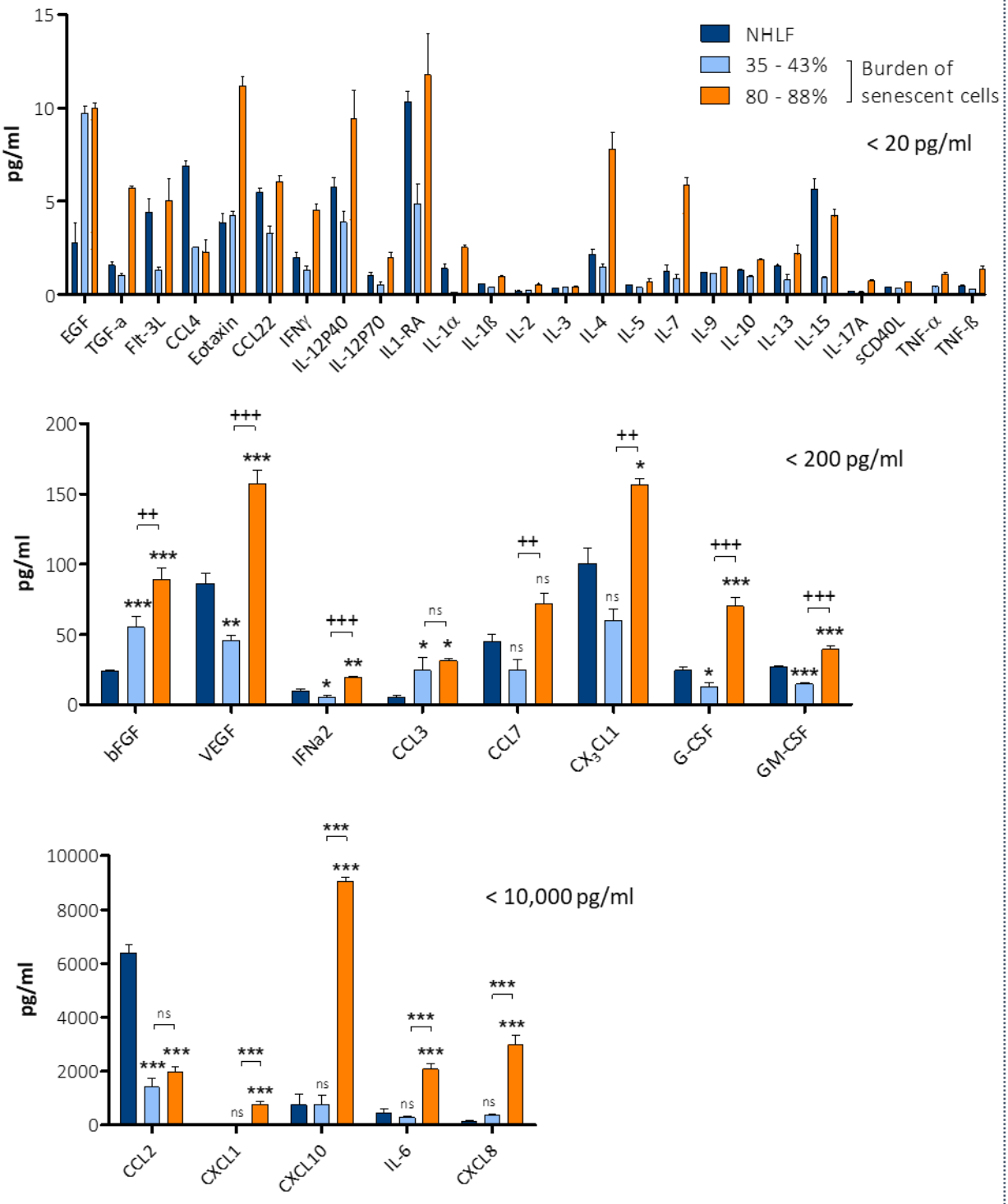

Figure 3.4.7. Multiplex cytokine array comparing NHLF and SIPS CM after 72 hrs of mono-culture. Basolateral media were collected and stored at -80°c. After thawing, conditioned media were analysed via Luminex Multiplex array, screening for immuno-modulating cytokines, chemokines and growth factors. Results are shown across 3 graphs of differing y-axis scales. Across all analytes detected at a concentration >100 pg/ml there was a significant increase in all analytes between the high percentage burden of senescence and NHLFs, with the exception of CCL7 in which there was no significant difference and CCL2 in which there was a significant decrease. There were also significant differences between high and low burden populations and several low burden populations had significantly lower analyte concentrations when compared to NHLFs. *** $p < 0.001$, ** $p < 0.01$, * $p < 0.05$ (vs NHLF), +++ $p < 0.001$, ++ $p < 0.01$ (vs low burden). NHLF n = 12 (4x donors: TB0912 [3], TB0917 [3], TB0932 [3], TB0918 [3]), SIPS n = 9 (3x donors: TB0917 [3], TB0918 [3], TB0932 [3]). 1-way ANOVA, Tukey's multiple comparison.

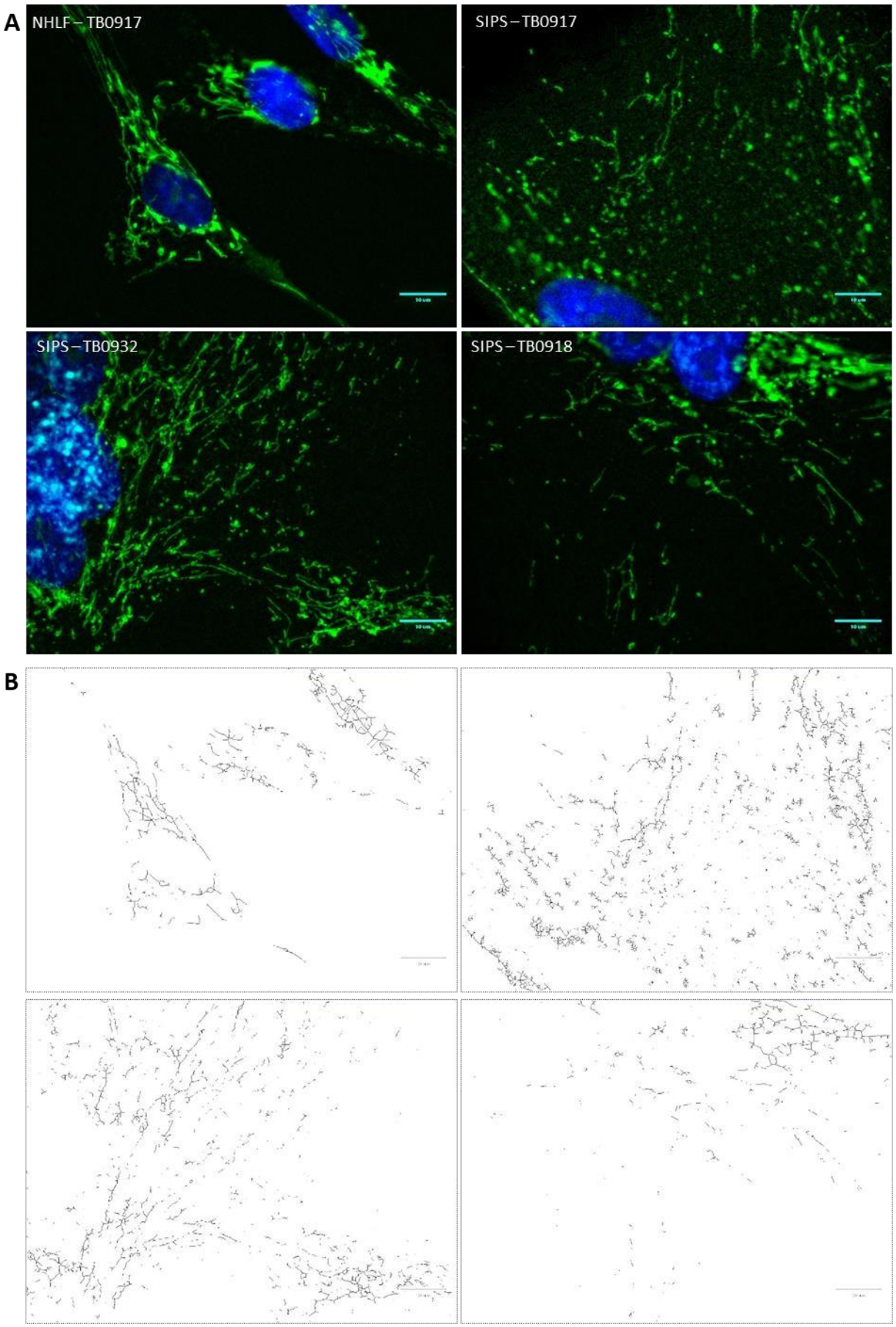

Figure 3.4.8. Immunofluorescent imaging of SIPS mitochondria. (A) Representative images of mono-cultured SIPS and NHLFs. 24 hrs post-seeding HLFs were fixed and stained for ATP5B (green) with additional DAPI (blue) nuclear staining. 100x magnification. Scale bar = 10 µm. **(B)** Corresponding skeletonised images of ATP5B staining for morphological quantification via ImageJ.

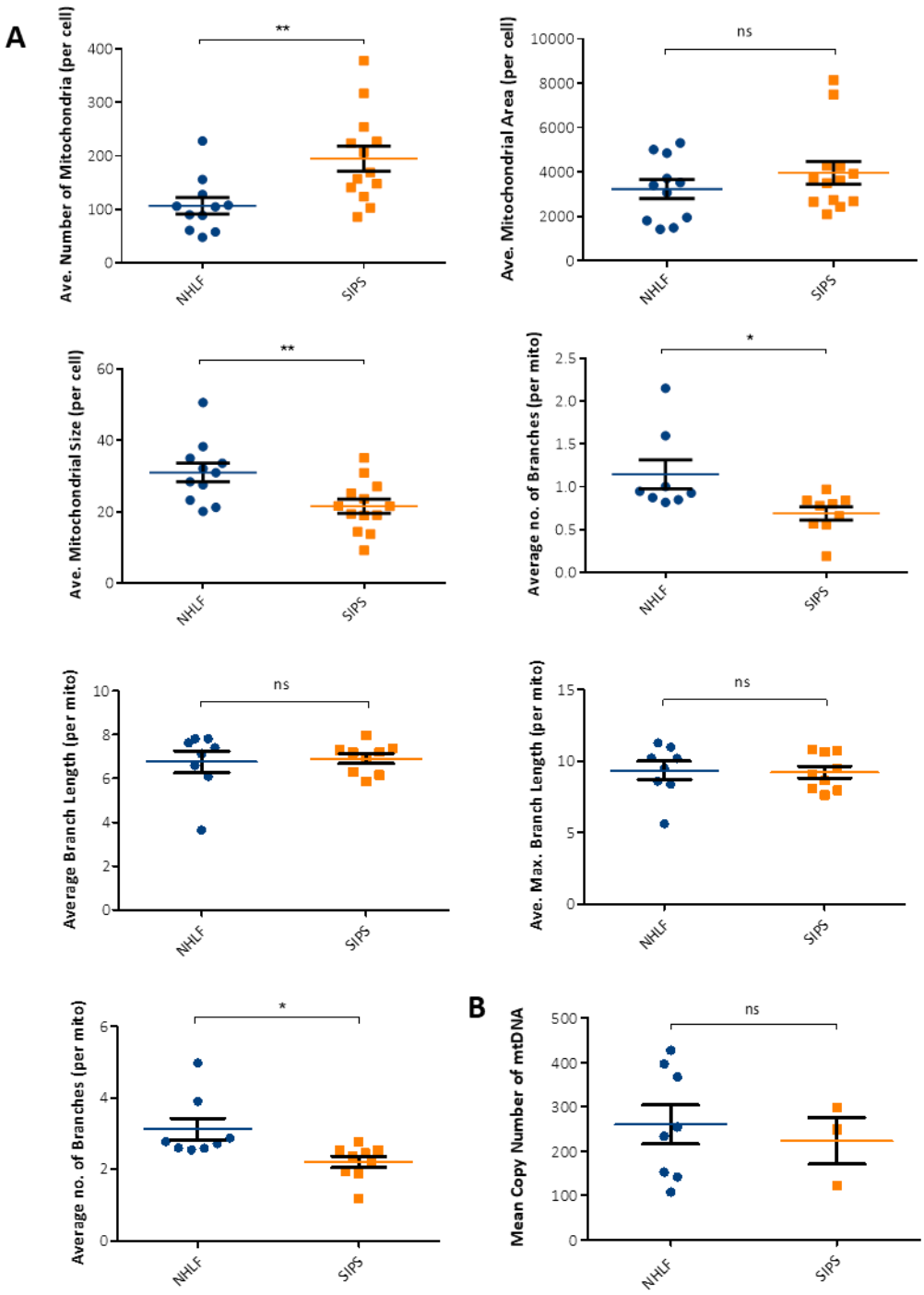

Figure 3.4.9. Quantification of mitochondrial DNA copy number and mitochondrial morphology between NHLF and SIPS. (A) Skeletonised, immunofluorescent ATP5B signal was quantified via ImageJ. Within a cell, the average number of mitochondria per cell was higher in SIPS yet the total area was not significantly different. Average size was decreased in SIPS. NHLF n = 11, SIPS n =13 Within mitochondria, the number of branches was decreased. There was no difference in average branch length or the maximum number of branches per mitochondria. The average number of junctions was significantly decreased. Data points are the average of 3 cells within an independent experiment. NHLF n = 8. SIPS n = 9. ** $p < 0.01$, * $p < 0.05$. Two-tailed, unpaired t-test. **(B)** DNA was isolated from 24 hr mono-cultured NHLFs and SIPS. RT-qPCR was performed with the nDNA primers *ND1* and *ND5,* and the mtDNA primers, *SCLO2B1* and *SERPINA1*. *ND1* and *ND5* were used as reference genes. The relative number of mtDNA copies was determined by the difference in Ct values between nuclear and mitochondrial DNA. There was no significant difference between NHLFs and SIPS. NHLF n = 8 (3x donors: TB0917 [3], TB0918 [2], TB0932 [3]). SIPS n = 3 (3x donors, TB0917, TB0918, TB0932). Two-tailed, unpaired t-test.

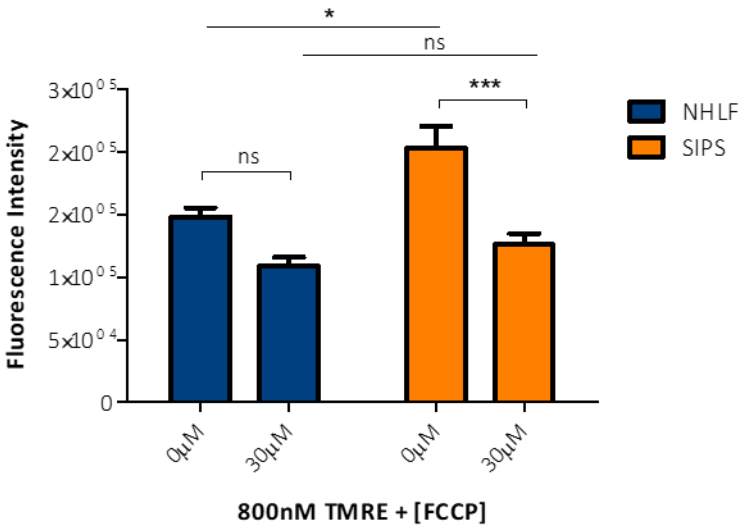

Figure 3.1.10. Assessment of mitochondrial membrane potential in mono-cultured NHLF and SIPS Comparison of NHLF and SIPS membrane potential 24 hrs post-seeding with 800 nM TMRE and 30μM FCCP. FCCP significantly decreased membrane potential in SIPS but not in NHLFs. There was no significant difference in uncoupled potential between NHLF and SIPS but, when coupled, SIPS potential was significantly higher. NHLF n = 4 (3x donors: TB0917, TB0918, TB0932 [2]), SIPS n = 4 (3x donors: TB0917 [2], TB0918, TB0932). *** $p < 0.001$, * $p < 0.05$. 2-way ANOVA, Bonferroni multiple comparison.

(*Figure* 3.4.9A.). The average number of mitochondria per cell was significantly increased in SIPS, although there was no difference in the area of this network. The average size of each mitochondrion within each cell was significantly less in SIPS, as was the average number of branches that each mitochondrion had. The average length of these branches was no different, nor was average maximum length of each branch. The average number of branches per mitochondrion was, however, significantly decreased in SIPS. The mean copy number of mtDNA was also measured via RT-qPCR. Isolated DNA was analysed, revealing that the mean copy number for SIPS fell within the range of that measured in NHLFs, with no significant difference between the two **(*Figure* 3.4.9B.)**. Therefore, SIPS do display a less interconnected mitochondrial network, composed of smaller and less branched organelles.

In an attempt to understand mitochondrial membrane polarity, $\Delta_{\psi m}$ was measured in NHLF and SIPS, after 24 hrs of mono-culture. TMRE and FCCP were again used **(*Figure* 3.4.10.)**. The fluorescence intensity of coupled mitochondrial was significantly higher in SIPS when compared to NHLFs. FCCP also significantly reduced this intensity in SIPS and there was no statistical difference between the uncoupled intensity of these cell types. In summary, this suggest that SIPS mitochondria, as well as being more fragmented and punctate, have hyperpolarised membranes in comparison to NHLFs. This potentially indicates increased ATP production and increased mitochondrial activity; however, it would be worth using an extracellular flux analyser to investigate this further.

3.4.2.4. SIPS RCN is decreased in culture and SIPS express greater levels of inflammatory and senescence-associated markers.

Senescence is defined by proliferative arrest. To begin to understand this in SIPS, cells were counted using a haemocytometer at 24 hr intervals, over a period of 72 hrs, to quantify RCN. SIPS were seeded at -24 hrs in either mono- or co-culture. Cell counts are shown relative to the initial seeding density. With the exception of a small drop at 0 hrs, RCN remains flat for 72 hrs, never significantly elevating above 1.0 for any culture

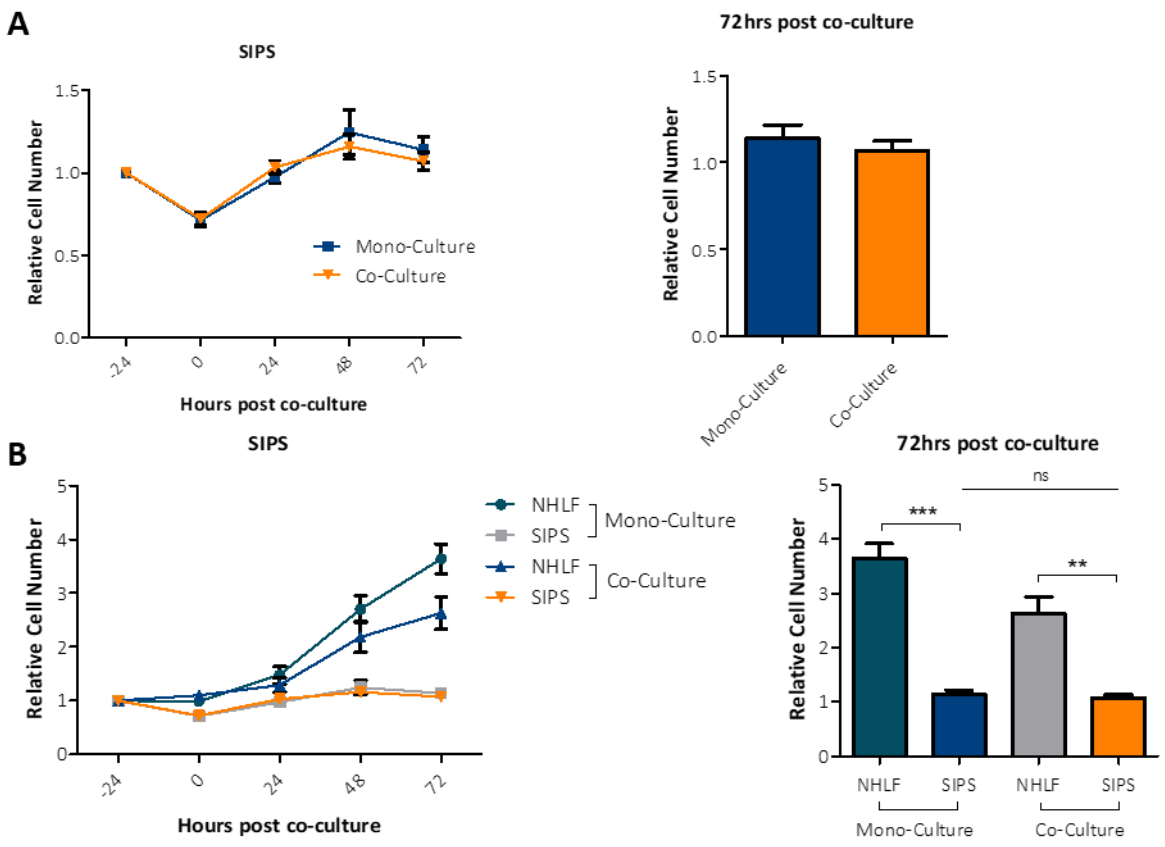

Figure 3.4.11. SIPS cell number over 72 hrs in mono- or co-culture. (A) SIPS were cultured in DMEM / αMEM 10% FBS media. At 24 hr intervals, over 72 hrs, SIPS cell numbers were counted using a haemocytometer. Cell numbers are shown relative to the initial seeding density. SIPS did not proliferate past their original seeding density and there was no significant difference between culture conditions. 1-way ANOVA, Tukey's multiple comparison. **(B)** Comparison of SIPS proliferation in mono- or co-culture with that of NHLFs. NHLF proliferation was significantly higher that that of SIPS at 72 hrs. NHLF n = 6 (3x donors: TB0917 [2], TB0918 [2], TB0932 [2]), SIPS n = 9 (3x donors: TB0917 [3], TB0918 [3], TB0932 [3]). *** $p < 0.001$, ** $p < 0.01$ (vs NHLF mono). 1-way ANOVA, Tukey's multiple comparison.

condition. At 72 hrs post co-culture, there was no significant difference between the RCN of either condition **(*Figure* 3.4.11A.)**. When comparing the values of SIPS in mono- or co-culture to equivalent data from NHLFs, RCN failed to rise in SIPS yet increased over 72 hrs for both NHLF conditions. At 72 hrs, NHLF mono-culture RCN and NHLF co-culture RCN were both significantly higher than the corresponding RCN of SIPS. Though not a measure of proliferation these results suggest a potential proliferative arrest in SIPS, under any culture condition, consistent with the underlying principles of the senescence phenotype **(*Figure* 3.2.11B.)**.

Though not increasing in cell number, after 72 hrs of co-culture there were significant changes to levels of SIPS RNA and protein secretion. RNA was isolated from SIPS and NHLFs at this time point and RT-qPCR performed. SASP and inflammatory wound associated RNA levels were quantified, as well as the regulators of senescence *CDKN1A* and *CDKN2A*. Average fold change was calculated in comparison to NHLF levels. There was a significant elevation in RNA levels of all factors, with the exception of *CDKN2A*, for which there was no significant change **(*Figure* 3.4.12.)**. The most significant increase was in levels of *IL33*, with an average change of 14.8-fold. *IL6, CXCL8* and *IL1B* were all increased on average over 5-fold. The smallest increase was in *HGF* levels, which increased 2-fold on average. The concentrations of secretory proteins were also measured, again via multiplex ELISA. The concentrations of proteins detected above 100 pg/ml are shown in **(*Figure* 3.4.13.)**. There were no significant differences in concentrations of VEGF and GM-CSF and concentrations of CCL2 and CXCL10 were significantly reduced. Concentrations of IL6, CXCL8, CXCL1 and GCSF were significantly increased. In SIPS co-culture CM concentrations of these proteins more than doubled when compared to their NHLF counterparts. The concentration of CXCL8 in SIPS CM was also the highest detected across all ELISA experiments, averaging at a concentration of roughly 14,000 pg/ml. As in previous experiments, the concentrations of IL-1α, IL-1β and IL-33 (measured via standard ELISA) were exceptionally low and there was no difference between CM types. These results highlight that with robust, p21-dependent senescence induction, cells experience severe stress, with upregulation of alarmin expression, concomitant with the upregulation of numerous SASP proteins that are secreted into the micro-environment.

These results describe the characteristics of SIPS in mono- and co-culture, the following experiments were aimed at understanding how these characteristics influence HBEC function.

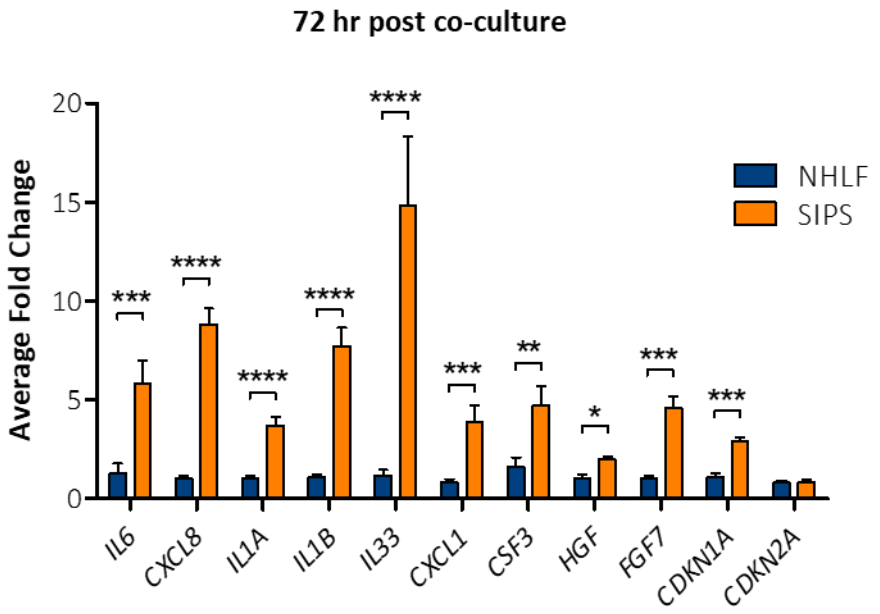

Figure 3.4.12. Comparison of NHLF and SIPS RNA levels after 72 hrs of co-culture. NHLF and SIPS were co-cultured in DMEM/αMEM 10% FBS. RT-qPCR was performed with genes of interest normalised to the reference genes *B2M* and *GAPDH.* SIPS RNA levels were calibrated to NHLF levels and the data is shown as an average fold change. There was a significant increase in levels of all genes of interest, except *CDKN2A*. NHLF n = 5 (3x donors: TB0917 [2], TB0918 [2], TB0932), SIPS n = 6 (3x donors: TB0917 [2], TB0918 [2], TB0932 [2]). **** p < 0.0001, *** p < 0.001, ** p < 0.01, * p < 0.05. Two-tailed, unpaired t-test performed on ddCt values.

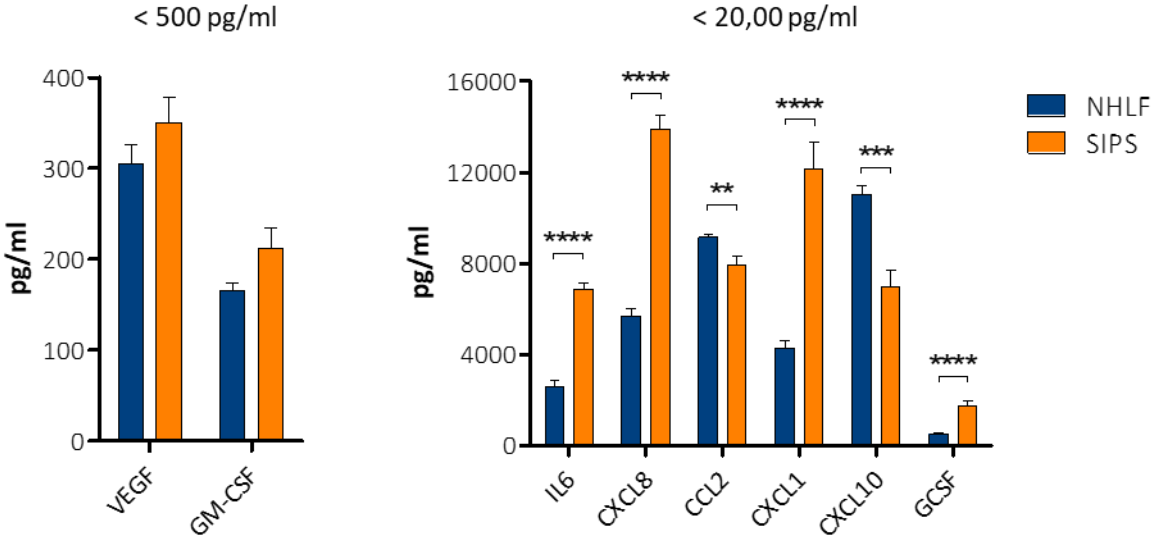

Figure 3.4.13. Multiplex cytokine array comparing NHLF and SIPS CM after 72 hrs of co-culture. Basolateral media were collected and stored at -80 °C. After thawing, conditioned media were analysed via Luminex Multiplex array, screening for immuno-modulating cytokines, chemokines and growth factors. Results are shown across 2 graphs of differing y-axis scales. SIPS CM has significantly increased concentrations of IL6, CXCL8, CXCL1 and GCSF compared to NHLFs and decreased concentrations of CCL2 and CXCL10. NHLF n = 12 (4x donors: TB0912 [3], TB0917 [3], TB0932 [3], TB0918 [3]), SIPS n = 9 (3x donors: TB0917 [3], TB0918 [3], TB0932 [3]). **** p < 0.0001, *** p < 0.001, ** p < 0.01. 1-way ANOVA, Tukey's multiple comparison.

3.4.2.5. The regeneration of HBEC barrier impermeability is impeded by both coculture with SIPS, or treatment with SIPS CM.

Firstly, the effect of SIPS co-culture on R_{TE} and the regeneration of epithelial ion impermeability was investigated. R_{TE} was measured over 72 hrs, at 24 hr intervals, in either HBEC mono-cultures or NHLF/SIPS co-cultures **(*Figure* 3.4.14A.)**. R_{TE} values did not significantly differ over the first 24 hrs. By 48 hrs, values for both co-culture types were significantly greater than mono-culture, although there was no difference between them. By 72 hrs there were significant differences between all three culture conditions **(*Figure* 3.4.14B.)**. R_{TE} values for both co-culture conditions were still significantly greater than those of mono-culture but the values for SIPS co-culture were significantly less than those for NHLF co-culture.

To investigate this further, an experiment was devised utilising an important aspect of SIPS induction. The period of recovery after H_2O_2 treatment is key to allowing the senescence phenotype to establish itself and the longer cells are left to recover, the greater the percentage of SA-βgal positivity. This property of SIPS induction was used to create SIPS mono-cultures of varying burdens of SA-βgal positive cells **(*Figure* 3.4.15A.)**. By taking cells at either recovery day 2, 4, or 6, a culture of increasing senescence burden could be created **(*Figure* 3.4.15B.)**. These populations of cells were then seeded at a density of 12,000 cells/well of a 24-well plate and subsequently given fresh medium and maintained for 72 hrs to produce CM. NHLFs were also cultured for 72hrs creating control CM. The CM, generated by differing levels of senescent HLFs, was then used to treat HBEC mono-cultures. As a further control, HBEC mono-cultures were also treated with CM, generated over 72 hrs but in the absence of cells. Treated HBECs were then cultured for 72 hrs and R_{TE} was measured **(*Figure* 3.4.15C.)**. When compared to the values of control CM, R_{TE} was significantly higher in NHLF co-culture and significantly

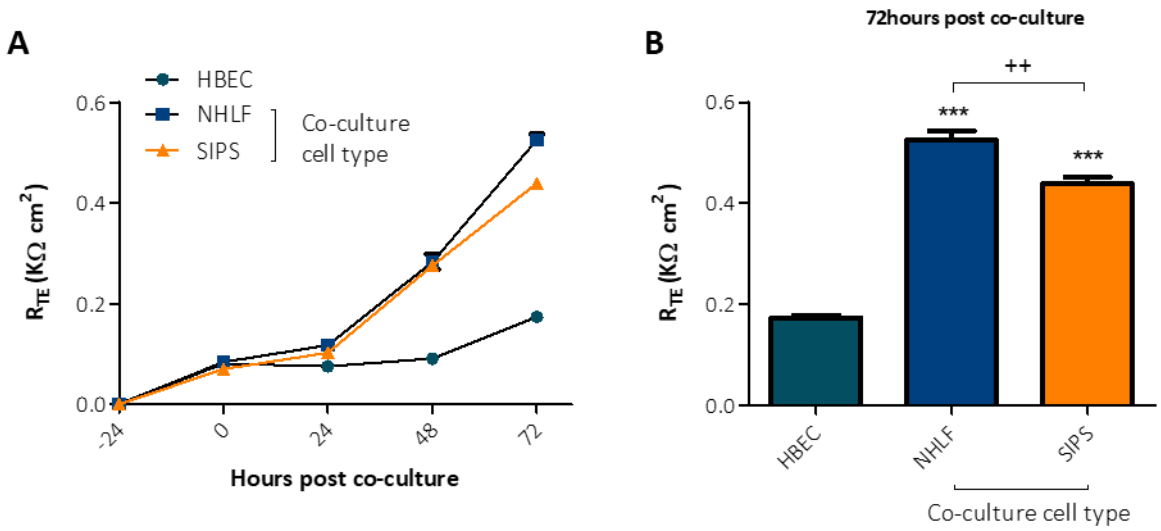

Figure 3.4.14. Effect of SIPS co-culture on HBEC R_{TE} over 72 hrs. (A) NHLFs and SIPS were seeded in equal densities at -24 hrs and co-cultured in DMEM/αMEM 10% for 72 hrs. R_{TE} was measured every 24 hrs hours. **(B)** At 72 hrs R_{TE} values from (A) are significantly higher for NHLFs and SIPS co-culture compared to HBEC mono-culture. SIPS values are significantly lower when compared to NHLFs. HBEC n = 4, NHLF n = 5 (4x donors: TB0912, TB0917 [2], TB0918, TB0932), SIPS n = 6 (3x donors: TB0917 [2], TB0918 [2], TB0932 [2]). *** $p < 0.001$ (vs HBEC), ++ $p < 0.01$ (vs NHLF). 1-way ANOVA, Tukey's multiple comparison.

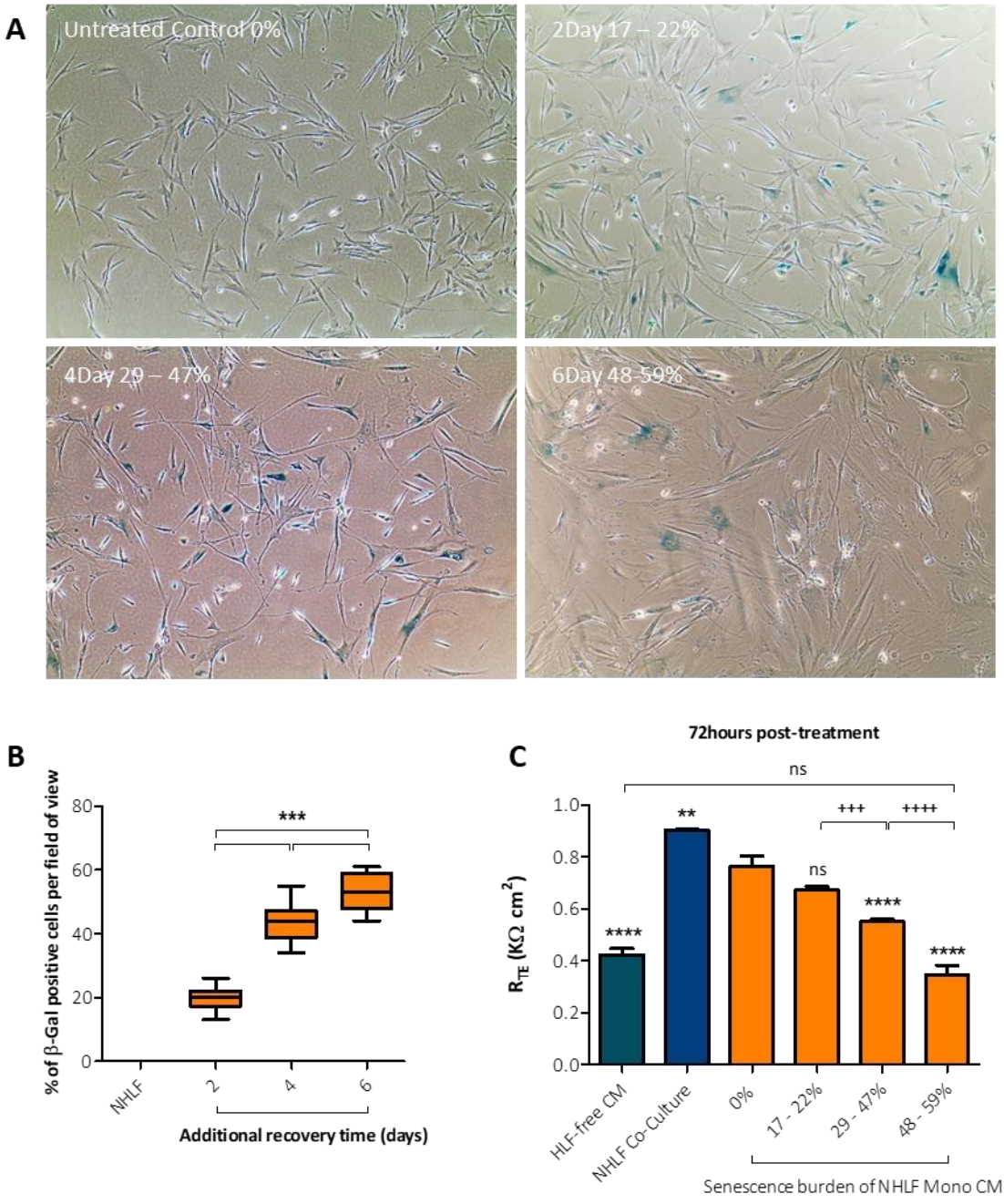

Figure 3.4.15. Effect of SIPS mono-culture CM on HBEC R_{TE} over 72 hrs. (A) The induction of SIPS was staggered over differing periods of recovery time prior to seeding in experiments. With an increase in recovery the percentage burden of senescent cells increased. Representative images of β-galactosidase activity are shown. **(B)** Quantification of β-galactosidase positivity. SIPS n = 7. *** $p < 0.001$. 1-way ANOVA, Tukey's multiple comparisons. **(C)** SIPS generated were mono-cultured for 72 hrs with the subsequent CM collected. HBEC mono-cultures were then seeded and treated with the CM from SIPS cultures of varying percentage burdens of senescence. R_{TE} was measured over 72 hrs in these cultures, alongside NHLF co-culture and HBEC mono-culture, treated with CM from a 72 hr cell-free culture. With an increase in burden of senescence, subsequent CM fails to significantly increase R_{TE} values at 72 hrs. SIPS n = 6, NHLF n = 5. **** $p < 0.0001$, ** $p < 0.01$ (vs 0% SIPS CM), ++++ $p < 0.0001$ (vs 29-47% SIPS CM), +++ $p < 0.001$ (17-22% SIPS CM). 2-way RM ANOVA, Bonferroni multiple comparison.

lower in HLF-free CM, consistent with earlier experiments investigating CM and R_{TE} **(*Figure* 3.2.7.)**. With an increasing burden of senescent cells, the subsequent CM has an increasingly attenuated ability to elevate R_{TE}, to the extent that, when the range of SAβgal positivity is between 48-59%, the CM fails to increase R_{TE} to a level significantly greater than that of control CM. SA-βgal activity was quantified prior to CM-production and therefore, over the 72 hr culture period, the senescence burden was likely to increase in all cultures. However, linear regression analysis of the data in ***Figure* 3.4.15B.** highlights a linear relationship between time and percentage positivity (r^2 = 0.93). Therefore, though the percentage burden will have changed by the end of CM production, the differences between cultures are likely to be maintained. Taken together, these results indicate that the microenvironment generated by SIPS is unable to promote epithelial regeneration.

3.4.2.6. In co-culture, SIPS reduce HBEC cell number and alter HBEC RNA levels.

To try and understand the cause of these differences, HBEC cell number was investigated. HBEC RCN was calculated over 72 hrs, following the protocol previously used to assess HBEC proliferation in NHLF co-culture. HBEC cell number was counted every 24 hrs in either mono-culture or co-culture with SIPS and RCN calculated **(*Figure* 3.4.16A.)**. HBEC RCN in mono-culture was significantly greater at 72 hrs than in coculture. This effect of co-culture was, however, not observed in SIPS co-culture, with no significant difference in RCN between co-culture conditions. Comparing the results of SIPS co-culture to those of NHLF co-culture and HBEC mono-culture, it can be seen that, at 72 hrs, HBEC RCN is significantly less in SIPS co-culture **(*Figure* 3.4.16B.)**. As found previously, there was an inverse relationship between HBEC RCN and R_{TE}, with a smaller RCN equalling a greater R_{TE}. The results from SIPS co-culture, however, do not fit this trend. Although there is a smaller RCN in this condition, R_{TE} is not greater **(*Figure* 3.4.17.)**.

SIPS co-culture also has an effect on HBEC RNA levels, as measured by RT-qPCR at 72 hrs post co-culture **(*Figure* 3.4.18)**. RNA levels of *VIM, KRT5, IL1A, CXCL1* and *TNFA* were all

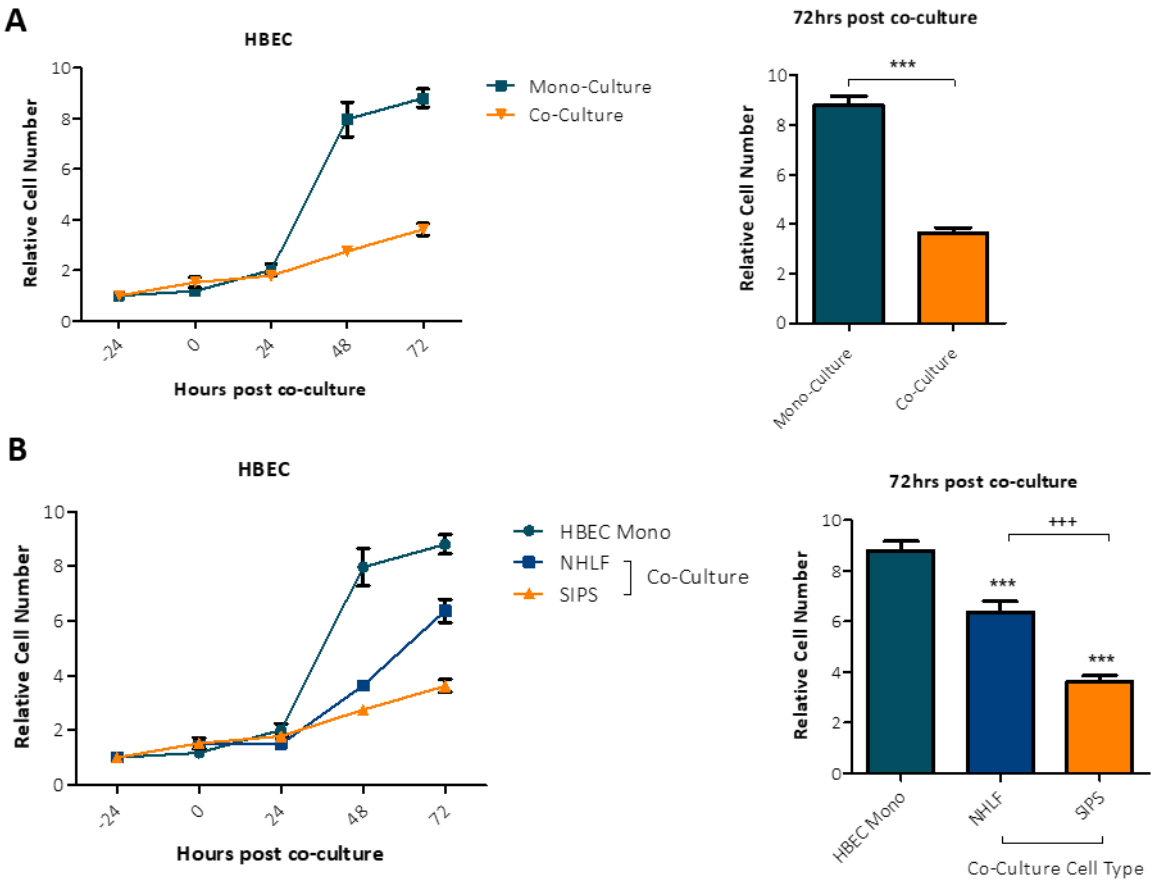

Figure 3.4.16. Effect of SIPS co-culture on HBEC cell number over 72 hrs. (A) HBECs were cultured in DMEM / αMEM 10% FBS media. At 24 hr intervals, over 72 hrs, HBEC cell numbers were counted using a haemocytometer. Cell numbers are shown relative to the initial seeding density. HBEC proliferation was significantly reduced in co-culture with SIPS. HBEC n = 6, SIPS n = 9 (3x donors: TB0917 [3], TB0918 [3], TB0917 [3]). *** $p < 0.001$, ** $p < 0.01$. 1-way ANOVA, Tukey's multiple comparison. **(B)** Comparison of HBEC proliferation in either mono-culture or co-culture with NHLF / SIPS. HBEC proliferation was greatest in mono-culture, significantly reduced with NHLF co-culture and even further reduced with SIPS co-culture. There was a significant difference between NHLF and SIPS co-culturing. HBEC n = 6, NHLF n = 6 (3x donors: TB0917 [2], TB0918 [2], TB0932 [2]). , SIPS n = 9 (3x donors: TB0917 [3], TB0918 [3], TB0932 [3]). *** $p < 0.001$ (vs HBEC mono), +++ $p < 0.001$ (vs NHLF). 1-way ANOVA, Tukey's multiple comparison.

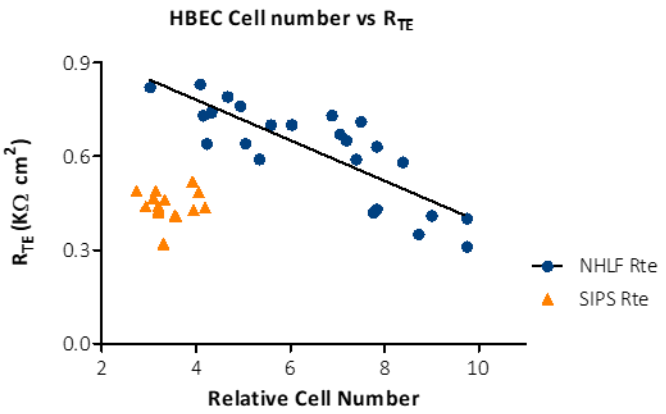

Figure 3.4.17. Relationship between RCN and R_{TE} with SIPS co-culture. As previously shown, there is an inverse relationship between RCN and R_{TE} when investigating with NHLF co-cultures or HBEC mono-culture. Plotting SIPS co-culture values on this graph highlights that, although HBEC RCN is decreased under these conditions, R_{TE} is not increased. Each point represents 1x insert.

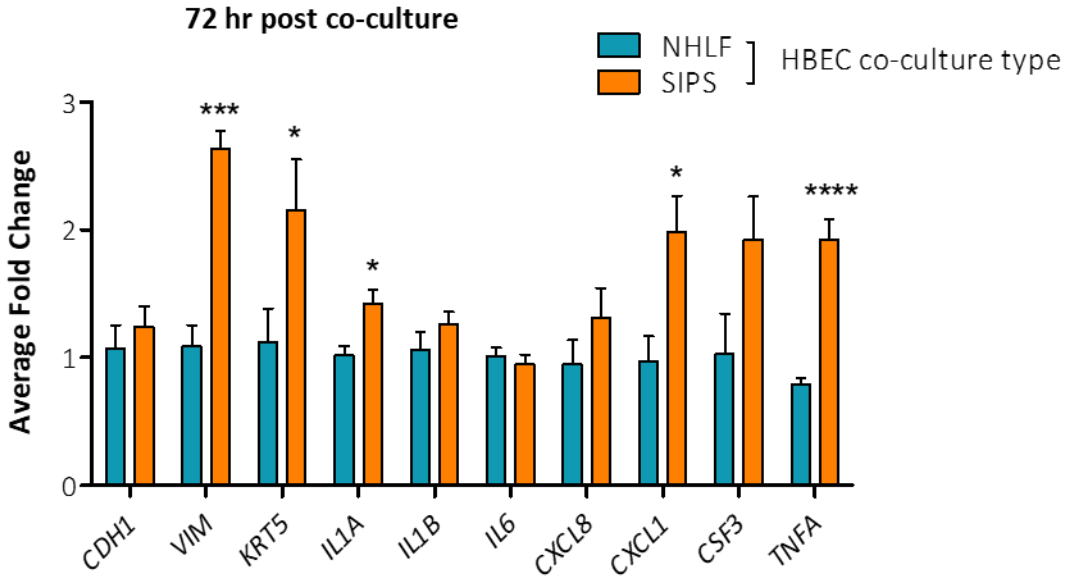

Figure 3.4.18. Effect of SIPS co-culture on HBEC RNA levels after 72 hrs. RT-qPCR was performed with genes of interest normalised to the reference genes *B2M* and *GAPDH.* HBEC co-culture RNA levels were calibrated to mono-culture levels and the data is shown as an average fold change. RNA levels of *VIM, KRT5, IL1A, CXCL1 and TNFA* were significantly increase in SIPS co-culture. There was no significant change in other genes of interest. NHLF co-culture n = 7 (3x donors: TB0917 [2], TB0918 [3], TB0932 [2]), SIPS co-culture n = 7 (3x donors: TB0917 [2], TB0918 [3], TB0932 [2]). **** $p < 0.0001$, *** $p < 0.001$, * $p < 0.05$. Two-tailed, unpaired t-test performed on ddCt values.

significantly elevated. There was no significant difference between levels of *CDH1, IL1B, IL6, CXCL8* or *CSF3*. This suggests a more inflammatory HBEC phenotype in SIPS coculture and also a potential resemblance to the epithelial phenotype found in IPF, with an increase in *VIM* and *KRT5* suggesting a more mesenchymal and a more basal epithelial phenotype.

3.4.2.7. SIPS in co-culture impair HBEC re-epithelialisation after wounding, associated with altered levels of inflammatory RNA transcripts.

Co-culture with SIPS fails to promote epithelial regeneration, decreases HBEC proliferation and increases mesenchymal and inflammatory RNA levels. The effect of SIPS on re-epithelialisation was next evaluated. Co-cultures were maintained for 72 hrs prior to mechanical wounding via scratch. Phase-contrast images were then taken at 0, 6 and 9 hrs, allowing quantification of wound closure with ImageJ **(*Figure* 3.4.19A)**. Representative images are shown in ***Figure* 3.4.19B**. By 6hrs there was a significant decrease in the percentage wound closure of HBECs co-cultured with SIPS, when compared to both HBEC mono-culture and NHLF co-culture. At 9 hrs these differences were maintained **(*Figure* 3.4.19C.)**. Re-epithelialisation was significantly impaired in SIPS co-culture over the course of 9 hrs, further highlighting the detriment of the SIPSgenerated micro-environment to epithelial function.

The effect that epithelial wounding had on SIPS RNA levels was also quantified. After 72 hrs of co-culture, NHLF or SIPS RNA was collected, prior to and 9 hrs after wounding. Though already significantly elevated compared to NHLFs, RNA levels of *IL1A, HGF, FGF7, CDKN1A, IL6, CXCL8* and *IL33* did not significantly change with wounding **(*Figure* 3.4.20)**. The average fold change of *HGF* levels remained greater than NHLFs but this did not reach significance after wound. Levels of *CDKN2A* were not elevated either pre- or postwounding. RT-qPCR did, however, reveal that wounding lead to an increase in RNA levels of *IL1B, CXCL1* and *CSF3.* The average fold change of both *IL1B* and *CXCL1* more than tripled and the average fold change of *CSF3* went from 3.9 to 42.7 in response to wounding, highlighting that SIPS are responsive to epithelial wounding and able to

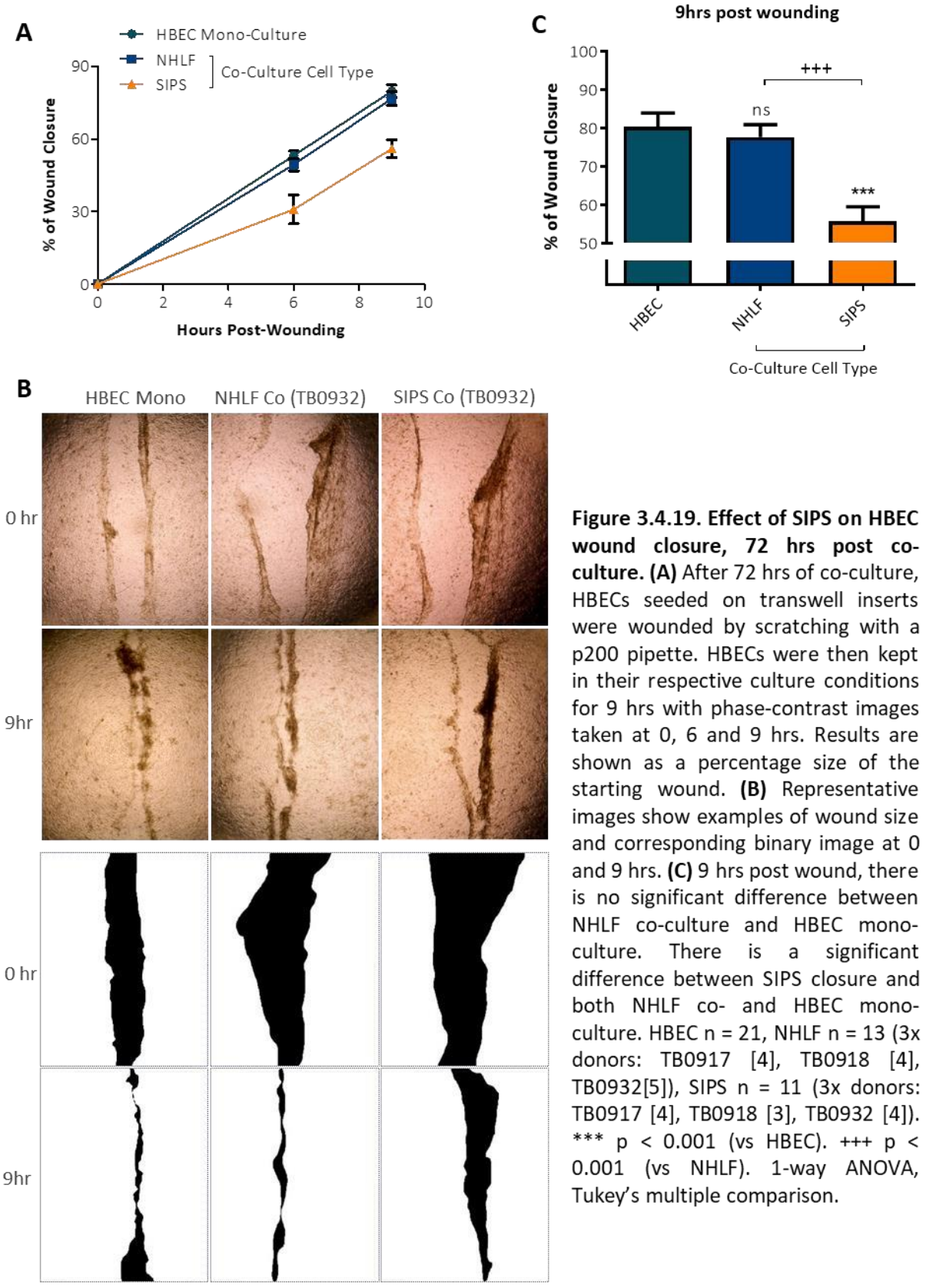

Figure 3.4.19. Effect of SIPS on HBEC wound closure, 72 hrs post co-culture. (A) After 72 hrs of co-culture, HBECs seeded on transwell inserts were wounded by scratching with a p200 pipette. HBECs were then kept in their respective culture conditions for 9 hrs with phase-contrast images taken at 0, 6 and 9 hrs. Results are shown as a percentage size of the starting wound. **(B)** Representative images show examples of wound size and corresponding binary image at 0 and 9 hrs. **(C)** 9 hrs post wound, there is no significant difference between NHLF co-culture and HBEC mono-culture. There is a significant difference between SIPS closure and both NHLF co- and HBEC mono-culture. HBEC n = 21, NHLF n = 13 (3x donors: TB0917 [4], TB0918 [4], TB0932[5]), SIPS n = 11 (3x donors: TB0917 [4], TB0918 [3], TB0932 [4]). *** $p < 0.001$ (vs HBEC). +++ $p < 0.001$ (vs NHLF). 1-way ANOVA, Tukey's multiple comparison.

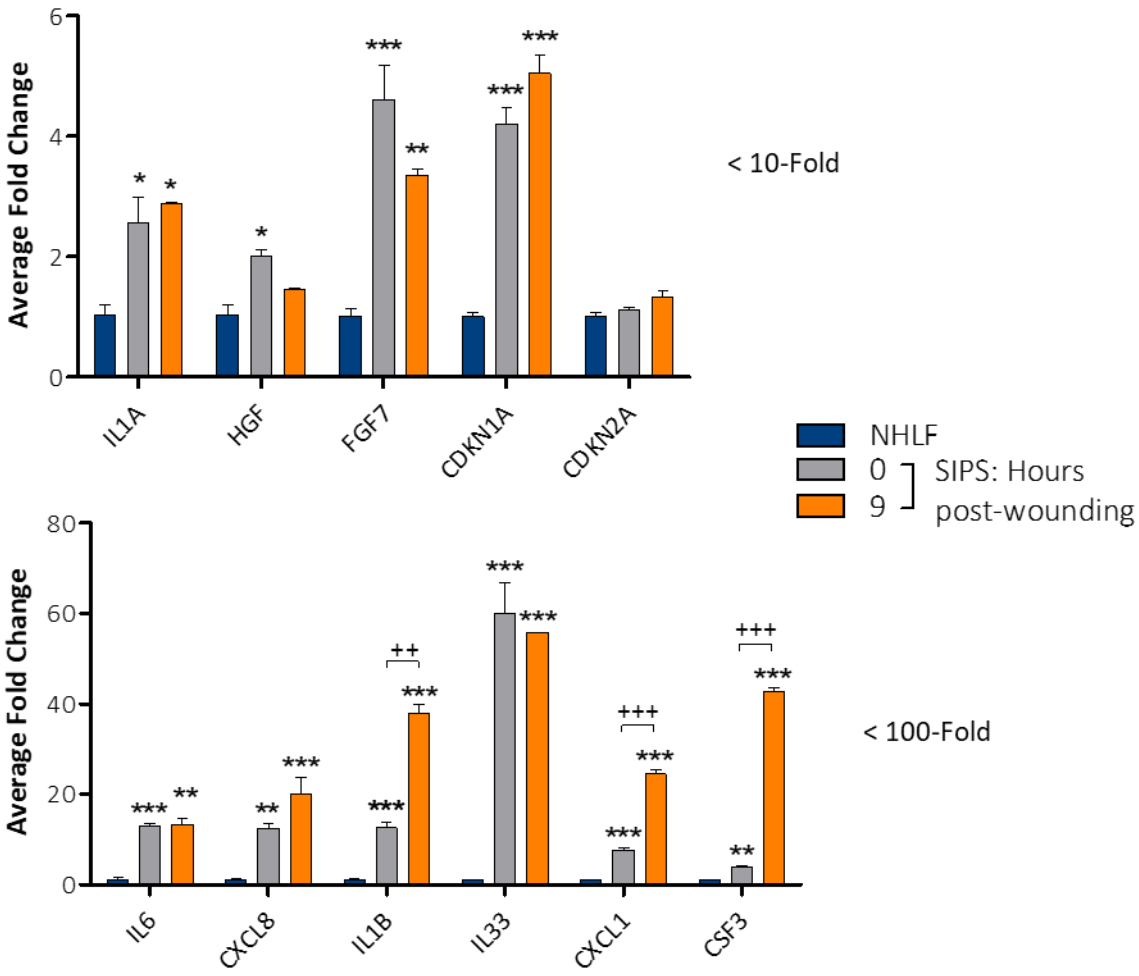

Figure 3.4.20. Comparison of RNA levels of NHLFs and SIPS at 0 and 9 hrs post-wounding, after 72 hrs of co-culture. RNA was isolated from NHLFs and SIPS pre- and post-wounding. RT-qPCR was performed with genes of interest normalised to the reference genes *B2M* and *GAPDH.* SIPS RNA levels were calibrated to NHLF co-culture levels and the data is shown as an average fold change. Results are shown across 3 graphs of differing y-axis scales. At 0 hrs SIPS RNA levels of all genes (except *CDKN2A*) were elevated when compared to NHLFs. At 9 hrs there were further elevations of *IL1B, CXCL1* and *GCSF*, which were significantly higher compared to 0 hrs. NHLF n = 4 (3x donors: TB0917, TB0918, TB0932 [2]), SIPS 0 hr n = 3 (3x donors: TB0917, TB0918, TB0932), SIPS 9hr n = 2 (2x donors: TB0918, TB0932). *** $p < 0.001$, ** $p < 0.01$, * $p < 0.05$ (vs NHLF), +++ $p < 0.001$, + $p < 0.05$ (vs SIPS 0 hr). 1-way ANOVA, Tukey's multiple comparison performed on ddCt values.

further increase expression of certain pro-inflammatory factors. *IL1B* is potentially elevated in response to epithelial cell death occurring during wounding, with necrotic cells releasing damage-associated molecular patterns that stimulate upregulation. Likewise, *CXCL1* and *CSF3* are secretory factors associated with wound repair and therefore expected to be elevated [306]. It is interesting however that the other key wound-associated factors, such as IL-6 and CXCL8, were not elevated and perhaps this

is demonstrative of the SIPS phenotype at baseline recapitulating the that of normal fibroblasts responding to epithelial injury.

3.4.2.8. SIPS CM can alter RNA levels of COL3A1 in NHLFs.

The primary focus of this section of experiments was to induce SIPS and to understand their relationship with HBECs in co-culture. Another area of intrigue however was the effect that SIPS could have on otherwise normal NHLFs. Hecker *et al.* described fibrotic foci in the aged, BLM-treated mouse as being comprised of an internal core of nonproliferative, senescent myofibroblasts surrounded by proliferative fibroblasts, with the suggestion that senescent fibroblasts promote proliferation and fibrogenic processes in their neighbours [242]. Schafer *et al.* have since been able to demonstrate that the CM from senescent fibroblasts can promote an increase in the relative expression of the collagen encoding genes *COL1A1* and *COL1A2*, genes important for matrix deposition and this fibrogenic process **(*Figure* 1.3.7B.)** [247]. Therefore, the effect that SIPS had on fibrotic processes in NHLFs was also of interest and it was hypothesised that the CM from SIPS would up-regulate expression of ECM producing genes. Consequently, an experiment was setup in which mono-cultured NHLFs were treated with SIPS CM or NHLF CM for 72 hrs, with RNA collected at this time point. SIPS CM was generated after 72 hrs of mono-culture, with cells seeded in 12-well plates at a density of 30,000 cells/well. Treated NHLFs were also seeded in this format. RT-qPCR was performed for the collagen encoding transcripts *COL1A1* and *COL3A1*, and the elastin encoding transcript *ELN*, key components of the ECM deposited in fibrosis. As a positive control, NHLFs were also treated with 1ng/ml of recombinant TGF-β1 (PrepoTech, USA), which is known to robustly increase expression of these ECM encoding genes. TGF-β1

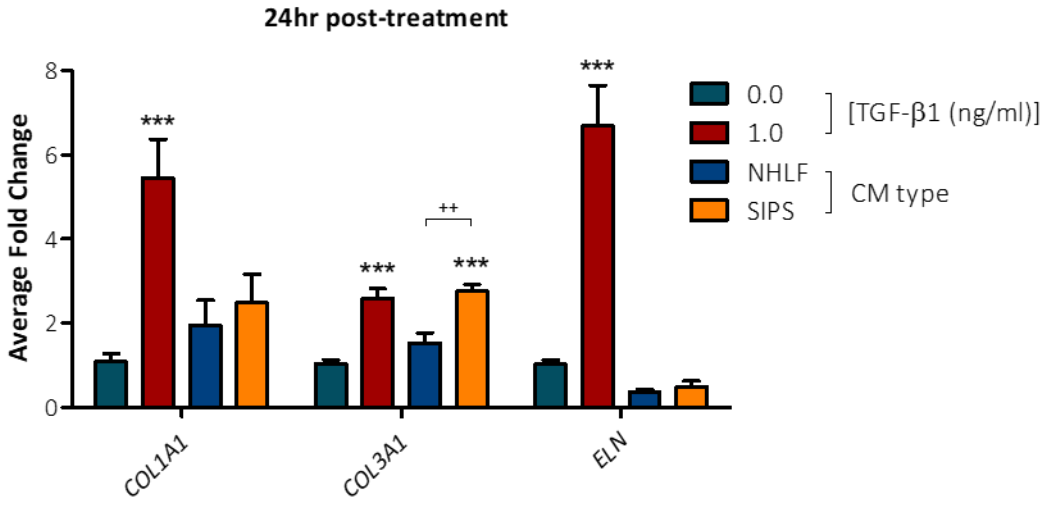

Figure 3.4.21. Effect of SIPS CM treatment on collagen and elastin RNA levels in NHLFs. NHLFs were treated with pre-incubation media containing: 4mM L-glutamine, 50 µg/ml ascorbic acid, 0.2 mM proline and 0.4% FBS for 24 hrs. media were then removed and replaced with DMEM 10% FBS with either 0.0 or 1.0 ng/ml recombinant TGF-β1, or the CM from 72 hr mono-cultured NHLFs or SIPS. Cells were treated for 24 hrs prior to RNA extraction and RT-qPCR. Genes of interest are normalised to the reference genes *B2M* and *GAPDH* and RNA levels are calibrated to the 0.0 ng/ml TGF-β1 treatment group. The data is shown as an average fold change. Treatment with 1.0 ng/ml TGF-β1 significantly elevated RNA levels of all genes. CM treatment did not significantly alter levels except for *COL3A1*, where SIPS CM treatment significantly elevated RNA levels when compared to control and NHLF CM. NHLF n = 6 (3x donors: TB0917 [2], TB0918 [2], TB0932 [2]). *** $p < 0.001$ (vs 0.0ng/ml TGF-β1), ++ $p < 0.01$ (vs SIPS CM). 1-way ANOVA, Tukey's multiple comparisons.

treatment significantly elevated levels of all three RNA transcripts when compared to untreated cells **(*Figure* 3.4.21.)**. NHLF and SIPS CM treatment had no significant effect on levels of either *COL1A1* or *ELN*, although the average fold change was greater in *COL1A1* levels and smaller in *ELN* levels. Treatment with NHLF CM had no significant effect on levels of *COL3A1* but treatment with SIPS CM led to a significant increase, matching the effect of TGF-β1 treatment. Though only evidenced at an RNA level, this result could also begin to suggest that SIPS can stimulate collagen type-3 α-1 production in non-senescent, neighbouring HLF. It is interesting that the CM could modulate NHLF gene expression and this further exemplified a role for senescence in the pathology of IPF.

3.4.2.9. SIPS recapitulate the functional behaviour of FHLFs, acting as a positive control and highlighting the senescence-like phenotype of these cells.

This section has thus far considered senescent cells, their characteristics and effects, in their own right. The rationale behind investigating this cellular phenomenon was, however, to understand how they relate to the previously described results concerning FHLFs. SIPS were designed to act as a positive control for FHLFs, under the hypothesis that FHLFs display a senescent-like phenotype that causes their pathological attributes. Due to an equivalence of experimental set ups and conditions, a direct comparison of data generated from FHLFs and SIPS can be made, allowing this hypothesis to be tested.

When comparing mitochondrial morphology, it is evident that both SIPS and FHLFs share similar characteristics **(*Figure* 3.4.22.)**. In comparison to NHLFs, both had an increased average number of mitochondria per cell whilst the mitochondria themselves were smaller and less branched. Mitochondrial junctions were also less prevalent in both. Therefore, both cell types have an altered mitochondrial phenotype, characterised by a high prevalence of mitochondria, but which are more punctate and part of a less wellconnected network.

Both cell types also have significantly smaller RCNs after 72 hrs of compared to NHLFs **(*Figure* 3.4.23A.)**. Both also significantly impaired re-epithelialisation **(*Figure* 3.4.23B.)**. SIPS were on average more detrimental to the process but there was no significant difference between the effect of them and the effect of FHLFs. Likewise, both also attenuated the beneficial effect of NHLF co-culture on R_{TE} development and epithelial regeneration **(*Figure* 3.4.23C.)**. R_{TE}, after 72 hrs of co-culture, was significantly less than in co-culture with NHLFs, with no statistical difference between the R_{TE} of monocultured HBECs, and again there was no difference between FHLFs and SIPS. Together these results highlight that SIPS and FHLFs are a detriment to epithelial function.

After 24 hrs of mono-culture and RT-qPCR, the evidence for similarities in phenotype was less robust **(*Figure* 3.2.24.)**. Both cell types showed a non-significant and modest increase in *IL6* expression, with no statistical difference between the two. FHLFs showed a non-significant increase in *CXCL8* expression but this was significantly less than the expression in SIPS. This was also true for expression of *IL1B*. *IL1A* was again

nonsignificantly upregulated in FHLFs, whereas in SIPS it was, but this time there was no statistical difference between the two. *CDKN1A* was upregulated exclusively in SIPS whereas, conversely, *CDKN2A* was upregulated exclusively in FHLFs. Therefore, only a trend of similarity can be described at an RNA level, although it is evident that changes in RNA levels are likely to be mediated by different pathways.

Protein concentrations in the CM, after 72 hrs of co-culture, can also be compared **(*Figure* 3.2.25.)**. Regarding IL-6 and CXCL8 protein secretion, both SIPS and FHLFs produce a higher concentration of these products than NHLFs. The average protein concentration was greatest in SIPS co-culture, significantly so for CXCL8, suggesting that SIPS represent a more pro-inflammatory phenotype than FHLFs. CCL2 and CXCL10 were both produced less by SIPS whereas there was no difference in FHLFs, indicating that this phenotypic alteration is unique to SIPS. There was a non-significant trend towards an increase in FHLFs CXCL1 production, with SIPS producing a significantly greater concentration. Conversely, for GM-CSF and G-CSF, FHLFs produced a significantly higher concentration than controls whereas SIPS did not. Taken together, these results suggest that, when looking at IL-6 and CXCL8, SIPS serve as a benchmark for a senescent-like phenotype in FHLFs. This is non-significantly evident for CXCL1 production as well and, in terms of GM-CSF and G-CSF, both cell types share a trend towards increased production. Overall, the comparison of data from these different experiments highlights how SIPS recapitulate many of the phenotypic characteristics of FHLFs.

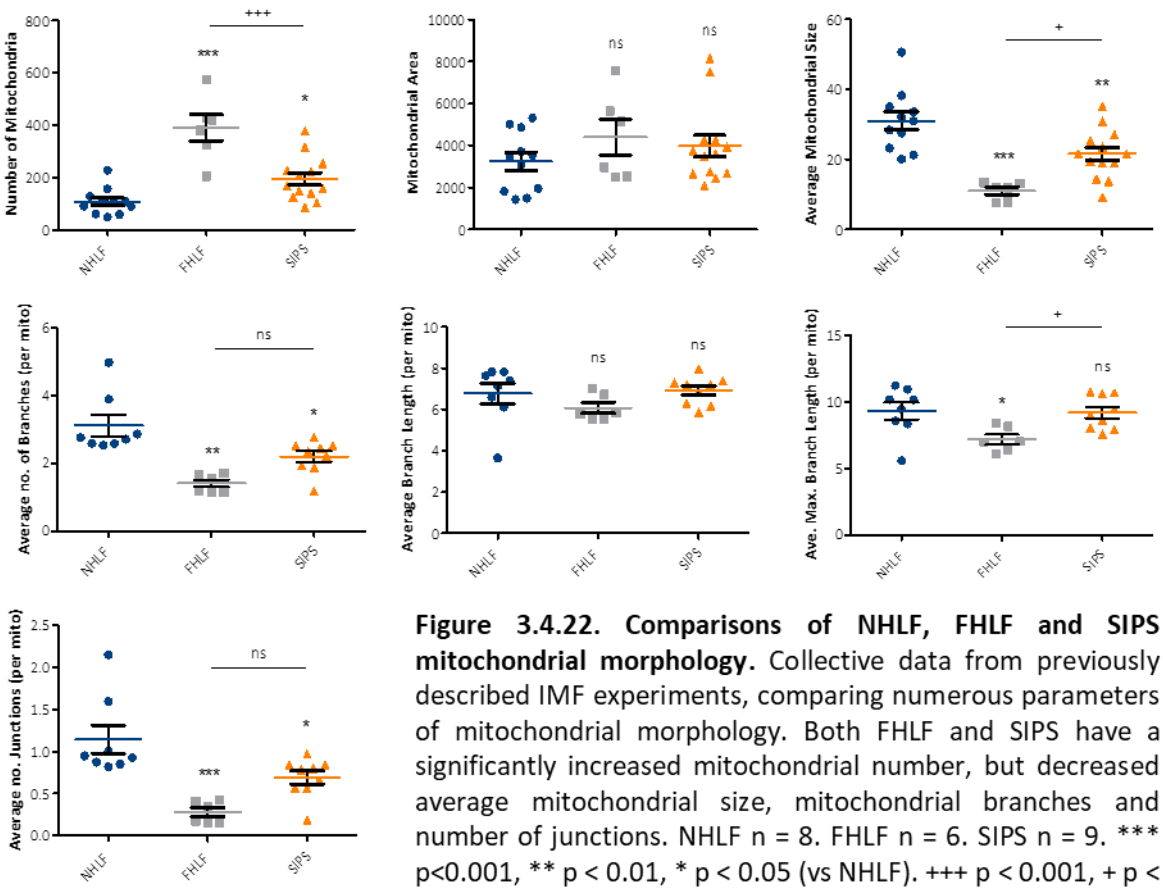

Figure 3.4.22. Comparisons of NHLF, FHLF and SIPS mitochondrial morphology. Collective data from previously described IMF experiments, comparing numerous parameters of mitochondrial morphology. Both FHLF and SIPS have a significantly increased mitochondrial number, but decreased average mitochondrial size, mitochondrial branches and number of junctions. NHLF n = 8. FHLF n = 6. SIPS n = 9. *** $p<0.001$, ** $p < 0.01$, * $p < 0.05$ (vs NHLF). +++ $p < 0.001$, + $p < 0.05$ (vs FHLF). 1-way ANOVA, Tukey's multiple comparisons.

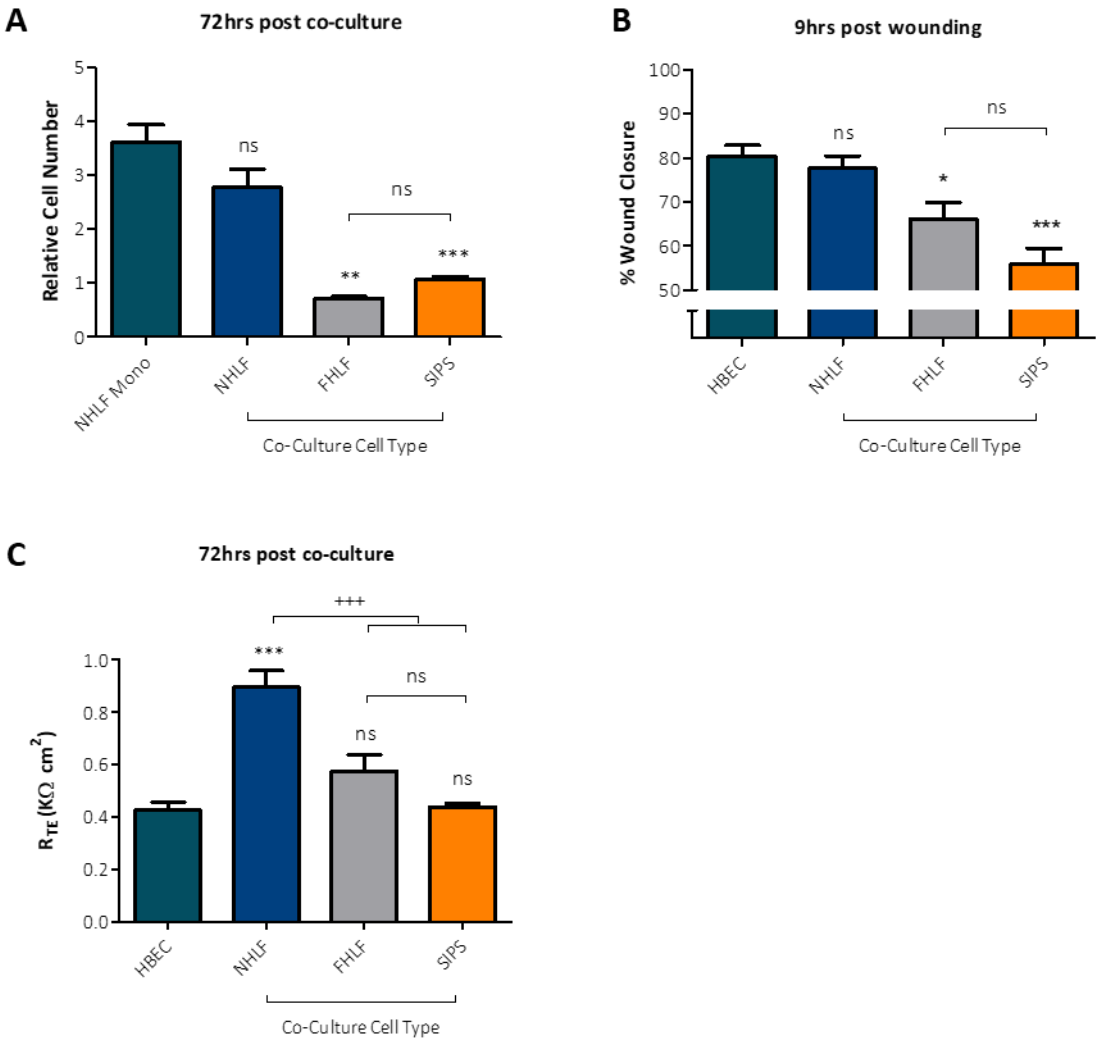

Figure 3.4.23. Comparisons of cell number, wound closure and R_{TE} of NHLFs, FHLFs and SIPS in co-culture. (A) HLF RCN measurements were made after 72 hrs of culture. Compared to mono-cultured NHLFs, the RCN of both FHLFs and SIPS was significantly less. There was no difference between these cell types. NHLF mono n = 18, NHLF n = 18, FHLF n = 3, SIPS n = 9. *** $p < 0.001$, ** $p < 0.01$ (vs NHLF mono). 1-way ANOVA, Tukey's multiple comparisons. **(B)** Percentage wound closure 9 hrs post scratch. Wound closure was significantly impaired when HBECs are co-cultured with both FHLF and SIPS. There was no difference between these culture conditions. HBEC n = 21, NHLF n = 38, FHLF n = 38, SIPS n = 32. *** $p < 0.001$, * $p < 0.05$ (vs HBEC). 1-way ANOVA, Tukey's multiple comparisons. **(C)** Comparison of R_{TE} after 72 hrs of culture. Co-culture with NHLF significantly increased R_{TE} compared to HBEC mono-culture, there was no statistical increase when co-cultured with FHLFs and SIPS. R_{TE} was significantly lower in these two conditions when compared to NHLFs. HBEC n = 11, NHLF n = 11, FHLF n = 11, SIPS n = 6. *** $p < 0.001$ (vs HBEC), +++ $p < 0.001$ (vs NHLF). 1-way ANOVA, Tukey's multiple comparisons.

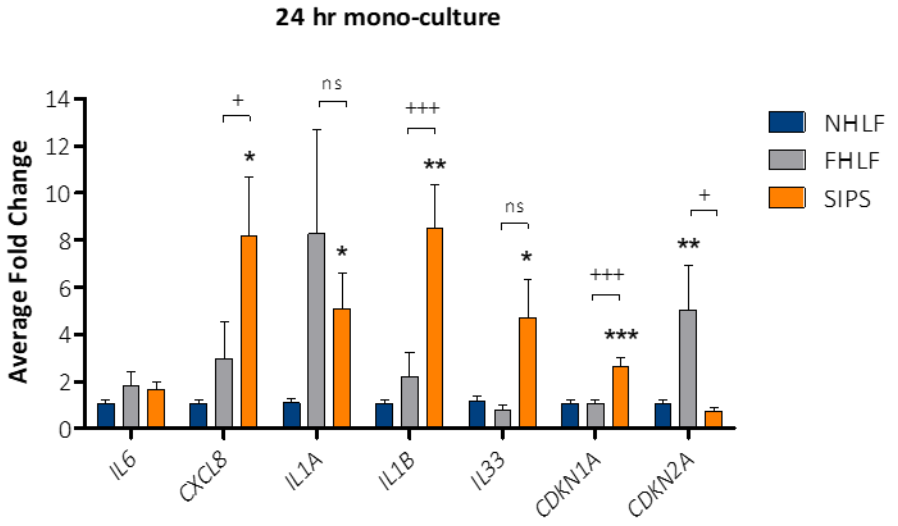

Figure 3.4.24. Comparison of NHLF, FHLF and SIPS RNA levels after 24 hrs of mono-culture. RNA was analysed after 24 hrs of mono-culture. Genes of interest are normalised to the reference genes *B2M* and *GAPDH* and RNA levels are calibrated to NHLFs. Levels of *CXCL8, IL1B* and *CDKN1A* were significantly greater in SIPS than NHLFs and FHLFs. Levels of *IL1A* and *IL33* were significantly greater in SIPS when compared to NHLFs but not FHLFs. Levels of *CDKN2A* were significantly greater in FHLFs then NHLFs and SIPS. NHLF n = 8, FHLF n = 6, SIPS n = 8. *** $p < 0.001$, ** $p < 0.01$, * $p < 0.05$ (vs NHLF). +++ $p < 0.001$, + $p < 0.05$ (vs FHLF). 1-way ANOVA, Tukey's multiple comparisons.

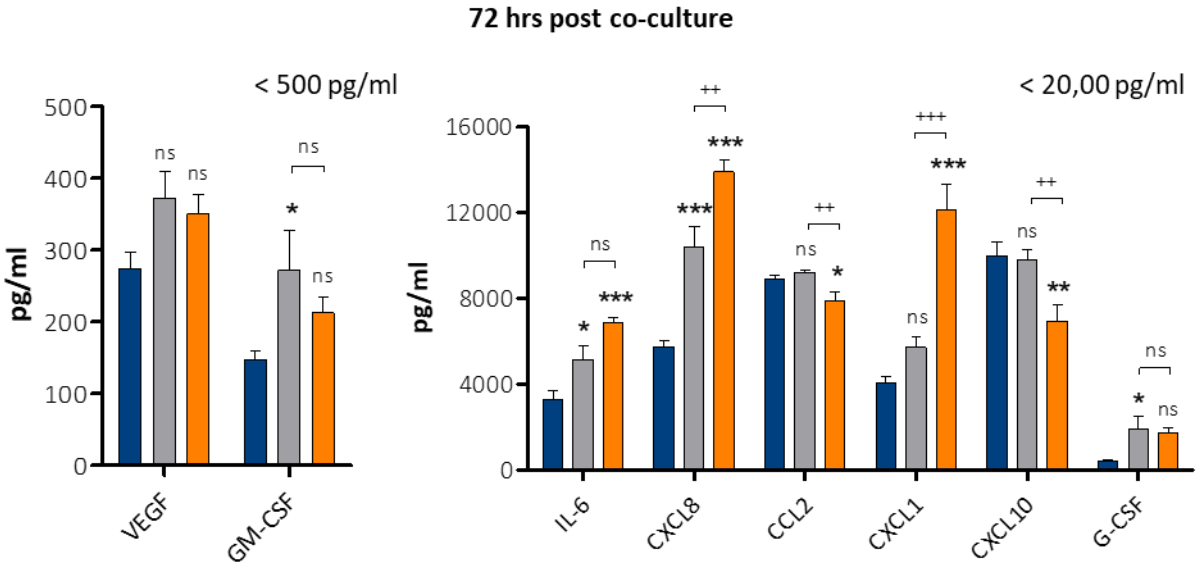

Figure 3.4.25. Comparisons of protein concentrations detected in the CM of NHLF, FHLF and SIPS co-cultures. Protein concentration was quantified in basolateral CM after 72 hrs of co-culture via multiplex ELISA. Results are shown across 2 graphs of differing y-axis scales. Compared to NHLF co-culture, concentrations of IL-6 and CXCL8 were both significantly greater in FHLF and SIPS co-culture. Concentrations of GM-CSF and G-CSF were increased in FHLFs co-cultures only. Concentrations of CCL2 and CXCL10 were decreased whilst CXCL1 concentrations are increased in SIPS co-cultures only. NHLF n = 12, FHLF n = 12, SIPS n = 9. *** $p < 0.001$, ** $p < 0.01$, * $p < 0.05$ (vs NHLF), +++ $p < 0.001$, ++ $p < 0.01$ (vs FHLF). 1-way ANOVA, Tukey's multiple comparisons.

3.4.3. Discussion

This section set out to induce senescence in NHLFs, ultimately allowing an investigation of their phenotype in co-culture and how they alter HBEC function. Senescence was robustly induced, as evidenced by several markers, and SIPS upregulated expression of a range of inflammatory signalling factors, concomitant with impaired HBEC reepithelialisation and an attenuation of HBEC regeneration.

Characterising SIPS in mono-culture

The successful and repeatable induction of SIPS was only achieved by providing each NHLF cell line with a tailored regimen of H_2O_2 treatments. The idiosyncratic response of differing cell lines was unanticipated and has not been discussed in previous literature. Why such differences existed was not specifically investigated in this study but numerous reasons may be relevant. H_2O_2 is a ROS that acts as a genotoxic agent, causing

DNA damage. Cells have several intrinsic mechanisms capable of responding to both ROS and DNA damage. These may be differentially regulated in the NHLF cell lines used. For example, the enzyme catalase is capable of decomposing H_2O_2 to form O_2 and H_2O. This may be differentially expressed, allowing some lines to tolerate much greater treatments with exogenous H_2O_2 than others. Secondly, DSBs created by genotoxic agents are repaired via homologous recombination and non-homologous end joining. A complex repertoire of nuclear machinery is required to facilitate these processes, all of which may also be differentially expressed. This could allow some lines to better repair DNA damage during treatment intervals and better respond to subsequent damage. γH2Ax is a marker of DNA damage and could be used in future to assess the severity of damage in differing cell lines, indicating how well they tolerate peroxide treatment. This could be achieved by both IMF imaging and flow cytometry.

The results from this section have demonstrated that SIPS induction is robust, with cells undergoing classical morphological alterations, acquiring SA-βgal activity and undergoing proliferative arrest. p21 was upregulated at both the RNA and protein level and this protein has been implicated as a key mediator of DNA damage induced senescence [197]. It was interesting that *CDKN2A* was not upregulated in SIPS whereas it was in FHLFs. Although its expression was only assessed by RT-qPCR, this would begin to suggest a different pathway for phenotype induction, an area for future experimentation.

Expression of classical SASP factors were upregulated in mono-cultured SIPS, further confirming the induction of senescence. These included IL-6, CXCL8, CXCL1, GM-CSF and VEGF, which have been previously identified in SASP [213]. It was interesting however that the levels of VEGF and GM-CSF were found at lower concentrations with a low burden of senescence in mono-culture. Though the reason for this is unclear, it further highlights that senescence is likely to play differing physiological roles dependent on the number of senescent cells present in the local environment, something that may be important for the role of senescence in IPF. Another point of interest was that the concentrations of certain proteins cold be so dramatically elevated in SIPS compared to NHLFs. Due to

the 72 hr culture period, and due to cell cycle arrest being concurrent with senescence, the number of NHLFs and SIPS is likely to be very different, with more cells available to produce the proteins analysed in NHLF cultures. Protein concentration was not corrected to cell number but it is therefore intriguing that with fewer cells, SIPS can produce significantly greater protein concentrations in the CM, further highlighting that senescence is not a state of dormancy but one of intensive activity.

The results from investigating SIPS mitochondria were in some instances consistent and in some instances inconsistent with the current literature. Peroxide induced senescence causes mitochondrial network fragmentation in immortalised mouse auditory cells, as assessed by skeletonised mitochondrial analysis [307], an observation also found in this study. However, shRNA knockdown of mitochondrial fission proteins in Chang cells (HeLa derived epithelial cell line) leads to extensive mitochondrial fusion and increased connectivity, causing senescence [262]. This is in agreement with other studies in which senescence is associated with increased mitochondrial mass, number and volume fraction, taken to mean an increase in mitochondrial biogenesis [201]. This investigation did find an increase in mitochondrial number but this was due to increased fragmentation and a greater dispersal throughout the enlarged cell cytoplasm. The network area was no different in SIPS suggesting that biogenesis has not occurred and increased fusion was not apparent. Adding further inconsistency were the results from assessing mitochondrial membrane potential, which revealed an increase in polarity when compared to NHLFs. Senescent cells exhibit a depolarised mitochondrial membrane when analysed via JC-1 IMF [200,307]. However, though further experimentation is required, it is clear that there are significant differences in mitochondrial morphology after SIPS induction.

The effect of SIPS in co-culture

SIPS in co-culture displayed upregulation of a range of inflammatory, SASP related proteins that, as hypothesised, occurred concomitantly with both an impairment of HBEC re-epithelialisation and an attenuation of regeneration. The experiments performed to uncover this effect have thus far been unreported in the literature.

That SIPS were of no benefit to the epithelium in co-culture is reflective of the persistent nature of these cells in the assays used. An acute, short acting induction of senescence is beneficial to development, wound repair and regeneration. This benefit however is dependent on immune-mediated clearance and no such clearance was facilitated in these experiments. This, coupled with the typically high burden of SA-βgal positive cells in culture is the likely reason for the concomitant reduction in epithelial function. Regarding wound healing, the parallels between SASP proteins and wound-associated inflammatory proteins is intriguing. Indeed, initially the panel of proteins investigated in this study were viewed under the guise of wound repair. The argument could be put forward that SIPS, and senescent cells *in vivo* occurring as a result of injury, re-enforce micro-environmental wound signalling, promoting repair. it would be interesting to see if having a lower burden of senescent cells in co-culture promotes re-epithelialisation and whether transient epithelia exposure to SIPS CM promotes R_{TE} development.

In an attempt to understand why SIPS impair these aspects of HBEC function, proliferation and RNA expression were assessed. Regarding proliferation, it was interesting that SIPS co-culture led to a decrease in growth. Previous literature would suggest that the interaction of senescent cells with their local environment is protumourigenic, causing epithelial cells to undergo full malignant transformation: proliferating excessively and becoming more invasive, in association with dedifferentiation [231,303]. This would also agree with the previously described, inverse relationship between proliferation and R_{TE}. That it did not was interesting. The reduction of growth may again be related to resource competition, in which SIPS out-compete the HBECs. Although senescent cells remain metabolic active, this activity would disagree with prior literature highlighting mitochondrial dysfunction in senescence. Any other reason for decreased proliferation could be related to the non-cell autonomous effects of SASP, whereby its components are able to induce senescence in neighbouring cells [191]. This would reduce HBEC growth by causing them to senesce. Assessing this via SAβgal staining after co-culture is difficult though, as it is hard to distinguish individual cells in the densely packed, pseudostratified epithelial layer. However, p21 / p16

expression could be assessed, by either IMF staining and imaging via confocal microscopy or via western blotting.

Regarding RNA expression, clues from this investigation were derived to suggest that the attenuation of function was related to a change in cell phenotype. RT-qPCR revealed that SIPS co-culture led to an upregulation of HBEC *VIM* and *KRT5*. *VIM* upregulation indicates that the cells are adopting a more mesenchymal phenotype and *KRT5* upregulation suggest a more basal-like phenotype. Re-epithelialisation is facilitated my epithelial sheet migration, in which the cells migrate as a unit. Cells of a more mesenchymal phenotype would be less conducive to this form of migration, potentially impeding the process. Their more basal nature may also limit the ability to form an impermeable ionic barrier. To further understand phenotypic changes in co-cultured HBECs, IMF experiments could be utilised to look at the protein expression of these RNA transcripts. Similarly, other epithelial markers could be analysed. Because ZO-1 expression was previously found not to be associated with changes in R_{TE} it was not assessed in HBECs after SIPS co-culture. To make sure that it is not playing a role in this scenario it could again be analysed via western blot.

Overall the results from these experiments highlight the detrimental role of senescent fibroblasts on the local epithelium. This is important in the context of IPF, in which recurrent injury requires the epithelium to be able to adequately respond. An epithelial niche dominated by senescent HLFs that contribute to a highly pro-inflammatory microenvironment would be detrimental to repair and regeneration, thereby accentuating the pathogenesis of the disease.

Comparing SIPS and FHLFs

An important aspect of this section was to understand how the phenotype of SIPS relates to that of FHLFs. This was achieved by comparing data from previous experiments. It was interesting that, by treating NHLFs with hydrogen peroxide, many of the characteristics of FHLFs could be recapitulated. SIPS and FHLFs shared a similar mitochondrial morphology, had lower cell counts, impaired HBEC re-epithelialisation and regeneration,

and also expressed elevated levels of several pro-inflammatory proteins. These results substantiate the hypothesis that the characteristics of senescence are an important driving force in the pathology of IPF.

The mitochondrial morphology of SIPS and FHLFs were similar across several parameters. In terms of SIPS, these results point towards a stress-induced, senescenceassociated mitochondrial morphology. If this morphology is a result of senescence induction, occurring after the establishment of senescence pathways, or if these changes actually drive the process of induction remains unclear. Oxidative stress causes greater, more persistent DNA damage in mitochondria and therefore it is possible that the mitochondria represent a weak spot in the capacity of HLFs to respond to H_2O_2 mediated stress [308]. Subsequently, loss of mtDNA integrity may lead to the increased production of ROS, accentuating DNA damage in the nucleus, aligning with the current paradigm that mitochondria are the key drivers of senescence [201]. Though based more on speculation than evidence, it would be tempting to hypothesise that the apparent mitochondrial fragmentation observed in these cells is part of a cellular response aimed at mitigating the impact of mtDNA damage, quarantining mitochondria with damaged DNA (which can result in deleterious mutations) and allowing mechanisms such as mitophagy to alleviate the burden of defective organelles. What is more important however, is that the equivalent morphology in FHLFs would suggest that these cells have also been previously exposed to similar insults. It suggests that in the lung, oxidative stress is also in abundance, capable of causing the same changes as found in SIPS.

That both FHLFs and SIPS display comparative cell cycle arrest is also indicative of the activation of similar, senescence-associated pathways in both. Unfortunately, as previously discussed, the data regarding FHLF proliferation is limited. However, it is still of interest that FHLFs, a cell type isolated from patients with a disease characterised by excess fibroproliferation, are non-proliferative, even in the presence of numerous growth factors, suggesting that this is also their behaviour in the IPF lung.

SIPS also recapitulate the effect of FHLFs in co-culture, impairing re-epithelialisation and attenuating regeneration. This again suggests that FHLFs have a senescence-like phenotype, one that is a detriment to the overlying epithelium in the IPF lung. Likewise, though at an RNA level the pattern is less clear, the proteins secreted by both cell types share many similarities, indicative of a common phenotype, characterised by an increased production of pro-inflammatory proteins that alter the local microenvironment. IL-6 and CXCL8 are the best examples of this shared phenotype, being significantly elevated in both co-cultures. These factors are elevated in IPF and in SASP and this direct comparison of results provides novel evidence for a role of SASP in IPF.

Gaining a better understanding of the phenotype of FHLFs within the context of senescence would be useful in further substantiating this hypothesis. RT-qPCR results would suggest that the phenotype, contrary to SIPS, is mediated by the p16-pRB pathway. However, it would be appropriate to establish this further by investigating protein expression and considering the roles of other senescence-regulating pathways. For example, western blotting and IMF imaging of p16, p53 and p38 would be suitable as all contribute to regulating the DNA damage response. Furthermore, as ROS is a key, upstream initiator of the p16-pRB pathway, it would be interesting to investigate ROS production these cells. Linking with hypotheses concerning the mitochondria, this could be achieved with dyes such as MitoSox, which highlight mitochondrial ROS. Interestingly, the redox imbalance and subsequent H_2O_2 production previously described in FHLFs could be a cause of the phenotype observed in this study [119].

In conclusion, it is evident that FHLFs and SIPS share similarities of phenotype, both of which are ultimately detrimental to the overlying epithelium in co-culture. This is indicative of an exposure of FHLFs to sub-lethal, yet recurrent, oxidative stress in the lung, which leads to the acquisition of a pro-inflammatory phenotype. Though much more could be done to understand these similarities and the mechanisms driving them, it is also worth attempting to understand if this phenotype can be modulated, with an

aim to attenuating the epithelial impairments caused by these cells. The next section of this study will investigate such questions.

3.5 Targeting the Senescence Associated Secretory Phenotype in Fibrotic and Senescent Human Lung Fibroblasts

3.5.1. Introduction

Co-culture with SIPS and FHLFs impairs post-wound re-epithelialisation and attenuates epithelial regeneration *in vitro*. In this model, this is due to an altered microenvironment generated by the secretory factors of these cells. Significantly elevated proteins, detected in both co-culture types, included IL-6, CXCL8, CXCL1, and G-CSF, all of which are strongly implicated in SASP and inflammation. These collective results led to the question, "can the secretome of SIPS and FHLFs be either suppressed or altered to better promote epithelial function?".

Pathways regulating inflammation

NF-□B is an important regulator of senescence induction and SASP production [214,309,310]. It is the archetypal, transcriptional regulator of inflammation and is implicated in both the ageing process and in tumourigenesis [174,311]. The pathways mediating NF-□B signalling are interconnected with those of STAT signalling, most notably STAT-3 [312]. NF□B-initiated IL-6 production is maintained by activated STAT-3 and, in cancer, direct interaction between the two prolongs NF-□B nuclear retention, increasing inflammation [313,314]. Direct STAT-3 signalling also leads to upregulation of proteins such as IL-6, CXCL8, CCL2, PAI-1, IL-1β and VEGF [236,312,315].

Role of the IL-6 / JAKs1-2 / STAT-3 signalling pathway

STAT-3 lies downstream of a signalling pathway involving IL-6 and JAKs 1 and 2. Activation of this pathway is initiated with IL-6 binding to its receptor IL-6R. IL-6R is a dimerised complex of two IL-6Rα subunits, which are either expressed on the cell surface or, more typically, found in a soluble form (sIL-6Rα). The receptor-ligand complex binds to, and dimerises, cell-surface bound gp130 molecules, which are associated with JAKs. Dimerisation of gp130s activates these JAKs, which in turn phosphorylate the cytosolic domains of gp130, allowing recruitment and activation of STAT-3. STAT-3 subsequently

becomes phosphorylated, forming a homodimer (or heterodimer with STAT1) and translocating to the nucleus where it can bind to enhancer sequences in numerous target genes [316].

JAK/STAT signalling in disease and age

Underpinned by increased inflammation, the result of JAK/STAT signalling can be diverse. It plays a role in tumourigenesis, it reinforces the senescence phenotype and it contributes to ageing [218,236,317–319]. It is also prominent in fibrosis in general. Via IL-6 signalling, STAT-3 activation mediates an indirect enhancement of TGF-β signalling that promotes collagen production. Subsequently, blocking JAK 1/2 signalling with the molecular inhibitor, Ruxolitinib, reduces dermal fibroblast *COL1A1* expression [320].

JAK/STAT signalling has also been investigated in the context of pulmonary fibrosis. Treatment of primary AEC2s *in vitro* with an inhibitor of STAT-3 phosphorylation, C-1889 [321], decreases TGF-β and IL-6/sIL-6Rα induced expression of injury and EMT associated markers, including *Pai1, Hif1a, Twist* and *Snail*. Likewise, nuclear-located phosphorylated STAT3 (pSTAT-3) is highly enriched in IPF derived fibroblasts, alveolar macrophages and epithelium [322]. In BLM-induced mouse fibrosis, soluble IL-6Rα is elevated and neutralising this signalling with a gp130 recombinant Fc fragment reduces pulmonary inflammation and attenuates pathology [323]. Similarly, genetically reducing systemic STAT-3 expression, prior to BLM instillation, decreases the susceptibility of mice to fibrosis [324]. Blocking the phosphorylation of STAT-3 with C-188-9, from days 1530 post-BLM, also attenuates fibrotic development [322]. In human patients, there are also increases in soluble IL-6Rα in tissue protein lysates, and pSTAT-3 is excessively abundant in the IPF lung, located primarily in non-epithelial parenchymal cells [323,324].

The drug Ruxolitinib (INCB18424) has also been used in the suppression of SASP production. Preadipocytes, induced to senescence by irradiation *in vitro*, produce elevated levels of secreted IL-6, CXCL8, CXCL1, CCL2, CXCL10, VEGF, GM-CSF, G-CSF and CCL5. At an RNA level, *IL1A* and *IL1B* are also elevated. With the exception of VEGF, JAK

1/2 inhibition (with an unnamed, alternative inhibitor) significantly decreases production of these proteins. Ruxolitinib, after a 72 hr treatment at a concentration of 1.0 μm, also reduces RNA levels of *IL6, CXCL8, CCL2* and *PAI1*. The result of this inhibition *in vivo* is a reduction in age-associated systemic inflammation. It also enhances physical activity in aged mice, suggesting that SASP is a key driver of the ageing phenotype, mediated by JAK/STAT signalling [236].

The implications of over-active signalling in both IPF and ageing, coupled with the increase in inflammatory proteins in FHLF and SIPS co-cultures, make inhibition of this pathway an attractive answer to the question of secretome suppression. Ruxolitinib was identified as a potential compound to achieve this.

Ruxolitinib

Ruxolitinib is a small, molecular compound that functions as an ATP mimetic, selectively inhibiting JAK 1 and 2. This leads to a decrease in STAT-3 phosphorylation and inhibition of IL-6 signalling. As well as inhibition at the RNA level, it also reduces circulating levels of IL-6 and TNF-α, evidenced in a mouse model of myelofibrosis, and it is currently used to treat patients with this disease [325]. Myelofibrosis is a myeloproliferative neoplasm, in which there are abnormal blood cell counts and systemic inflammation, resulting from scarring of haemopoietic centres in the bone marrow. Ruxolitinib has improved survival rates across several clinical trials [326,327]. Only modest histological improvements in bone marrow fibrosis were identified in these trials, but a case report of a patient treated for three years with the drug found that treatment lead to fibrosis resolution [328].

Taken together, this evidence suggested Ruxolitinib may be an appropriate treatment for suppressing the production of inflammatory proteins evident in FHLF and SIPS coculture.

Hypotheses

1. Ruxolitinib will reduce production of inflammatory cytokines in FHLFs and SIPS, improving epithelial regeneration and re-epithelialisation.

3.5.2. Results

3.5.2.1. Treatment with Ruxolitinib is non-toxic to HBECs or HLFs.

Prior to investigating the effects of Ruxolitinib treatment in co-culture, the effect of the drug on mono-cultured HLFs was assessed. First the toxicity of the drug was evaluated across all cell types used, with cells initially seeded in 96-well plates at a density of 2,000 cells/well. For HBECs, it was important to understand the effects of the drug on proliferation, since HBEC cell number is related to R_{TE} in co-culture. HBECs were treated with Ruxolitinib at 0.0, 0.1, 0.5 and 1.0 μM, diluted in media containing 0.1% DMSO, 72 hrs prior to proliferative assessment via Alamar Blue staining. No effect on HBEC cell number was observed following treatment **(*Figure* 3.5.1A.)**. Extending this to HLF cultures revealed that the drug also had no detrimental effects on either NHLFs, FHLFs or SIPS, with no significant differences in cell number between any treatment concentrations **(*Figure* 3.5.1.)**. Also, in accordance with prior experiments, the cell numbers of both FHLF and SIPS were significantly lower than those of NHLFs after 72 hrs. Taken together, it is unlikely that any effect of the drug in co-culture is related to increased cell toxicity or increased proliferation.

3.5.2.2. Ruxolitinib does not alter SA-βgal activity in SIPS but does reduces STAT-3 phosphorylation.

Whether Ruxolitinib reverses the senescence phenotype has thus far been unreported. Conceivably, the reduction in cytokine and chemokine production could act as a brake on paracrine mediated senescence, preventing non-senescent cells from adopting this phenotype. However, in cells that are chronically senescent, Ruxolitinib is unlikely to interfere with already established senescence pathways and the state of senescence is understood to be irreversible. To test this, SIPS were treated for 72 hrs with Ruxolitinib prior to fixing and SA-βgal staining. Representative images highlight staining across NHLFs and three SIPS cell lines **(*Figure* 3.5.2.)**. The staining suggests that the drug has no effect on SA-βgal activity over this time course, with the majority of SIPS staining blue

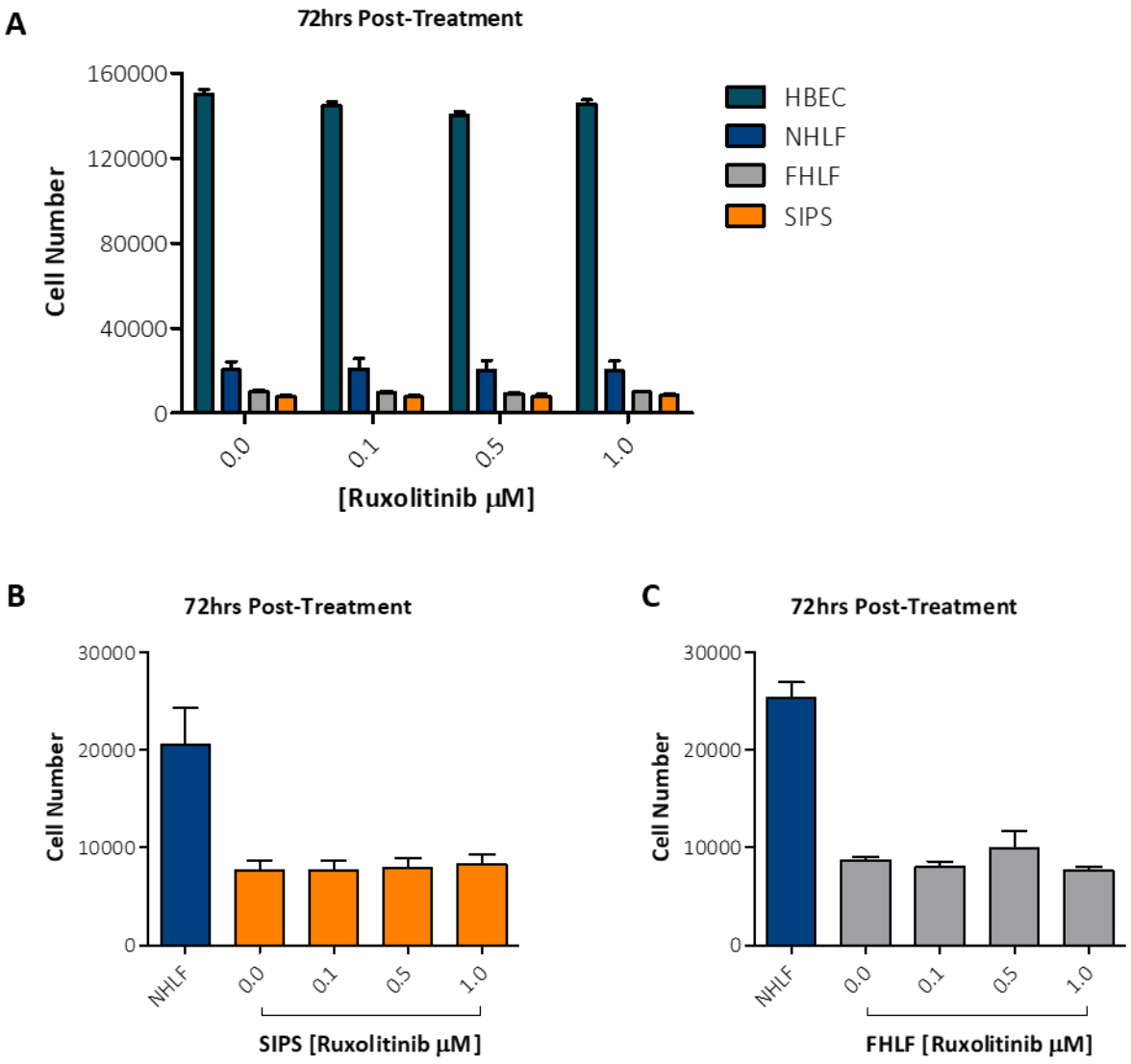

Figure 3.5.1. Effect of 72 hr Ruxolitinib treatment on HBEC and HLF cell number in mono-culture. **(A)** Cells were seeded in 96-well plates at -24 hrs and allowed to adhere. At 0 hr, media were changed for DMEM / αMEM 10% with a range of Ruxolitinib concentrations. For final concentrations, the drug was diluted 1:100 from a working stock of media containing 10% DMSO. Cells were treated for 72 hrs prior to addition of Alamar Blue. This was incubated for 2 hr 30 min before removal, washing and fluorescence measurement using a plate reader. A serial dilution of cells were also seeded, and fluorescence intensity and cell number was used to calculate a standard curve for each cell type. Fluorescence intensity was used to calculate cell number. **(A)** shows results for all cell types. **(B)** Effect of Ruxolitinib on SIPS cell number, which again had no significant effect. NHLF n = 3 (3x donors: TB0917, TB0918, TB0932), SIPS n = 7 (3x donors: TB0917 [2], TB0918 [3], TB0932 [2]). 1-way ANOVA, Tukey's multiple comparison. **(C)** Effect of Ruxolitinib on FHLF cell number. The drug had no significant effect on FHLF proliferation. NHLF n = 4 (3x donors: TB0917 [2], TB0918, TB0932), FHLF n = 3 (3x donors: BR001, BR002, BR003). 1-way ANOVA, Tukey's multiple comparison.

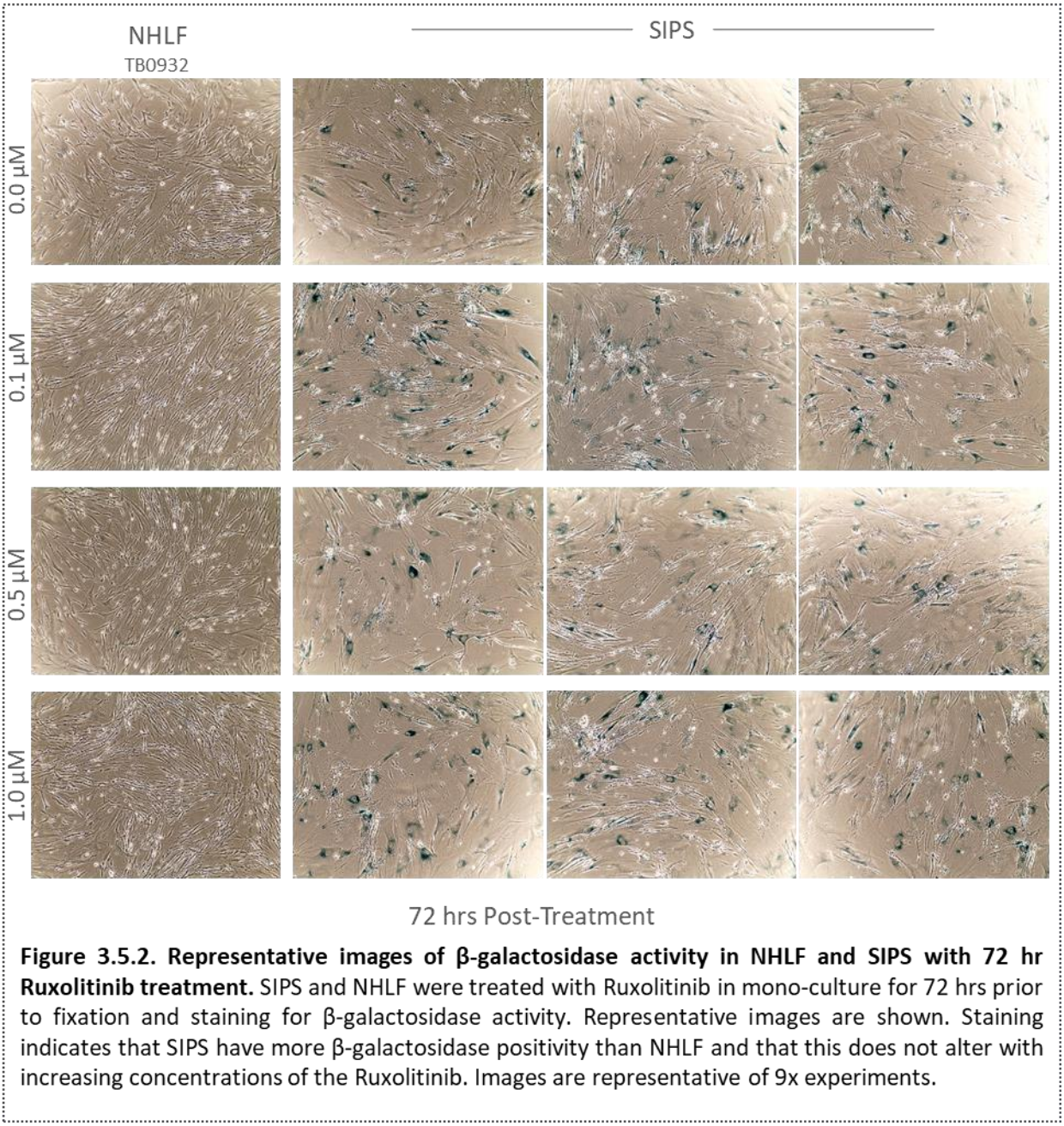

Figure 3.5.2. Representative images of β-galactosidase activity in NHLF and SIPS with 72 hr Ruxolitinib treatment. SIPS and NHLF were treated with Ruxolitinib in mono-culture for 72 hrs prior to fixation and staining for β-galactosidase activity. Representative images are shown. Staining indicates that SIPS have more β-galactosidase positivity than NHLF and that this does not alter with increasing concentrations of the Ruxolitinib. Images are representative of 9x experiments.

across all four drug concentrations. Therefore, treatment is unlikely to be mediating effects by reducing the burden of senescence.

To test whether Ruxolitinib was inhibiting JAK 1/2 activity and thereby preventing STAT3 phosphorylation, western blotting was performed on NHLF and SIPS lysates. Cells were seeded at a density of 60,000 cells/well in 6-well plates and treated for 72 hrs prior to protein isolation. The resulting blot was probed for total STAT-3 (tSTAT-3), pSTAT-3, p21 and β-actin (as a loading control) **(*Figure* 3.5.3.)**. Ostensibly, all cells expressed similar levels of tSTAT-3. SIPS however displayed much stronger expression of p21 and

untreated SIPS also displayed increased expression of pSTAT-3. Treatment with 1.0 µM Ruxolitinib abrogated STAT-3 phosphorylation in all three SIPS lines, whilst having no effect on the levels of p21. Therefore, it is evident that Ruxolitinib reduces STAT-3 phosphorylation in SIPS, and a 1.0 µM concentration was sufficient to achieve complete inhibition.

3.5.2.3. Treatment with Ruxolitinib promotes post-wound re-epithelialisation and epithelial regeneration in both FHLF and SIPS co-cultures.

The effect that Ruxolitinib had when used to treat co-cultures was next examined. NHLF, FHLF and SIPS co-cultures, as well as HBEC mono-cultures, were established in which cells were treated with Ruxolitinib at 0 hrs, concurrent with the change of media. Drug was only added to the basolateral compartment of co-cultures and all culture types were treated with a range of drug concentrations. Re-epithelialisation was first assessed (using the methods previously described). A treatment of 0.0 µM and 1.0 µM of drug was used in mono-cultured HBECs **(*Figure* 3.5.4A.)** and HBECs co-cultured with NHLFs **(*Figure* 3.5.4B.)**. Treatment lead to a significant improvement in mono-cultured reepithelialisation, increasing wound closure by roughly 10%. Interestingly, treatment had no additional benefit in NHLF-HBEC co-cultures, with both conditions displaying a higher percentage closure when compared to mono-culture. Therefore, despite the lack of proliferation noted in **Results 5.2.1.**, Ruxolitinib can directly alter HBEC function to promote re-epithelialisation in mono-culture following wounding. The effect of drug

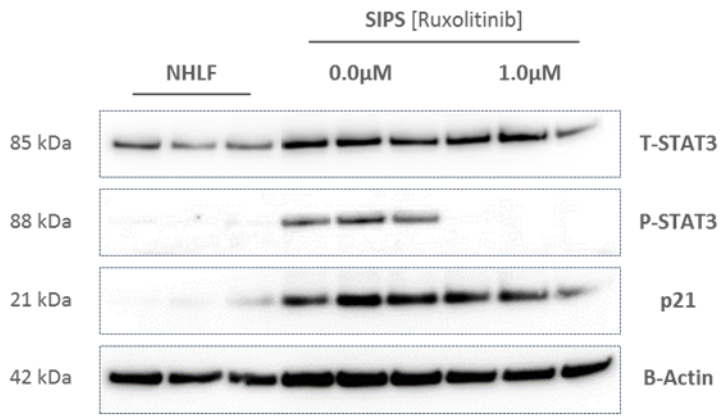

Figure 3.5.3. STAT-3 western blot analysis in Ruxolitinib treated SIPS. Cells were seeded in mono-culture. NHLFs were allowed to adhere overnight, the media was changed and cells treated for 1 hr with 0.0 µM Ruxolitinib. Protein was then collected with PhosphoSafe extraction reagent. SIPS were cultured for 72 hrs prior to media change and a 1hr treatment with Ruxolitinib. Protein was collected with PhosphoSafe buffer. HRP conjugated secondary antibodies were used for chemiluminescent imaging. 1x blot was performed. NHLF 0.0 µM n = 3 (3x donors: TB0917, TB0918, TB0932), SIPS 0.0 µM n = 3 (3x donors: TB0917, TB0918, TB0932), SIPS 1.0 µM n = 3 (3x donors: TB0917, TB0918, TB0932). The same 3x donors were used for each condition.

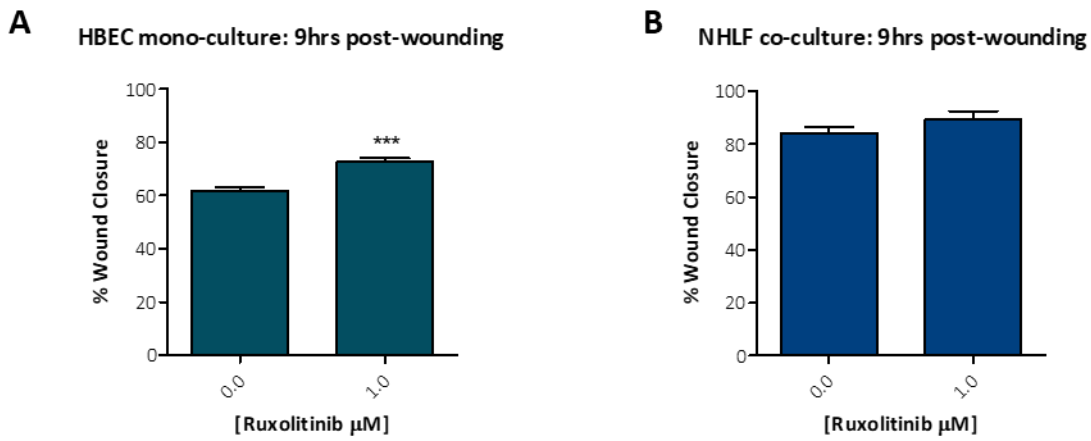

Figure 3.5.4. Effect of 72 hr Ruxolitinib treatment on HEBC wound closure, in mono- and NHLF co-culture. Cells were seeded at -24 hrs and at 0 hrs media were changed to DMEM / αMEM 10% FBS with a range of Ruxolitinib concentrations. 72 hrs post-treatment HBEC were mechanically wounded and cultured for a further 9 hrs with phase-contrast images taken at 0 and 9 hrs. Images were used to calculate the percentage of wound closure. **(A)** 1.0 µM of Ruxolitinib significantly improves wound closure in mono-cultured HBECs. HBEC (0.0 and 1.0 µm) n = 7. *** $p < 0.001$. Two-way, unpaired t-test. **(B)** 1.0 µM of Ruxolitinib has no effect on wound closure in HBECs co-cultured with NHLFs. NHLF (0.0 and 1.0 µm) n = 12 (3x donors: TB0917 [3], TB0918 [3], TB0932 [3]). Two-way, unpaired t-test.

treatment was subsequently assessed in SIPS co-cultures, using 0.0 µM treated HBEC mono-cultures and NHLF co-cultures as controls. Representative phase-contrast images,

and corresponding 9 hr binary images, are shown ***Figure* 3.5.5A**. The results, 9 hrs postwounding are shown in ***Figure* 3.5.5B**. Wound closure in both 0.0 µM and 0.1 µM treated SIPS co-cultures was significantly less than in NHLF co-cultures, as previously observed in ***Figure* 3.2.19**. Treatment with 0.5 µM and 1.0 µM of drug increased percentage wound closure to the extent that there were no significant differences when compared to NHLF controls. 1.0 µM Ruxolitinib also significantly improved wound closure when compared to 0.0 µM SIPS co-culture. Therefore, Ruxolitinib is able to promote reepithelialisation, attenuating the impairment of closure found in SIPS co-culture.

This experiment was repeated using FHLFs, with phase contrast images and 9 hr postwounding results shown in ***Figure* 3.5.6**. As with SIPS, wound closure was significantly less in 0.0 µM and 0.1 µM treated FHLF co-cultures but improved with 0.5 µM and 1.0 µM treatments. The improvement in closure was non-significant between 0.0 µM and 1.0 µM treatment but was significantly elevated between 0.1 µM and 1.0 µM treated cultures. Therefore, Ruxolitinib is able to promote re-epithelialisation in both SIPS and FHLFs co-cultures, an effect that, could in part, be mediated through the drug influencing the epithelium.

Epithelial regeneration was next investigated, assessed via R_{TE} measurement over 72 hrs with a full range of Ruxolitinib concentrations. At 72 hrs, treatment had no effect on mono-cultured HBEC R_{TE} **(*Figure* 3.5.7A.)** but, with an increase in drug concentration, there were significant increases in R_{TE} in NHLF-HBEC co-cultures **(*Figure* 3.5.7B.)**, suggesting that Ruxolitinib does not directly influence the epithelium but does elicit changes in the basolateral NHLFs. The effect of treatment on SIPS and FHLF co-cultures was assessed, in comparison to 0.0 µM treated HBEC mono-cultures and NHLF cocultures. At 72 hrs, the R_{TE} of 0.0 µM treated SIPS co-cultures was significantly less than that of NHLF co-cultures, consistent with previous experiments **(*Figure* 3.5.7C.)**. Treatment with 0.1 µM and 0.5 µM increased SIPS R_{TE} making these differences nonsignificant. Treatment with 1.0 µM resulted in a significant increase in R_{TE}, greater than

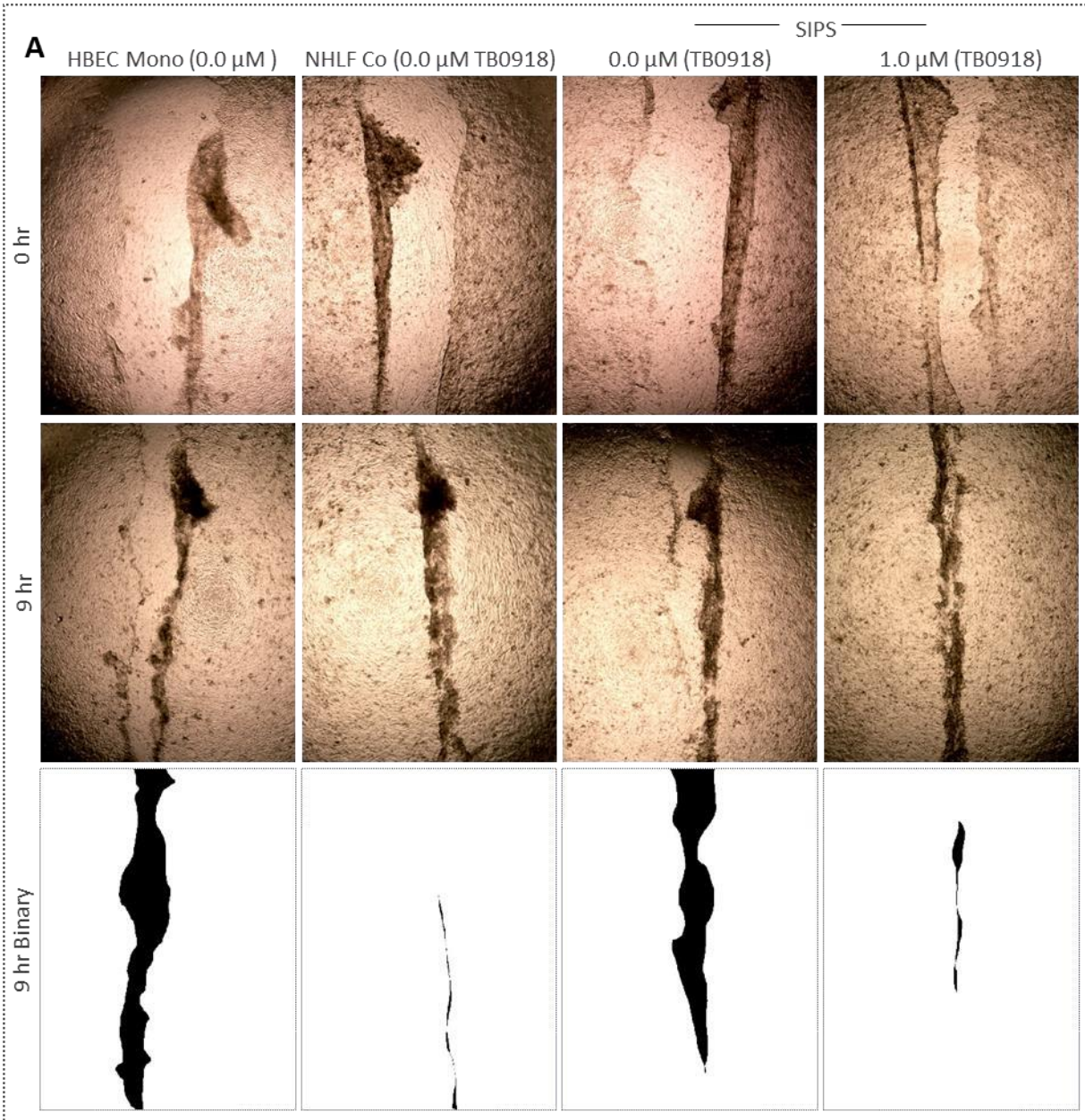

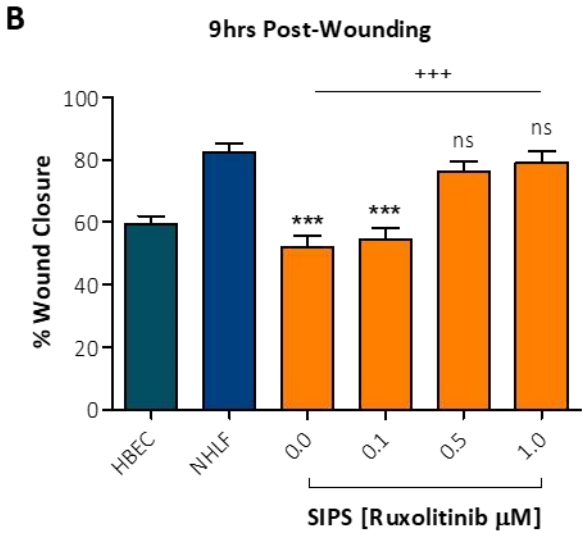

Figure 3.5.5. Effect of Ruxolitinib treatment on SIPS co-culture wound closure. (A) Images were taken at 0 and 9 hrs with quantification of wound closure achieved by converting images to binary using ImageJ. Representative images from all experiments of wounds under phase-contrast at 0 and 9 hrs with the corresponding 9hr binary image are shown. **(B)** Percentage closure at 9 hrs post-wounding, comparing SIPS co-culture to HBEC mono-culture and NHLF co-culture. HBEC n = 4, NHLF n = 4 (3x donors: TB0917, TB0918, TB0932 [2]), SIPS n = 6 (3x donors: TB0917 [2], TB0918 [2], TB0932 [2]). *** p<0.001 (vs NHLF), +++ p<0.001 (vs 0.0 µM SIPS). 1-way ANOVA, Tukey's multiple comparisons.

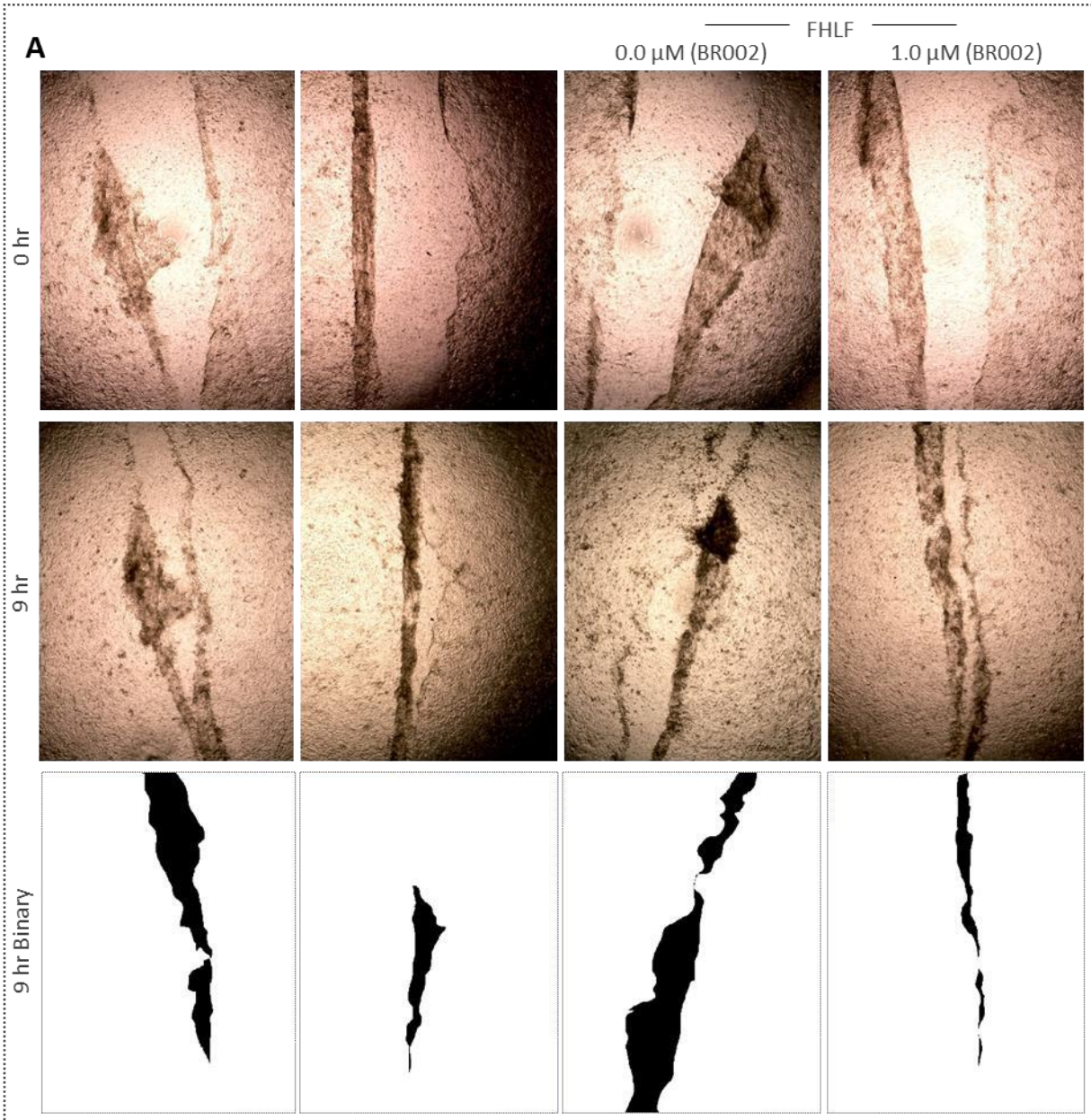

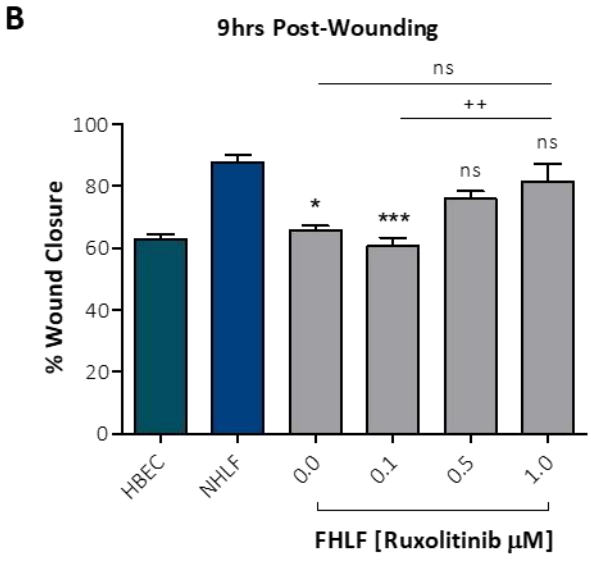

Figure 3.5.6. Effect of Ruxolitinib treatment on FHLF co-culture wound closure. (A) Images were taken at 0 and 9 hrs with quantification of wound closure achieved by converting images to binary using ImageJ. Representative images from all experiments of wounds under phase-contrast at 0 and 9 hrs with the corresponding 9 hr binary image are shown. **(B)** Percentage closure at 9 hrs post-wounding, comparing FHLF co-culture to HBEC mono-culture and NHLF co-culture. HBEC n = 7, NHLF n = 7 (3x donors: TB0917 [2], TB0918 [3], TB0932 [3]), FHLF n = 9 (3x donors: BR001 [3], BR002 [3], BR003 [3]). * $p<0.05$, *** $p<0.001$ (vs NHLF), ++ $p<0.01$ (vs 0.1 µM SIPS). 1-way ANOVA, Tukey's multiple comparisons.

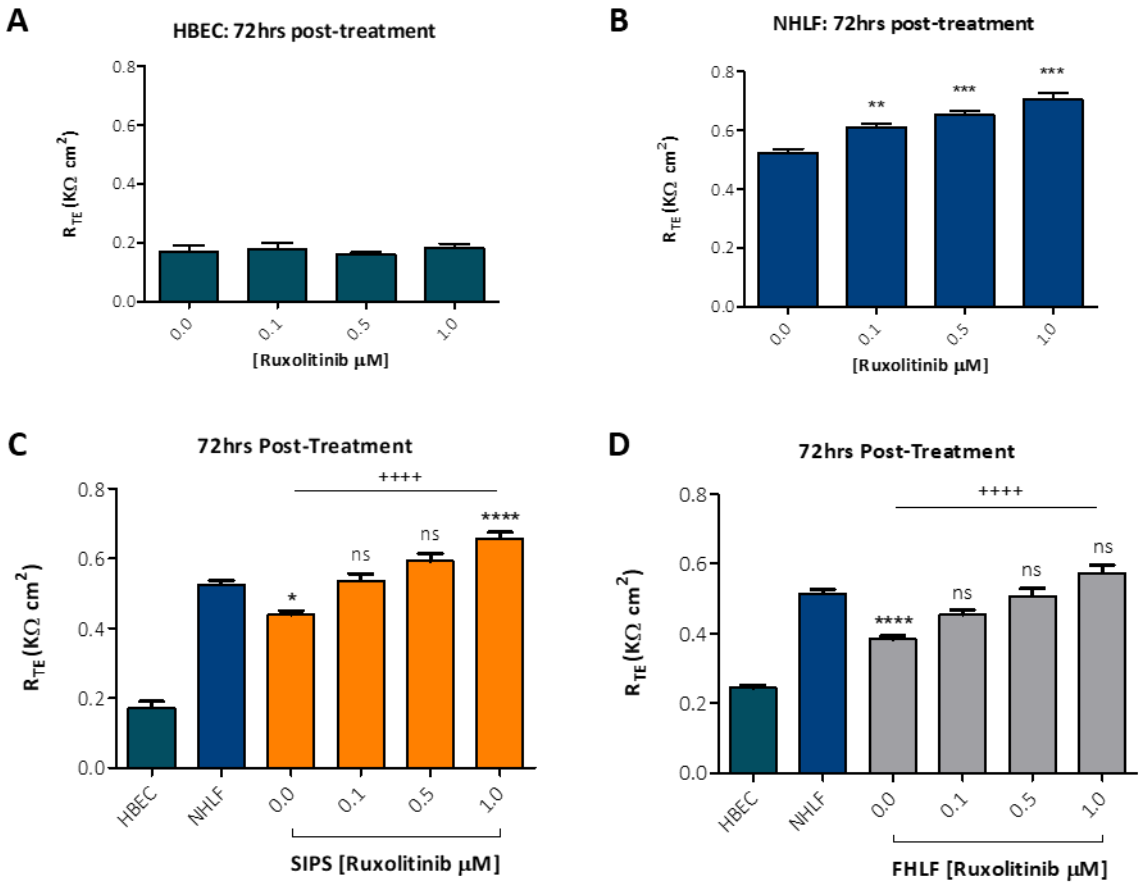

Figure 3.5.7. Effect of 72 hr Ruxolitinib treatment on HBEC R_{TE} in HLF co-culture. Cells were seeded at -24 hrs and at 0 hrs media were changed to DMEM / αMEM 10% FBS with a range of Ruxolitinib concentrations. R_{TE} was measured up to 72 hrs. **(A)** Effect of Ruxolitinib on HBEC R_{TE}. At 72 hrs treatment has no effect. HBEC n = 4. 1-way ANOVA, Tukey's multiple comparisons. **(B)** Effect of Ruxolitinib on NHLF R_{TE}. 72 hrs of treatment leads to significant increases in R_{TE}. NHLF n = 6 (3x donors: TB0917 [2], TB0918 [2], TB0932 [2]). ** $p < 0.01$, *** $p < 0.001$ (vs 0.0 µM). 1-way ANOVA, Tukey's multiple comparisons. **(C)** Comparison of SIPS R_{TE} at 72 hrs post co-culture. R_{TE} of SIPS 0.0 µM co-culture is significantly less than NHLF co-culture, SIPS 1.0 µM is significantly greater. HBEC n = 4, NHLF n = 5 (3x donors: TB0917 [2], TB0918 [2], TB0932), SIPS n = 6 (3x donors: TB0917 [2], TB0918 [2], TB0932 [2]). * $p < 0.05$, **** $p < 0.0001$ (vs NHLF), ++++ $p < 0.0001$ (vs 0.0 µM SIPS). 2-way RM ANOVA, Bonferroni multiple comparisons. **(D)** Comparison of FHLF R_{TE} at 72 hrs post co-culture. R_{TE} of FHLF 0.0µM co-culture is significantly less than NHLF co-culture. HBEC n = 4, NHLF n = 6 (3x donors: TB0917 [2], TB0918 [2], TB0932 [2]), FHLF n = 5 (3x donors: BR001, BR002 [2], BR003 [2]). **** $p<0.0001$ (vs NHLF), ++++ $p<0.0001$ (vs 0.0 µM FHLF). 2-way RM ANOVA, Bonferroni multiple comparisons.

both controls and 0.0 µM treated SIPS co-culture. Therefore, Ruxolitinib improves the regenerative potential of HBECs, attenuating the detrimental effect of co-culture with SIPS. The same was also found to be true for co-culture with FHLFs **(*Figure* 3.5.7D.)**. 0.0 µM treated FHLF R_{TE} was significantly less than NHLF co-culture but again R_{TE} was increased with drug treatment, making this attenuation non-significant. Treatment with

1.0 µM did not increase R_{TE} to a level greater than that of NHLF 0.0 µM co-culture but did significantly improve upon 0.0 µM treated FHLF co-cultures. In summary, Ruxolitinib promotes HBEC regeneration when in co-culture with SIPS and FHLFs.

3.5.2.3. Treatment with Ruxolitinib does not alter RNA levels of inflammatory factors in SIPS.

Ruxolitinib was shown to reduce STAT-3 phosphorylation in SIPS and promote HBEC reepithelialisation and regeneration. It was hypothesised that this was due to a suppression of the inflammatory mediators secreted by SIPS into the microenvironment. Therefore, RNA levels for proteins previously assessed were quantified after Ruxolitinib treatment. This was performed in both SIPS mono- and co-culture, with RNA analysed 72 hrs after treatment in each **(*Figure* 3.5.8.)**. In both set-ups treatment with Ruxolitinib had no effect on SIPS RNA levels. All transcripts were elevated in SIPS when compared to NHLFs, with the exception of *CDKN2A*, which was not upregulated. A 1.0 µM treatment in co-culture did significantly increase RNA levels of *CXCL1* but this was the only observable effect of treatment. These results, as well as being inconsistent with previous literature, strongly suggested that Ruxolitinib had no effect on transcriptional regulation in SIPS, at least at this timepoint. Though treatment had positive effects on R_{TE}, measurable at 72 hrs, it was thought that, in terms of RNA levels, by 72 hrs any transcriptional changes may have reverted to baseline. Inhibition of STAT3 phosphorylation was measured only 1 hr after treatment and therefore it was deemed that a shorter treatment period may allow transcriptional changes to be observed. Consequently, RT-qPCR was again performed, this time in mono-cultured cells treated for only an 8 hr period **(*Figure* 3.5.9.)**. As before, treatment with 1.0 µM of Ruxolitinib had no effect on SIPS RNA levels. These results strongly suggest that Ruxolitinib does not improve epithelial function by reducing gene expression of SIPS inflammatory proteins. Subsequently, the mechanism by which functional improvement is attained remains undetermined and requires further investigation. Experiments such as multiplex ELISA on the CM could offer a more definitive answer.

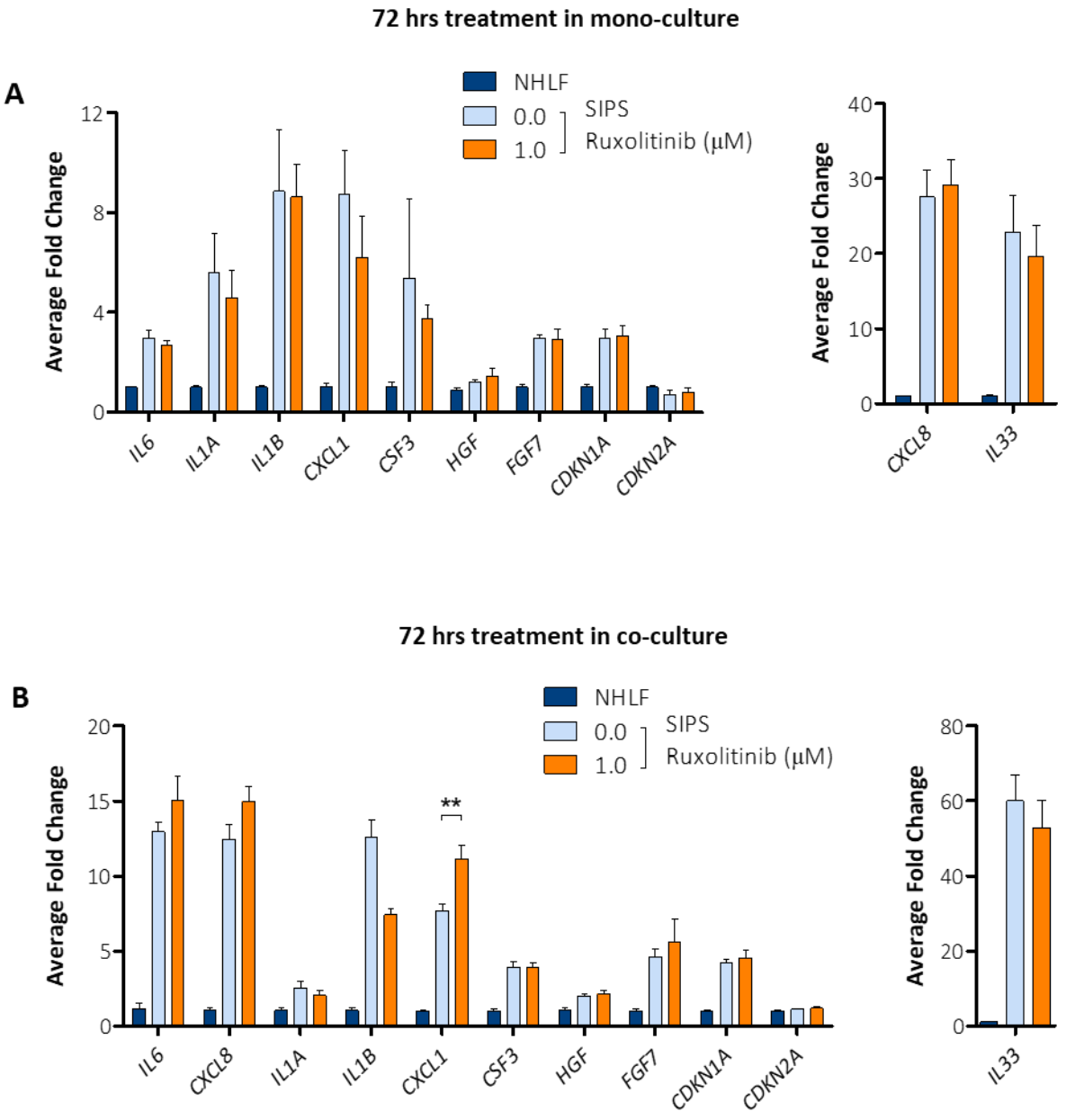

Figure 3.5.8. Effect of 72 hr Ruxolitinib treatment on RNA levels of SIPS in mono- and co-culture. RT-qPCR was performed with genes of interest normalised to the reference genes *B2M* and *GAPDH.* SIPS RNA levels were calibrated to NHLF levels and the data is shown as an average fold change. Results are shown across 2 graphs of differing y-axis scales. **(A)** RNA was isolated from cells after 72 hrs treatment with Ruxolitinib in mono-culture. The drug had no significant effect on RNA levels. NHLF n = 4 (3x donors: TB0917, TB0918, TB0932 [2]), SIPS n = 6 (3x donors: TB0917 [2], TB0918 [2], TB0932 [2]). 1-way ANOVA, Tukey's multiple comparison performed on ddCt values. **(B)** RNA was isolated from cells after 72 hrs treatment in co-culture. 1.0 µM Ruxolitinib significantly increased levels of CXCL1 and had no effect on other genes. NHLF n = 4 (3x donors: TB0917, TB0918, TB0932 [2]), SIPS n = 3 (3x donors: TB0917, TB0918, TB0932). ** $p < 0.01$ (vs 0.0 µM SIPS) 1-way ANOVA, Tukey's multiple comparison performed on ddCt values.

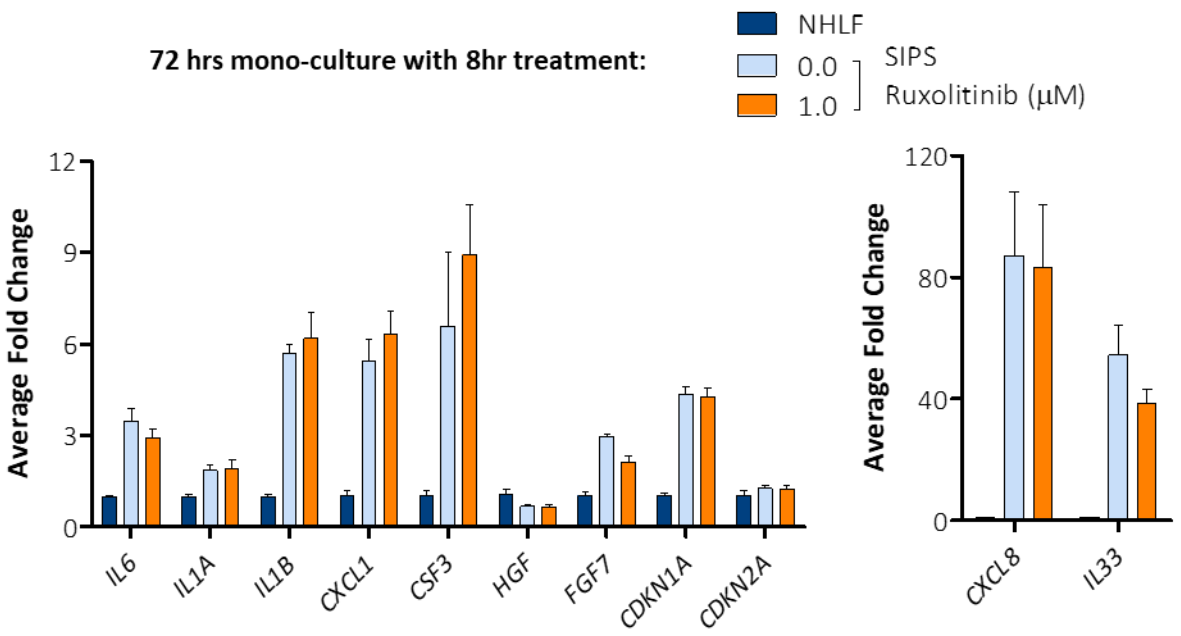

Figure 3.5.9. Effect of 8hr Ruxolitinib treatment on RNA levels of SIPS in mono-culture. NHLF and SIPS were mono-cultured for 72 hrs in DMEM / αMEM (10% FBS) prior to media change and 8hr incubation with Ruxolitinib. RNA was then extracted. RT-qPCR was performed with genes of interest normalised to the reference genes *B2M* and *GAPDH.* SIPS RNA levels were calibrated to NHLF levels and the data is shown as an average fold change. Results are shown across 2 graphs of differing y-axis scales. Ruxolitinib treatment had no effect on SIPS RNA levels. NHLF n = 4 (3x donors: TB0917 [2], TB0918, TB0932), SIPS n = 5 (3x donors: TB0917, TB0918 [2], TB0932 [2]). 1-way ANOVA, Tukey's multiple comparison, performed on ddCt values.

3.5.3. Discussion

As a result of previous experiments, this section set out to investigate whether epithelial-mesenchymal crosstalk could be modulated via pharmacological intervention, in an attempt to suppress the secretion of the numerous inflammatory proteins that were found to be elevated in co-culture with SIPS and FHLFs, under the assumption that they were detrimental to epithelial function. The results from this investigation found that by targeting the JAK/STAT signalling pathway, HBEC re-epithelialisation and regeneration could be improved. These results also provide rationale for a range of further investigations.

Firstly, though STAT-3 phosphorylation was assessed in SIPS, it would be interesting to understand if there was also an increase in phosphorylation in FHLFs. As SIPS reflect the

phenotype of FHLFs it would be hypothesised that there is an increase and that treatment with Ruxolitinib could also reduce this. Likewise, it would be interesting to better elucidate the effect of Ruxolitinib on the wider JAK/STAT signalling pathway, identifying alterations in other signalling proteins, most notably by identifying the phosphorylation status of JAKs 1 and 2 and also the intracellular localisation of STAT-3 - which should localise to the nucleus when activated [316]. It would also be appropriate to revisit these experiments using structurally different, but functionally equivalent JAK 1 and 2 inhibitors. For example, the compounds Baricitinib and Tofacitinib which also inhibit these kinases [329,330]. Finding similar results with these drugs would reduce the likelihood of the effects of Ruxolitinib being non-specific and off-target, further supporting the validity of targeting this pathway.

That re-epithelialisation in mono-cultured HBECs is improved with Ruxolitinib is a point of interest, reflecting a difficulty of co-culture in which selective treatment of one cell type is not straightforward. One way to gain a more discriminate understanding of the role of JAK/STAT signalling in co-culture would be to silence JAKs 1 and 2, or STAT-3, via the use of siRNA knockdown – or similar approaches. This would evade the issue of Ruxolitinib directly effecting the epithelium. If this method of signalling inhibition was also found to promote re-epithelialisation it would more conclusively demonstrate its importance, further validating the use of this treatment.

Regarding R_{TE} and HBEC regeneration, results found that drug treatment did not effect HBEC mono-cultures. It was interesting however that it did have an effect on NHLF cocultures. From previous experiments with mono- and co-cultures it is evident that NHLFs produce significantly more inflammatory factors when co-cultured **(*Figure* 3.2.4.)**, the same factors that are produced at even greater levels in SIPS and FHLFs. This upregulation is understood to be due to a post-wounding, regenerative process occurring in co-culture, in which the epithelial cells repopulate a denuded basement membrane. That regeneration is also improved in both SIPS and FHLF co-cultures suggests that treatment may be useful in targeting crosstalk in IPF and attenuating the pathological impact of recurrent lung injury. It would be interesting to test the effects of

treatment in more complex systems, such as *in vivo* models of lung injury. The most obvious of these would include the mouse model of BLM-induced fibrosis, in which BLM causes widespread AEC1 death, however other approaches could include mechanical de-epithelialisation *in vivo*, using an intra-tracheal probe to mechanical remove upper airway epithelium [76].

When attempting to understand why treatment with Ruxolitinib promotes reepithelialisation and regeneration, analysis of RNA expression offered limited assistance. It was expected that treatment would decrease expression of IL6 and CXCL8, as observed by Xu *et al.* [236]. That it did not could be interpreted as there being a temporal disconnect between intracellular RNA levels and protein production, or it could be due to other, compensatory pathways, upregulating this inflammatory signalling. This could be identified by a repeat of the multiplex ELISA assays on Ruxolitinib-treated CM. The results could also reflect the more salient importance of other secretory proteins in mediating HBEC function, again suggesting the potential for investigating changes in global gene expression. Predominantly immune-modulating proteins were assessed in this study but a whole range of other proteins may be relevant to the effects seen in coculture, the expression of which may also be modulated by Ruxolitinib. Because of this, it can only be stated that the elevation of inflammatory proteins, observed with SIPS and FHLFs, correlates to the functional alterations found in HBECs, with their elevation in the micro-environment not a causal reason for impairment. To establish a causal relationship, it would be worth attempting to more directly target some of the key secretory proteins elevated. The use of neutralising antibodies, targeted to proteins such as IL-6 and CXCL8, could be used. It would be hypothesised however that their effect would not be as significant as treatment with Ruxolitinib. Part of the rationale for targeting an upstream signalling pathway is that IPF is a complex disease. An imbalance in expression of a single secretory protein is unlikely to be the cause and it therefore makes sense to pharmacologically suppress a range of proteins. Indeed, the success of Nintedanib and Pirfenidone has been attributed to their pleiotropic effects. However, the use of neutralising antibodies would be useful *in vitro* to validate targeting this pathway.

One other consideration to make, regarding targeting this pathway, is that although evidenced to play an important role in SASP and IPF, JAK/STAT signalling is also an important mediator of BC airway regeneration, with pathway activation critical for the regeneration of differentiated ciliated cells [88]. This differentiation occurs after epithelial barrier establishment in BC cultures exposed apically to the air, a phase of regeneration not investigated in this study. It highlights however the complexity of cytokine signalling in the lungs response to injury and suggests that an over-reduction of this signalling would be detrimental to regeneration if sustained into the period of differentiation.

In summary, this section represents an attempt at modulating HLF secretion, providing some rationale for investigating the use of SASP suppressing drugs in further *in vitro* experiments, with the hope of continuation in *in vivo* models of IPF. That the current therapeutic options for IPF are somewhat limited **(Intro 2.2.)** and that Ruxolitinib is already used clinically mean it remains an attractive and viable option. Though it would be premature to offer the appellation of therapeutic candidate to Ruxolitinib, it is worth furthering our understanding of how this drug functions within the context of IPF and how it may be used to potentially treat the disease.

4. Discussion

4.1 Summary of Results

The results from this thesis have demonstrated several important and interesting aspects of IPF biology, revolving around the human lung fibroblast and its relationship with the epithelium. Understanding this relationship has focused most prominently on the role of inflammatory secretory signalling, investigating production of a broad range of immune-modulating cytokines, chemokines and growth factors. When normal and diseased HLFs were cultured on their own, without exogenous stimulation, it was difficult to discern any substantial pathological differences **(Results.3.1.)**. There were significant alterations in mitochondrial morphology, yet fully understanding the importance of this requires extensive experimentation. The lack of differences in monoculture did not necessarily conflict with current literature; in which studies typically apply some form of stimulant to their cultures, such as patient derived matrix or profibrotic stimuli, but it did suggest that in order to develop a more profound understanding of the role of HLFs in IPF, an *in vitro* system would have to be established that better recapitulated specific cell-cell interactions in the lung.

This was achieved by a method of co-culture **(Results.3.2.)**. Utilising an epithelial cell line and semi-permeable transwell inserts, a system was established that allowed cocultured cell types to communicate via secretion. The simple addition of an epithelial layer to fibroblast cultures had interesting effects and facilitated the investigation of epithelial-mesenchymal crosstalk along with several of the key characteristics and driving forces of IPF. Co-culture with NHLFs created a micro-environment that promoted epithelial function. Though postulated to reflect epithelial development *ab initio*, coculture experiments were re-evaluated as a model of injury, in which epithelial cells are required to repopulate a denuded basement membrane (in this case, the transwell insert). This was coupled with scratch assays that aimed to recapitulate the process of re-epithelialisation, in sum allowing an *in vitro* investigation of the airways response to injury. NHLFs were found to enhance both of these processes, signifying that healthy fibroblasts are supportive of their epithelial neighbours and promote their function through secretory communication. FHLFs, by contrast, failed to demonstrate such

abilities. Reluctant to proliferate and pro-inflammatory, these cells impaired the process of re-epithelialisation. Not only this, but they could not match the ability of NHLFs to enhance regeneration **(Results.3.3.)**. These results better aligned with the current understanding of IPF, complying with a paradigm in which pathological fibroblasts contribute to aberrant and dysfunctional epithelial repair. Importantly, such was the repertoire of secretory factors produced by these cells and its similarity to the secretory phenotype of cells in a state of senescence, that it was thought that this phenotype could be important in unlocking the detrimental role of fibrotic fibroblasts in IPF. There was much evidence for this, from both the literature and prior experiments with these cells. As well as displaying a reduced proliferative capacity, FHLFs were also shown to upregulate expression of *CDKN2A*, an important regulator of senescence. It was therefore hypothesised that a senescent-like phenotype was in operation in these cells.

To further understand this, NHLFs were recurrently treated with hydrogen peroxide, an agent used to cause DNA damage and an important signalling factor in airway injury. The treatment regimens adopted were able to reproducibly and robustly induce a state of cell cycle arrest, typified by the acquisition of numerous senescence-associated hallmarks **(Results.3.4.)**. Critically these cells recapitulated many of the functional effects of FHLFs in co-culture, impairing re-epithelialisation and failing to promote regeneration. Indeed, even the mitochondrial morphology of both cell types was found to be defined by similar characteristics. The implications from these results were that the secretory factors, produced by both cell types, were an appropriate target for pharmacological intervention. The nature of SASP, and the elevation of several of its core proteins in FHLFs and SIPS, led to the decision to target its regulation upstream, inhibiting the JAK/STAT signalling pathway, a pathway important to IPF, senescence and ageing. Inhibition of this pathway did yield success, restoring re-epithelialisation and reinstating the regenerative process, yet this was not without several limitations, and the creation of several unanswered questions **(Results.3.5.)**. Whether Ruxolitinib is a viable therapeutic option for IPF cannot be confidently stated, yet these results, and this body of work, have opened up the potential for further investigation that may offer future success. In sum, this investigation has highlighted important characteristics of

FHLFs and how these cells alter the function of the epithelium. A resulting question however is, what can these results suggest about the activity of FHLFs *in vivo*, and what do these results mean regarding the pathobiology of IPF?

4.2 Implications for Disease Pathobiology

4.2.1. Senescence in the context of IPF

The inability of FHLFs to facilitate epithelial repair and regeneration reflects one of the defining characteristics of the disease, an aberrant and dysfunctional wound healing response, and implicates the FHLF as the central mediator of this defect. That they are detrimental to these processes is of real significance in a disease characterised by recurrent injury [164,275]. Because injury is seemingly frequent, it makes the importance of adequate repair all the more salient and focuses the implications of fibroblast pathology onto their paracrine abilities to dictate airway repair, as well as their ability to excessively deposit extracellular matrix. This investigation has attributed the pathological effects of FHFLs to senescent-like properties, a phenotype highly relevant against the backdrop of the ageing lung in which this disease arises [174,229,242]. Fibroblast senescence does however present somewhat of a paradox in the context of a disease also characterised by excessive fibroblast proliferation and matrix deposition. The two phenotypes of senescence and fibroproliferation are however not mutually exclusive in a population of cells defined by its heterogeneity. It may well be that the results of this investigation have struck upon a subset of fibroblasts in which the characteristics of senescence predominate.

This does however raise the question of how these cells arise themselves, but it is possible to describe a narrative, that is novel yet complicit with the current literature, which describes the endowment of these senescent-like properties. Firstly, injury to the lung airways would induce activation of a series of homeostatic repair pathways, which encompass signalling via developmental pathways and the use of hydrogen peroxide

[41,81,86]. These pathways ultimately result in the induction of an acute senescence response, whereby previously activated fibroblasts enter a state of cell cycle arrest, signalling to the immune system for clearance [220,223]. Senescent cells come and go during normal, infrequent repair yet in the IPF lung recurrent injury and the recurrent activation of these pathways would create a sustained burden of senescent cells. Though these cells could and would normally be cleared by immune cells, the decline of this system with age would lead to their accumulation [234], reaching a threshold in which the burden of senescent cells becomes detrimental to epithelial repair, as evidenced in this investigation. The micro-environment created by these senescent cells would have detrimental ramifications for both the epithelium and the mesenchyme. The secretome of these cells limits the differential potential of epithelial progenitors [222] and, coupled with an over-compensatory attempt at regeneration, could result in the AEC2 hyperplasia and distal BC colonisation observed in the disease [128,130]. The proinflammatory elements of the secretome also stimulate pro-repair responses in neighbouring, normal fibroblasts. However, because this signalling is chronic, it would result in an overexuberant response, associated with fibroproliferation and matrix deposition [247]. Through these effects, it is feasible that senescent-like fibroblasts could orchestrate the demise of normal lung physiology, acting as central mediators in the pathogenesis of IPF **(*Figure* 4.1.1.)**.

That FHLFs are representative of senescent cells has interesting implications for IPF in terms of research and therapeutics. Clinically, IPF is beset by the issue of a lack of therapeutic options that reverse pathology [103]. Likewise, the only two currently available treatments are promiscuous in their activity, having a broad range of effects on numerous cell types with several side-effects. Investigations into senescence however have thus far been able to produce strategies that selectively target and clear senescent cells [235,237,238]. Therefore, if senescent-like fibroblasts are indeed the key to IPF pathology then they present a viable pharmacological target that can utilise already existing therapeutic strategies, such as treatment with D+Q or ABT263.

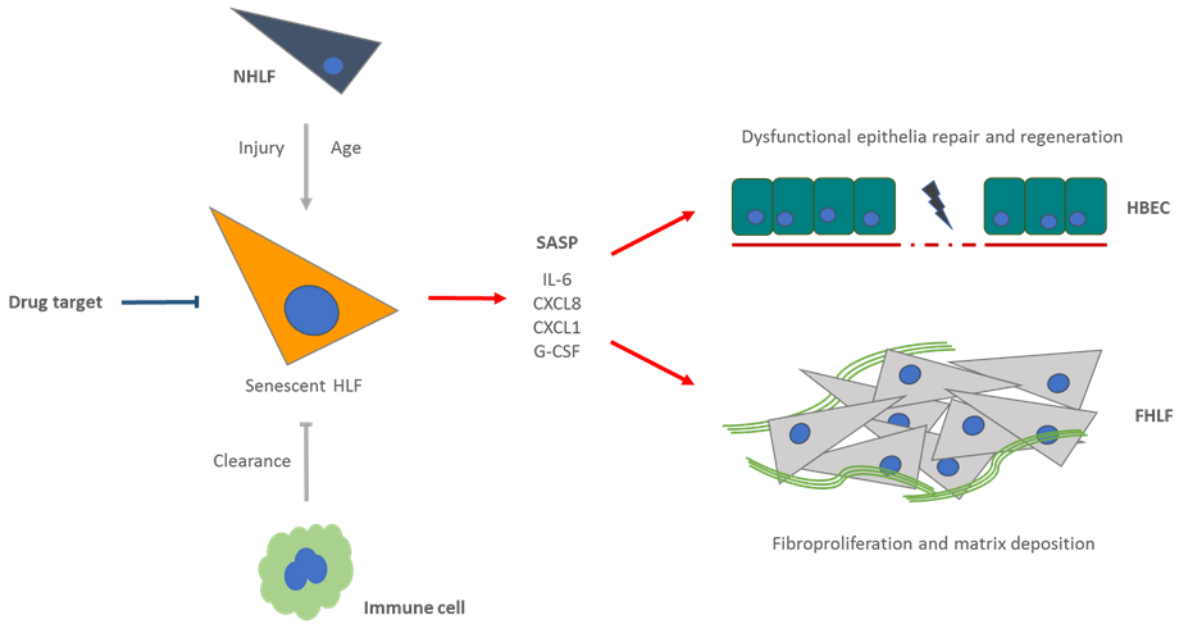

Figure 4.1.1. Proposed concept of the role of fibroblast senescence in IPF. NHLFs maintain the trophic environment of the healthy airway but in IPF, a permissive genetic background, coupled with recurrent injury and ageing leads to the accumulation of senescent fibroblasts, which are not cleared by the immune system. These cells acquire a SASP, altering the local micro-environment. This reduces the ability of the epithelium to respond to injury, leading to dysfunctional repair, and promotes fibrogenic processes in local, normal fibroblasts. Together this drives the pathobiology of IPF but also provides a target for pharmacological intervention. Further proof of this concept requires additional experimentation but it begins to align with recently published literature, in particular that of Schafer *et al.* [246].

4.2.2. Modelling secretory crosstalk in the context of IPF

The model system used throughout this investigation involved the use of primary human lung fibroblasts in co-culture with a human, bronchial epithelial cell line, in system that restricted cell-cell contact but facilitated secretory communication. This model allowed investigation of epithelial-mesenchymal crosstalk, focusing on the role of secretory proteins in an attempt to better recapitulate airway physiology. However, it is worth identifying how this model fits into the wider concepts of IPF cell biology, as well as the other types of secretory communication prominent in the lung and the more complex interactions that drive the disease.

4.2.2.1. Patient-derived HLFs

Patient-derived HLFs were an extremely important element of this investigation, as such it is important to consider the way in which they were used. One of the limitations of this study was that more patient information was not available. For a variety of reasons information pertaining to smoker-status, weight, co-morbidities, and outcome postdiagnosis was not available. This information would have been both useful and interesting, providing a potential explanation for any large variations in *in vitro* data. Ideally, future experiments would use a greater number of patients stratifying them along clinical outcome and patient history.

Another possible limitation was that population doublings were not thoroughly accounted for, instead relying on the assumption that passage of cells upon roughly 80% confluency would maintain broadly equivalent population doublings between differing populations. This assumption creates the potential that certain populations of cells used in an experiment could be considerably more biologically 'aged' than passage matched counterparts, a potential pitfall when investigating senescence. Future experiments could be made more robust by passaging cells on the basis of population doublings and using kinetically matched populations of cells for experiments.

Regarding IPF cell biology, one of the merits of the normal and diseased fibroblasts used in this investigation was that they were all derived from patients of older age. This meant two things: firstly, that when comparing FHLFs to these cells, differences in phenotype and behaviour were less likely to be the result of age-associated alterations and more likely to be the result of pathology-associated changes; secondly, it meant that these age-related changes were likely to affect both cell types and that these cells were likely different to those from young patients. This means that differences, especially relating to senescence, may have been harder to distinguish between cell types, as even in NHLFs, senescent-like alterations could have begun to develop as part of the natural process of ageing.

Another important consideration, especially when focusing on senescent-like properties, is the method by which primary HLFs were derived **(Methods 2.1.4.)**. Explantation requires fibroblasts to migrate and proliferate from their resident lung environment onto a tissue culture environment, which vastly differs. Only a select subset of cells would achieve this, and it was these cells that were used in subsequent experiments. Consequently, this process acted to select for fibroblasts that had a sufficient migratory and proliferative capacity to allow them to leave their native environment and grow on plastic. Previous work from this lab has shown that because of this, the yield of cells is dramatically less than if lung tissue is enzymatically digested (removing matrix to leave all cells on plastic). Therefore, cells in the lung that are either in a senescent or pre-senescent state are not likely to be found in the cohort of cells derived from explantation. This has meant that the ability of this investigation to assess senescence has most likely been restricted, but it has also meant that the senescent-like properties identified in FHLFs could reflect a phenotype that is in fact much more prominent in the IPF lung. The FHLF phenotype and its relationship to senescence may therefore be more accentuated *in vivo* and makes future investigation into this phenomenon even more worthwhile.

4.2.2.2. The use of the HBEC cell line

Turning now to the epithelium, this investigation utilised a bronchial epithelial cell line. This was preferred as it provided consistency and avoided issues of inter-donor variation. Results using this line in co-culture were interesting and allowed investigation into aspects of re-epithelialisation and regeneration. However, although these cells have been widely evidenced to recapitulate many of the *in vivo* characteristics of primary HBECs across multiple passages, they are still a transformed line and some aspects of HBEC biology may be lost. The use of primary HBECs would therefore more faithfully represent the lung epithelium *in* vitro. Primary HBECs could be obtained either by isolation from human tissue samples or by purchasing from commercial sources.

Regardless, experimenting with these cells is a viable option for future experiments that could further corroborate the findings of this investigation.

Similarly, using one epithelial cell type raises questions about the effect of HLF coculture on other types of epithelial cell in the lung. HBECs, in particular BCs, are implicated in the pathology of IPF, inappropriately propagating in a distal direction and colonising both the small airways and honeycomb cysts **(Intro 1.2.3.2.)**. However, there are also substantial alterations to AEC2 cells, which hyperpolarise and overlay fibrotic foci, and AEC1s, which appear to be lost through injury. Subsequently, how HLF secretory crosstalk influences these two cell types could also be considered, with similar experimentation creating a more complete picture of epithelial-mesenchymal interactions in the lung.

Finally, one of the unique characteristics regarding epithelial cells in the lung is that their apical surface is exposed to the air. Though, fluids such as ASL in the airways or surfactant in the alveoli form a barrier to direct contact, this exposure is important in epithelial function, providing a cue for the establishment of polarity and influencing airway homeostasis. Interestingly, during development airway epithelium does not experience this environmental stimulus but it is important to consider that the HBECs in this study were kept in submerged culture. Exposing them to the air would have allowed a potentially better recapitulation of the *in vivo* airway and again could be performed in the future using standard air-liquid interface cultures.

4.2.2.3. Different types of crosstalk

This investigation has focused specifically on the role of secretory crosstalk in the pathology of IPF, using a method of co-culture that restricts cell-cell contact and cellmatrix interactions. Though secretory crosstalk is fundamental to the numerous processes of development, homeostasis and repair, how cells communicate via direct contact, both with other cells and the ECM are also very important. For example, the AEC2 niche is maintained by basement membrane fenestrations that allow AEC2 foot processes to make contact with pericytes **(*Figure* 1.1.8.)**. Similarly, the invasive

properties of IPF fibroblasts are mediated, in part, by an increase in integrin signalling that interacts with stiffened ECM **(*Figure* 1.2.5.)**. Not only this, but epithelial and mesenchymal cell types also communicate with a broad range of other cells in the lung. Interactions with endothelial cells, lipofibroblasts, pericytes and an extensive repertoire of immune cells are also important in both disease and health. Indeed, additional dialogue with these cell types may have important ramifications for epithelialmesenchymal crosstalk. Therefore, understanding these interactions would also add to the overall understanding of crosstalk in IPF and, in sum, it is clear that the model utilised in this investigation, although well-suited to assess secretory communication, doesn't fully capture the complex interactions between differing cell types, using differing modes of communication, that are likely to have a significant influence on IPF pathology.

4.3 Future experiments

An appreciation of where the model of secretory communication sits within the complex pathology of IPF raises possibilities for a whole range of future experiments, aimed at corroborating the results from this investigation whilst also widening its scope.

4.3.1. Understanding HLF mitochondrial function

This investigation attempted to assess mitochondrial phenotype in isolated HLFs by looking at mitochondrial morphology and membrane potential. These two parameters however, though in some cases highlighting interesting differences between cell types, provided an incomplete picture of mitochondrial function and what this meant for cell activity. As previously alluded to, further understanding membrane potential and how it relates to ROS production could be achieved by both repeating the TMRE experiments with the dyes JC-1 and MitoSox, and also by investigating their fluorescence via microscopy **(Results 3.1.3.)**. Mitochondrial function itself could also be assessed using an extracellular flux analyser (Seahorse). This machine allows investigation of glycolytic

function and mitochondrial respiration, by measuring extracellular acidification rate and oxygen consumption rate respectively. It would be hypothesised that FHLFs and SIPS would display more mitochondrial stress, indicative of increased oxidative stress, which could then be attributed to changes in mitochondrial morphology. With SIPS, it would also be interesting to measure changes in glycolytic function and mitochondrial respiration, over the time-course of senescence induction. Coupled with further morphological quantitation, this would highlight if changes in mitochondrial function occur before or after fragmentation, answering the question of whether changes in morphology are a cause of a consequence of altered function.

4.3.2. Epithelial differentiation at air-liquid interface (ALI)

Results 3.2.2.2. began to suggest that NHLF co-culture promoted epithelial function not through increased HBEC proliferation or tight junction formation but through potentially modulating differentiation. This was not investigated further but could prove an interesting avenue of future research. Fully examining epithelial differentiation requires a more complicated approach to maintaining co-cultures but is possible, allowing determination of how mono-culture and co-culture with NHLF, FHLF and SIPS alters differentiation. Ideally, a primary HBEC line would be utilised for these experiments as these cells have greater potency and more readily differentiate under appropriate conditions. These cells could be seeded in conjunction with HLFs in adherence with the method used in this study **(Method 2.1.6.)**, allowing formation of a confluent and integral epithelial barrier by 72 hrs. At this time point, the cells would then be moved to ALI by removing the apical media. This exposes the polarised epithelium to the atmosphere, and can provide contextual cues for differentiation whilst the basolateral surface remains in contact with the media and retains the ability to communicate with fibroblasts. Evaluating differentiation is best achieved after periods of culture up to 3 weeks. To avoid fibroblast overcrowding or apoptosis, ALI HBEC inserts would have to be transferred to fresh HLF cultures every 72 hrs. Across varying time intervals, extending up to 3 weeks post-ALI, HBEC cultures could be fixed and stained, using primary antibodies for BCs (KRT5), mucosal cells (MUC5AC) and multi-ciliated cells

(FOXJ1). Via confocal microscopy, z-stack images would be produced allowing a 3D reconstruction of the epithelial layer. By counting the numbers of different cell types present, the ratio of basal to mucosal or ciliated cells could be calculated providing a quantitative score of differentiation that could be compared across differing co-culture types. It would be hypothesised that, compared to mono-culture, NHLF co-culture increases differentiation, indicative of these cells creating a micro-environment that benefits the epithelium. It would also be hypothesised that both FHLFs and SIPS would fail to provide this support. In fact, it could be expected that the epithelium would be densely packed with undifferentiated BCs, reminiscent of the distal BC colonisation observed in IPF.

4.3.3. Effect of senescence on NHLFs

A preliminary attempt was made at understanding how the secretory factors of SIPS influence fibrogenic processes in NHLFs, a question that remains extremely important in understanding the role of senescence in IPF. To test the hypothesis that SIPS promote ECM deposition in NHLFs, RNA levels of *COL1A1*, *COL3A1* and *ELN* were measured in cells treated for 72 hrs with SIPS CM **(*Figure* 3.4.22.)**. This however provided only a limited answer and future experiments could be performed to better understand this interaction. Firstly, as the cells in this experiment were pre-treated with media containing factors that assist in matrix deposition, protein levels could also be measured post-treatment. Protein would be extracted with RIPA buffer and western blot performed, staining for the different collagen proteins, allowing investigation of differential expression. Similarly, collagen levels could be determined by utilising highperformance liquid chromatography (HPLC). After 72 hrs, treated cells would be incubated at -80 ^{o}C for 24 hrs and then defrosted and scraped to disrupt the cell layer and ECM. Protein would then be precipitated in 67% (v/v) ethanol at 4 ^{o}C overnight, then hydrolysed via a 16 hr incubation in 6M hydrochloric acid at 110 ^{o}C. Hydrolysates would then be evaporated to dryness under vacuum in a centrifuge and re-dissolved in HPLCgrade H_2O. Further derivatisation would be achieved, ultimately allowing samples to be run on HPLC. Collagen content would be quantified by measuring hydroxyproline

content (a component of collagen that makes up 12.2% w/w) with the hypothesis that both SIPS CM treatment and recombinant TGF-β1 treatment would significantly increase collagen deposition in NHLFs, providing further evidence that the characteristics of senescence play a central role in IPF pathology. Similarly, this series of experiments could be repeated using the CM from FHLFs, operating under the same hypothesis.

4.3.4. Interactions with the immune system

One other area of substantial interest, that it was not possible to study in this investigation, is how epithelial-mesenchymal crosstalk links with the cells of the immune system. The immune system is extremely important in facilitating the pathology of IPF and understanding how fibroblasts mediate its function would be of interest. Firstly, it would be interesting to investigate how the CM of various culture conditions influences chemotaxis of macrophages, neutrophils or NK cells, with the hypothesis that there would be greater migration towards CM from FHLF and SIPS cultures, indicative of these cell types producing elevated levels of chemoattractant. As a preliminary study, this could be achieved by investigating the simple migration of THP-1 cells (a human, monocytic cell line) in Boyden chemotaxis chambers. Varying CM types would be placed in the basolateral chamber and immune cells seeded into the apical chamber. As a control for chemotaxis, certain chambers would also contain varying concentrations of recombinant CCL2, an archetypal chemoattractant, or volumes of unconditioned media. Similarly, to control for the effects of chemokinesis, pelleted THP-1s would also be resuspended in CM or chemoattractant-containing media. Across a period of 2-3 hrs, and at intervals of 30 min, the basolateral media would be extracted and the number of THP1s counted, providing information on chemotaxis.

Extending investigations into the role of the immune system could also be performed, with IPF patient derived immune cells providing a good platform for investigation. When using these cells (for example circulating monocytes derived from IPF blood samples) in a similar chemotaxis experiment it may be expected that these cells fail to respond to chemotactic signals in the CM, indicative of immune alterations. Likewise, with patient

and control immune cells it would be interesting to investigate their ability to clear senescent cells. An inability of the immune system to clear senescent cells is potentially important in both the process of ageing and the pathology of IPF. Understanding clearance *in vitro* could be achieved by incubating SIPS with patient derived monocytes and counting SIPS cell number after incubation. It could also be achieved by transfecting the cells with fluorescent proteins. Immune cells that perform phagocytosis would then acquire a degree of fluorescence that could be measured via spectroscopy or microscopy. Again, it would be hypothesised that IPF derived cells lack the capacity for senescence mediated clearance and together this could provide another reason for the accumulation of senescent-like cells in IPF.

4.3.5. Investigating senescence *in vivo*

As discussed previously, the model of crosstalk used in this investigation doesn't fully recapitulate the complex interactions between cell types of the human airways. The use of an *in vivo* model of fibrosis would provide a better opportunity to understand the significance of the fibrotic fibroblast phenotype and the role of senescence in IPF. The classical method of investigating fibrosis *in vivo* involves the treatment of mice with BLM, either via intra-tracheal or intra-nasal instillation, or by intraperitoneal injection. In this model, a period of inflammation occurs with subsequent fibrosis establishing itself by around 21 days post-treatment. This method is normally performed using young mice (2 – 3 months-old), however, as already discussed, age is an important driving force in IPF **(Intro 1.2.4.4.)**, which is also underpinned by senescence **(Intro 1.3.3.1.)**. Therefore, the use of aged mice (>18 months-old) would better suit this investigation. Developing a model of established fibrosis in aged mice would provide a useful platform for studying the involvement of senescence-like hallmarks in IPF. This could be achieved histologically, by comparing sections of normal and fibrotic lung (from both young and aged mice) for the classical markers of senescence such as p16 and p21, as well as performing staining for SA-βgal activity. Importantly it would be interesting to understand the cellular localisation of these markers, if expressed, hypothesising that they would be found most prominently in fibroblasts. Markers of SASP could also be

assessed, focusing in particular on IL-6 and CXCL8 expression, as well as the phosphorylation status and intracellular localisation of STAT-3, again hypothesising that there will be an enrichment for nuclear located pSTAT-3 in fibroblasts of aged, fibrotic mice. Taking a more global approach to gene expression could also yield interesting findings, giving a broader overview of senescence and fibrosis-associated pathways. This could be achieved by performing microarray analysis on whole lung homogenates from these mice. Though this restricts discrimination between cell types, subsequent gene ontology analysis could further identify pathways of interest.

As well as investigating these aspects in animal models, it would also be interesting to repeat these histological and gene expression analyses on sections of human tissue, comparing sections from IPF patients and normal controls. Evidence for elevation of senescence markers, SASP proteins and JAK/STAT enrichment would provide a more compelling rationale for attempting to target senescence *in vivo*.

4.3.6. Targeting senescence in *in vivo* models of IPF

With an established model of BLM-induced fibrosis in aged mice, and the identification of hallmarks of senescence in both this model and patient samples, subsequent investigations would focus on pharmacological intervention, to either slow the progression of fibrosis or even reverse the pathology. The choice of therapeutic would primarily revolve around targeting the JAK/STAT signalling pathway, utilising Ruxolitinib. Other JAK inhibitors could also be used, such as Baricitinib and Tofacitinib, to validate the on-target effects of Ruxolitinib. Treatment could be administered via oral gavage or, following the method of Xu *et al.*, administered in the animal feed [236]. The regimen adopted by this study utilised a 60 mg/kg treatment for 10 consecutive days and this approach could be adopted in preliminary experiments. Inhibition of JAK/STAT signalling would be assessed via the same histological analysis as previously discussed. The effect of drug treatment would then be assessed across several parameters. Blood oxygen levels would be measured at multiple timepoints, with decreases in pO_2 indicative of declining lung function. *Post mortem*, whole lungs would be digested and protein

expression of αSMA assessed via western blot, with increased expression indicative of myofibroblast propagation and a worsening of fibrosis. Similarly, whole lung collagen content could be quantified via HPLC, highlighting the extent of matrix deposition. Likewise, all of these markers of fibrotic progression could be corroborated by histological staining. Finally, survival curves could be plotted. It would be hypothesised that, compared to vehicle-treated animals, treatment with JAK inhibitors would lead to an attenuation of fibrotic progression across all of these parameters, ultimately resulting in increased survival rates in Ruxolitinib-treated mice. As well as controlling for drug vehicle, it would also be appropriate to compare the effects of these treatments to equivalent mice treated with Nintedanib and Pirfenidone. As these are the current therapeutic options for IPF patients it would be important to demonstrate that JAK/STAT inhibition has a greater effect on fibrotic progression than either of these drugs.

4.4 Concluding remarks

In summary, this investigation into the role of epithelial-mesenchymal crosstalk has resulted in: the successful isolation, propagation and experimentation with primary HLFs, from both fibrotic and non-fibrotic patients; the establishment of a method of coculture, creating a system with which to test the direct effects of HLFs on epithelial cells; the successful induction of premature senescence in NHLFs and has proposed a new potential option for the treatment of IPF. This investigation has also opened up many novel avenues of research, providing rationale for the further investigation of senescence *in vivo*, both in mouse and human, and for the further investigation of JAK/STAT signalling and its role in the disease. Overall, the concluding point of this work is that key to the pathology of IPF is a breakdown in the relationship between fibroblast and epithelial cells, the result of fibroblasts acquiring a secretory phenotype that is proinflammatory and reflective of the characteristics of cellular senescence. Ultimately, this investigation has highlighted the complexity of IPF pathology, yet regardless, there is much promise for future research.

Bibliography

1. Domyan, E. T. *et al.* Signaling through BMP receptors promotes respiratory identity in the foregut via repression of Sox2. *Dev. Camb. Engl.* **138,** 971–981 (2011).
2. Goss, A. M. *et al.* Wnt2/2b and beta-catenin signaling are necessary and sufficient to specify lung progenitors in the foregut. *Dev. Cell* **17,** 290–298 (2009).
3. Ornitz, D. M. & Yin, Y. Signaling networks regulating development of the lower respiratory tract. *Cold Spring Harb. Perspect. Biol.* **4,** (2012).
4. Metzger, R. J., Klein, O. D., Martin, G. R. & Krasnow, M. A. The branching programme of mouse lung development. *Nature* **453,** 745–750 (2008).
5. Bellusci, S., Grindley, J., Emoto, H., Itoh, N. & Hogan, B. L. Fibroblast growth factor 10 (FGF10) and branching morphogenesis in the embryonic mouse lung. *Development* **124,** 4867–4878 (1997).
6. Weaver, M., Dunn, N. R. & Hogan, B. L. Bmp4 and Fgf10 play opposing roles during lung bud morphogenesis. *Development* **127,** 2695–2704 (2000).
7. Tang, N., Marshall, W. F., McMahon, M., Metzger, R. J. & Martin, G. R. Control of Mitotic Spindle Angle by the RAS-Regulated ERK1/2 Pathway Determines Lung Tube Shape. *Science* **333,** 342–345 (2011).
8. Chen, J. & Krasnow, M. A. Integrin Beta 1 Suppresses Multilayering of a Simple Epithelium. *PLOS ONE* **7,** e52886 (2012).
9. Perl, A.-K. T., Wert, S. E., Nagy, A., Lobe, C. G. & Whitsett, J. A. Early restriction of peripheral and proximal cell lineages during formation of the lung. *Proc. Natl. Acad. Sci.* **99,** 10482–10487 (2002).
10. Hashimoto, S. *et al.* β-Catenin-SOX2 signaling regulates the fate of developing airway epithelium. *J. Cell Sci.* **125,** 932–942 (2012).
11. Gontan, C. *et al.* Sox2 is important for two crucial processes in lung development: Branching morphogenesis and epithelial cell differentiation. *Dev. Biol.* **317,** 296–309 (2008).
12. Rawlins, E. L., Clark, C. P., Xue, Y. & Hogan, B. L. M. The Id2+ distal tip lung epithelium contains individual multipotent embryonic progenitor cells. *Dev. Camb. Engl.* **136,** 3741–3745 (2009).
13. Rockich, B. E. *et al.* Sox9 plays multiple roles in the lung epithelium during branching morphogenesis. *Proc. Natl. Acad. Sci. U. S. A.* **110,** E4456–E4464 (2013).
14. Treutlein, B. *et al.* Reconstructing lineage hierarchies of the distal lung epithelium using single-cell RNA-seq. *Nature* **509,** 371–375 (2014).
15. Alanis, D. M., Chang, D. R., Akiyama, H., Krasnow, M. A. & Chen, J. Two nested developmental waves demarcate a compartment boundary in the mouse lung. *Nat. Commun.* **5,** ncomms4923 (2014).
16. Chang, D. R. *et al.* Lung epithelial branching program antagonizes alveolar differentiation. *Proc. Natl. Acad. Sci.* **110,** 18042–18051 (2013).

17. Peng, T. *et al.* Coordination of heart and lung co-development by a multipotent cardiopulmonary progenitor. *Nature* **500,** 589–592 (2013).
18. Lindahl, P. *et al.* Alveogenesis failure in PDGF-A-deficient mice is coupled to lack of distal spreading of alveolar smooth muscle cell progenitors during lung development. *Development* **124,** 3943–3953 (1997).
19. Kugler, M. C. *et al.* Sonic Hedgehog Signaling Regulates Myofibroblast Function During Alveolar Septum Formation in Murine Postnatal Lung. *Am. J. Respir. Cell Mol. Biol.* **57,** 280-293 (2017).
20. Suki, B., Ito, S., Stamenović, D., Lutchen, K. R. & Ingenito, E. P. Biomechanics of the lung parenchyma: critical roles of collagen and mechanical forces. *J. Appl. Physiol.* **98,** 1892–1899 (2005).
21. Weibel, E. R. It Takes More than Cells to Make a Good Lung. *Am. J. Respir. Crit. Care Med.* **187,** 342–346 (2013).
22. Selman, M. & Pardo, A. Role of Epithelial Cells in Idiopathic Pulmonary Fibrosis. *Proc. Am. Thorac. Soc.* **3,** 364–372 (2006).
23. Hogan, B. L. M. *et al.* Repair and regeneration of the respiratory system: complexity, plasticity, and mechanisms of lung stem cell function. *Cell Stem Cell* **15,** 123–138 (2014).
24. Breeze, R. & Turk, M. Cellular structure, function and organization in the lower respiratory tract. *Environ. Health Perspect.* **55,** 3–24 (1984).
25. Herriges, M. & Morrisey, E. E. Lung development: orchestrating the generation and regeneration of a complex organ. *Development* **141,** 502–513 (2014).
26. Roy, M. G. *et al.* Muc5b is required for airway defence. *Nature* **505,** 412–416 (2014).
27. Fahy, J. V. & Dickey, B. F. Airway Mucus Function and Dysfunction. *N. Engl. J. Med.* **363,** 2233–2247 (2010).
28. Chen, Y., Zhao, Y. H., Di, Y. P. & Wu, R. Characterization of human mucin 5B gene expression in airway epithelium and the genomic clone of the amino-terminal and 5'-flanking region. *Am. J. Respir. Cell Mol. Biol.* **25,** 542–553 (2001).
29. Evans, C. M. *et al.* Mucin is produced by clara cells in the proximal airways of antigen-challenged mice. *Am. J. Respir. Cell Mol. Biol.* **31,** 382–394 (2004).
30. Knowles, M. R. & Boucher, R. C. Mucus clearance as a primary innate defense mechanism for mammalian airways. *J. Clin. Invest.* **109,** 571–577 (2002).
31. Song, H. *et al.* Functional characterization of pulmonary neuroendocrine cells in lung development, injury, and tumorigenesis. *Proc. Natl. Acad. Sci.* **109,** 17531–17536 (2012).
32. Krasteva, G. *et al.* Cholinergic chemosensory cells in the trachea regulate breathing. *Proc. Natl. Acad. Sci. U. S. A.* **108,** 9478–9483 (2011).
33. Hong, K. U., Reynolds, S. D., Watkins, S., Fuchs, E. & Stripp, B. R. Basal Cells Are a Multipotent Progenitor Capable of Renewing the Bronchial Epithelium. *Am. J. Pathol.* **164,** 577–588 (2004).

34. Rock, J. R. *et al.* Basal cells as stem cells of the mouse trachea and human airway epithelium. *Proc. Natl. Acad. Sci.* **106,** 12771–12775 (2009).
35. Watson, J. K. *et al.* Clonal Dynamics Reveal Two Distinct Populations of Basal Cells in Slow-Turnover Airway Epithelium. *Cell Rep.* **12,** 90–101 (2015).
36. Hegab, A. E. *et al.* Novel stem/progenitor cell population from murine tracheal submucosal gland ducts with multipotent regenerative potential. *Stem Cells Dayt. Ohio* **29,** 1283–1293 (2011).
37. Cole, B. B. *et al.* Tracheal Basal cells: a facultative progenitor cell pool. *Am. J. Pathol.* **177,** 362–376 (2010).
38. Ghosh, M. *et al.* Context-dependent differentiation of multipotential keratin 14expressing tracheal basal cells. *Am. J. Respir. Cell Mol. Biol.* **45,** 403–410 (2011).
39. Volckaert, T. *et al.* Parabronchial smooth muscle constitutes an airway epithelial stem cell niche in the mouse lung after injury. *J. Clin. Invest.* **121,** 4409–4419 (2011).
40. Bowden, D. H. Cell turnover in the lung. *Am. Rev. Respir. Dis.* **128,** S46-48 (1983).
41. Tadokoro, T., Gao, X., Hong, C. C., Hotten, D. & Hogan, B. L. M. BMP signaling and cellular dynamics during regeneration of airway epithelium from basal progenitors. *Development* **143,** 764–773 (2016).
42. Zhao, R. *et al.* Yap Tunes Airway Epithelial Size and Architecture by Regulating the Identity, Maintenance, and Self-Renewal of Stem Cells. *Dev. Cell* **30,** 151–165 (2014).
43. Hackett, N. R. *et al.* The Human Airway Epithelial Basal Cell Transcriptome. *PLOS ONE* **6,** e18378 (2011).
44. Araya, J., Cambier, S., Morris, A., Finkbeiner, W. & Nishimura, S. L. IntegrinMediated Transforming Growth Factor-β Activation Regulates Homeostasis of the Pulmonary Epithelial-Mesenchymal Trophic Unit. *Am. J. Pathol.* **169,** 405–415 (2006).
45. McQualter, J. L., Yuen, K., Williams, B. & Bertoncello, I. Evidence of an epithelial stem/progenitor cell hierarchy in the adult mouse lung. *Proc. Natl. Acad. Sci.* **107,** 1414–1419 (2010).
46. Peng, T. *et al.* Hedgehog actively maintains adult lung quiescence and regulates repair and regeneration. *Nature* **526,** 578–582 (2015).
47. Adamson, I. Y., Hedgecock, C. & Bowden, D. H. Epithelial cell-fibroblast interactions in lung injury and repair. *Am. J. Pathol.* **137,** 385–392 (1990).
48. Crapo, J. D., Barry, B. E., Gehr, P., Bachofen, M. & Weibel, E. R. Cell number and cell characteristics of the normal human lung. *Am. Rev. Respir. Dis.* **126,** 332–337 (1982).
49. Barkauskas, C. E. *et al.* Type 2 alveolar cells are stem cells in adult lung. *J. Clin. Invest.* **123,** 3025–3036 (2013).
50. Desai, T. J., Brownfield, D. G. & Krasnow, M. A. Alveolar progenitor and stem cells in lung development, renewal and cancer. *Nature* **507,** 190–194 (2014).

51. Jain, R. *et al.* Plasticity of Hopx+ Type I alveolar cells to regenerate Type II cells in the lung. *Nat. Commun.* **6,** 6727 (2015).
52. Sirianni, F. E., Chu, F. S. F. & Walker, D. C. Human Alveolar Wall Fibroblasts Directly Link Epithelial Type 2 Cells to Capillary Endothelium. *Am. J. Respir. Crit. Care Med.* **168,** 1532–1537 (2003).
53. Panos, R. J., Rubin, J. S., Csaky, K. G., Aaronson, S. A. & Mason, R. J. Keratinocyte growth factor and hepatocyte growth factor/scatter factor are heparin-binding growth factors for alveolar type II cells in fibroblast-conditioned medium. *J. Clin. Invest.* **92,** 969–977 (1993).
54. Qiao, R. *et al.* Effects of KGF on alveolar epithelial cell transdifferentiation are mediated by JNK signaling. *Am. J. Respir. Cell Mol. Biol.* **38,** 239–246 (2008).
55. Young, L. & Adamson, I. Y. Epithelial-fibroblast interactions in bleomycin-induced lung injury and repair. *Environ. Health Perspect.* **101,** 56–61 (1993).
56. Rawlins, E. L. *et al.* The role of Scgb1a1+ Clara cells in the long-term maintenance and repair of lung airway, but not alveolar, epithelium. *Cell Stem Cell* **4,** 525–534 (2009).
57. Kaplan, M. J. & Radic, M. Neutrophil extracellular traps (NETs): Double-edged swords of innate immunity. *J. Immunol. Baltim. Md 1950* **189,** 2689–2695 (2012).
58. Grommes, J. & Soehnlein, O. Contribution of neutrophils to acute lung injury. *Mol. Med. Camb. Mass* **17,** 293–307 (2011).
59. Rodero, M. P. *et al.* In Vivo Imaging Reveals a Pioneer Wave of Monocyte Recruitment into Mouse Skin Wounds. *PLOS ONE* **9,** e108212 (2014).
60. Holzheimer, R. G. & Steinmetz, W. Local and systemic concentrations of pro- and anti-inflammatory cytokines in human wounds. *Eur. J. Med. Res.* **5,** 347–355 (2000).
61. Daley, J. M., Brancato, S. K., Thomay, A. A., Reichner, J. S. & Albina, J. E. The phenotype of murine wound macrophages. *J. Leukoc. Biol.* **87,** 59–67 (2010).
62. Lucas, T. *et al.* Differential Roles of Macrophages in Diverse Phases of Skin Repair. *J. Immunol.* **184,** 3964–3977 (2010).
63. Martin, P. *et al.* Wound Healing in the PU.1 Null Mouse—Tissue Repair Is Not Dependent on Inflammatory Cells. *Curr. Biol.* **13,** 1122–1128 (2003).
64. Schneider, L. *et al.* Directional Cell Migration and Chemotaxis in Wound Healing Response to PDGF-AA are Coordinated by the Primary Cilium in Fibroblasts. *Cell. Physiol. Biochem.* **25,** 279–292 (2010).
65. Driskell, R. R. *et al.* Distinct fibroblast lineages determine dermal architecture in skin development and repair. *Nature* **504,** 277–281 (2013).
66. Darby, I., Skalli, O. & Gabbiani, G. α-Smooth muscle actin is transiently expressed by myofibroblasts during experimental wound healing. *Lab. Invest.* **63,** 21–29 (1990).
67. Desmoulière, A., Geinoz, A., Gabbiani, F. & Gabbiani, G. Transforming growth factor-beta 1 induces alpha-smooth muscle actin expression in granulation tissue

myofibroblasts and in quiescent and growing cultured fibroblasts. *J. Cell Biol.* **122,** 103–111 (1993).

68. Gs, A. *et al.* Mice lacking Smad3 show accelerated wound healing and an impaired local inflammatory response. *Nat. Cell Biol.* **1,** 260–266 (1999).
69. Shah, M., Foreman, D. M. & Ferguson, M. W. Neutralisation of TGF-beta 1 and TGFbeta 2 or exogenous addition of TGF-beta 3 to cutaneous rat wounds reduces scarring. *J. Cell Sci.* **108,** 985–1002 (1995).
70. Koyama, H., Raines, E. W., Bornfeldt, K. E., Roberts, J. M. & Ross, R. Fibrillar collagen inhibits arterial smooth muscle proliferation through regulation of Cdk2 inhibitors. *Cell* **87,** 1069–1078 (1996).
71. Knipper, J. A. *et al.* Interleukin-4 Receptor α Signaling in Myeloid Cells Controls Collagen Fibril Assembly in Skin Repair. *Immunity* **43,** 803–816 (2015).
72. Ito, Y. *et al.* Influenza induces IL-8 and GM-CSF secretion by human alveolar epithelial cells through HGF/c-Met and TGF-α/EGFR signaling. *Am. J. Physiol. - Lung Cell. Mol. Physiol.* **308,** L1178–L1188 (2015).
73. Grimstad, Ø. *et al.* Cellular sources and inducers of cytokines present in acute wound fluid. *Wound Repair Regen.* **19,** 337–347 (2011).
74. Pottier, N. *et al.* Identification of Keratinocyte Growth Factor as a Target of microRNA-155 in Lung Fibroblasts: Implication in Epithelial-Mesenchymal Interactions. *PLOS ONE* **4,** e6718 (2009).
75. Zahm, J. M. *et al.* Cell migration and proliferation during the in vitro wound repair of the respiratory epithelium. *Cell Motil. Cytoskeleton* **37,** 33–43 (1997).
76. Erjefält, J. S., Erjefält, I., Sundler, F. & Persson, C. G. A. In vivo restitution of airway epithelium. *Cell Tissue Res.* **281,** 305–316 (1995).
77. Fenteany, G., Janmey, P. A. & Stossel, T. P. Signaling pathways and cell mechanics involved in wound closure by epithelial cell sheets. *Curr. Biol.* **10,** 831–838 (2000).
78. Desai, L. P., Aryal, A. M., Ceacareanu, B., Hassid, A. & Waters, C. M. RhoA and Rac1 are both required for efficient wound closure of airway epithelial cells. *Am. J. Physiol. - Lung Cell. Mol. Physiol.* **287,** L1134–L1144 (2004).
79. Nunan, R. *et al.* Ephrin-Bs Drive Junctional Downregulation and Actin Stress Fiber Disassembly to Enable Wound Re-epithelialization. *Cell Rep.* **13,** 1380–1395 (2015).
80. Razzell, W., Wood, W. & Martin, P. Recapitulation of morphogenetic cell shape changes enables wound re-epithelialisation. *Development* **141,** 1814–1820 (2014).
81. Lisse, T. S., King, B. L. & Rieger, S. Comparative transcriptomic profiling of hydrogen peroxide signaling networks in zebrafish and human keratinocytes: Implications toward conservation, migration and wound healing. *Sci. Rep.* **6,** (2016).
82. Ito, Y. *et al.* Lung fibroblasts accelerate wound closure in human alveolar epithelial cells through hepatocyte growth factor/c-Met signaling. *Am. J. Physiol. Lung Cell. Mol. Physiol.* **307,** L94-105 (2014).

83. Myerburg, M. M. *et al.* Hepatocyte growth factor and other fibroblast secretions modulate the phenotype of human bronchial epithelial cells. *Am. J. Physiol. - Lung Cell. Mol. Physiol.* **292,** L1352–L1360 (2007).
84. Dupuit, F. *et al.* Differentiated and functional human airway epithelium regeneration in tracheal xenografts. *Am. J. Physiol. Lung Cell. Mol. Physiol.* **278,** L165-176 (2000).
85. Heguy, A. *et al.* Responses of the human airway epithelium transcriptome to in vivo injury. *Physiol. Genomics* **29,** 139–148 (2007).
86. Paul, M. K. *et al.* Dynamic Changes in Intracellular ROS Levels Regulate Airway Basal Stem Cell Homeostasis through Nrf2-Dependent Notch Signaling. *Cell Stem Cell* **15,** 199–214 (2014).
87. Pardo-Saganta, A. *et al.* Injury Induces Direct Lineage Segregation of Functionally Distinct Airway Basal Stem/Progenitor Cell Subpopulations. *Cell Stem Cell* **16,** 184–197 (2015).
88. Tadokoro, T. *et al.* IL-6/STAT3 promotes regeneration of airway ciliated cells from basal stem cells. *Proc. Natl. Acad. Sci. U. S. A.* **111,** E3641-3649 (2014).
89. Sponsel, H. T., Breckon, R., Hammond, W. & Anderson, R. J. Mechanisms of recovery from mechanical injury of renal tubular epithelial cells. *Am. J. Physiol.* **267,** F257-264 (1994).
90. Tonnesen, M. G., Feng, X. & Clark, R. A. Angiogenesis in wound healing. *J. Investig. Dermatol. Symp. Proc.* **5,** 40–46 (2000).
91. Maher, T. M. Diffuse parenchymal lung disease. *Medicine (Baltimore)* **40,** 314–321 (2012).
92. Raghu, G. *et al.* An Official ATS/ERS/JRS/ALAT Statement: Idiopathic Pulmonary Fibrosis: Evidence-based Guidelines for Diagnosis and Management. *Am. J. Respir. Crit. Care Med.* **183,** 788–824 (2011).
93. King, T. E., Pardo, A. & Selman, M. Idiopathic pulmonary fibrosis. *The Lancet* **378,** 1949–1961 (2011).
94. Visscher, D. W. & Myers, J. L. Histologic Spectrum of Idiopathic Interstitial Pneumonias. *Proc. Am. Thorac. Soc.* **3,** 322–329 (2006).
95. Snell, N. *et al.* Burden of lung disease in the UK; findings from the British Lung Foundation's 'respiratory health of the nation' project. *Eur. Respir. J.* **48,** PA4913 (2016).
96. Ley, B., Collard, H. R. & King, T. E. Clinical course and prediction of survival in idiopathic pulmonary fibrosis. *Am. J. Respir. Crit. Care Med.* **183,** 431–440 (2011).
97. Hutchinson, J. P., McKeever, T. M., Fogarty, A. W., Navaratnam, V. & Hubbard, R. B. Increasing global mortality from idiopathic pulmonary fibrosis in the twenty-first century. *Ann. Am. Thorac. Soc.* **11,** 1176–1185 (2014).
98. Navaratnam, V. *et al.* The rising incidence of idiopathic pulmonary fibrosis in the UK. *Thorax* **66,** 462–467 (2011).

99. Population Themes - United Nations Population Division | Department of Economic and Social Affairs. Available at: http://www.un.org/en/development/desa/population/theme/ageing/WPA2015.shtml. (Accessed: 14th July 2017)
100. du Bois, R. M. *et al.* Forced vital capacity in patients with idiopathic pulmonary fibrosis: test properties and minimal clinically important difference. *Am. J. Respir. Crit. Care Med.* **184,** 1382–1389 (2011).
101. Behr, J. Disease Progression in Idiopathic Pulmonary Fibrosis - FVC is Not Enough. *Am. J. Respir. Crit. Care Med.* (2017). doi:10.1164/rccm.201706-1246ED
102. Wollin, L. *et al.* Mode of action of nintedanib in the treatment of idiopathic pulmonary fibrosis. *Eur. Respir. J.* **45,** 1434-1445 (2015).
103. Raghu, G. *et al.* An Official ATS/ERS/JRS/ALAT Clinical Practice Guideline: Treatment of Idiopathic Pulmonary Fibrosis. An Update of the 2011 Clinical Practice Guideline. *Am. J. Respir. Crit. Care Med.* **192,** e3–e19 (2015).
104. Richeldi, L. *et al.* Efficacy of a Tyrosine Kinase Inhibitor in Idiopathic Pulmonary Fibrosis. *N. Engl. J. Med.* **365,** 1079–1087 (2011).
105. Richeldi, L. *et al.* Efficacy and Safety of Nintedanib in Idiopathic Pulmonary Fibrosis. *N. Engl. J. Med.* **370,** 2071–2082 (2014).
106. Nakazato, H., Oku, H., Yamane, S., Tsuruta, Y. & Suzuki, R. A novel anti-fibrotic agent pirfenidone suppresses tumor necrosis factor-alpha at the translational level. *Eur. J. Pharmacol.* **446,** 177–185 (2002).
107. Oku, H. *et al.* Antifibrotic action of pirfenidone and prednisolone: different effects on pulmonary cytokines and growth factors in bleomycin-induced murine pulmonary fibrosis. *Eur. J. Pharmacol.* **590,** 400–408 (2008).
108. King, T. E. *et al.* A Phase 3 Trial of Pirfenidone in Patients with Idiopathic Pulmonary Fibrosis. *N. Engl. J. Med.* **370,** 2083–2092 (2014).
109. Noble, P. W. *et al.* Pirfenidone in patients with idiopathic pulmonary fibrosis (CAPACITY): two randomised trials. *The Lancet* **377,** 1760–1769 (2011).
110. Raghu, G. *et al.* Efficacy of simtuzumab versus placebo in patients with idiopathic pulmonary fibrosis: a randomised, double-blind, controlled, phase 2 trial. *Lancet Respir. Med.* **0,** (2016).
111. Barry-Hamilton, V. *et al.* Allosteric inhibition of lysyl oxidase-like-2 impedes the development of a pathologic microenvironment. *Nat. Med.* **16,** 1009–1017 (2010).
112. Behr, J. *et al.* Safety and tolerability of acetylcysteine and pirfenidone combination therapy in idiopathic pulmonary fibrosis: a randomised, double-blind, placebocontrolled, phase 2 trial. *Lancet Respir. Med.* **4,** 445–453 (2016).
113. Daniels, C. E. *et al.* Imatinib treatment for idiopathic pulmonary fibrosis: Randomized placebo-controlled trial results. *Am. J. Respir. Crit. Care Med.* **181,** 604–610 (2010).
114. Network, T. I. P. F. C. R. Randomized Trial of Acetylcysteine in Idiopathic Pulmonary Fibrosis. *N. Engl. J. Med.* **370,** 2093–2101 (2014).

115. Noth, I. *et al.* A placebo-controlled randomized trial of warfarin in idiopathic pulmonary fibrosis. *Am. J. Respir. Crit. Care Med.* **186,** 88–95 (2012).
116. Wilkes, D. S. *et al.* Oral immunotherapy with type V collagen in idiopathic pulmonary fibrosis. *Eur. Respir. J.* **45,** 1393–1402 (2015).
117. Shaw, T. J. & Martin, P. Wound repair: a showcase for cell plasticity and migration. *Curr. Opin. Cell Biol.* **42,** 29–37 (2016).
118. Thannickal, V. J. & Fanburg, B. L. Activation of an H2O2-generating NADH oxidase in human lung fibroblasts by transforming growth factor beta 1. *J. Biol. Chem.* **270,** 30334–30338 (1995).
119. Hecker, L. *et al.* NADPH Oxidase-4 Mediates Myofibroblast Activation and Fibrogenic Responses to Lung Injury. *Nat. Med.* **15,** 1077–1081 (2009).
120. Xia, H. *et al.* Pathological integrin signaling enhances proliferation of primary lung fibroblasts from patients with idiopathic pulmonary fibrosis. *J. Exp. Med.* **205,** 1659–1672 (2008).
121. Nho, R. S., Hergert, P., Kahm, J., Jessurun, J. & Henke, C. Pathological Alteration of FoxO3a Activity Promotes Idiopathic Pulmonary Fibrosis Fibroblast Proliferation on Type I Collagen Matrix. *Am. J. Pathol.* **179,** 2420–2430 (2011).
122. Bühling, F. *et al.* Altered expression of membrane-bound and soluble CD95/Fas contributes to the resistance of fibrotic lung fibroblasts to FasL induced apoptosis. *Respir. Res.* **6,** 37 (2005).
123. Romero, Y. *et al.* mTORC1 activation decreases autophagy in aging and idiopathic pulmonary fibrosis and contributes to apoptosis resistance in IPF fibroblasts. *Aging Cell* **15,** 1103–1112 (2016).
124. Li, Y. *et al.* Severe lung fibrosis requires an invasive fibroblast phenotype regulated by hyaluronan and CD44. *J. Exp. Med.* **208,** 1459–1471 (2011).
125. Chen, H. *et al.* Mechanosensing by the α6-integrin confers an invasive fibroblast phenotype and mediates lung fibrosis. *Nat. Commun.* **7,** 12564 (2016).
126. Oehrle, B. *et al.* Validated prediction of pro-invasive growth factors using a transcriptome-wide invasion signature derived from a complex 3D invasion assay. *Sci. Rep.* **5,** 12673 (2015).
127. Uhal, B. D. *et al.* Alveolar epithelial cell death adjacent to underlying myofibroblasts in advanced fibrotic human lung. *Am. J. Physiol. - Lung Cell. Mol. Physiol.* **275,** L1192–L1199 (1998).
128. Seibold, M. A. *et al.* The Idiopathic Pulmonary Fibrosis Honeycomb Cyst Contains A Mucocilary Pseudostratified Epithelium. *PLOS ONE* **8,** e58658 (2013).
129. Bueno, M. *et al.* PINK1 deficiency impairs mitochondrial homeostasis and promotes lung fibrosis. *J. Clin. Invest.* **125,** 521–538 (2015).
130. Chilosi, M. *et al.* Abnormal Re-epithelialization and Lung Remodeling in Idiopathic Pulmonary Fibrosis: The Role of ΔN-p63. *Lab. Invest.* **82,** 1335–1345 (2002).
131. Plantier, L. *et al.* Ectopic respiratory epithelial cell differentiation in bronchiolised distal airspaces in idiopathic pulmonary fibrosis. *Thorax* **66,** 651–657 (2011).

132. Xu, Y. *et al.* Single-cell RNA sequencing identifies diverse roles of epithelial cells in idiopathic pulmonary fibrosis. *JCI Insight* **1,** (2017).
133. O'Dwyer, D. N. *et al.* The peripheral blood proteome signature of idiopathic pulmonary fibrosis is distinct from normal and is associated with novel immunological processes. *Sci. Rep.* **7,** 46560 (2017).
134. Molyneaux, P. L. *et al.* The role of bacteria in the pathogenesis and progression of idiopathic pulmonary fibrosis. *Am. J. Respir. Crit. Care Med.* **190,** 906–913 (2014).
135. Molyneaux, P. L. *et al.* Changes in the respiratory microbiome during acute exacerbations of idiopathic pulmonary fibrosis. *Respir. Res.* **18,** 29 (2017).
136. Hyldgaard, C., Hilberg, O. & Bendstrup, E. How does comorbidity influence survival in idiopathic pulmonary fibrosis? *Respir. Med.* **108,** 647–653 (2014).
137. Kreuter, M. *et al.* Impact of Comorbidities on Mortality in Patients with Idiopathic Pulmonary Fibrosis. *PLOS ONE* **11,** e0151425 (2016).
138. Nogee, L. M. *et al.* A Mutation in the Surfactant Protein C Gene Associated with Familial Interstitial Lung Disease. *N. Engl. J. Med.* **344,** 573–579 (2001).
139. Lawson, W. E. *et al.* Genetic mutations in surfactant protein C are a rare cause of sporadic cases of IPF. *Thorax* **59,** 977–980 (2004).
140. Markart, P. *et al.* Surfactant protein C mutations in sporadic forms of idiopathic interstitial pneumonias. *Eur. Respir. J.* **29,** 134-137 (2006).
141. Zhang, Y., Noth, I., Garcia, J. G. N. & Kaminski, N. A Variant in the Promoter of MUC5B and Idiopathic Pulmonary Fibrosis. *N. Engl. J. Med.* **364,** 1576–1577 (2011).
142. van der Vis, J. J. *et al.* Effect of Muc5b promoter polymorphism on disease predisposition and survival in idiopathic interstitial pneumonias. *Respirology* **21,** 712-717 (2016).
143. Tsakiri, K. D. *et al.* Adult-onset pulmonary fibrosis caused by mutations in telomerase. *Proc. Natl. Acad. Sci. U. S. A.* **104,** 7552–7557 (2007).
144. Armanios, M. Y. *et al.* Telomerase Mutations in Families with Idiopathic Pulmonary Fibrosis. *N. Engl. J. Med.* **356,** 1317–1326 (2007).
145. Alder, J. K. *et al.* Telomere dysfunction causes alveolar stem cell failure. *Proc. Natl. Acad. Sci. U. S. A.* **112,** 5099–5104 (2015).
146. Allen, R. J. *et al.* Genetic variants associated with susceptibility to idiopathic pulmonary fibrosis in people of European ancestry: a genome-wide association study. *Lancet Respir. Med.* **5,** 869–880 (2017).
147. Kropski, J. A., Blackwell, T. S. & Loyd, J. E. The genetic basis of idiopathic pulmonary fibrosis. *Eur. Respir. J.* **45,** 1717-1727 (2015).
148. Huang, X. *et al.* Matrix Stiffness–Induced Myofibroblast Differentiation Is Mediated by Intrinsic Mechanotransduction. *Am. J. Respir. Cell Mol. Biol.* **47,** 340–348 (2012).
149. Asano, S. *et al.* Matrix stiffness regulates migration of human lung fibroblasts. *Physiol. Rep.* **5,** (2017).
150. Liu, F. *et al.* Mechanosignaling through YAP and TAZ drives fibroblast activation and fibrosis. *Am. J. Physiol. - Lung Cell. Mol. Physiol.* **308,** L344–L357 (2015).

151. Parker, M. W. *et al.* Fibrotic extracellular matrix activates a profibrotic positive feedback loop. *J. Clin. Invest.* **124,** 1622–1635 (2014).
152. Chanda, D. *et al.* Developmental Reprogramming in Mesenchymal Stromal Cells of Human Subjects with Idiopathic Pulmonary Fibrosis. *Sci. Rep.* **6,** (2016).
153. Hu, B. *et al.* Reemergence of Hedgehog Mediates Epithelial–Mesenchymal Crosstalk in Pulmonary Fibrosis. *Am. J. Respir. Cell Mol. Biol.* **52,** 418–428 (2014).
154. Ding, H. *et al.* Sonic Hedgehog Signaling Mediates Epithelial–Mesenchymal Communication and Promotes Renal Fibrosis. *J. Am. Soc. Nephrol.* **23,** 801–813 (2012).
155. Bolaños, A. L. *et al.* Role of Sonic Hedgehog in idiopathic pulmonary fibrosis. *Am. J. Physiol. - Lung Cell. Mol. Physiol.* **303,** L978–L990 (2012).
156. Moshai, E. F. *et al.* Targeting the Hedgehog–Glioma-Associated Oncogene Homolog Pathway Inhibits Bleomycin-Induced Lung Fibrosis in Mice. *Am. J. Respir. Cell Mol. Biol.* **51,** 11–25 (2014).
157. Königshoff, M. *et al.* Functional Wnt Signaling Is Increased in Idiopathic Pulmonary Fibrosis. *PLOS ONE* **3,** e2142 (2008).
158. Königshoff, M. *et al.* WNT1-inducible signaling protein–1 mediates pulmonary fibrosis in mice and is upregulated in humans with idiopathic pulmonary fibrosis. *J. Clin. Invest.* **119,** 772–787 (2009).
159. Henderson, W. R. *et al.* Inhibition of Wnt/beta-catenin/CREB binding protein (CBP) signaling reverses pulmonary fibrosis. *Proc. Natl. Acad. Sci. U. S. A.* **107,** 14309–14314 (2010).
160. Aumiller, V., Balsara, N., Wilhelm, J., Günther, A. & Königshoff, M. WNT/β-catenin signaling induces IL-1β expression by alveolar epithelial cells in pulmonary fibrosis. *Am. J. Respir. Cell Mol. Biol.* **49,** 96–104 (2013).
161. Akhmetshina, A. *et al.* Activation of canonical Wnt signalling is required for TGF-βmediated fibrosis. *Nat. Commun.* **3,** 735 (2012).
162. McQualter, J. L. *et al.* TGF-β signaling in stromal cells acts upstream of FGF-10 to regulate epithelial stem cell growth in the adult lung. *Stem Cell Res.* **11,** 1222–1233 (2013).
163. Li, M. *et al.* Epithelium-specific deletion of TGF-β receptor type II protects mice from bleomycin-induced pulmonary fibrosis. *J. Clin. Invest.* **121,** 277–287 (2011).
164. Mutsaers, S. E., Bishop, J. E., McGrouther, G. & Laurent, G. J. Mechanisms of tissue repair: from wound healing to fibrosis. *Int. J. Biochem. Cell Biol.* **29,** 5–17 (1997).
165. Scotton, C. J. *et al.* Increased local expression of coagulation factor X contributes to the fibrotic response in human and murine lung injury. *J. Clin. Invest.* **119,** 25501563 (2009).
166. Car, B. D. *et al.* Elevated IL-8 and MCP-1 in the bronchoalveolar lavage fluid of patients with idiopathic pulmonary fibrosis and pulmonary sarcoidosis. *Am. J. Respir. Crit. Care Med.* **149,** 655–659 (1994).

167. Papiris, S. A. *et al.* High levels of IL-6 and IL-8 characterize early-on idiopathic pulmonary fibrosis acute exacerbations. *Cytokine* **102,** 168-172 (2017)
168. Cao, Z. *et al.* Targeting of the pulmonary capillary vascular niche promotes lung alveolar repair and ameliorates fibrosis. *Nat. Med.* **22,** 154–162 (2016).
169. Meiners, S., Eickelberg, O. & Königshoff, M. Hallmarks of the ageing lung. *Eur. Respir. J.* **45,** 807-827 (2015).
170. Utz, J. P., Ryu, J. H., Myers, J. L. & Michels, V. V. Usual interstitial pneumonia complicating dyskeratosis congenita. *Mayo Clin. Proc.* **80,** 817–821 (2005).
171. Alder, J. K. *et al.* Short telomeres are a risk factor for idiopathic pulmonary fibrosis. *Proc. Natl. Acad. Sci.* **105,** 13051–13056 (2008).
172. Redente, E. F. *et al.* Age and sex dimorphisms contribute to the severity of bleomycin-induced lung injury and fibrosis. *Am. J. Physiol. Lung Cell. Mol. Physiol.* **301,** L510-518 (2011).
173. Chung, H. Y. *et al.* Molecular inflammation: underpinnings of aging and age-related diseases. *Ageing Res. Rev.* **8,** 18–30 (2009).
174. Jurk, D. *et al.* Chronic inflammation induces telomere dysfunction and accelerates ageing in mice. *Nat. Commun.* **5,** 4172 (2014).
175. Yu, B. *et al.* Wnt4 signaling prevents skeletal aging and inflammation by inhibiting nuclear factor-κB. *Nat. Med.* **20,** 1009–1017 (2014).
176. Sousa-Victor, P. *et al.* Geriatric muscle stem cells switch reversible quiescence into senescence. *Nature* **506,** 316–321 (2014).
177. Doles, J., Storer, M., Cozzuto, L., Roma, G. & Keyes, W. M. Age-associated inflammation inhibits epidermal stem cell function. *Genes Dev.* **26,** 2144–2153 (2012).
178. Hayflick, L. The limited in vitro lifetime of human diploid cell strains. *Exp. Cell Res.* **37,** 614–636 (1965).
179. Ventura, A. *et al.* Restoration of p53 function leads to tumour regression in vivo. *Nature* **445,** 661–665 (2007).
180. Chen, Z. *et al.* Crucial role of p53-dependent cellular senescence in suppression of Pten-deficient tumorigenesis. *Nature* **436,** 725–730 (2005).
181. Braig, M. *et al.* Oncogene-induced senescence as an initial barrier in lymphoma development. *Nature* **436,** 660–665 (2005).
182. Naylor, R., Baker, D. & van Deursen, J. Senescent Cells: A Novel Therapeutic Target for Aging and Age-Related Diseases. *Clin. Pharmacol. Ther.* **93,** 105–116 (2013).
183. Harley, C. B., Futcher, A. B. & Greider, C. W. Telomeres shorten during ageing of human fibroblasts. *Nature* **345,** 458–460 (1990).
184. Bunz, F. *et al.* Requirement for p53 and p21 to Sustain G_2 Arrest After DNA Damage. *Science* **282,** 1497–1501 (1998).
185. Robles, S. J. & Adami, G. R. Agents that cause DNA double strand breaks lead to p16INK4a enrichment and the premature senescence of normal fibroblasts. *Oncogene* **16,** 1113–1123 (1998).

186. Sedelnikova, O. A. *et al.* Senescing human cells and ageing mice accumulate DNA lesions with unrepairable double-strand breaks. *Nat. Cell Biol.* **6,** 168–170 (2004).
187. Hubackova, S. *et al.* IFNγ induces oxidative stress, DNA damage and tumor cell senescence via TGFβ/SMAD signaling-dependent induction of Nox4 and suppression of ANT2. *Oncogene* **35,** 1236–1249 (2016).
188. Moiseeva, O., Mallette, F. A., Mukhopadhyay, U. K., Moores, A. & Ferbeyre, G. DNA Damage Signaling and p53-dependent Senescence after Prolonged β-Interferon Stimulation. *Mol. Biol. Cell* **17,** 1583–1592 (2006).
189. Lugo, R. *et al.* Heterotypic paracrine signaling drives fibroblast senescence and tumor progression of large cell carcinoma of the lung. *Oncotarget* **5,** (2016).
190. Storer, M. *et al.* Senescence is a developmental mechanism that contributes to embryonic growth and patterning. *Cell* **155,** 1119–1130 (2013).
191. Acosta, J. C. *et al.* A complex secretory program orchestrated by the inflammasome controls paracrine senescence. *Nat. Cell Biol.* **15,** 978–990 (2013).
192. Muñoz-Espín, D. *et al.* Programmed Cell Senescence during Mammalian Embryonic Development. *Cell* **155,** 1104–1118 (2013).
193. Nelson, G. *et al.* A senescent cell bystander effect: senescence-induced senescence. *Aging Cell* **11,** 345–349 (2012).
194. Wiley, C. D. *et al.* Mitochondrial Dysfunction Induces Senescence with a Distinct Secretory Phenotype. *Cell Metab.* **23,** 303–314 (2016).
195. Pomerantz, J. *et al.* The Ink4a Tumor Suppressor Gene Product, p19Arf, Interacts with MDM2 and Neutralizes MDM2's Inhibition of p53. *Cell* **92,** 713–723 (1998).
196. Stein, G. H., Drullinger, L. F., Soulard, A. & Dulić, V. Differential Roles for CyclinDependent Kinase Inhibitors p21 and p16 in the Mechanisms of Senescence and Differentiation in Human Fibroblasts. *Mol. Cell. Biol.* **19,** 2109–2117 (1999).
197. Muñoz-Espín, D. & Serrano, M. Cellular senescence: from physiology to pathology. *Nat. Rev. Mol. Cell Biol.* **15,** 482–496 (2014).
198. Purvis, J. E. *et al.* p53 Dynamics Control Cell Fate. *Science* **336,** 1440–1444 (2012).
199. Geisler, S. *et al.* PINK1/Parkin-mediated mitophagy is dependent on VDAC1 and p62/SQSTM1. *Nat. Cell Biol.* **12,** 119–131 (2010).
200. Passos, J. F. *et al.* Feedback between p21 and reactive oxygen production is necessary for cell senescence. *Mol. Syst. Biol.* **6,** 347 (2010).
201. Correia-Melo, C. *et al.* Mitochondria are required for pro-ageing features of the senescent phenotype. *EMBO J.* **35,** 724-742(2016).
202. Swanson, E. C., Manning, B., Zhang, H. & Lawrence, J. B. Higher-order unfolding of satellite heterochromatin is a consistent and early event in cell senescence. *J. Cell Biol.* **203,** 929–942 (2013).
203. De Cecco, M. *et al.* Genomes of replicatively senescent cells undergo global epigenetic changes leading to gene silencing and activation of transposable elements. *Aging Cell* **12,** 247–256 (2013).

204. Narita, M. *et al.* Rb-Mediated Heterochromatin Formation and Silencing of E2F Target Genes during Cellular Senescence. *Cell* **113,** 703–716 (2003).
205. Shah, P. P. *et al.* Lamin B1 depletion in senescent cells triggers large-scale changes in gene expression and the chromatin landscape. *Genes Dev.* **27,** 1787–1799 (2013).
206. Lukášová, E., Kovarˇík, A., Bacˇíková, A., Falk, M. & Kozubek, S. Loss of lamin B receptor is necessary to induce cellular senescence. *Biochem. J.* **474,** 281–300 (2017).
207. Zhang, H., Pan, K.-H. & Cohen, S. N. Senescence-specific gene expression fingerprints reveal cell-type-dependent physical clustering of up-regulated chromosomal loci. *Proc. Natl. Acad. Sci.* **100,** 3251–3256 (2003).
208. Shelton, D. N., Chang, E., Whittier, P. S., Choi, D. & Funk, W. D. Microarray analysis of replicative senescence. *Curr. Biol.* **9,** 939–945 (1999).
209. Apel, K. & Hirt, H. REACTIVE OXYGEN SPECIES: Metabolism, Oxidative Stress, and Signal Transduction. *Annu. Rev. Plant Biol.* **55,** 373–399 (2004).
210. James, E. L., Lane, J. A. E., Michalek, R. D., Karoly, E. D. & Parkinson, E. K. Replicatively senescent human fibroblasts reveal a distinct intracellular metabolic profile with alterations in NAD+ and nicotinamide metabolism. *Sci. Rep.* **6,** srep38489 (2016).
211. Reis, R. J. S. & Goldstein, S. Mitochondrial DNA in mortal and immortal human cells. Genome number, integrity, and methylation. *J. Biol. Chem.* **258,** 9078–9085 (1983).
212. Rodier, F. *et al.* Persistent DNA damage signalling triggers senescence-associated inflammatory cytokine secretion. *Nat. Cell Biol.* **11,** 973–979 (2009).
213. Coppé, J.-P. *et al.* Senescence-Associated Secretory Phenotypes Reveal CellNonautonomous Functions of Oncogenic RAS and the p53 Tumor Suppressor. *PLOS Biol* **6,** e301 (2008).
214. Rovillain, E. *et al.* Activation of nuclear factor-kappa B signalling promotes cellular senescence. *Oncogene* **30,** 2356–2366 (2011).
215. Keller, M., Rüegg, A., Werner, S. & Beer, H.-D. Active Caspase-1 Is a Regulator of Unconventional Protein Secretion. *Cell* **132,** 818–831 (2008).
216. Ogura, Y., Sutterwala, F. S. & Flavell, R. A. The Inflammasome: First Line of the Immune Response to Cell Stress. *Cell* **126,** 659–662 (2006).
217. Orjalo, A. V., Bhaumik, D., Gengler, B. K., Scott, G. K. & Campisi, J. Cell surfacebound IL-1α is an upstream regulator of the senescence-associated IL-6/IL-8 cytokine network. *Proc. Natl. Acad. Sci.* **106,** 17031–17036 (2009).
218. Kuilman, T. *et al.* Oncogene-Induced Senescence Relayed by an InterleukinDependent Inflammatory Network. *Cell* **133,** 1019–1031 (2008).
219. Binet, R. *et al.* WNT16B Is a New Marker of Cellular Senescence That Regulates p53 Activity and the Phosphoinositide 3-Kinase/AKT Pathway. *Cancer Res.* **69,** 9183–9191 (2009).

220. Demaria, M. *et al.* An Essential Role for Senescent Cells in Optimal Wound Healing through Secretion of PDGF-AA. *Dev. Cell* **31,** 722–733 (2014).
221. Jun, J.-I. & Lau, L. F. The matricellular protein CCN1 induces fibroblast senescence and restricts fibrosis in cutaneous wound healing. *Nat. Cell Biol.* **12,** 676–685 (2010).
222. Ritschka, B. *et al.* The senescence-associated secretory phenotype induces cellular plasticity and tissue regeneration. *Genes Dev.* **31,** 172–183 (2017).
223. Krizhanovsky, V. *et al.* Senescence of activated stellate cells limits liver fibrosis. *Cell* **134,** 657–667 (2008).
224. Wolstein, J. M. *et al.* INK4a knockout mice exhibit increased fibrosis under normal conditions and in response to unilateral ureteral obstruction. *Am. J. Physiol. Renal Physiol.* **299,** F1486-1495 (2010).
225. Meyer, K., Hodwin, B., Ramanujam, D., Engelhardt, S. & Sarikas, A. Essential Role for Premature Senescence of Myofibroblasts in Myocardial Fibrosis. *J. Am. Coll. Cardiol.* **67,** 2018–2028 (2016).
226. Herbig, U., Ferreira, M., Condel, L., Carey, D. & Sedivy, J. M. Cellular Senescence in Aging Primates. *Science* **311,** 1257–1257 (2006).
227. Jeyapalan, J. C., Ferreira, M., Sedivy, J. M. & Herbig, U. Accumulation of senescent cells in mitotic tissue of aging primates. *Mech. Ageing Dev.* **128,** 36–44 (2007).
228. Baker, D. J. *et al.* Opposing roles for p16Ink4a and p19Arf in senescence and ageing caused by BubR1 insufficiency. *Nat. Cell Biol.* **10,** 825–836 (2008).
229. Baker, D. J. *et al.* Clearance of p16Ink4a-positive senescent cells delays ageingassociated disorders. *Nature* **479,** 232–236 (2011).
230. Lee, B. P. *et al.* Changes in the expression of splicing factor transcripts and variations in alternative splicing are associated with lifespan in mice and humans. *Aging Cell* **15,** 903–913 (2016).
231. Parrinello, S., Coppe, J.-P., Krtolica, A. & Campisi, J. Stromal-epithelial interactions in aging and cancer: senescent fibroblasts alter epithelial cell differentiation. *J. Cell Sci.* **118,** 485–496 (2005).
232. Laberge, R.-M. *et al.* MTOR regulates the pro-tumorigenic senescence-associated secretory phenotype by promoting IL1A translation. *Nat. Cell Biol.* **17,** 1049–1061 (2015).
233. Sagiv, A. *et al.* Granule exocytosis mediates immune surveillance of senescent cells. *Oncogene* **32,** 1971–1977 (2013).
234. Hall, B. M. *et al.* Aging of mice is associated with p16(Ink4a)- and β-galactosidasepositive macrophage accumulation that can be induced in young mice by senescent cells. *Aging* **8,** 1294–1315 (2016).
235. Baar, M. P. *et al.* Targeted Apoptosis of Senescent Cells Restores Tissue Homeostasis in Response to Chemotoxicity and Aging. *Cell* **169,** 132-147.e16 (2017).

236. Xu, M. *et al.* JAK inhibition alleviates the cellular senescence-associated secretory phenotype and frailty in old age. *Proc. Natl. Acad. Sci.* **112,** E6301–E6310 (2015).
237. Zhu, Y. *et al.* The Achilles' heel of senescent cells: from transcriptome to senolytic drugs. *Aging Cell* **14,** 644-658 (2015).
238. Chang, J. *et al.* Clearance of senescent cells by ABT263 rejuvenates aged hematopoietic stem cells in mice. *Nat. Med.* **22,** 78–83 (2016).
239. Yanai, H. *et al.* Cellular senescence-like features of lung fibroblasts derived from idiopathic pulmonary fibrosis patients. *Aging* **7,** 664–672 (2015).
240. Li, Y. *et al.* Hyaluronan synthase 2 regulates fibroblast senescence in pulmonary fibrosis. *Matrix Biol. J. Int. Soc. Matrix Biol.* **55,** 35–48 (2016).
241. Cui, H. *et al.* miR-34a Inhibits Lung Fibrosis by Inducing Lung Fibroblast Senescence. *Am. J. Respir. Cell Mol. Biol.* **56,** 168–178 (2017).
242. Hecker, L. *et al.* Reversal of Persistent Fibrosis in Aging by Targeting Nox4-Nrf2 Redox Imbalance. *Sci. Transl. Med.* **6,** 231ra47-231ra47 (2014).
243. Chen, R. *et al.* Telomerase Deficiency Causes Alveolar Stem Cell Senescenceassociated Low-grade Inflammation in Lungs. *J. Biol. Chem.* **290,** 30813–30829 (2015).
244. Minagawa, S. *et al.* Accelerated epithelial cell senescence in IPF and the inhibitory role of SIRT6 in TGF-β-induced senescence of human bronchial epithelial cells. *Am. J. Physiol. Lung Cell. Mol. Physiol.* **300,** L391-401 (2011).
245. Shivshankar, P. *et al.* Caveolin-1 deficiency protects from pulmonary fibrosis by modulating epithelial cell senescence in mice. *Am. J. Respir. Cell Mol. Biol.* **47,** 28–36 (2012).
246. Disayabutr, S. *et al.* miR-34 miRNAs Regulate Cellular Senescence in Type II Alveolar Epithelial Cells of Patients with Idiopathic Pulmonary Fibrosis. *PloS One* **11,** e0158367 (2016).
247. Schafer, M. J. *et al.* Cellular senescence mediates fibrotic pulmonary disease. *Nat. Commun.* **8,** 14532 (2017).
248. Cozens, A. L. *et al.* CFTR expression and chloride secretion in polarized immortal human bronchial epithelial cells. *Am. J. Respir. Cell Mol. Biol.* **10,** 38–47 (1994).
249. Debacq-Chainiaux, F., Erusalimsky, J. D., Campisi, J. & Toussaint, O. Protocols to detect senescence-associated beta-galactosidase (SA-betagal) activity, a biomarker of senescent cells in culture and in vivo. *Nat. Protoc.* **4,** 1798–1806 (2009).
250. Murray, L. A. *et al.* Hyper-responsiveness of IPF/UIP fibroblasts: Interplay between TGFβ1, IL-13 and CCL2. *Int. J. Biochem. Cell Biol.* **40,** 2174–2182 (2008).
251. Nho, R. S., Hergert, P., Kahm, J., Jessurun, J. & Henke, C. Pathological Alteration of FoxO3a Activity Promotes Idiopathic Pulmonary Fibrosis Fibroblast Proliferation on Type I Collagen Matrix. *Am. J. Pathol.* **179,** 2420–2430 (2011).
252. Li, Y. *et al.* Severe lung fibrosis requires an invasive fibroblast phenotype regulated by hyaluronan and CD44. *J. Exp. Med.* **208,** 1459–1471 (2011).

253. Engelhardt, E. *et al.* Chemokines IL-8, GROα, MCP-1, IP-10, and Mig Are Sequentially and Differentially Expressed During Phase-Specific Infiltration of Leukocyte Subsets in Human Wound Healing. *Am. J. Pathol.* **153,** 1849–1860 (1998).
254. Di Paolo, N. C. & Shayakhmetov, D. M. Interleukin 1α and the inflammatory process. *Nat. Immunol.* **17,** 906–913 (2016).
255. Suwara, M. I. *et al.* IL-1α released from damaged epithelial cells is sufficient and essential to trigger inflammatory responses in human lung fibroblasts. *Mucosal Immunol.* **7,** 684–693 (2014).
256. Borthwick, L. A. The IL-1 cytokine family and its role in inflammation and fibrosis in the lung. *Semin. Immunopathol.* **38,** 517–534 (2016).
257. McDonald, B. *et al.* Intravascular Danger Signals Guide Neutrophils to Sites of Sterile Inflammation. *Science* **330,** 362–366 (2010).
258. Bajrami, B. *et al.* G-CSF maintains controlled neutrophil mobilization during acute inflammation by negatively regulating CXCR2 signaling. *J. Exp. Med.* **213,** 19992018 (2016).
259. Kitamura, H. *et al.* Mouse and human lung fibroblasts regulate dendritic cell trafficking, airway inflammation, and fibrosis through integrin αvβ8–mediated activation of TGF-β. *J. Clin. Invest.* **121,** 2863–2875 (2011).
260. Jordana, M., Särnstrand, B., Sime, P. J. & Ramis, I. Immune-inflammatory functions of fibroblasts. *Eur. Respir. J.* **7,** 2212–2222 (1994).
261. Acosta, J. C. *et al.* Chemokine signaling via the CXCR2 receptor reinforces senescence. *Cell* **133,** 1006–1018 (2008).
262. Lee, S. *et al.* Mitochondrial Fission and Fusion Mediators, hFis1 and OPA1, Modulate Cellular Senescence. *J. Biol. Chem.* **282,** 22977–22983 (2007).
263. Cai, X. Y., Gommoll, C. P., Justice, L., Narula, S. K. & Fine, J. S. Regulation of granulocyte colony-stimulating factor gene expression by interleukin-17. *Immunol. Lett.* **62,** 51–58 (1998).
264. Kessler, D. J., Duyao, M. P., Spicer, D. B. & Sonenshein, G. E. NF-kappa B-like factors mediate interleukin 1 induction of c-myc gene transcription in fibroblasts. *J. Exp. Med.* **176,** 787–792 (1992).
265. Keane, M. P. *et al.* IFN-gamma-inducible protein-10 attenuates bleomycin-induced pulmonary fibrosis via inhibition of angiogenesis. *J. Immunol. Baltim. Md 1950* **163,** 5686–5692 (1999).
266. Tager, A. M. *et al.* Inhibition of pulmonary fibrosis by the chemokine IP-10/CXCL10. *Am. J. Respir. Cell Mol. Biol.* **31,** 395–404 (2004).
267. Jiang, D. *et al.* Inhibition of pulmonary fibrosis in mice by CXCL10 requires glycosaminoglycan binding and syndecan-4. *J. Clin. Invest.* **120,** 2049–2057 (2010).
268. Barratt, S. L. *et al.* Differential Expression of VEGF-Axxx Isoforms is Critical for Development of Pulmonary Fibrosis. *Am. J. Respir. Crit. Care Med.* **196,** 479-493 (2017).

269. Rodriguez, L. R. *et al.* Global Gene Expression Analysis in an in vitro Fibroblast Model of Idiopathic Pulmonary Fibrosis Reveals Potential Role for CXCL14/CXCR4. *Sci. Rep.* **8,** 3983 (2018).
270. Hill, A. R. *et al.* IL-1α mediates cellular cross-talk in the airway epithelial mesenchymal trophic unit. *Tissue Barriers* **4,** e1206378 (2016).
271. Forbes, B., Shah, A., Martin, G. P. & Lansley, A. B. The human bronchial epithelial cell line 16HBE14o− as a model system of the airways for studying drug transport. *ResearchGate* **257,** 161–7 (2003).
272. Mercer, P. F. *et al.* Proteinase-Activated Receptor-1, CCL2, and CCL7 Regulate Acute Neutrophilic Lung Inflammation. *Am. J. Respir. Cell Mol. Biol.* **50,** 144–157 (2014).
273. Gomperts, B. N. *et al.* Keratinocyte Growth Factor Improves Repair in the Injured Tracheal Epithelium. *Am. J. Respir. Cell Mol. Biol.* **37,** 48–56 (2007).
274. Stewart, C. E., Torr, E. E., Mohd Jamili, N. H., Bosquillon, C. & Sayers, I. Evaluation of Differentiated Human Bronchial Epithelial Cell Culture Systems for Asthma Research. *Journal of Allergy* **2012,** (2012).
275. Barkauskas, C. E. & Noble, P. W. Cellular mechanisms of tissue fibrosis. 7. New insights into the cellular mechanisms of pulmonary fibrosis. *Am. J. Physiol. Cell Physiol.* **306,** C987-996 (2014).
276. Morishima, Y. *et al.* Triggering the Induction of Myofibroblast and Fibrogenesis by Airway Epithelial Shedding. *Am. J. Respir. Cell Mol. Biol.* **24,** 1–11 (2001).
277. Kolodsick, J. E. *et al.* Prostaglandin E2 inhibits fibroblast to myofibroblast transition via E. prostanoid receptor 2 signaling and cyclic adenosine monophosphate elevation. *Am. J. Respir. Cell Mol. Biol.* **29,** 537–544 (2003).
278. Goldstein, R. H. & Polgar, P. The effect and interaction of bradykinin and prostaglandins on protein and collagen production by lung fibroblasts. *J. Biol. Chem.* **257,** 8630–8633 (1982).
279. Huang, S. K. *et al.* Variable Prostaglandin E2 Resistance in Fibroblasts from Patients with Usual Interstitial Pneumonia. *Am. J. Respir. Crit. Care Med.* **177,** 66–74 (2008).
280. Uhal, B. D. *et al.* Fibroblasts isolated after fibrotic lung injury induce apoptosis of alveolar epithelial cells in vitro. *Am. J. Physiol.* **269,** L819-828 (1995).
281. Waghray, M. *et al.* Hydrogen peroxide is a diffusible paracrine signal for the induction of epithelial cell death by activated myofibroblasts. *FASEB J. Off. Publ. Fed. Am. Soc. Exp. Biol.* **19,** 854–856 (2005).
282. Geiser, T., Ishigaki, M., van Leer, C., Matthay, M. A. & Broaddus, V. C. H(2)O(2) inhibits alveolar epithelial wound repair in vitro by induction of apoptosis. *Am. J. Physiol. Lung Cell. Mol. Physiol.* **287,** L448-453 (2004).
283. Larsson, O. *et al.* Fibrotic Myofibroblasts Manifest Genome-Wide Derangements of Translational Control. *PLOS ONE* **3,** e3220 (2008).
284. Pan, J. *et al.* Inhibition of Bcl-2/xl With ABT-263 Selectively Kills Senescent Type II Pneumocytes and Reverses Persistent Pulmonary Fibrosis Induced by Ionizing Radiation in Mice. *Int. J. Radiat. Oncol.* **99,** 353-361 (2017).

285. Chang, T.-C., Hsu, M.-F. & Wu, K. K. High Glucose Induces Bone Marrow-Derived Mesenchymal Stem Cell Senescence by Upregulating Autophagy. *PLOS ONE* **10,** e0126537 (2015).
286. Lorenzi, M., Montisano, D. F., Toledo, S. & Barrieux, A. High glucose induces DNA damage in cultured human endothelial cells. *J. Clin. Invest.* **77,** 322–325 (1986).
287. Burdon, R. H., Gill, V., Boyd, P. A. & Rahim, R. A. Hydrogen peroxide and sequencespecific DNA damage in human cells. *FEBS Lett.* **383,** 150–154 (1996).
288. Driessens, N. *et al.* Hydrogen peroxide induces DNA single- and double-strand breaks in thyroid cells and is therefore a potential mutagen for this organ. *Endocr. Relat. Cancer* **16,** 845–856 (2009).
289. Mirzayans, R., Andrais, B., Scott, A., Wang, Y. W. & Murray, D. Ionizing RadiationInduced Responses in Human Cells with Differing TP53 Status. *Int. J. Mol. Sci.* **14,** 22409–22435 (2013).
290. Sohn, D., Essmann, F., Schulze-Osthoff, K. & Jänicke, R. U. p21 blocks irradiationinduced apoptosis downstream of mitochondria by inhibition of cyclin-dependent kinase-mediated caspase-9 activation. *Cancer Res.* **66,** 11254–11262 (2006).
291. Dasari, A., Bartholomew, J. N., Volonte, D. & Galbiati, F. Oxidative Stress Induces Premature Senescence by Stimulating Caveolin-1 Gene Transcription through p38 Mitogen-Activated Protein Kinase/Sp1–Mediated Activation of Two GC-Rich Promoter Elements. *Cancer Res.* **66,** 10805–10814 (2006).
292. Zdanov, S., Remacle, J. & Toussaint, O. Establishment of H2O2-induced premature senescence in human fibroblasts concomitant with increased cellular production of H2O2. *Ann. N. Y. Acad. Sci.* **1067,** 210–216 (2006).
293. Volonte, D., Zhang, K., Lisanti, M. P. & Galbiati, F. Expression of Caveolin-1 Induces Premature Cellular Senescence in Primary Cultures of Murine Fibroblasts StressInduced Premature Senescence Upregulates the Expression of Endogenous Caveolin-1. *Mol. Biol. Cell* **13,** 2502–2517 (2002).
294. Psathakis, K. *et al.* Exhaled markers of oxidative stress in idiopathic pulmonary fibrosis. *Eur. J. Clin. Invest.* **36,** 362–367 (2006).
295. Frippiat, C. *et al.* Subcytotoxic H2O2 stress triggers a release of transforming growth factor-beta 1, which induces biomarkers of cellular senescence of human diploid fibroblasts. *J. Biol. Chem.* **276,** 2531–2537 (2001).
296. Toussaint, O., Medrano, E. E. & von Zglinicki, T. Cellular and molecular mechanisms of stress-induced premature senescence (SIPS) of human diploid fibroblasts and melanocytes. *Exp. Gerontol.* **35,** 927–945 (2000).
297. Chen, Q. & Ames, B. N. Senescence-like growth arrest induced by hydrogen peroxide in human diploid fibroblast F65 cells. *Proc. Natl. Acad. Sci.* **91,** 4130–4134 (1994).

298. Chen, Q. M. *et al.* Molecular analysis of H2O2-induced senescent-like growth arrest in normal human fibroblasts: p53 and Rb control G1 arrest but not cell replication. *Biochem. J.* **332,** 43–50 (1998).
299. Dimri, G. P. *et al.* A biomarker that identifies senescent human cells in culture and in aging skin in vivo. *Proc. Natl. Acad. Sci. U. S. A.* **92,** 9363–9367 (1995).
300. Kurz, D. J., Decary, S., Hong, Y. & Erusalimsky, J. D. Senescence-associated (beta)galactosidase reflects an increase in lysosomal mass during replicative ageing of human endothelial cells. *J. Cell Sci.* **113 (Pt 20),** 3613–3622 (2000).
301. Lee, B. Y. *et al.* Senescence-associated beta-galactosidase is lysosomal betagalactosidase. *Aging Cell* **5,** 187–195 (2006).
302. Val, M. M. *et al.* Senescent bronchial fibroblasts induced to senescence by Cr(VI) promote epithelial–mesenchymal transition when co-cultured with bronchial epithelial cells in the presence of Cr(VI). *Mutagenesis* **30,** 277–286 (2015).
303. Krtolica, A., Parrinello, S., Lockett, S., Desprez, P.-Y. & Campisi, J. Senescent fibroblasts promote epithelial cell growth and tumorigenesis: A link between cancer and aging. *Proc. Natl. Acad. Sci.* **98,** 12072–12077 (2001).
304. Papadopoulou, A. & Kletsas, D. Human lung fibroblasts prematurely senescent after exposure to ionizing radiation enhance the growth of malignant lung epithelial cells in vitro and in vivo. *Int. J. Oncol.* **39,** 989–999 (2011).
305. Ohuchida, K. *et al.* Radiation to stromal fibroblasts increases invasiveness of pancreatic cancer cells through tumor-stromal interactions. *Cancer Res.* **64,** 3215–3222 (2004).
306. Chen, L., Tredget, E. E., Wu, P. Y. G. & Wu, Y. Paracrine Factors of Mesenchymal Stem Cells Recruit Macrophages and Endothelial Lineage Cells and Enhance Wound Healing. *PLOS ONE* **3,** e1886 (2008).
307. Kamogashira, T., Hayashi, K., Fujimoto, C., Iwasaki, S. & Yamasoba, T. Functionally and morphologically damaged mitochondria observed in auditory cells under senescence-inducing stress. *Npj Aging Mech. Dis.* **3,** 2 (2017).
308. Yakes, F. M. & Van Houten, B. Mitochondrial DNA damage is more extensive and persists longer than nuclear DNA damage in human cells following oxidative stress. *Proc. Natl. Acad. Sci. U. S. A.* **94,** 514–519 (1997).
309. Salminen, A., Kauppinen, A. & Kaarniranta, K. Emerging role of NF-κB signaling in the induction of senescence-associated secretory phenotype (SASP). *Cell. Signal.* **24,** 835–845 (2012).
310. Chien, Y. *et al.* Control of the senescence-associated secretory phenotype by NFκB promotes senescence and enhances chemosensitivity. *Genes Dev.* **25,** 2125– 2136 (2011).
311. Mantovani, A., Allavena, P., Sica, A. & Balkwill, F. Cancer-related inflammation. *Nature* **454,** 436–444 (2008).
312. Yu, H., Pardoll, D. & Jove, R. STATs in cancer inflammation and immunity: a leading role for STAT3. *Nat. Rev. Cancer* **9,** 798–809 (2009).

313. Grivennikov, S. *et al.* IL-6 and Stat3 are required for survival of intestinal epithelial cells and development of colitis-associated cancer. *Cancer Cell* **15,** 103–113 (2009).
314. Lee, H. *et al.* Persistently activated Stat3 maintains constitutive NF-kappaB activity in tumors. *Cancer Cell* **15,** 283–293 (2009).
315. Lee, C. *et al.* Janus Kinase-Signal Transducer and Activator of Transcription Mediates Phosphatidic Acid-Induced Interleukin (IL)-1β and IL-6 Production. *Mol. Pharmacol.* **69,** 1041–1047 (2006).
316. Heinrich, P. C., Behrmann, I., Müller-Newen, G., Schaper, F. & Graeve, L. Interleukin-6-type cytokine signalling through the gp130/Jak/STAT pathway. *Biochem. J.* **334,** 297–314 (1998).
317. Bollrath, J. *et al.* gp130-mediated Stat3 activation in enterocytes regulates cell survival and cell-cycle progression during colitis-associated tumorigenesis. *Cancer Cell* **15,** 91–102 (2009).
318. Kujawski, M. *et al.* Stat3 mediates myeloid cell-dependent tumor angiogenesis in mice. *J. Clin. Invest.* **118,** 3367–3377 (2008).
319. Ohanna, M. *et al.* Secretome from senescent melanoma engages the STAT3 pathway to favor reprogramming of naive melanoma towards a tumor-initiating cell phenotype. *Oncotarget* **4,** 2212–2224 (2013).
320. O'Reilly, S., Ciechomska, M., Cant, R. & Laar, J. M. van. Interleukin-6 (IL-6) Trans Signaling Drives a STAT3-dependent Pathway That Leads to Hyperactive Transforming Growth Factor-β (TGF-β) Signaling Promoting SMAD3 Activation and Fibrosis via Gremlin Protein. *J. Biol. Chem.* **289,** 9952–9960 (2014).
321. Xu, X., Kasembeli, M. M., Jiang, X., Tweardy, B. J. & Tweardy, D. J. Chemical Probes that Competitively and Selectively Inhibit Stat3 Activation. *PLOS ONE* **4,** e4783 (2009).
322. Pedroza, M. *et al.* STAT-3 contributes to pulmonary fibrosis through epithelial injury and fibroblast-myofibroblast differentiation. *FASEB J.* **30,** 129–140 (2016).
323. Le, T.-T. T. *et al.* Blockade of IL-6 Trans Signaling Attenuates Pulmonary Fibrosis. *J. Immunol. Author Choice* **193,** 3755–3768 (2014).
324. O'Donoghue, R. J. J. *et al.* Genetic partitioning of interleukin-6 signalling in mice dissociates Stat3 from Smad3-mediated lung fibrosis. *EMBO Mol. Med.* **4,** 939–951 (2012).
325. Quintás-Cardama, A. *et al.* Preclinical characterization of the selective JAK1/2 inhibitor INCB018424: therapeutic implications for the treatment of myeloproliferative neoplasms. *Blood* **115,** 3109–3117 (2010).
326. Vannucchi, A. M. *et al.* A pooled analysis of overall survival in COMFORT-I and COMFORT-II, 2 randomized phase 3 trials of ruxolitinib for the treatment of myelofibrosis. *Haematologica* **100,** 1139-1145 (2015).
327. Verstovsek, S. *et al.* A Double-Blind, Placebo-Controlled Trial of Ruxolitinib for Myelofibrosis. *N. Engl. J. Med.* **366,** 799–807 (2012).

328. Wilkins, B. S. *et al.* Resolution of bone marrow fibrosis in a patient receiving JAK1/JAK2 inhibitor treatment with ruxolitinib. *Haematologica* **98,** 1872–1876 (2013).
329. Genovese, M. C. *et al.* Baricitinib in Patients with Refractory Rheumatoid Arthritis. *N. Engl. J. Med.* **374,** 1243–1252 (2016).
330. Boyle, D. L. *et al.* The JAK inhibitor tofacitinib suppresses synovial JAK1-STAT signalling in rheumatoid arthritis. *Ann. Rheum. Dis.* **74,** 1311-1316 (2014).

Appendix

List of acknowledgements for reproduced figures:

Figure 1.1.1. Lung budding from the anterior foregut.
Reproduced from ref. [3] with the permission of © Cold Spring Harbor Laboratory Press

Figure 1.1.2. Commitment of lung endodermal epithelium to a conducting or acinar lineage. **(A)**
Reproduced form ref. [25] with the permission of © *Development*.

Figure 1.1.2. Commitment of lung endodermal epithelium to a conducting or acinar lineage. **(B)**
Reprinted by permission from Macmillan Publishers Ltd: *Nature* (ref [4]), © 2008.

Figure. 1.1.3. Stages of distal lung development.
Reproduced from ref. [3] with the permission of © Cold Spring Harbor Laboratory Press

Figure 1.1.4. Myofibroblast alveolar infiltration and secondary septae formation.
Reprinted with permission of the American Thoracic Society. Copyright © 2017 American Thoracic Society. Kugler, M. C. *et al.* (2017) Sonic Hedgehog Signaling Regulates Myofibroblast Function During Alveolar Septum Formation in Murine Postnatal Lung. *Am. J. Respir. Cell Mol. Biol.*
The American Journal of Respiratory Cell and Molecular Biology is an official journal of the American Thoracic Society.

Figure 1.1.5. Differential organisation of the conducting and acinar airway.
Reprinted from *Cell Stem Cell*, Hogan, B. L. M. *et al.* Repair and regeneration of the respiratory system: complexity, plasticity, and mechanisms of lung stem cell function. Volume **15,** issue 2**,** 123–138 © 2014 with permission from Elsevier.

Figure 1.1.6. Hierarchy of lung epithelial cell progenitors and expression markers of their lineage.
Reproduced form ref. [25] with the permission of © *Development*.

Figure 1.1.7. Postnatal, epithelial Shh signalling is required for maintaining mesenchymal quiescence.
Reprinted by permission from Macmillan Publishers Ltd: *Nature* (ref [19]), © 2015.

Figure 1.1.8. Structure and cell types of the AEC2 niche **(A)**
Reprinted from *American Journal of Pathology*. Adamson, I. *et al*. Epithelial cellfibroblast interactions in lung injury and repair. Volume **137**, issue 2, p385-392 © 1990 with permission from Elsevier.

Figure 1.1.8. Structure and cell types of the AEC2 niche **(B)**
Reprinted from *Cell Stem Cell*, Hogan, B. L. M. *et al.* Repair and regeneration of the respiratory system: complexity, plasticity, and mechanisms of lung stem cell function. Volume **15,** issue 2**,** p123–138 © 2014 with permission from Elsevier.

Figure 1.1.9. BMP4 signalling and epithelial dynamics in homeostasis and wound repair.
Reproduced from ref. [41]. Freely distributed under a Creative Commons CC-BY Licence.

Figure 1.2.1. The general classification of the diffuse parenchymal lung disease.
Reprinted from *Medicine (Baltimore)* Maher, T. M. Diffuse parenchymal lung disease. Volume **40,** issue 6, p314–321 © 2014 with permission from Elsevier.

Figure 1.2.2. The pattern of UIP found under HRCT scan.
Reprinted from *Medicine (Baltimore)* Maher, T. M. Diffuse parenchymal lung disease. Volume **40,** issue 6, p314–321 © 2014 with permission from Elsevier.

Figure 1.2.3. Histological identification of UIP.
Reprinted from *The Lancet*, King, T. E., Pardo, A. & Selman, M. Idiopathic pulmonary fibrosis. Volume **378**, issue 9807, p1949–1961 © 2011 with permission from Elsevier.

Figure 1.2.4. Epidemiological issues associated with IPF. **(A)**
Reprinted with permission of the American Thoracic Society. Copyright © 2017 American Thoracic Society. Ley, B., Collard, H. R. & King, T. E. (2011) Clinical course and prediction of survival in idiopathic pulmonary fibrosis. *Am. J. Respir. Crit. Care Med.* **183,** 431–440. *The American Journal of Respiratory and Critical Care Medicine* is an official journal of the American Thoracic Society.

Figure 1.2.4. Epidemiological issues associated with IPF. **(B)**
Reprinted with permission of the American Thoracic Society. Copyright © 2017 American Thoracic Society. Hutchinson, J. P., McKeever, T. M., Fogarty, A. W., Navaratnam, V. & Hubbard, R. B. (2014) Increasing global mortality from idiopathic pulmonary fibrosis in the twenty-first century. *Ann. Am. Thorac. Soc.* **11,** 1176–1185. *Annals of the American Thoracic Society* is an official journal of the American Thoracic Society.

Figure 1.2.5. α_6–integrin signalling on stiff ECM confers an invasive fibroblast phenotype and contributed to lung fibrosis.
Reproduced from ref. [125]. Freely distributed under a Creative Commons CC-BY Licence.

Figure. 1.2.6. Epithelial alteration in the parenchyma of IPF lungs.
Reproduced from ref. [128]. Freely distributed under a Creative Commons CC-BY Licence.

Figure 1.2.7. Recurrent injury establishes long lasting fibrosis.
Reprinted by permission from Macmillan Publishers Ltd: *Nature Medicine* (ref [168]), © 2016.

Figure 1.2.8. Age as a driving factor in IPF. **(A)**
Reproduced with permission of the ERS ©. European Respiratory Journal Mar 2015, 45 (3) 807-827; DOI: 10.1183/09031936.00186914

Figure 1.2.8. Age as a driving factor in IPF. **(B)**
Reproduced from ref. [172] with the permission of The American Physiological Society.

Figure 1.3.1. The origins of senescent cells.
Reproduced from ref. [182] with the permission of John Wiley and Sons

Figure 1.3.3. Key components of the senescence associated secretory phenotype in fibroblasts.
Reproduced from ref. [213]. Freely distributed under a Creative Commons CC-BY Licence.

Figure 1.3.4. Presence of senescent cells over the course of forelimb development in mouse.
Reprinted from *Cell*, Storer, M. *et al.* Senescence is a developmental mechanism that contributes to embryonic growth and patterning. Volume **155**, issue 5, p1119–1130 © 2013 with permission from Elsevier.

Figure 1.3.5. Senescent cells in AER of the developing mouse forelimb.
Reprinted from *Cell*, Storer, M. *et al.* Senescence is a developmental mechanism that contributes to embryonic growth and patterning. Volume **155**, issue 5, p1119–1130 © 2013 with permission from Elsevier.

Figure 1.3.6. Senescence promotes wound healing in young mice.
Reprinted from *Dev. Cell*, Demaria, M. *et al*. An Essential Role for Senescent Cells in Optimal Wound Healing through Secretion of PDGF-AA. Volume **31**, issue 6, p722–733 © 2014 with permission from Elsevier.

Figure 1.3.7. Cellular senescence is evident in IPF and clearance of senescent cells can improve health.
Reproduced from ref. [247]. Freely distributed under a Creative Commons CC-BY Licence.

A

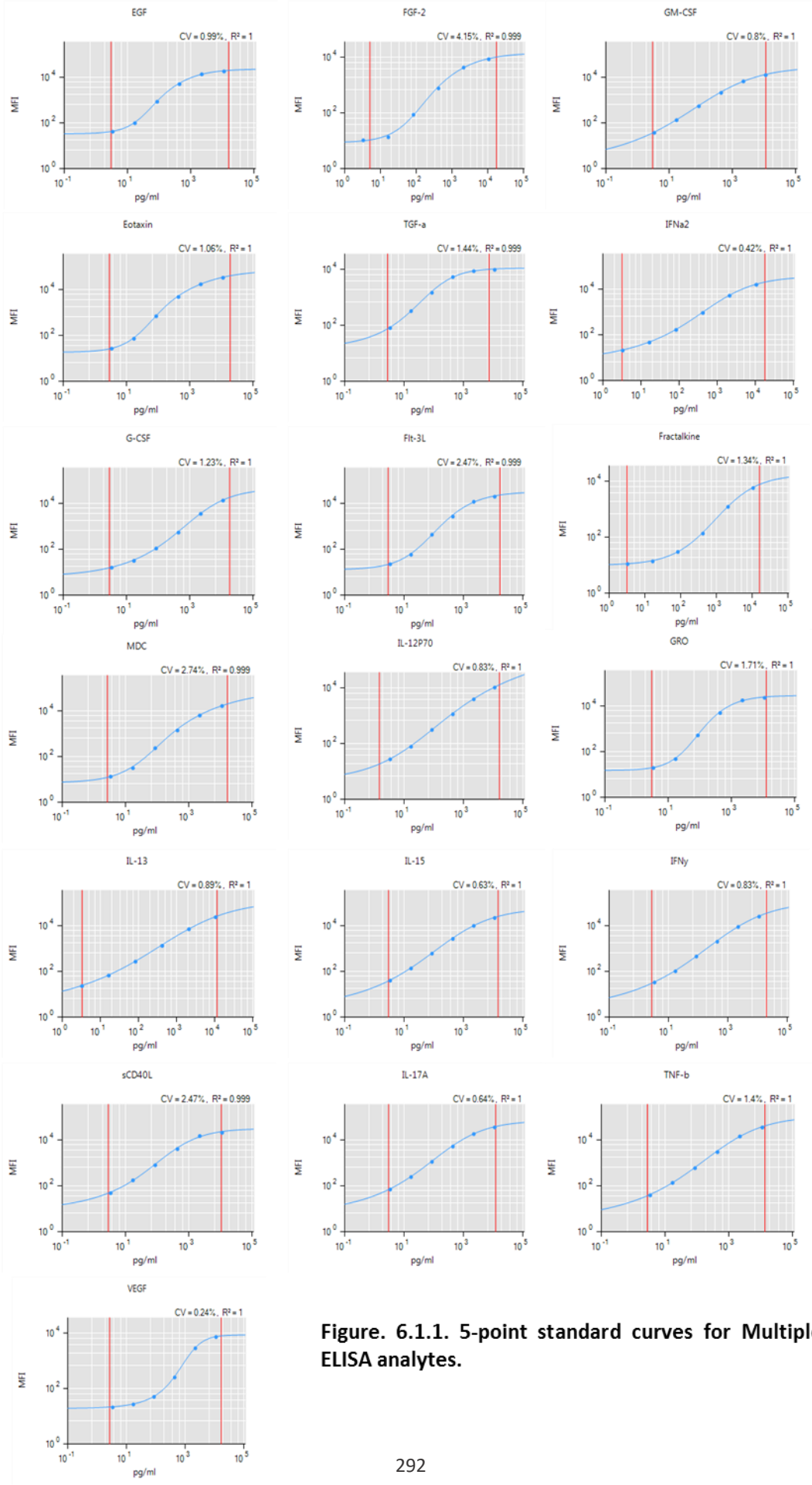

Figure. 6.1.1. 5-point standard curves for Multiplex ELISA analytes.

B

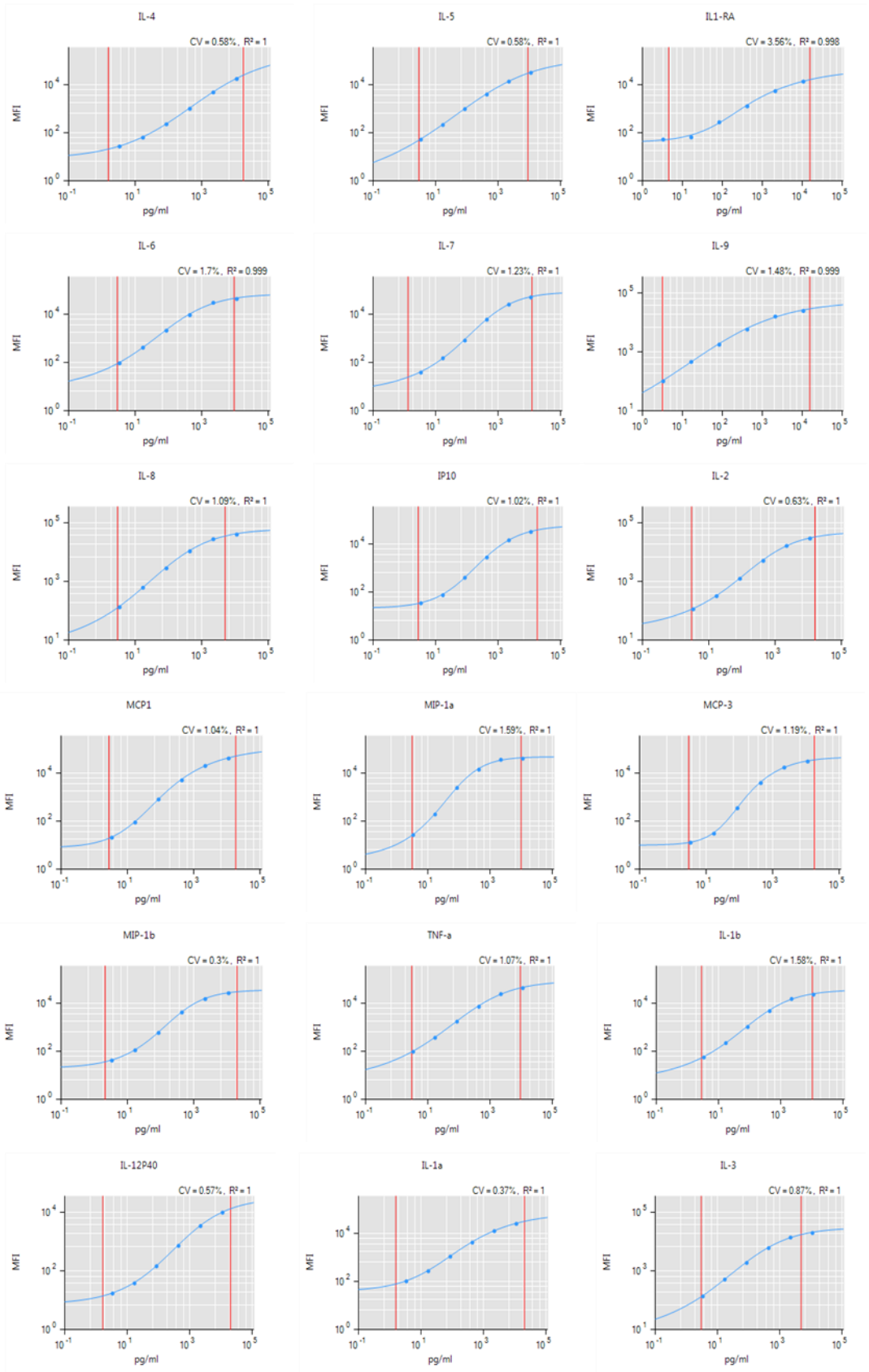
IL-4
CV = 0.58%, R² = 1
IL-5
CV = 0.58%, R² = 1
IL1-RA
CV = 3.56%, R² = 0.998
IL-6
CV = 1.7%, R² = 0.999
IL-7
CV = 1.23%, R² = 1
IL-9
CV = 1.48%, R² = 0.999
IL-8
CV = 1.09%, R² = 1
IP10
CV = 1.02%, R² = 1
IL-2
CV = 0.63%, R² = 1
MCP1
CV = 1.04%, R² = 1
MIP-1a
CV = 1.59%, R² = 1
MCP-3
CV = 1.19%, R² = 1
MIP-1b
CV = 0.3%, R² = 1
TNF-a
CV = 1.07%, R² = 1
IL-1b
CV = 1.58%, R² = 1
IL-12P40
CV = 0.57%, R² = 1
IL-1a
CV = 0.37%, R² = 1
IL-3
CV = 0.87%, R² = 1
MFI
pg/ml

Cytokine	Minimum Detectable Concentration (pg/ml)	Intra-assay % Confidence Variable	% Recovery in Matrix
EGF	2.8	2.3	97.5
bFGF	7.6	2.3	99.0
Eotaxin	4.0	7.2	100.5
TGFα	0.8	4.1	91.7
G-CSF	1.8	1.8	100.3
Flt-3L	5.4	2.4	98.2
GM-CSF	7.5	3.1	100.7
CX_3CL1	22.7	4.5	87.2
IFNα2	2.9	2.4	93.9
IFNγ	0.8	1.6	98.1
CXCL1	9.9	2.1	97.5
IL-10	1.1	1.6	97.7
CCL7	3.8	1.6	97.0
IL-12P40	7.4	2.8	93.0
CCL22	3.6	1.6	102.3
IL-12P70	0.6	2.2	104.0
IL-13	1.3	2.2	95.0
IL-15	1.2	2.7	95.3
sCD40L	5.1	3.7	95.2
IL-17	0.7	2.2	103.8
IL-1RA	8.3	2.1	93.5
IL-1α	9.4	3.3	92.9
IL-9	1.2	2.4	99.4
IL-1β	0.8	2.3	94.9
IL-2	1.0	2.1	5.4
IL-3	0.7	3.4	101.0
IL-4	4.5	2.9	94.5
IL-5	0.5	2.6	99.9
IL-6	0.9	2.0	96.1
IL-7	1.4	1.7	93.0
CXCL8	0.4	1.9	98.3
CXCL10	8.6	2.6	93.8
CCL2	1.9	1.5	98.3
CCL3	2.9	1.9	105.0
CCL4	3.0	2.4	92.4
TNFα	0.7	1.6	97.8
TNFβ	1.5	3.7	97.5
VEGF	26.3	4.3	91.8

Figure. 6.1.2. Multiplex ELISA sensitivities and accuracy. As per the manufacturer, minimum detection concentrations, intra assay confidence variables and recovery in matrix are stated. Intra-assay precision is generated from the mean of the % CV's from sixteen reportable results across two different concentration of cytokines in a single assay. Spike recovery: the data represents mean recovery of three concentration levels (low, medium and high) of spiked standards ranging from 3-10,000pg/mL in serum matrix

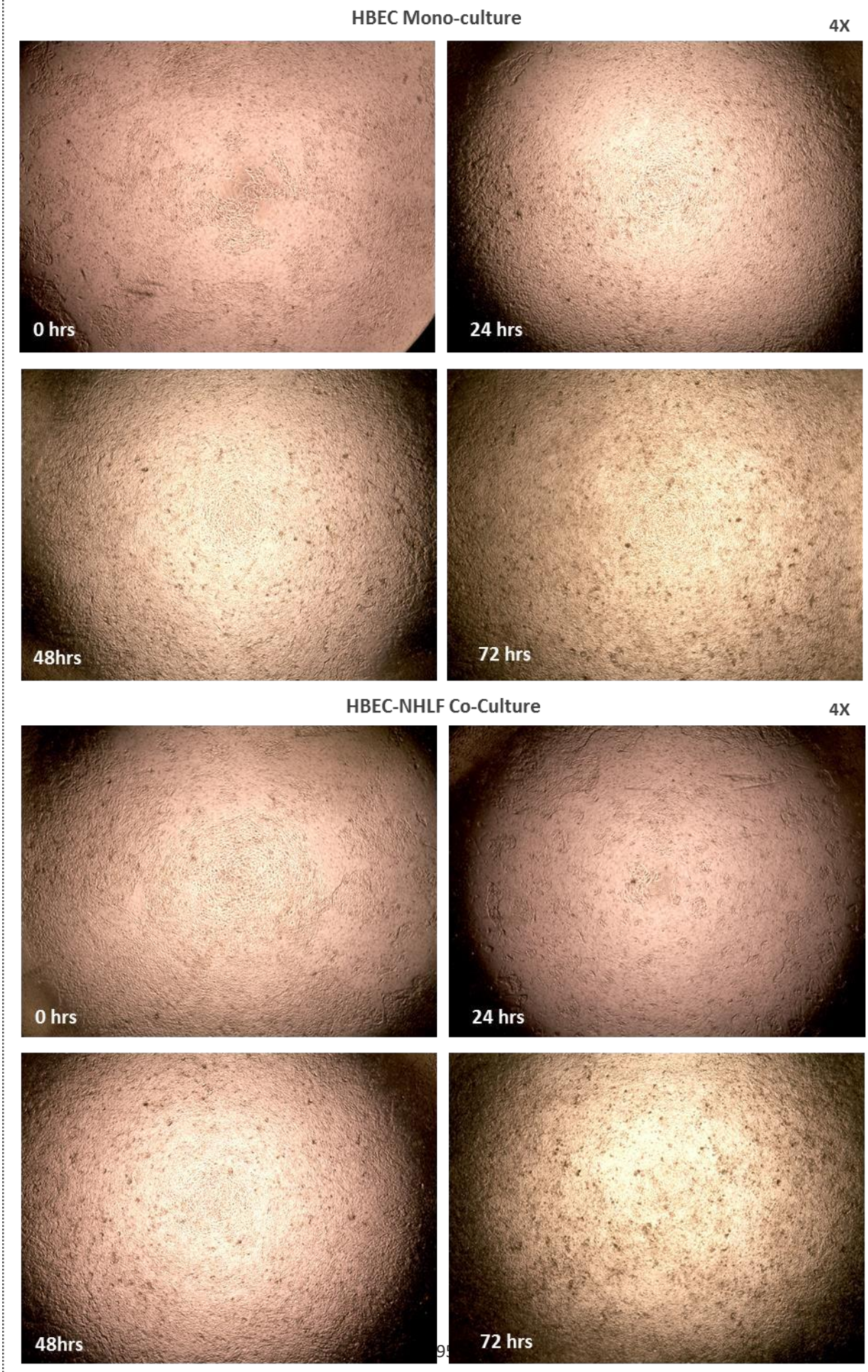

Figure. 6.1.2. Phase-contrast images of HBECs seeded in mono- and co-culture.

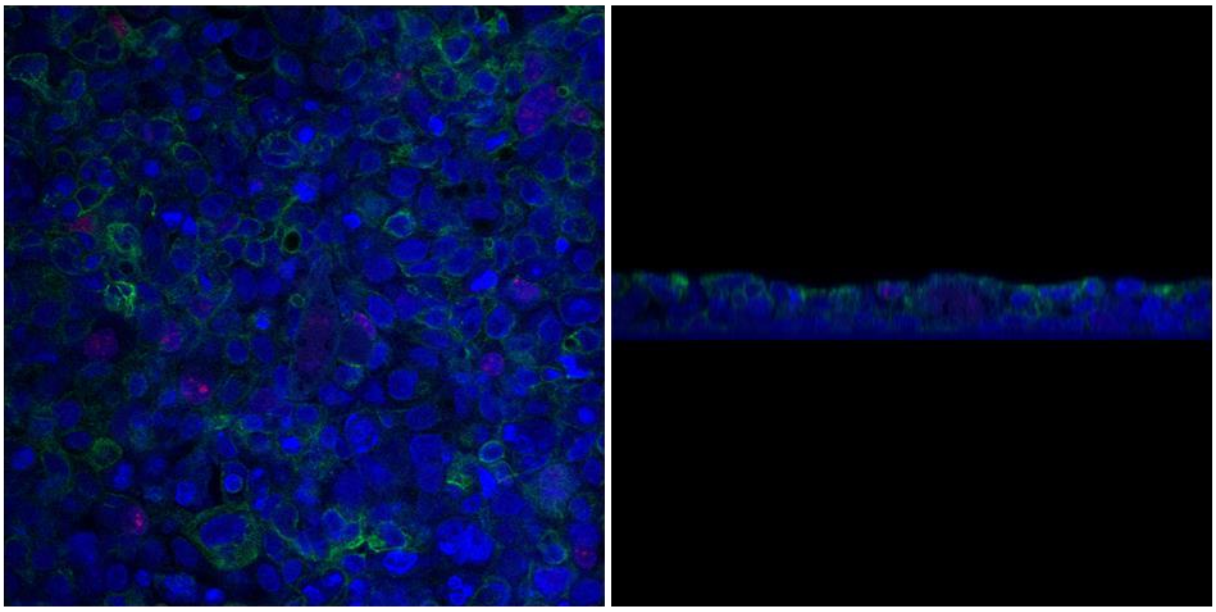

Figure 6.1.3. Confocal microscopy of HBECs. Mono-culture HBECs were cultured in transwell inserts for 96hrs, they were then fixed and stained with KRT-5 (Alexa 488), Ki67 (Alexa 595) and DAPI, images were taken via confocal microscopy, showing the axial and frontal planes.